Faculdade de Engenharia da Universidade do Porto

Development of a New Computational Approach to Simulate Blood Coagulation

Maria Inês Araújo Barbosa

Dissertation carried out under the
Master in Biomedical Engineering

Supervisor: Prof. Dr. Jorge Américo Oliveira Pinto Belinha
Co-Supervisor: Prof. Dr. Renato Manuel Natal Jorge

Porto, June 2019

Resumo

Atualmente as doenças cardiovasculares são a principal causa de morte em todo o mundo, apresentando um grande impacto económico e social. O sistema cardiovascular é composto pelo coração, vasos sanguíneos e sangue, desempenhando funções vitais para o normal funcionamento de todo o corpo, das quais se pode destacar o processo de paragem de hemorragias através dos mecanismos de hemostasia. O sangue possui os componentes necessários para desencadear uma resposta adequada para intervir, como por exemplo, no caso de rutura de um vaso. Nesta situação, as plaquetas são ativadas para parar a hemorragia e pode iniciar-se o processo de coagulação. No fim, forma-se um material gelatinoso sobre a lesão, ao qual se dá o nome coágulo ou trombo que mais tarde é dissolvido através do processo de fibrinólise. Em condições normais, este conjunto de mecanismos só ocorre em situações de emergência, no entanto, alterações, por exemplo, no fluxo ou nos compostos intervenientes, podem levar à uma formação ou crescimento anormal do coágulo, o que muitas vezes pode estar associada a determinadas doenças cardíacas, como é o caso do enfarte do miocárdio. Deste modo, é importante compreender este processo de modo a evitar estes casos e poder intervir atempadamente, o que pode contribuir para a diminuição dos números associados às doenças cardiovasculares. Nesta sequência, os estudos numéricos surgem como alternativa aos métodos convencionais e clínicos, sendo já possível obter resultados coerentes com dados experimentais. No entanto, é importante referir que o processo envolvido na formação de um coágulo é bastante complexo e ainda não completamente compreendido, pelo que os modelos até agora desenvolvidos para o representar ainda não são capazes de simular todo o processo. Assim, o presente trabalho tem como objetivo a simulação do fluxo sanguíneo e a previsão da formação de coágulos através do método dos elementos finitos e de métodos sem malha. Para além disso, um novo modelo numérico e um algoritmo inovador, capazes de prever a formação de coágulos, serão desenvolvidos e testados em diferentes condições fisiológicas de modo a serem validados.

Abstract

Nowadays, cardiovascular diseases are the leading cause of death in the world, with a major economic and social impact. The cardiovascular system is formed by the heart, blood vessels and blood, performing vital functions for the normal functioning of the whole body. One of these vital functions is the process of stopping haemorrhages through haemostasis mechanisms. The blood has the required components to trigger an adequate response to intervene, for example, in case of rupture of a vessel. In this situation, the platelets are activated to stop the bleeding and the coagulation process can occur. At the end, a gelatinous material is formed on the lesion site, which is called the clot or thrombus, which will later be dissolved through the fibrinolysis process. Under normal conditions, this set of mechanisms only occurs in emergencies however, changes, for example, in the flow or in the intervening compounds, can lead to abnormal formation and/or growth of the clot, which can often be associated with certain cardiovascular diseases, such as myocardial infarction. Therefore, it is important to understand this process in order to avoid these cases and to be able to intervene in time, which may contribute to a decrease in the numbers associated with these types of diseases. In this sequence, numerical studies appear as an alternative to conventional and clinical methods, being capable to deliver coherent results with experimental data. However, it is important to mention that the process involved in the formation of a clot is quite complex and is not yet completely understood, so the developed models to represent it, so far, are still unable to simulate the whole process. Thus, the present work aims to simulate blood flow and clot formation, through the Finite Element method and through meshless methods. In addition, a new numerical model and an innovative algorithm capable of predicting the formation of clots will be developed and tested under different physiological conditions in order to be validated.

Agradecimentos

Antes de mais, o meu agradecimento ao professor Jorge Belinha, por todo o apoio, confiança, disponibilidade e motivação ao longo destes 2 anos. Pelas oportunidades que tanto me fizeram crescer.

A todos aqueles que fizeram parte do meu percurso e que contribuíram para chegar ao fim de mais uma etapa importante da minha vida. Em especial aos meus amigos, que me ajudaram sempre ao longo destes anos. Pelo carinho, amizade, companheirismo e bons momentos.

Ao Marcelo, pela paciência, ajuda, carinho e compreensão durante este percurso. Por acreditar em mim mas, acima de tudo, por fazer com que tudo seja sempre melhor.

Por fim, à minha família, pelo apoio incondicional, por todas as palavras e ensinamentos. Aos meus Pais que me deram tudo, que estiveram sempre presentes, que me ajudaram a cumprir os meus objetivos e que sempre me incentivaram a seguir os meus sonhos. Sem eles, nada seria possível.

A todos, obrigada.

Institutional Acknowledgments

The author truly acknowledges the work conditions provided by the Applied Mechanics Division (SMAp) of the department of mechanical engineering (DEMec) of Faculty of Engineering of the University of Porto (FEUP), and by the MIT-Portugal project "MIT-EXPL/ISF/0084/2017", funded by Massachusetts Institute of Technology (USA) and "Ministério da Ciência, Tecnologia e Ensino Superior - Fundação para a Ciência e a Tecnologia" (Portugal).

Additionally, the authors gratefully acknowledge the funding of Project NORTE-01-0145-FEDER-000022 - SciTech - Science and Technology for Competitive and Sustrainable Industries, cofinanced by Programa Operacional Regional do Norte (NORTE2020), through Fundo Europeu de Desenvolvimento Regional (FEDER).

Furthermore, the author acknowledges the inter-institutional collaboration with clinical partners of the Vascular Surgery department of "Hospital de São João do Porto" – Dr. Isabel B. Vilaça and Dr.João Rocha Neves.

Finally, the author acknowledges the synergetic collaboration with the collaborators of "Computational Mechanics Research Laboratory CMech-Lab" (ISEP/FEUP/INEGI), and its director, Prof.Dr. Jorge Belinha, and its senior advisors, Prof.Dr. Renato Natal Jorge and Prof.Dr. Lúcia Dinis.

"Remember to look up at the stars and not down at your feet.
Try to make sense of what you see and wonder about what makes the universe exist. Be curious.
And however difficult life may seem, there is always something you can do and succeed at.
It matters that you don't just give up."

Stephen Hawking

Contents

List of Figures

List of Tables

List of Abbreviations and Symbols

Abbreviations

1D - One-dimensional

2D - Two-dimensional

3D - Three-dimensional

ATIII – Antithrombin III

BDFM - Backward Differentiation Formula Method

BEM - Boundary Element Method

CVD - Cardiovascular disease

CT- Computed Tomography

CFD - Computational Fluid Dynamics

CRD - Convection-Reaction–Diffusion

DPD - Dissipative Particle Dynamics method

DVT - Deep vein thrombosis

EFGM - Element Free Galerkin method

FDM - Finite Difference method

FEM – Finite Element method

FPM - Finite Point Method

FVM – Finite Volume method

MRI - Magnetic Resonance Imaging

MLPG - Meshless Local Petrov–Galerkin method

MPS - Moving Particles Semi-Implicit method

NNRPIM – Natural Neighbour Radial Point Interpolation method

ODE's - Ordinary Differential Equations

PC – Protein C

PDE's - Partial Differential Equations

PAI-1- Plasminogen Activator Inhibitor-1

PGI2 - Prostacyclin I2

RBF - Radial Basis Function

RPIM – Radial Point Interpolation method

Re - Reynolds Number

RKM - Runge-Kutta method

SPH - Smoothed Particle Hydrodynamics

TF –Tissue Factor

TFPI - Tissue Factor Pathway Inhibitor

t-PA - Tissue Plasminogen Activator

TAFI - Thrombin-activatable Fibrinolysis Inhibitor

TM - Thrombomodulin

vWF - VonWillebrand Factor

u-PA - Urokinase Plasminogen Activator

Symbols

μ - viscosity

$\dot{\tau}$ - shear stress

$\dot{\gamma}$ - shear rate

$\dot{\varepsilon}$ – strain rate

Chapter 1

Introduction

1.1 - Framework

Cardiovascular disease (CVD) is the leading cause of death around the world [1-3], representing a global public health crisis [4]. The increase of the prevalence of CVD and mortality associated with it has, in recent years, encouraged the development and use of new techniques to control this world problem. [1]

According to World Health Organization (WHO), CVD was responsible for 30% of all deaths in 2008 [4]. Later, in 2015, 19.9 million deaths occurred, one-third of all global deaths caused by CVD [3], a number that is expected to rise to 23.6 million by 2030 [2].

The cost of CVD to both families and society is related to the loss of productivity and income of the patient possessing CVD and the respective caregiver, who may have to stop working in order to provide the necessary assistance. Between 2010 and 2030, real total direct medical costs of CVD are projected to triple, from $272.5 billion to $818.1 billion [2].

CVD remains the number one killer of Americans. With the aging of the population, the prevalence and cost of care associated with CVD conditions like heart failure and stroke, is expected to increase over the next decades. By the year 2035, nearly half of the U.S. population is projected to have CVD, generating $1.1 trillion annually in direct and indirect medical costs, representing a steep price for society [5].

Alterations in the haemostatic system are related to CVD [6]. The formation of a clot in coronary or cerebral circulation can cause acute myocardial infarction or ischemic stroke, respectively, is one of the most common causes of morbidity and mortality, with the prevalence of these diseases increasing in developing nations [7]. About 5 million Americans have heart failure, with an

incidence of 10 per 1000 population, being more prevalent in elders and representing 20% of all hospital admissions among this group [8].

Deep vein thrombosis (DVT) and pulmonary embolism also affect more than 1 million Americans per year, a number which has been increasing with the aging population [9, 10]. These conditions can be initiated by inflammation and blood stasis, which leads to the formation of a red blood clot and, some factors, like the abnormal expression of cellular and/or plasma procoagulant activity, increase the risk of these occurrences [10].

Beyond the risk of death (30%), from one third to one half of the individuals develop recurrent thrombosis, long-term morbidity associated with post-thrombotic syndrome or chronic venous insufficiency, representing a significant economic problem [9, 10]. The treatment of a single event costs from $10 000 to more than $16 000 per person, which corresponds to $2 billion dollars per year [9].

Due to the ageing of the population, and the consequent increase of health care costs, the identification and development of new and effective techniques and treatments are required to tackle this global issue [7, 11]. The medical field requires more rigorous methods. Computer simulations are an important tool to analyse the behaviour of the circulatory system. Numerical simulations are noninvasive and, comparing with in vitro experiments, possibly more accurate and flexible [11]. Furthermore, it is important to understand the normal and pathologic behaviour of the vascular system. Thus, numerical methods, have also been used to obtain detailed information on blood flow and the response of blood vessels [12].

In the present work, the blood flow and the formation of blood clots through biomechanical simulations will be studied, using discretization numerical methods. Furthermore, a new numerical model capable of predicting and studding the formation of clots will be developed and tested under different conditions with the aim of validating it, taking into account some parameters, which will also be investigated.

1.2 - Motivation

Haemodynamic conditions, including velocity, shear and pressure, play an important role in the modulation of vascular adaptation and the localization of vascular disease. Consequently, understanding the local haemodynamic environment in a region of the vascular system is an important field of research, particularly in haemostasis and in thrombotic situations [12].

The available numerical models can provide simulations quite realistic since they can resort to the patient's available data. This patient-specific data can be obtained through radiological acquisition with computed tomography (CT), magnetic resonance imaging (MRI), etc. [11], which allows for the realistic definition of the shape of the computational domain (the organ or tissue under study).

In recent years, numerical analyses have increased in popularity [13]. For the last four decades, Finite Element method (FEM) has been the most commonly used discrete numerical method for analysing physical phenomena, both in solid and fluid mechanics [14, 15]. In fluid flow analyses, these methods can solve complex problems, making it a very powerful tool. Besides that, they are relatively low cost, and can be an alternative to experimental tests, which is quite beneficial in engineering and, more particularly, in clinical studies [13]. FEM can be used to compute, for example, pressure, velocity or/and shear stresses in biological flows, properties that are essentials to understand specific processes [15].

However, it is important to stress that other methods have been successfully used for this purpose, as in the case of meshless methods. However, the number of papers presented in the literature is reduced, when compared to the ones performed with FEM. Regarding the meshless method chosen for this work, it was never been used before to study blood flow or blood coagulation. Thus, it is important to understand the viability of these methods applied to blood and blood processes in order to improve this gap in the literature.

1.3 - Objectives

The main objective of this work is to simulate blood flow, with and without clot, in order to understand how it influence the blood flow dynamics, taking into account features like size, form and constitution, using different methods. The other main objective of this work is to develop a new algorithm to simulate blood clot formation, verifying its viability through different examples and situations and through the study of different mechanical properties that are related with the growth of the clot and with the algorithm created, namely velocity or viscosity of the domain.

Thus, to achieve these goals, secondary objectives were defined:

- Perform a steady flow analysis of the blood flow using recent meshless methods;
- Compare different numerical methods;
- Study the effect of a clot in blood flow;
- Simulate the flow of the bio-system blood-clot;
- Investigate the optimal parameters for the fluid (blood) and for the viscous solid (clot).

Furthermore, this dissertation aims to perform a detailed survey in the following topics:

- Cardiovascular system (physiology)
- Blood flow (physiology and mathematical models to describe it).
- Blood clot formation (physiology and mathematical models to describe it).
- Discrete numerical techniques (mathematical formulation and state-of-the-arte)

1.4 - Document Structure

The present dissertation is organized in ten chapters, with them being divided into several subsections. Chapter 1 is a brief summary on the importance and relevance of studies such as the one that will be performed in this project. Besides, the motivation for such work and the main objectives defined are also presented. Chapter 2 is an introductory chapter to the cardiovascular system, which allows to understand its behaviour, as well as its constituents in normal conditions. Chapter 3 explains the complexity of the formation of blood clots and the conditions and abnormalities that lead to their formation, the participants of the process are presented and why this process is difficult to explain and modulate/simulate. It is one of the most important chapters because simulating blood coagulation is the focus of the dissertation. Chapter 4 presents the discrete techniques and the fluid flow formulation that will be used in this work. Chapter 5 corresponds to the state of the art of previous works on fluids, blood flow and blood coagulation, reviewing published papers in this field, and the importance of these studies to medicine is stressed. Chapter 6 shows the preliminary work, which allow to understand the influence of the clot in the blood flow but also, the influence of the viscosity in this type of system. Chapter 7 presents the new developed algorithm, being explain each part of the new code in different subsections. Chapter 8 and 9 correspond to the results obtained with the algorithm. Chapter 8 presents the results that validate the algorithm and Chapter 9 presents other examples, where some parameters and boundary conditions were changed in order to verify the robustness and stability of the proposed algorithm. Lastly, Chapter 10 shows some conclusions about all the work performed.

Chapter 2

Cardiovascular System

Maintaining the haemostasis is one of the main functions of the cardiovascular system. However, to understand this process it is important to first understand how the system normally behaves, as well as their main constituents and their respective functions. Thus, this chapter is a review on the cardiovascular system (taking into account its anatomy and main functions) and, more particularly, on blood and other main players in the haemostasis process. So, this chapter also presents the process that leads to the formation of the constituents of blood, its mechanical properties and constitutive models to represent it.

2.1 - Introduction

The cardiovascular system, also known as circulatory system, is made up of the heart (pump) and vasculature (**Figure 2.1**). The heart is a complex organ and is it turn made up of four chambers (two auricles and two ventricles) that pump blood into the vasculature - a network of arteries, arterioles, capillaries, venules and veins, that carry blood to whole body [16, 17].

This system is normally divided into two parts: the pulmonary and systemic circulations. Both are comprised by the three main types of vessels (arteries, capillaries and veins), subdivided according to their diameters and wall thickness [16].

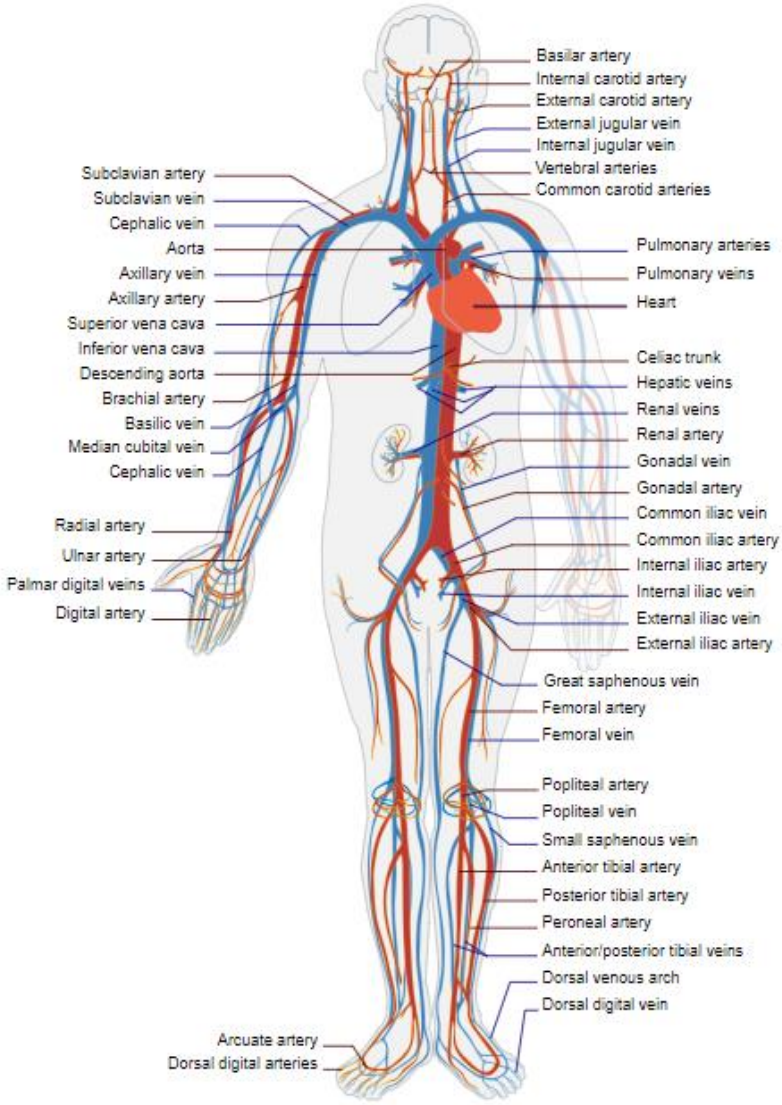

Figure 2.1 - Schematic representation of the cardiovascular system. Adapted from [18].

Regarding the tissues that make up the wall of the vessels, they are formed by [17]:

- **Endothelium**: a special epithelium that acts like a semipermeable barrier between blood plasma and interstitial fluid, allowing mediation of the bi-directional exchanges of small molecules and transport of macromolecules. Thus, it is responsible for monitoring the exchanges between blood and tissues.
- **Smooth Muscle**: It is part of all vessels except capillaries and some venules. Its main function is the regulation of the volume and local pressure of blood through contraction and relaxation, monitoring the calibre of the vessels.
- **Connective Tissue**: its quantity and proportion varies according to the type and functional necessity of vessels. This tissue is abundant in collagen, which contributes to the physical properties of the walls, being able to affect the diffusion and permeability of the vessel.

Besides that, the combination of these tissues form three layers, also known as [17, 19]:

- **Tunica Intima**: The innermost layer of the blood vessels and made up of a layer of endothelium cells and one of connective tissue (the subendothelium layer), being in contact with the flowing blood. In larger vessels, this layer is separated from Tunica Media by an elastic lamina, mainly composed of elastin and with small gaps that allow the diffusion of substances to nourish the cells in deeper zones.
- **Tunica Media**: this layer is mainly formed by smooth muscle cells and, between them, variable amounts of extracellular matrix, depending on the type of vessel. Extracellular matrix is composed of elastic and connective fibers, being also dependent on the type of vessel.
- **Tunica Adventitia**: also known as tunica externa, it is the outermost layer. This layer consists of connective fibers mainly of collagen I layered in a spiral shape and elastic fibers that become continuous with the connective tissue of the organs.

The following figure (**Figure 2.2**) represents a schematic illustration of the constitution of a vessel.

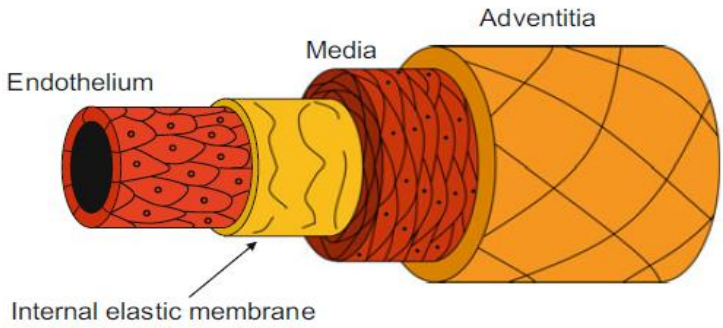

Figure 2.2 - Generic composition of a vessel. Adapted from [18].

It is important to notice that each type of vessel presents specific structural features that allows its distinction from the others [17].

From a mechanical perspective, vessel walls are essential made up of elastin and collagen, with their ratio being the main determinant of the elastic behaviour of a vessel. Elastin is highly deformable under pressure, presenting a low Young's modulus when compared with collagen. On the other hand, collagen presents a higher breaking strength [18].

Arteries are a group of vessels that become smaller as they branch out and have thick walls containing large quantities of elastic tissue. Their main function is to carry oxygenated blood (with oxygen and nutrients), from the heart to the tissues. They are subdivided in elastic arteries, muscular arteries and arterioles (**Figure 2.3**). However, due to their elasticity, they also maintain blood flow through the tissues during the cardiac cycle [17, 19].

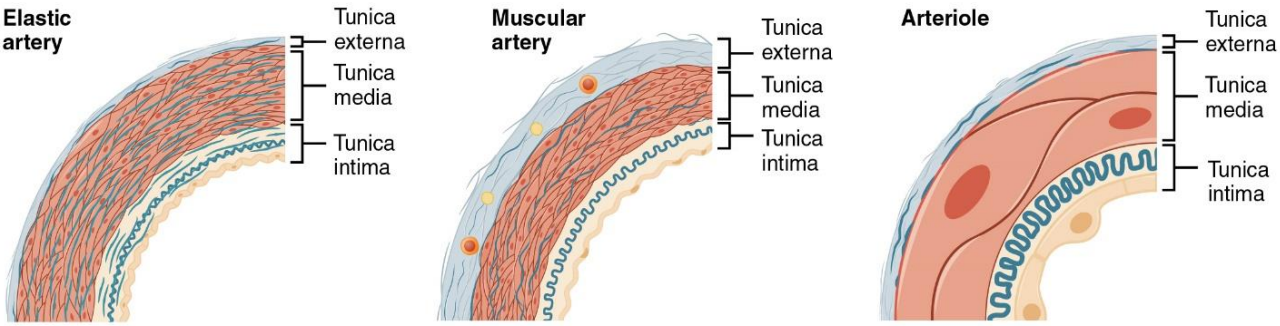

Figure 2.3 - Composition of the walls of different arteries. Adapted from [18].

Capillaries perform the ultimate function of the cardiovascular system: the exchange of nutrients, metabolic end products, and cell secretions between blood and target tissues. They are composed of only a layer of endothelium cells on a basement membrane, without any surrounding smooth muscle or elastic tissue. Besides that, they are divided into continuous, fenestrated and sinusoid capillaries (**Figure 2.4**) [17-19].

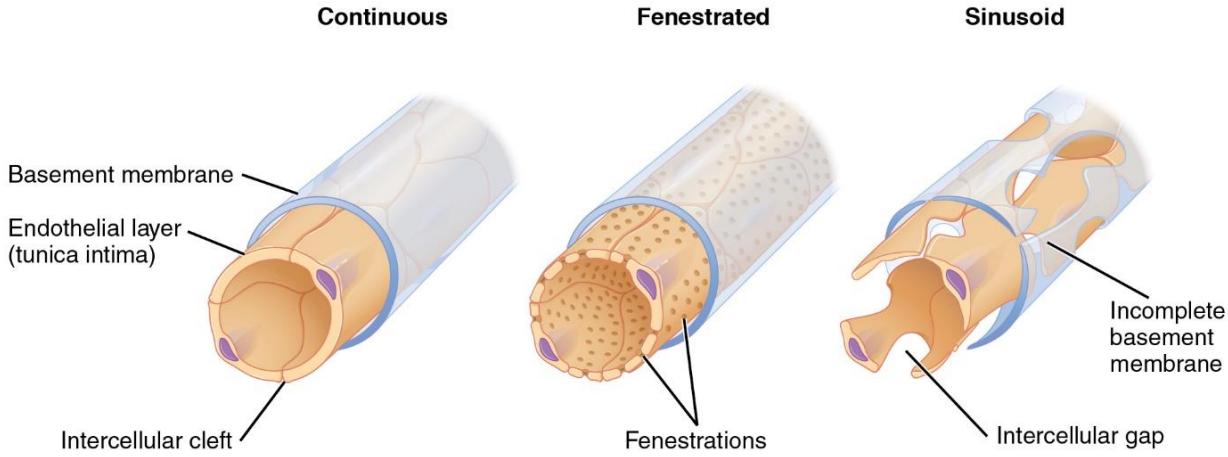

Figure 2.4 - Composition of the walls of different capillaries. Adapted from [18].

Veins receive blood from venules who receive it from capillaries and re-route the blood to the heart [17, 19]. Comparing with arteries, veins are low pressure vessels with a slow flow, thin walls and their elastin/collagen ratio is small [16, 18]. These vessels are divided in veins with small, medium and large calibre (**Figure 2.5**) [17].

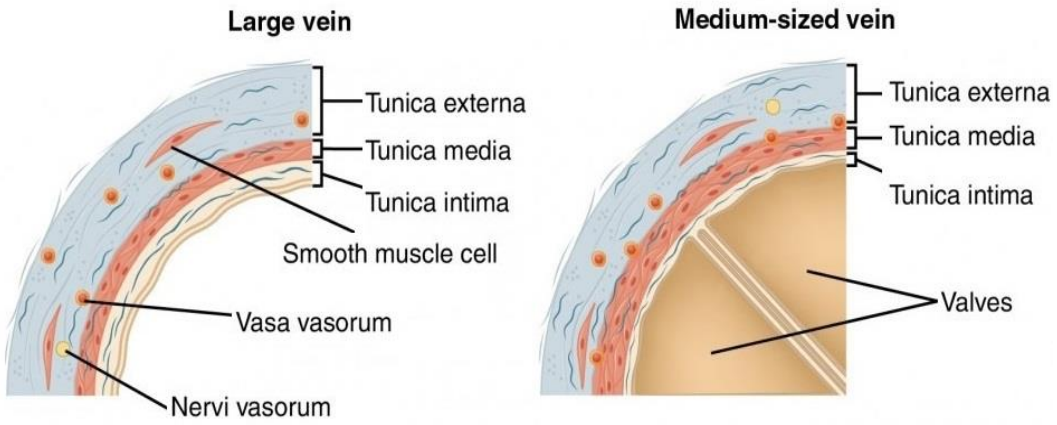

Figure 2.5 - Composition of the walls of different veins. Adapted from [18].

Besides that, the following table (**Table 2.1**) presents generic features of blood vessels.

Table 2.1 – Characteristics of blood vessels. Adapted from [18].

Vessel	Diameter (mm)	Length (mm)	Number	Volume (mL)	Cross Sectional Area (cm^2)	Mean Velocity (cm/s)	Mean Pressure (mmHg)
Aorta	22	600	1	228	4	25	95
Large Arteries	6	300	40	339	11	8.3	93
Small Arteries	2	50	2400	377	75	1.2	87
Arterioles	0.02	3	1.1×10^8	104	346	0.3	54
Capillaries	0.01	1	3.3×10^9	259	2592	0.04	25
Venules	0.04	3	2.2×10^8	829	2765	0.03	7
Small Veins	2	50	2400	377	75	1.2	4
Large Veins	10	300	40	943	31	3	2
Venae Cava	22	500	2	228	4	25	0

The main functions of the cardiovascular system are [18]:

- **Transport of Molecules**: oxygen, carbon dioxide, glucose, amino acids, vitamins and minerals are some examples of products that come in and out from the vascular system and organs, transported by blood, to contribute for the normal function of the entire body.
- **Defence and Healing**: the immune system and tissue repair system are part of the cardiovascular, involving particles transported in the blood.
- **Thermoregulation**: combined with sweating, 4% of blood, flows close to the skin surface to regulate the temperature of the body, however, under conditions of excessive heat, this quantity may be increased in order to maintain the normal body temperature.
- **Fluid Balance**: controls the volumes and electrolyte concentration of intracellular fluid and extracellular fluid (interstitial fluid, blood and lymph).

Thus, blood in an essential element of the cardiovascular system. Blood is a complex fluid that circulates throughout the body and its correct behaviour is essential to maintain the normal function of the organism [20]. So, it is important to understand how this fluid works.

2.2 - Blood

It is important to study blood flows during normal and abnormal physiologic conditions since the most common CVD are associated with some form of abnormal blood flow and, as said before, they are a major cause of death around the world [20].

2.2.1 - Biological Description of Blood

There are about 5 L of blood in the human body (about 7% of the body weight). This fluid is a heterogeneous multi-phase (semisolid and liquid) mixture of blood cells suspended in plasma, a liquid with proteins, organic molecules, minerals and ions (**Figure 2.6**) that performs some important functions in the human body (**Table 2.2**) [20-22].

Thus, blood is mainly made up of three components:

- **Plasma**: a colour fluid composed of organic and inorganic substances dissolved in water (90 % water, 1 % electrolytes and 9% of various molecules) [19]. Plasma represents 55% of blood and its main function is the transportation and distribution of nutrients and metabolites [16, 18]. Besides that, plasma contains amino acids that are used by cells to make their own proteins [19].
- **Macromolecules and other Molecules**: their central role is the creation of an osmotic pressure to allow the absorption of extracellular fluid into capillaries. These correspond to proteins, such as globulins (immune system), albumin (maintenance of oncotic pressure) and fibrinogen

(clotting system); vitamins, hormones, waste products (urea, ammonia), carbon dioxide, oxygen and a variety of mineral electrolytes [18, 19].

- **Blood Cells**: also called corpuscles or "formed elements", they are the solid phase of blood and are divided in three major groups: the erythrocytes/red cells, leucocytes/white cells and platelets. They are involved in oxygen transport, blood coagulation and in the immune transport [17].

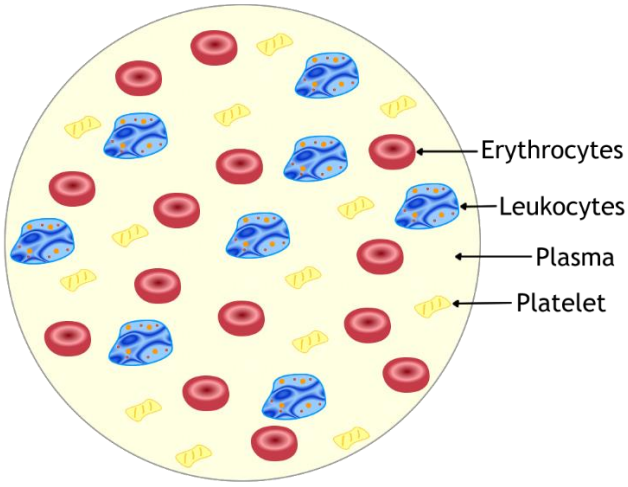

Figure 2.6 – Illustrative representation of blood components in blood.

Table 2.2 – Composition of blood. Adapted from [18].

Blood component	% By volume	Main Function
Plasma	50-60	Carbon Dioxide and Nutrient Transport
Red Cells	40-50	Oxygen Transport
White Cells	0.7	Immune System
Platelets	0.3	Blood Coagulation
Macromolecules: Albumin	2	Maintain the Osmotic Pressure
Other	1.5	Various

As seen previously, the main functions of the cardiovascular system are attributed to the blood. Among these, it is possible to highlight the transportation and diffusion of metabolic products of tissue cells and the maintenance of haemostasis [19, 21]. The rate of delivery is determined by blood concentration and the rate of blood flow and the rate of diffusion by its rheological properties [21]. Regarding haemeostasis, it is the constituents of the blood that prevent losses of blood and allow blood coagulation [19].

2.2.2 - Cellular Constitution

Blood cells are produced from the bone marrow, all descending from pluripotent hematopoietic stem (undifferentiated cells), by a process called Haematopoiesis (**Figure 2.7**). When these divide, they can become two types of cells: lymphoid stem cells or myeloid stem cells. Lymphoid stem cells only differentiate in lymphocytes, while myeloid stem cells can follow different paths of differentiation, giving origin to red blood cells, platelets and the other white cells [19].

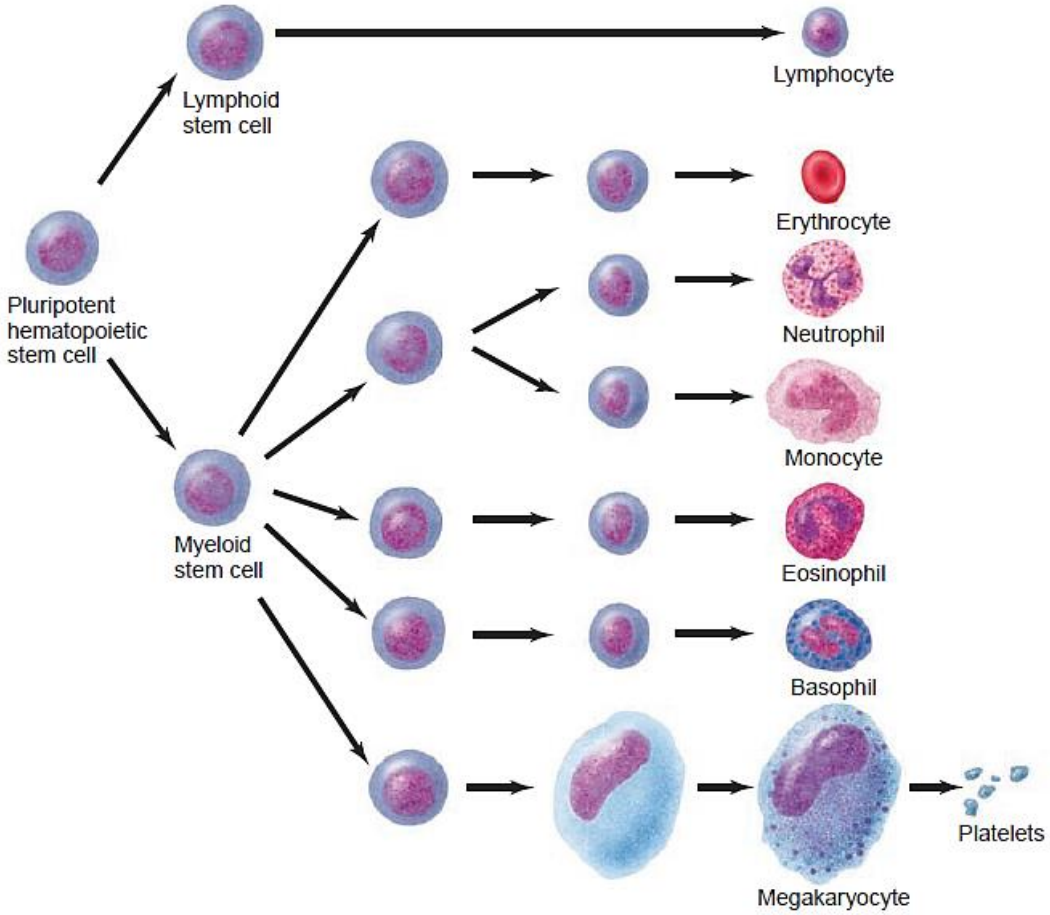

Figure 2.7 – Different pathways of the Haematopoiesis. Adapted from [19].

- **Red Blood Cells**: also known as erythrocytes, these are cells without nucleus (anucleated) and with a biconcave disc shape, which provides a large surface area that facilitates the exchange of gases (**Figure 2.8**). These cells have a diameter of 7.5 μm, a thickness of 2.6 μm and an effective diameter of 5.5 μm. Due to their high content of haemoglobin, red blood cells are involved in the transport of oxygen from the lungs to the tissues. In normal conditions, these

cells always remain inside the vessels and possess sufficient flexibility to pass through thin capillaries. The percentage by volume that red cells occupy in blood (called haematocrit) corresponds to 40–54 % in men and 35–49 % in women, and their normal concentration is 4-6 million per millilitre [17, 18].

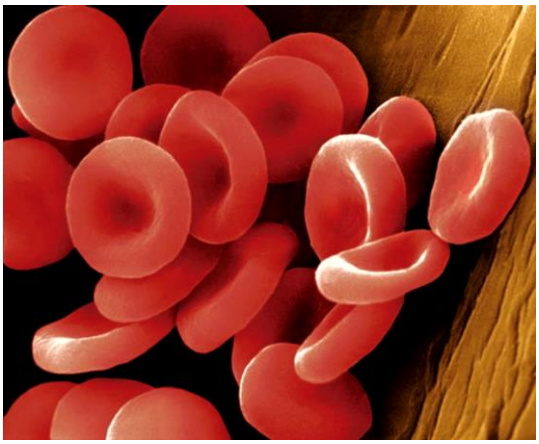

Figure 2.8 – Red blood cells/erythrocytes. Adapted from [19].

- **White Cells**: or leukocytes, are colourless, with spherical shape and represent 0.7 % of the blood volume with a concentration of 4500-11500 per millilitre. This type of cells is involved in the normal response to infection and remains temporarily in the bloodstream [17, 18]. Besides that, they are divided into two group: the granulocytes and the agranulocytes (**Figure 2.9**) [16]. Granulocytes have an irregular nucleus and present granules in their cytoplasm. Moreover, these are divided in three different types, each one with its specific function. One the other hand, agranulocytes present a more regular shape without granules in the cytoplasm and are divided in two types [17].

  Granulocytes [17, 19]:

  - Neutrophils: rounded cells and polymorphonuclear which are intended to ingest and digest bacteria and fungi. They represent 50-70% of the leukocytes.
  - Eosinophils: represent 1-3% of the leukocytes and present a bilobed nucleus. Their main function is to attack larger parasites and to partake in allergic responses.
  - Basophils: cells with a bulky nucleus with an irregular shape and with bigger granules when compared with the other granulocytes. 0-2% of the leukocytes are basophils and they are responsible for some symptoms of the response to allergic including histamine release.

Agranulocytes [17, 19]:

- Monocytes: the largest leukocytes, carried by the cardiovascular system to different tissues where they transform into cells called macrophages. 2-11% of the leukocytes are monocytes.
- Lymphocytes: recognize and attack foreign bodies and also help to destroy cells in the body which have become diseased through virus infection or cancer. They are small with spherical nucleus and scarce cytoplasm. Moreover, these cells can be divided in two main types – Lymphocytes T and B – and represent 18-42% of the leucocytes.

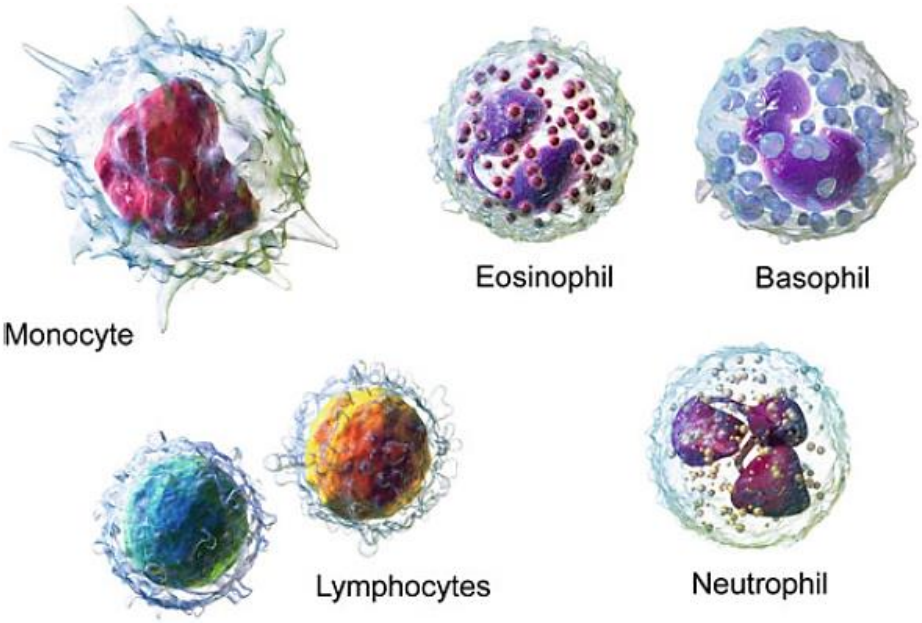

Figure 2.9 – Types of white blood cells/leukocytes. Adapted from [18].

- **Platelets**: represent 0.3 % of the blood volume and present a concentration of 150-450 thousands per millilitre. They are colourless, non-nucleated cell fragments of megakaryocytes that contain numerous granules and exist in inactivated (majority) and activated forms (**Figure 2.10**). Besides that, their shape is plate-like with a diameter of 2–3 μm. Once activated, they become sticky and more spherical with projections (pseudopods). Platelets are involved in blood clotting and in the repair of damaged endothelium [17-19].

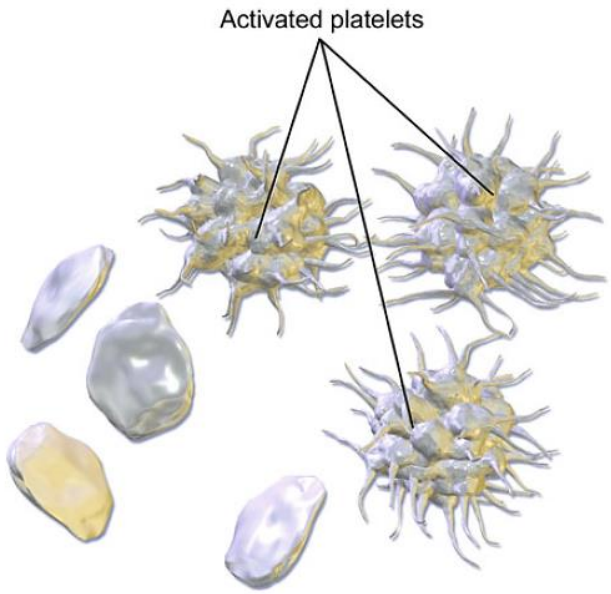

Figure 2.10 – Inactivated and activated platelets. Adapted from [18].

2.2.3 - Mechanical Properties

Since the total volume concentration of leukocytes and platelets is only about 1%, they have low influence in blood rheology. The rheological properties of blood depend on the intrinsic rheological characteristics of the plasma and red blood cells and on their interactions with each other as well as with surrounding structures [16, 21, 22]. It is also affected by the external physical conditions, like the temperature. However, if these are regulated, they do not significantly affect blood rheological properties [22].

To delay the flow, a shear stress occurs when blood flows in the endothelium [20]. This is proportional to the shear rate (velocity gradient) and fluid dynamic viscosity [20, 23]. The wall shear stress is the force per unit area applied by the fluid, tangentially to the wall, being related to some vascular diseases, since endothelium cells react to shear stresses [11]. In arteries, it is common to calculate the mean wall shear stress assuming a laminar steady flow in a straight tube since it is not easily measured for pulsatile flows [20]. Besides that, arteries usually adapt to keep the wall shear stress constant, which is only altered in some situations, such as thrombosis [20].

The viscosity (μ) is defined as a relation between shear stress (τ) and shear rate ($\dot{\gamma}$), which is given by $\tau = \mu \times \dot{\gamma}$ [21].

A Newtonian fluid is a fluid whose viscosity does not vary with shear rate (**Figure 2.11**), at a fixed temperature and pressure [16, 24], such is the case of plasma which presents a viscosity of 1.8 mPa s at 25 ºC [16, 21].

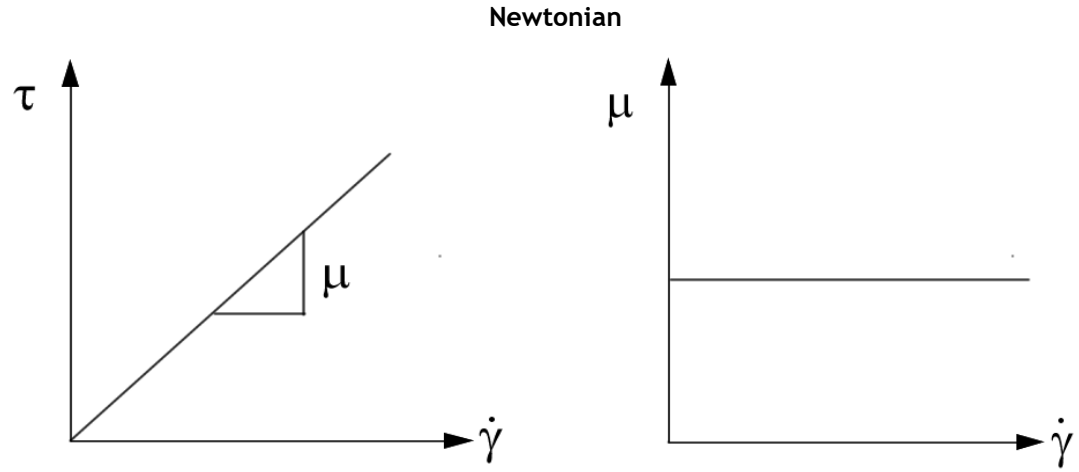

Figure 2.11- Newtonian fluid behaviour.

On the other hand, a non-Newtonian fluid is a fluid whose viscosity varies with shear rate and the shear stress-shear rate relation is non-linear (**Figure 2.12**) [21, 24].

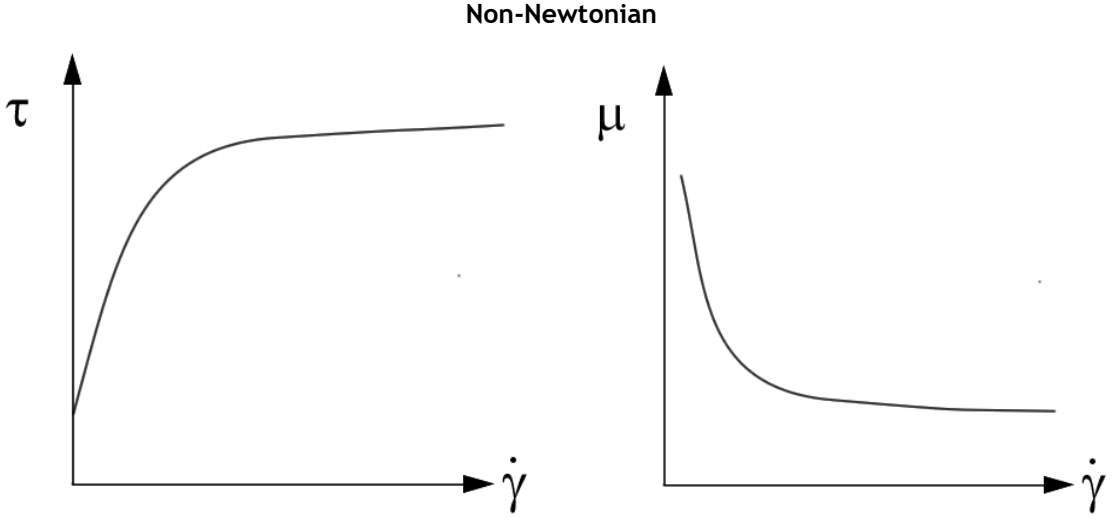

Figure 2.12 – Non-Newtonian fluid behaviour.

Compared to plasma, blood has a higher viscosity, which decreases with increasing shear rate, and it is considered a non-Newtonian fluid (**Figure 2.13**), presenting deformation rate dependency, viscoelasticity, yield stress and thixotropy [21, 22, 25].

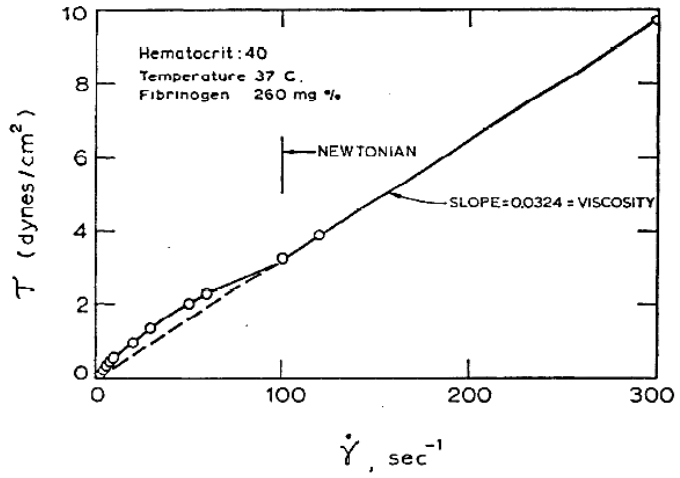

Figure 2.13 – Rheological curve of blood. Adapted from [24].

Blood viscosity depends on the viscosity of plasma, haematocrit level, blood cell distribution, mechanical properties of blood cells, deformation, extensional and shearing forces and on the environmental conditions [22].

At low shear, the high viscosity is due to the existence of rouleaux three-dimensional (3D) structures of stacks of red cells that form due to their elasticity and ability to aggregate [18, 25]. As shear rate increases, the formation of rouleaux is lower, which leads to a decrease in viscosity and, at shear rates of about 10 s^{-1}, the formation of these structures does not occur. With the increase of shear rate, red cells elongate and line up with the flow direction, leading to a decrease in viscosity [18]. Lastly, at the highest shear rates, the layers of red cells with plasma regions also decrease in viscosity, since plasma facilitates the movement of red cells [11, 18]. A summary of previous mentioned behaviours is presented in the **Table 2.3**:

Table 2.3 – Red cell behaviour taking into account the level of shear rate. Adapted from [18].

Shear Rate (s^{-1})	Red Cell Behaviour
0 – 0.01	Virtually all red cells form rouleaux There is a very small yield stress
0.01 – 1	Rouleaux length decreases Chains align themselves with respect to flow direction
1 – 100	Very few rouleaux present; none above about 5 s^{-1} Red cells begin to deform, elongating and aligning with flow direction
100 - 1000	Red cells are elongated Red cells may form layers with plasma in between

Thus, when the haematocrit increases, the viscosity also increases (**Figure 2.14**), making the non-Newtonian behaviour more evident, mainly in low shear rates [16]. Consequently, non-Newtonian behaviour is dependent on red blood cells since they are present in high concentrations and possess unique mechanical properties. However, this type of behaviour is not usually considered since it implies a more complex analysis. Thus, generally, blood flow models are considered as Newtonian [18, 22].

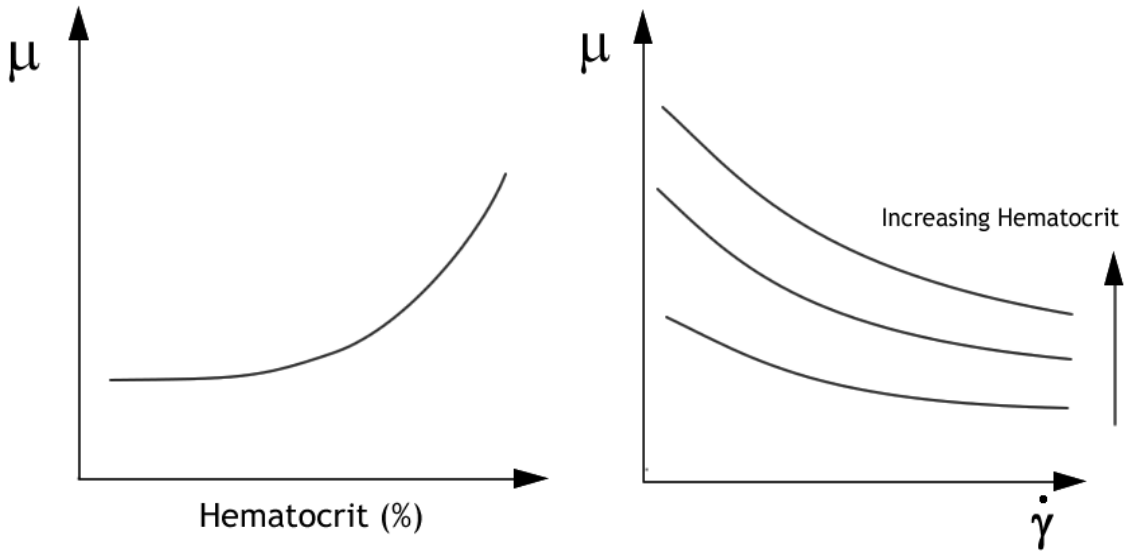

Figure 2.14 – Dependence of blood viscosity with the haematocrit level.

Furthermore, the non-Newtonian blood behaviour is smoother when compared with the one exhibited, for example, by typical polymeric systems. So, in some parts of the vascular system, such as large vessels, considering blood as a Newtonian fluid is acceptable and its viscosity can be assumed as constant [16, 20, 22]. This is due to the high shear rates (~200–300 s^{-1}) to which blood is exposed in large lumens and cavities which causes the extinction of non-Newtonian effects [18, 22]. Furthermore, in these structures, blood is considered as a homogeneous continuum medium because in the heart blood is mixed, which causes red blood cells to distribute uniformly, creating a homogeneous flow, where blood cell aggregation, deformation and interaction is minimal [18, 22]. Thereby, flow in arteries is laminar with red cells uniformly distributed and with a high velocity, which leads to the conclusion that it is reasonable to treat blood as a Newtonian fluid [18, 26].

On the other hand, in smaller vessels, as is the case with capillaries, this assumption is not valid. The blood must be viewed as a suspension of blood cells in plasma, and it is necessary to take into account the presence of the cellular elements and their interactions since they lead to significant changes in the blood rheological properties [16].

Some characteristics of blood in the different type of vessels are presented in **Table 2.4**.

Table 2.4 - Characteristics of blood in the different types of structures. Adapted from [18].

Component	Peak Reynolds Number (Re)	Turbulence	Red Cell Aggregation	Homogeneous Distribution of Cells
Heart	5000 - 20000	No	No	Yes
Arteries	500 – small arteries 5000 - aorta	No	No	Yes
Microcirculation	0.5 – arterioles 0.0003 – capillaries	Yes	Yes	No
Veins	100 – small veins 3000 – 4000 – vena cava	Yes	Yes	No

Blood also demonstrates yield stress (**Figure 2.15**). This type of stress is typically a constant property of the fluid and is treated as a constant. Yield stress is a critical shear stress value. Bellow yield stress the material shows deformation, over this threshold, it starts flowing like a fluid [16, 22]. However, in blood, there is some controversy since its yield stress is highly a variable, ranging from 0.002 to 0.40 dynes/cm^2. So, this must be considered as a function of time, instead of as a constant [16].

Furthermore, yield stress is associated to the aggregation of red blood cells, at low shear rates (to form rouleaux), and it is correlated to the concentration of fibrinogen and to the haematocrit level. Besides that, it contributes to blood clotting [22].

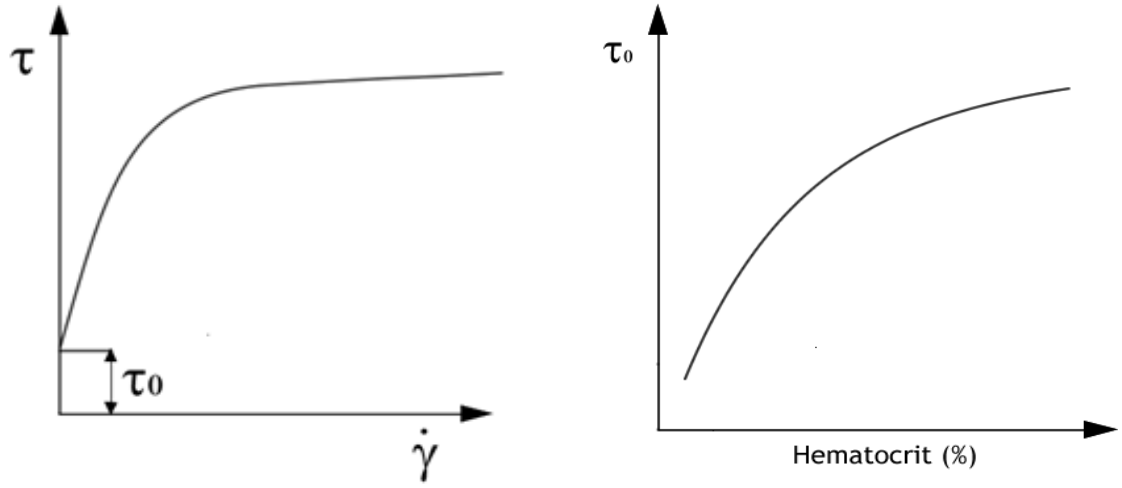

Figure 2.15 – Yield stress (τ_0) behaviour of blood.

Blood is also considered as a viscoelastic fluid, i.e., a fluid that has the ability to store and release elastic energy. At normal haematocrit level, this property is due to the reversible deformation of the RBCs 3D microstructures, thus being dependent on haematocrit and RBC properties, but also on temperature [16, 25]. The membrane of red blood cells exhibits stress relaxation and the necessary bridging mechanisms to form the 3D structures, which leads to the presence of elastic energy [16].

Thurston in 1972 was one of the first to recognize the viscoelastic nature of blood at low shear rates [16, 25] and that the viscoelastic behaviour is less prominent with increasing shear rate. Thus, Thurston proposed that, beyond a critical shear rate, the nonlinear behaviour is related to the microstructural changes that occur in blood. Viscoelastic properties present a small magnitude, being negligible by shear rates of the order of 10 s^{-1} [16].

Furthermore, blood presents a thixotropic behaviour too. Once again, red blood cells are the main culprits for this property, due to the formation and dissolution dynamics of the 3D aggregates that promote alterations in red blood cells, which can influence the rheology of blood [16].

In normal physiological conditions, the values of the Re reached in vessels do not allow the formation of relevant turbulence. Only in some cases, like at the exit of the aortic valve, the Re may reach the value of a few thousands, corresponding to flow instabilities. However, there is not enough time for a full turbulent flow to develop [11]. Typical values of the Re can be found in **Table 2.5**.

Table 2.5 – Features of some types of vessels. Adapted from [11].

Vessel	Diameter (mm)	Length (cm)	Peak Velocity (cm/s)	Wave Speed (m/s)	Re
Ascending Aorta	15	4	1.0	5	4000
Thoracic Aorta	11	15	0.8	6	2500
Iliac Artery	5	20	0.8	6	1000
Femoral Artery	4	45	0.8	7	800
Common Carotid Artery	4	20	0.8	7	800
Small Artery	2	10	0.2	20	100
Capillary	0.01	0.2	0.001	-	0.0003
Small Vein	2	10	0.6	2	100
Large Vein	8	50	0.8	1	1700

If the Re is at most in the order of 1000, the flow is stable and is called laminar [11].

Lastly, in blood flow simulations, it is common to assume blood as an incompressible flow with a fixed density of 1056 $kg.m^{-3}$ [18]. Besides that, and as mentioned before, when shear rate increases, the viscosity also increases, tending to the asymptotic value of 0.004 Pa.s [16, 18]. Thus, when larger vessels are considered and blood is treated as a Newtonian fluid, it is possible to assume this value [18].

2.3 - Constitutive/Rheological Models

In 1775, Euler developed the "Euler Equations" with the objective of describing blood flow in human arteries, but the application of these types of mathematical models in medical research only began to be used several years later, with the improvement of computers, imaging and geometry extraction techniques and numerical algorithms [11].

Although the mathematical equations of fluid dynamics are the basis for haemodynamics modelling, the mathematical models already developed to describe the cardiovascular system are still a challenging problem [11].

To describe the blood flow in large arteries, numerous models have been used. Thus, the characteristics of blood flow can be obtained through, for example, numerical methods, such as FEM [22].

The elastic one dimensional Navier-Stokes and the rigid Hagen-Poiseuille are the most common models used for Newtonian behaviour [22]. However, Navier-Stokes equations are usually used to describe blood flow in healthy arteries where flow is considered as a Newtonian fluid [11, 16, 22].

$$\frac{\partial \boldsymbol{u}}{\partial t} + \rho(\boldsymbol{u} \cdot \nabla)\boldsymbol{u} + \nabla P - \operatorname{div}\big(\mu\, \mathbf{D}(\boldsymbol{u})\big) = \boldsymbol{f}\ , \qquad \operatorname{div}(\boldsymbol{u}) = 0 \tag{2. 1}$$

With $\boldsymbol{u}$ as the velocity, P the pressure, ρ the density, ∇ the gradient operator, μ the viscosity and f the external forces.

The first equation represents the conservation of linear momentum, while the second equation represents the continuity equation [11].

Though, in some cases, it is necessary to use more complex models. So, most general models can be rewrite, as the case of the called Generalized Newtonian fluids, also known as Reiner-Rivlin fluids. An example of model that used the mentioned (and that it is used for blood) is the Power-Law fluid model, for which the viscosity function is given by:

$$2\mu(\dot{\gamma}) = K\,(\dot{\gamma})^{n-1} \tag{2. 2}$$

With $2\mu(\dot{\gamma})$ being a shear dependent viscosity function, $\dot{\gamma}$ the shear rate, n the power-law index and K the consistency constant.

When n is equal to 1, the fluid is considered Newtonian, while in other cases the viscosity increased or decreased as a function of the shear rate, being considered non-Newtonian. Besides that, a more general form can be written:

$$\frac{(\mu(\dot{\gamma}) - \mu_\infty)}{(\mu_0 - \mu_\infty)} = F(\dot{\gamma}) \quad (2.\ 3)$$

Where μ_0 and μ_∞ represent the asymptotic viscosity values at zero and infinite shear rates, respectively, and $F(\dot{\gamma})$ is a shear dependent function.

And, from this equation, different models emerge with different choices of the function $F(\dot{\gamma})$, as can be seen in **Table 2.6** [16].

Table 2.6 - Most common generalized Newtonian models for a Newtonian fluid. Adapted from [16].

Model	$\frac{(\mu(\dot{\gamma}) - \mu_\infty)}{(\mu_0 - \mu_\infty)}$	Material Constants for Blood
Powell-Eyring	$\frac{sinh^{-1}(\lambda\dot{\gamma})}{\lambda\dot{\gamma}}$	$\lambda = 5.383\ s$
Cross	$\frac{1}{1+(\lambda\dot{\gamma})^m}$	$\lambda = 1.007\ s \quad m = 1.028$
Modified Cross	$\frac{1}{(1+(\lambda\dot{\gamma})^m)^a}$	$\lambda = 3.736\ s \quad m = 2.406 \quad a = 0.254$
Carreau	$(1+(\lambda\dot{\gamma})^2)^{(n-1)/2}$	$\lambda = 3.313\ s \quad n = 0.3568$
Carreau-Yasuda	$(1+(\lambda\dot{\gamma})^a)^{(n-1)/a}$	$\lambda = 1.902\ s \quad n = 0.22 \quad a = 1.25$

Hereupon, one of the main differences between blood models is the use of Newtonian or non-Newtonian behaviour. However, it is important to highlight that for vessels with a diameter that is less than 1 mm and shear rate of <100 s^{-1}, the Newtonian models are not suitable [11, 22].

For non-Newtonian behaviour, several models were delineated, which are the cases of Carreau-Yasuda, Casson, Power Law, Cross, Herschel-Bulkley, Oldroyd-B, Quemada, Yeleswarapu, Bingham, Eyring-Powell and Ree-Eyring (**Table 2.7**). However, the most popular models used are Carreau-Yasuda and Casson [22].

Table 2.7 - Some examples of constitutive equations of Non-Newtonian models. Adapted from [22].

Model	Equation	Non-Newtonian Properties
Carreau-Yasuda	$\mu = \mu_\infty + \frac{\mu_0 - \mu_\infty}{\lvert 1 + (\lambda\dot{\gamma})^a \rvert^{\frac{1-n}{a}}}$	Shear Thinning
Casson	$\tau^{1/2} = (k\,\dot{\gamma})^{1/2} + \tau_0{}^{1/2}$	Yield Stress
Power Law	$\tau = k\,\dot{\gamma}^{\,n}$	Shear Thinning
Cross	$\mu = \mu_\infty + \frac{\mu_0 - \mu_\infty}{1 + \lambda\dot{\gamma}^{\,m}}$	Shear Thinning
Herschel-Bulkley	$\tau = k\,\dot{\gamma}^{\,n} + \tau_0$	Shear Thinning
Oldroyd-B	$\boldsymbol{\tau} + \lambda_1 \overset{\nabla}{\boldsymbol{\tau}} = \mu_0 \left(\dot{\boldsymbol{\gamma}} + \lambda_2 \overset{\nabla}{\dot{\boldsymbol{\gamma}}} \right)$	Viscoelasticity
Quemada	$\mu = \mu_p \left(1 - \frac{k_0 + k_\infty \sqrt{\dot{\gamma}/\dot{\gamma}_c}}{2\left(1 + \sqrt{\dot{\gamma}/\dot{\gamma}_c}\right)} \phi \right)^{-2}$	Shear Thinning
Yeleswarapu	$\mu = \mu_\infty + (\mu_0 - \mu_\infty) \frac{1 + \ln(1 + \lambda\dot{\gamma})}{1 + \lambda\dot{\gamma}}$	Shear Thinning
Bingham	$\tau = k\,\dot{\gamma} + \tau_0$	Yield Stress
Eyring-Powell	$\mu = \mu_\infty + \frac{(\mu_0 - \mu_\infty)\, sin\, h^{-1}(k\,\dot{\gamma})}{\lambda\dot{\gamma}}$	Shear Thinning
Ree-Eyring	$\tau = \tau_c \; sin\, h^{-1}\left(\frac{\mu_0\,\dot{\gamma}}{\tau_c}\right)$	Shear Thinning

With $\dot{\gamma}$ as the shear rate, $\dot{\gamma}_c$ the characteristic shear rate, $\dot{\boldsymbol{\gamma}}$ the rate of strain tensor, λ characteristic time constant, λ_1 the relaxation time, λ_2 the retardation time, μ the fluid viscosity, μ_p the plasma viscosity, μ_0 the zero-shear-rate viscosity, μ_∞ the infinite-shear-rate viscosity, τ the shear stress, $\boldsymbol{\tau}$ the stress tensor, τ_c the characteristic shear stress, τ_0 the yield-stress, ϕ the volume concentration, a the Carreau-Yasuda index, k the consistency coefficient, k_0 the maximum volume fraction for zero shear rate, k_∞ the maximum volume fraction for infinite shear rate, m the Cross model index, n the power law index and $\overset{\nabla}{\cdot}$ The upper convected time derivative.

The Non-Newtonian models presented may be expressed in other forms and the last column represents the properties that can be taken from these models in the context of blood modelling [22]. Besides that, it is important to refer that the use of expressions for viscosity where it is dependent on shear rate increase the cost of computations by 10%, due to extra calculations and increased non-linearity of the problem [11].

Furthermore, there is not one single model, Newtonian or non-Newtonian, that can represent all features of the blood complexities, with different models being used to represent different characteristics [22].

Also, it is possible to find in literature models to modulate the yield stress property of blood. However these models are more used for situations of low shear rate. It is important to refer that materials that present this property require a finite shear stress, in other words, the yield stress (τ_0), to start flowing. So, a simple yield criterion is given by:

$$\sqrt{|II|_\tau} = \tau_0 \tag{2. 4}$$

Being $|II|_\tau$ the second invariant of the extra stress tensor. If $\sqrt{|II|_\tau} < \tau_0$, the fluid do not flow [16].

Regarding the models, the simplest is the Bingham fluid model that can be written as:

$$\sqrt{|II|_\tau} < \tau_0 \rightarrow \boldsymbol{D} = 0 \tag{2. 5}$$

$$\sqrt{|II|_\tau} \geq \tau_0 \rightarrow \begin{cases} \boldsymbol{D} = \dfrac{1}{2\mu}\left(1 - \dfrac{\tau_0}{\sqrt{|II|_\tau}}\right) \\ \tau = 2\left(\mu - \dfrac{\tau_0}{\sqrt{2|II|_\tau}}\right) \end{cases} \tag{2. 6}$$

With $\boldsymbol{D}$ as the deformation tensor and μ as the viscosity.

Herschel-Bulkley and the Casson models are other examples that are inserted in these types of models. The first is similar to the Bingham fluid model but its formulation is given by [16]:

$$\sqrt{|II|_\tau} < \tau_0 \rightarrow \boldsymbol{D} = 0 \tag{2. 7}$$

$$\sqrt{|II|_\tau} \geq \tau_0 \rightarrow \begin{cases} \boldsymbol{D} = \dfrac{1}{2K\,\dot{\gamma}^{n-1}}\left(1 - \dfrac{\tau_0}{\sqrt{|II|_\tau}}\right) \\ \tau = 2\left(K\,\dot{\gamma}^{n-1} - \dfrac{\tau_0}{\sqrt{2|II|_\tau}}\right) \end{cases} \tag{2. 8}$$

However, the most common model is the Casson constitutive model which can be written as [16]:

$$\sqrt{|\mathrm{II}|_\tau} < \tau_0 \rightarrow \boldsymbol{D} = 0$$

$$\sqrt{|\mathrm{II}|_\tau} \geq \tau_0 \rightarrow \begin{cases} \boldsymbol{D} = \dfrac{1}{2\mu N}\left(1 - \dfrac{\sqrt{\tau_0}}{\sqrt[4]{4\,|\mathrm{II}|_\tau}}\right) \\ \tau = 2\left(\sqrt{\tau_0} - \dfrac{\sqrt{\tau_0}}{\sqrt[4]{4\,|\mathrm{II}|_\mathrm{D}}}\right) \end{cases} \tag{2. 9}$$

Towards the viscoelastic property, the majority of models available are very complex and for this reason they are not usually found in literature [16]. However, some viscoelastic constitutive models have been recently proposed to describe blood rheology [25]. One of the simplest models is the Maxwell model given by:

$$\tau + \lambda_1 \overset{\nabla}{\boldsymbol{\tau}} = 2\mu \boldsymbol{D} \tag{2. 10}$$

Being λ_1 the relaxation time [16].

Oldroyd-B models are a class of models that are more general [22]. This class is defined as:

$$\boldsymbol{\tau} + \lambda_1 \overset{\nabla}{\boldsymbol{\tau}} = \mu_0 \left(\dot{\boldsymbol{\gamma}} + \lambda_2 \overset{\nabla}{\dot{\boldsymbol{\gamma}}}\right) \tag{2. 11}$$

It is important to refer that the fluids represented by this class, with additional viscosity, can be considered as Maxwell fluids, being a particular case of these [16].

More recent, models of differential type have been emerged in literature, such as the empirical five-constant generalized Oldroyd-B model, where μ was substituted by a generalized Newtonian viscosity model like:

$$\mu = \mu_\infty + (\mu_0 - \mu_\infty)\ \frac{1 + \ln(1 + \lambda\dot{\gamma})}{1 + \lambda\dot{\gamma}} \tag{2. 12}$$

Although, the model covers a large range of shear rates, it has an important limitation. The relaxation times do not depend on the shear rate, which does not occur in reality [16].

Chapter 3

Blood Clots

The uncontrolled growth of a thrombus may result in vessel obstruction which consequently can lead to stroke or coronary vascular disease, conditions that cost more than $315 billion each year in losses of productivity and medical costs [27, 28]. Due to the prevalence of certain cofactors, such as smoking, high cholesterol, obesity, hypertension, diabetes mellitus and inactivity, complex thrombotic pathologies has been increasing over the years [27].

The formation and dissolution of blood clots is fundamental for life and is the result of a sequence of chemical reactions, involving platelets and a huge number of molecules. However, this is a complex process and a variety of conditions can promote insufficient or excessive coagulation, leading to severe problems that affect the lives of numerous people [16]. For example, venous thrombosis affect 1 in 1000 individuals per year, being more prevalent in elderly people [29], and DVT and pulmonary embolism result in more than 60 000 deaths per year in the US [27].

Every year, only in Europe, coagulation disorders cause more than half million deaths, more than the total number of deaths caused by AIDS, breast cancer, prostate cancer and road traffic accidents, combined together. Thus, to counter these numbers, it is essential to understand the mechanisms related to clot formation, growth and dissolution [25].

This chapter presents the haemostatic process, its participants and the causes that can lead to the formation of a blood clot. Moreover, the different types of clots that exist are also presented, their mechanical properties and the rheological models used to represent this process.

3.1 - Anatomy of a Thrombus

Thrombosis is the formation of a blood clot inside a vessel in order to protect the body from excessive blood loss [20].

A clot or a thrombus is a jelly material that is formed through the blood coagulation process, the clot surface dries up, forming a solid crust [16]. Normally, the main components of a clot are the platelets and the red blood cells, which are bounded by molecules in the cell membrane of the platelets (membrane glycoproteins) by plasma proteins and by a network of fibrin, which serves as a scaffold for endothelial cells, leukocytes, platelets, and plasma proteins bounded to the clot [10, 20, 30].

Platelets present an enormous number of membrane receptors (**Figure 3.1**), allowing their interaction with specific components and the formation of a plug [16, 31, 32]. However, these receptor-ligand interactions depend on the prevailing blood flow conditions and the extent of vascular injury [7]. They are also storage compartments of species involved in blood coagulation and its regulation [16, 31, 32].

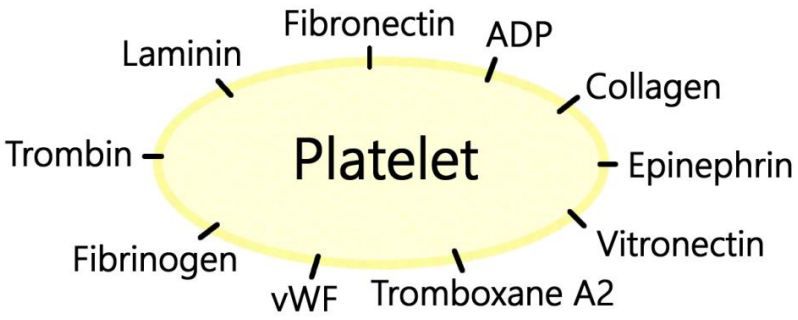

Figure 3.1 - Membrane receptors of platelets.

Red blood cells can also be found in the clot complex, as well as other components, since, when fibrin is formed, it can trap them in its network (**Figure 3.2**). They present passive action, contributing only to the volume of the clot [16].

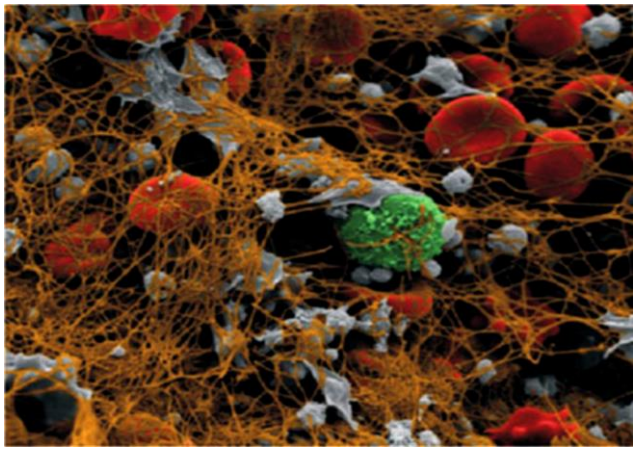

Figure 3.2 – Thrombus with fibrin network. Adapted from [16].

The formation of the fibrin network involves several elements, the so-called coagulation agents, that may also be present in the clot structure, to create a strong aggregate [16]:

- **VonWillebrand Factor (vWF),** a large plasma protein secreted by endothelial cells and platelets, being present in soluble state in plasma [19, 32]. It can be activated by shear stress and it is involved in platelet adhesion to fibrin and to the lesion site [16, 19].
- **Tissue Factor (TF)**, also known as thromboplastin or thrombokinase, it is an integral membrane glycoprotein, located in the tissue adventitia and in the outer plasma membrane of various tissue cells. When an injury occurs, it contacts with blood and initiates a sequence of reactions that will lead to fibrin formation [16, 19, 33, 34].
- **Plasma Proteins,** also known as the numbered factor pairs, usually present in blood in an inactive precursor form (zymogens). Nevertheless, they can be converted to the active state (serine protease) via enzymes [33, 35]. They are involved in the reactions that are initiated by TF and that lead to fibrin network formation that will strengthen the platelet plug [33]. They act together and can form different complexes between them (some factors do not possess an enzymatic activity, they bind in complexes that are present in a reaction), being also accompanied by antagonist reactions. Furthermore, to each one, a roman number was attributed according to the chronological order of their discovery (**Table 3.1**) [16].

Table 3.1 – Blood Coagulation Factors. Adapted from [36].

Roman Number	Alternative Name	Active Form	Description
FI	Fibrinogen	FIa: Fibrin	Plasmatic protein, synthetize in the liver
FII	Prothrombin	FIIa: Thrombin	Plasmatic protein, synthetize in the liver
FIII	Tissue Factor	-	Mix of lipoproteins, released by damaged tissues
FIV	Ca^{2+} ions	-	Needed in all coagulation process
FV	Proaccelerin	FVa: cofactor of FXa	Plasmatic protein, synthetize in the liver
FVI	-	FIVa: identical to FVa	Similar to FVa
FVII	Proconvertin	FVIIa	Plasmatic protein, synthetize in the liver
FVIII	AHG	FVIIIa: cofactor of FIXa	Plasmatic protein, synthetize in megakaryocytes
FIX	Christmas Factor	FIXa	Plasmatic protein, synthetize in the liver
FX	Stuart-Prower Factor	FXa	Plasmatic protein, synthetize in the liver
FXI	Plasma Thromboplastin Antecedent (PTA)	FXIa	Plasmatic protein, synthetize in the liver
FXII	Hageman Factor	FXIIa	Plasmatic protein
FXIII	Laki-Lorand Factor	FXIIIa	Protein of plasma and platelets

3.1.1 - Causes of Clot Formation

Blood contains all the necessary elements to generate a thrombus and to maintain a normal flow behaviour [35]. Haemostasis is a fast and complex process and the first step of wound healing. Its main objective is to stop the bleeding, in order to avoid blood losses [16, 37]. In normal and healthy circulation, coagulation activity is offset by the presence of anticoagulants and by fibrinolytic activity [35]. However, in blood vessels, it is normal for small lesions to occur spontaneously, leading to the formation of platelet aggregates in a effort to maintain haemostasis [16, 23].

Moreover, in disease states unwanted formation of clots (thrombosis) can occur, with risk of embolism, since the circulating platelets can become aggregated, forming a thrombus mass. Such occurrence augment the tendency of clotting under some circumstances, leading to hypercoagulability [23, 35]. This type of event is characteristic of thromboembolic diseases, which present serious consequences for various blood vessels and organs, such as limbs (DVT), lungs (pulmonary embolism), brain (stroke) and heart (myocardial infarction) [23], being related to anomalies of the vascular wall, anomalies of the blood flow and anomalies of blood components [38]. Although, it is important to stress that, even though a slower flow can contribute to thrombogenesis, it alone cannot cause it [39].

Besides that, FVII is a key factor in the initiation of the process so, thrombotic disorders are more frequent in subjects with higher plasma levels of FVII [40].

Examples of these diseases are listed below, and the main cause for the abnormal formation of clots is presented in each case.

- **Rupture of atherosclerotic plaque**: is a trigger of the acute myocardial infarction, as a result of the formation of a thrombus, and it is normally associated with obesity or high cholesterol [10, 32, 41]. TF is at high concentrations in the necrotic core of the atheroma and when plaque rupture occurs, at high shear rate (500-1500 s^{-1}), it becomes exposed. Since it is one of the triggers of coagulation, the formation of thrombus occurs [10, 20, 42].
- **Thrombocytosis**: is an unusually high platelet count that can be due to its excessive production by the bone marrow, spleen dysfunction or medical treatments, which can lead to thrombophilia [16].
- **Deep vein thrombosis (DVT)**: this condition leads to reduced circulation in the limbs due to clot formation in deep veins (femoral, popliteal, saphenous, etc.) [16]. Although it is difficult to explain how a clot is formed when there is no injury and in an environment of low stress (10-100 s^{-1}), alterations in blood flow can create favourable conditions to initiate blood coagulation, associated with an overexpression of TF, that can be secreted by the endothelium in the presence of abnormal condition of the flow, or it can be induced by leucocytes [10, 16]. Besides that, hypoxia stimulates TF release by platelets and red cells could release ADP, which

will activate platelets, or even by other risk conditions like smoking, trauma, prolonged immobility, infection, surgery, pregnancy or cancer [10, 16, 32]. Abnormalities in red blood cells number or function can also be related to DVT due to their effect on blood viscosity and their influence on the position of platelets, as abnormalities in fibrin level, that increase fibrin network and consequently the resistance of clots to fibrinolysis [10].

- **Heart Arrhythmia and Thromboembolism**: atrial fibrillation can lead to formation of clots related with altered blood flow. Clots can then reach the brain (causing a stroke) or the kidneys [16].

However, in addition to the previously listed, other causes may be responsible for abnormal formation of thrombus:

- **Recirculation and Residence Time**: in regions of complex flow, such as bifurcations or stenoses, platelets may recirculate long enough to become activated and form small aggregates since the balance between anticoagulation and coagulation is lost [20, 43]. In physiologic flow, 10 s residence is long enough for significant aggregation or fibrin accumulation [20].
- **Coagulation on Artificial Surfaces**: the insertion of artificial surfaces (heart valves, stents, etc.) is usually associated with blood coagulation, which can be caused by high shear stress in blood and alteration of platelets, leading to their aggregation and adhesion or even to the activation of coagulation [16, 35]. Some materials also have affinity to fibrinogen, which can produce platelet aggregation. FXII can also become activated on artificial surfaces [16].
- **Disturbance in the natural balance between procoagulants and anticoagulants**: it can occur due to genetic or acquired factors, as the case of genetic factors involved in the deficiency of anticoagulants, such as antithrombin III or protein C, and the presence of mutations, like in FV [29, 38]. These species maintain blood fluidity in the absence of an injury and generate a clot, when necessary, in the lesion site [32]. The proper balance between them is critical for proper haemostasis and to avoid pathological situations, since anticoagulants guarantee the control of the coagulation process and they prevail over the procoagulant in normal conditions [32, 38].

It is important to highlight that blood coagulation process changes with the physiological aging of humans [38, 40], along with vascular disease and thromboembolism associated with advancing age. Since the concentration of procoagulant factors in plasma increase, an acceleration of clotting activity can occur or a poorly balanced by natural anticoagulants may happen [40]. For example, plasma fibrinogen levels increase with the advancing age [38, 40], increasing from 280 mg/dL (47-54 years) to 300 mg/dL in individuals aged 65-79 years, with an expected increment of 10 mg/dL for each decade in healthy subjects. Besides that, changes like the impairment of vascular endothelium function, hyperreactivity of circulating platelets, depression of the fibrinolytic system, dyslipidaemia and hypertension, are related with hypercoagulability [40].

3.1.2 - Formation of Thrombus

Thrombosis is a complex interaction between platelets and plasma proteins [20]. The endothelium of vessels conserves an anticoagulant surface that serves to maintain a normal blood flow. However, disruption in its continuity causes platelets to adhere to this site, which is usually the primary event leading to thrombus formation [32, 35]. However, the activation of the endothelium by chemicals, cytokines, or inflammatory processes can also lead to this formation since TF may also be exposed/expressed in these circumstances [31].

As mentioned before, platelets are the central component in this process, being the ones that initiate and regulate a large number of components that are involved in this process. They interact with endothelium and verify if it presents any alteration. When platelets notice the presence of an injury, the haemostatic process initiates in seconds [16, 29, 37]. This process can be described by three platelet functions (adhesion, activation, and aggregation) - the primary haemostasis - and by the coagulation cascade, a sequence of complex reactions, both characterized by strong positive feedback - the secondary haemostasis [16, 20, 33, 37]. These different mechanisms usually occur simultaneously, having several interactions. Besides that, thrombin is the molecule that presents the central role in all this process [20, 29, 44].

3.1.2.1 - Primary Haemostasis

When a vascular injury occurs, platelets change their shape, emitting pseudopods, which allow their binding to the site of injury and between them, forming a bridge with the ligands vWF and fibrinogen, in order to form a plug that acts like a temporary barrier [16, 33, 35].

So, as mentioned, platelets present three main roles (**Figure 3.3**):

- **Adhesion**: when a thrombogenic surface (like subendothelial and medial layers of vessels) is exposed to blood, platelets adhere to proteins in its surface, through glycoproteins of its membrane (such as vWF), due to the presence of collagen in the lesion [32, 35]. Collagen present positively charged chemical groups, a characteristic that induces platelet adhesion [35].
- **Activation**: in the presence of chemical (such as ADP, thrombin, thromboxane A2 or collagen) or physical (such as shear stress or biomaterials) stimulus, platelet functions are triggered, becoming activated platelets [20, 35]. This activation promotes an alteration in their shape, releasing pseudopods that facilitate the adhesion. Besides that, platelets also contract, which combine cells and fibrin, and release their granular contents (for example ADP) when contact with collagen, acting locally to activate more platelets (positive feedback mechanism) and to

promote aggregation [19, 20, 45]. Lastly, it is important to stress that, platelets also catalyse thrombin and allow the assembly of coagulation complexes in their membranes [7, 20, 32].

- **Aggregation**: in this stage occurs the formation of the platelet plug, which is an agglomerate of platelets. The link between platelets can occur via fibrinogen, fibrin or vWF [20, 23]. This plug, in an initial phase, does not present erythrocytes and the contribution of fibrin is insignificant [35]. Furthermore, aggregated and activated platelets provide phospholipid-equivalent surfaces where the complex-dependent reactions of the coagulation cascade are performed [31].

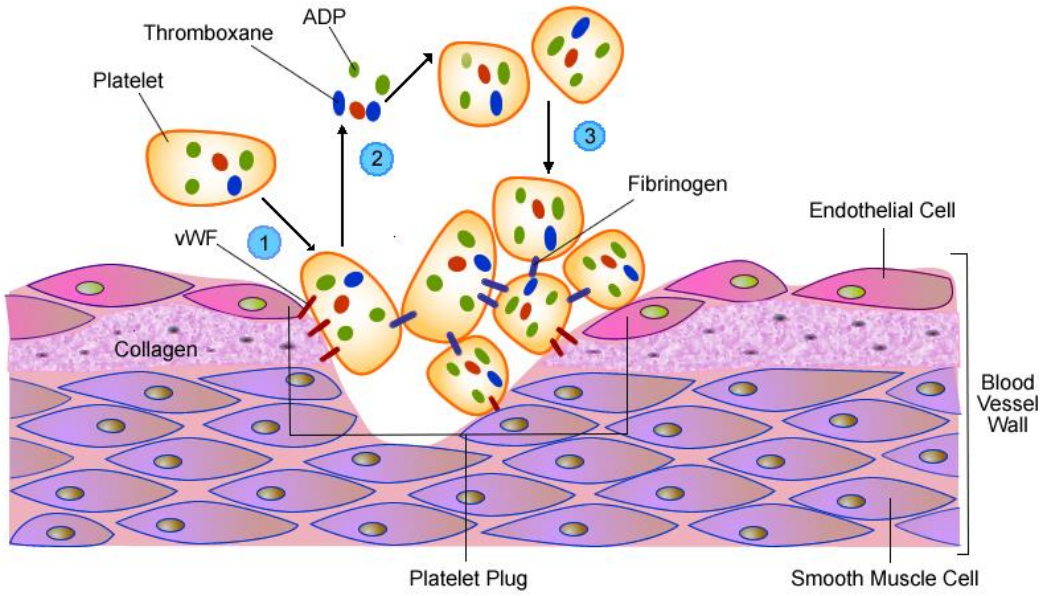

Figure 3.3 - Primary haemostasis: 1- Platelet adhesion; 2- Platelet activation; 3- Platelet aggregation.

Besides that, the activation of platelets also leads to the release of several molecules, such as the growth factor, that will increase the plug and begin the tissue repair [33]. Lymphocytes and monocytes are also activated by platelets, which adhere to the endothelium, promoting an inflammatory response [38].

While the plug is formed and compacted, the smooth muscle in the damaged vessel is stimulated to contract through compounds released by platelets, like thromboxane A2, which causes vasoconstriction and consequently decreases blood flow and blood pressure in the lesion site [19].

3.1.2.2 - Secondary Haemostasis

Similar to primary haemostasis, this process is also triggered by exposure of a thrombogenic surface. However, comparing with the previous process, secondary haemostasis is more complex [35].

In normal conditions, the lesion exposes TF and collagen, which will trigger blood coagulation (also known as clotting) [19, 20, 37]. This mechanism occurs around the platelet plug and it is the central haemostatic defence [19, 32]. Besides to solidify the blood that remains in the lesion, the final reaction of this proteolytic process converts prothrombin into thrombin, which cleaves fibrinogen into insoluble fibrin. This last compound will form a mesh that is incorporated into the plug, strengthening and stabilizing it [20, 32]. Furthermore, thrombin also interacts with platelets, causing their activation, release of their granular contents, and irreversible aggregation [20].

Regarding the biological models used to describe secondary haemostasis, the most famous and commonly used is the 3-pathway Cascade Model. However, the model currently believed as the most correct is the Cell-Based Model [16, 46]. The main difference between these two is the action of factor FXII. In the 3-pathway Cascade Model, FXII is the trigger of the intrinsic pathway, while in the Cell-Based Model, FXII do not enter in the process [16].

3.1.2.2.1 - The 3-Pathway Cascade Model

Also known as Cascade or Waterfall model, it was only proposed in 1964, being the basis of blood clotting until very recently. However, the more actual used model is based on it, having only been made some correction at the beginning of the present century [16].

As mentioned before, the Cascade Model explains the role of FXII [16]. Besides that, it is divided into three pathways (intrinsic, extrinsic, and common pathway) where the different zymogens participate and are transformed in their active form [6, 19].

Generically, intrinsic and extrinsic pathways are sequentially activated and, in the end, they combine to form the common pathway, where the prothrombin-thrombin reaction is present (**Figure 3.4**). Although, the two pathways have distinct mechanisms, thrombin forms a link between them [19].

- **Intrinsic pathway**: This pathway gets its name from the fact that all the necessary compounds for it to occur are found in the bloodstream. However, it is also known as contact activation pathway [19]. FXII, which circulates in blood, is the first plasma protein to act in this pathway, becoming active upon contact with collagen from the endothelium or the membrane of active platelets. FXIIa will catalyse the activation of FXI, which consequently will activate FIX [16, 19]. Then, this will activate FX, which is the enzyme that, in the presence of FVa, converts

prothrombin to thrombin [29, 32]. Besides that, FVIIIa (which circulates bonded to vWF before its activation) acts like a cofactor of FIXa, and not like an enzyme, in the activation of FX, forming a complex with it, named tenase [29].

- **Extrinsic pathway**: contrary to intrinsic pathway, this requires a cellular element found outside of blood, and due to that, it is called extrinsic pathway [19]. It is also known as TF pathway since it is initiated by TF, which is not a plasma protein, but a constituent of subendothelial cells. TF binds to FVII leading to the formation of a complex and activation of the this factor, starting the feedback mechanism [29]. This complex catalyses the activation of FV, which will form a complex with FXa (prothrombinase) [19, 33]. Therefore, FV is a cofactor in activation of prothrombin, which increase the velocity of the reaction, and it is further activated by FXa and thrombin [29, 33].

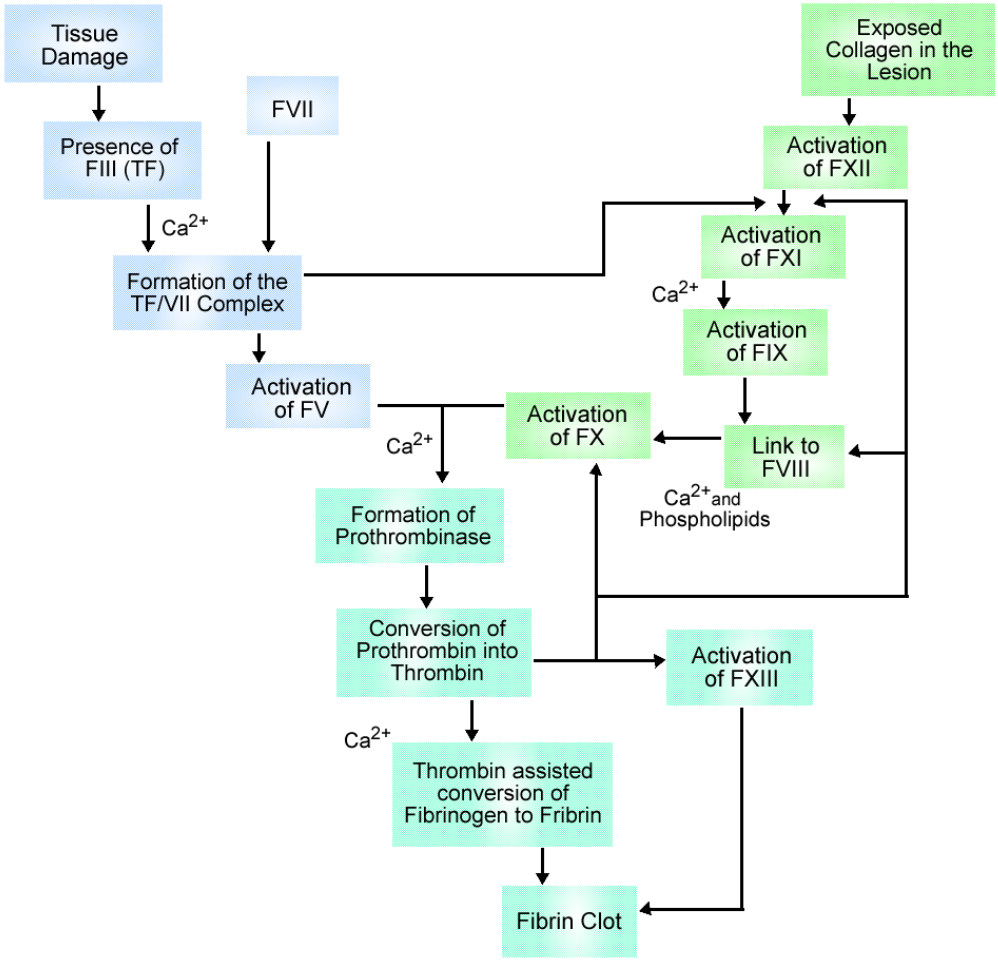

Figure 3.4 – Coagulation cascade.

Thus, blood coagulation has two ways to initiate. These two ways come together in a common pathway to catalyse thrombin from prothrombin, via a hydrolysis reaction that reduce its molecular weight. In the end of the common pathway, thrombin will form the fibrin monomers [19, 33] after forming the prothrombinase complex in the membrane surface of the active platelets [37]. When thrombin is formed, it converts fibrinogen into insoluble fibrin [10, 33], which polymerize to form a gel that mechanically will stabilize the platelet plug [47], occurring the maximum generation of thrombin after the development of the fibrin clot [29].

Thrombin also contributes to activate FXI, FVIII, FV and platelets [19, 29, 33]. Since it active FV and platelets, it also helps in the conversion of prothrombin to thrombin [19].

However, it is important to highlight that the extrinsic pathway is the most common way of initiating blood coagulation, with the intrinsic pathway as its alternative [6, 29]. Therefore, a small quantity of thrombin is generated only by the extrinsic pathway in the begging of this process, which initiate fibrin formation [33]. Besides, and as mentioned before, this small quantity of thrombin will also produce a positive feedback effect, activating FXI, FVIII and platelets, which are needed to trigger the intrinsic pathway, without FXII [19, 33].

On the other hand, intrinsic pathway generates the required thrombin for an adequate coagulation process, being important to formation, growth and maintenance of fibrin [19, 33].

The problem of the 3-pathway cascade model is the position of FVIII, which its deficiency is related with Haemophilia A. So, if the extrinsic pathway alone would be enough for the occurrence of the all process, this deficiency can be neglected. Besides that, FXII deficiency would eliminate FVIII of coagulation process, leading to the same effect, which is not true. Therefore, the cell-based model emerged to overcome this inconsistency, giving importance to FVIII, which is essential to clotting [16].

3.1.2.2.2 - Cell-Based Model

An update on haemostasis process was achieved by the introduction of the cell-based model, which focuses on the fact that the involved reactions are controlled by their localization on different cellular surfaces [32, 46]. The complexes formed (procoagulant and anticoagulant) are produced on negatively charged membrane surfaces of the active platelets, which is a critical point that restricts the reaction to the lesion site.

Furthermore, this model presents four main steps: initiation, amplification, propagation and termination [16, 32]. However, some author opt to present the initiation and the amplification phases as a unique step [31, 34].

- **Initiation**: the main objective of this phase is the formation of thrombin, while platelets adhere and aggregate to the lesion site [16]. When TF is exposed, it occurs the formation of FVII-TF complex, since in normal condition blood already present a small quantity of FVIIa [31, 34]. This complex activates FIX and FX, generating a small quantity of their active forms [16, 31, 34]. Then, FIXa acts in FV and forms a small quantity of FVa. Although, it is important to stress that thrombin is the main activator of FV, being this small production of FVa essential to form the FVa-FXa complex (prothrombinase), which will produce a nanomolar concentration of thrombin, at a low rate [16, 31, 32]. **Figure 3.5** presents a schematic representation of this phase.

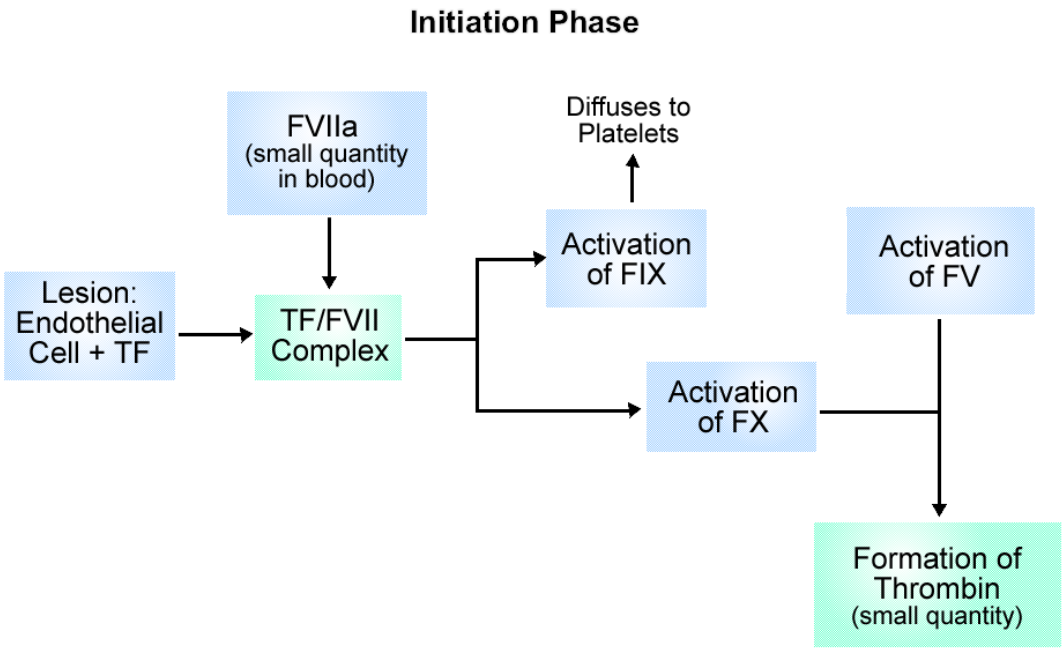

Figure 3.5 – Initiation phase of blood coagulation.

- **Amplification**: in the present phase, platelets become more active, releasing the contents of their granules, due to the small quantity of generated thrombin [16, 34, 38]. One the other hand, thrombin also dissociates the FVIII-vWF complex, which will activate FVIII (being its only activator), and promote platelet aggregation via vWF. Furthermore, it activates FV, stimulating its production by platelets and activates FXI, which will activate FIX on platelet surface [16, 38]. Moreover, in this phase, it already exists all the substrates necessary to produce the main quantity of thrombin, which will occur in the next phase [44]. **Figure 3.6** presents a schematic representation of this phase.

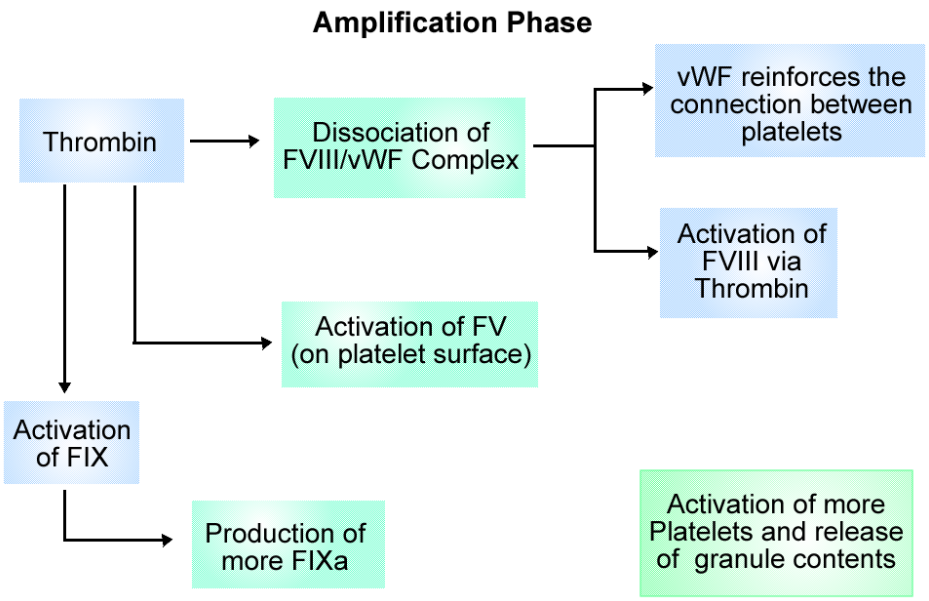

Figure 3.6 – Amplification phase of blood coagulation.

- **Propagation**: This phase produces 95% of all thrombin, since all procoagulant proteins are present at plasma, which favour exponentially its formation (**Figure 3.7**) [16, 31, 38].

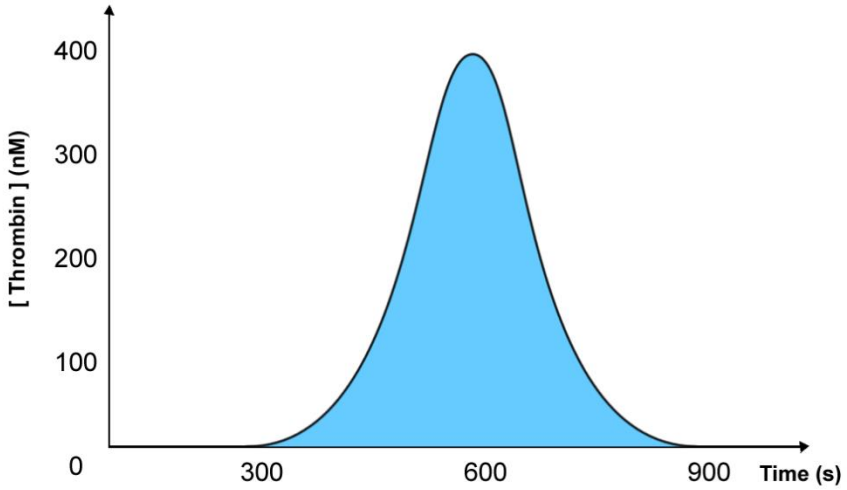

Figure 3.7 –Variation of thrombin concentration throughout the time of the coagulation process. Adapted from [16].

Active platelets present a surface that allows the combination of FVIIIa and FIXa in order to form the tenase complex, which will then activate FX. In its turn, FXa will combine with FVa on the surface of platelets, forming prothrombinase complex, which will activate prothrombin at a high rate [16, 31, 32, 46]. Coagulation process presents an effective positive feedback [16]

but, if it exists an absence of FVII or FXI during this phase, thrombin formation is suppressed [31]. In addition to the previously mentioned, in this phase thrombin also converts fibrinogen to fibrin by a polymerization reaction that cleaves its fibrinopeptides [16, 31, 43]. Thus, fibrin network traps blood constituents and strengthens the clot [16]. **Figure 3.8** represent a schematic representation of this phase.

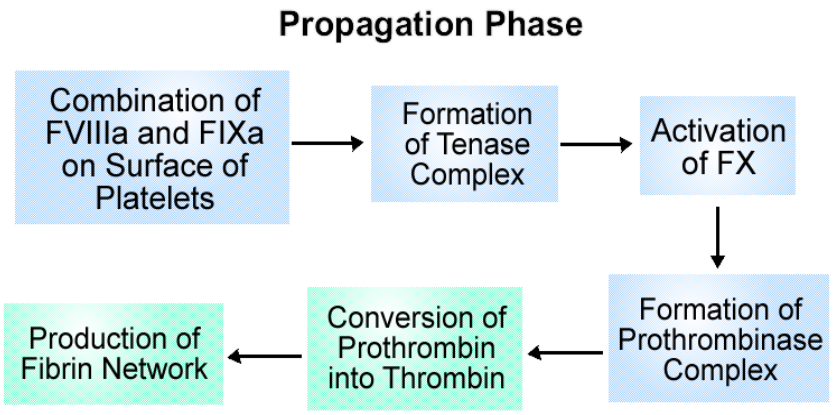

Figure 3.8 – Propagation phase of blood coagulation and formation of fibrin.

- **Termination**: The last phase of clotting process has the aim of to stop clot growth, leading to the cessation of prothrombin consumption, and inactivation of some enzymes due to the action of natural coagulants (**Figure 3.9**) [16, 34]. This process will be further explained in **3.3**.

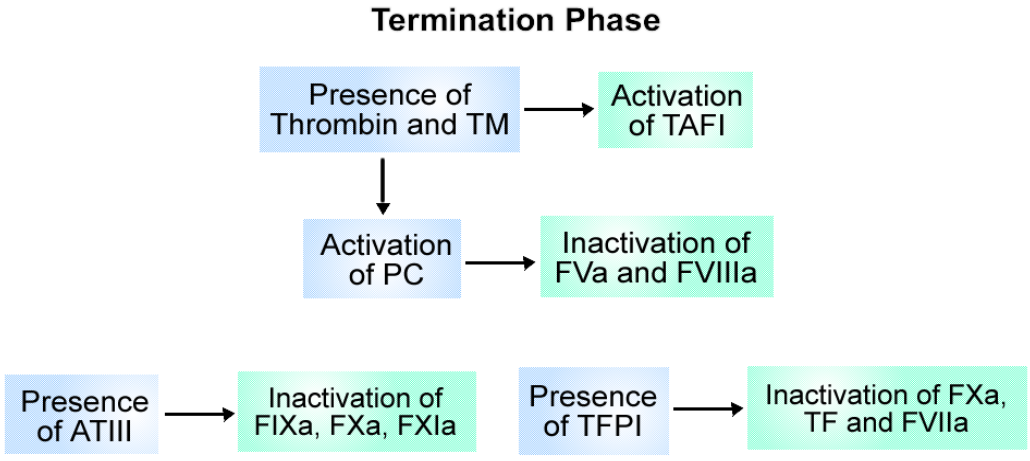

Figure 3.9 - Termination phase of blood coagulation.

Lastly, it is important to stress that the normal concentrations of the coagulation agents in blood (**Table 3.2**), depend on their roles in blood coagulation process. Thus, fibrinogen, due to its importance to all process, is the factor that presents higher concentration. One the other hand,

FVIII presents the lower concentration, being enough for its function of supporting FIXa in the activation of FX [29].

Table 3.2 - Normal Concentration in blood of clotting agents. Adapted from [25, 31, 48-50].

Component	Concentration (nM)
FI	7000
FII	1400
FIII (TF)	Variable
FV	20
FVII	10
FVIII	0.7
FIX	90
FX	170
FXI	30
FXIII	90
Platelets	10
Activated Platelets	0.001/0.5

Regarding activated factors, the majority of authors considers a concentration of 0 nM [25, 31, 49, 50]. However, it also possible to find in literature some considered concentrations in normal bloodstream:

Table 3.3 - Normal Concentration in blood of activated factors. Adapted from [48].

Component	Concentration (nM)
FIa	0.70
FIIa	0.140
FVa	0.002
FVIIa	0.1
FVIIIa	0.00007
FIXa	0.009
FXa	0.017
FXIa	0.003

3.2 - Types of Clots

Vessels possess several physiologic responses to maintain the normal behaviour of the circulatory system, such as when lesions occur. In these situations, the body must be able to deal with different problems [20].

One of the main factors that can determine the chemical environment near to clot formation is the blood flow, since it transports the essential cells and molecules to form the clot [16, 51]. Besides, it also maintains the concentration levels of clotting and anticlotting factors and the rate of species exchange between blood and the lesion [26, 43, 51]. However, the flow and the diffusion are dependent on the geometry of the system and on the rheological properties of blood [26, 51].

The diffusion coefficient is determined by the random movements of molecules that are induced thermally. If a molecule was assumed spherical, with a radius R, and if it is larger than solvent molecules, the diffusion coefficient D is given by the Stokes-Einstein equation [51]:

$$D = \frac{K\,T}{6\pi\,\mu\,R} \tag{3. 1}$$

With K as the Boltzmann's constant, T as the absolute temperature and μ as the viscosity.

If the molecule is small, the diffusion coefficient is considered 10^{-5} cm^2/s. One the other hand, for large proteins, such as the agents involved in the formation and dissolution of clot, the value is considered between 10^{-6} and 10^{-7} cm^2/s. For platelets, the value is near to 10^{-9} cm^2/s [51].

The tabulated values for common diffusion coefficient are presented in **Table 3.4** [49, 50].

Table 3.4 - Diffusion coefficients of clotting agents. Based on [49, 50].

Component	Diffusion Coefficient (cm^2/s)
Platelets	1.58×10^{-9}
Activated Platelets	1.58×10^{-9}
FI	3.1×10^{-7}
FIa	2.47×10^{-7}
FII	5.21×10^{-7}
FIIa	6.47×10^{-7}
FV	3.12×10^{-7}
FVa	3.82×10^{-7}
FVIII	3.12×10^{-7}
FVIIIa	3.92×10^{-7}

FIX	5.63×10^{-7}
FIXa	6.25×10^{-7}
FX	5.63×10^{-7}
FXa	7.37×10^{-7}
FXI	3.97×10^{-7}
FXIa	5.0×10^{-7}
Protein C	5.44×10^{-7}
ATIII	5.57×10^{-7}
TFPI	6.30×10^{-7}
tPA	5.28×10^{-7}

So, the characteristics of a clot strongly depend on the site where occurs its formation and on the local conditions. Thus, two principal types of clots are considered [20, 30]: white clot and red clot.

3.2.1 - White Clot

Endothelial defects can lead to the formation of white thrombus in veins or in arteries. Although, since the flow velocity is slower in veins, the formation of fibrin predominates. In arteries, fibrin cannot form, except in areas of disturbed flow like stagnation [35].

White thrombus normally occurs in the arterial tree, where flow is more rapid, so the accumulation of procoagulant does not occur, and where higher shear forces are present, such as in ruptured plaques. In these cases, platelets can adhere to the lesion site and forms a platelet thrombus, which presents a softer colour [20, 32, 35]. Besides that, the thrombus size can be estimated by counting the number of platelets in the clot [20]. White clots can also present leukocytes in its structure [39].

3.2.2 - Red Clot

In zones where shear is minimal, as in peripheral veins, the activation of coagulation process leads to higher concentrations of procoagulant [20, 35]. A venous thrombus is formed under slow flow, which enables the local accumulation and interation of procoagulant substances, allowing the development of a fibrin clot. This may occur both by local trauma or alterations in blood chemistry [35].

Moreover, this type of clot presents large amounts of fibrin and a homogeneous distribution of erythrocytes and fibrin. Since fibrin can trap erythrocytes in their network, the blood clot presents a reddish colour [32, 35].

3.3 - Fibrinolysis

After the formation of the clot, it is important that clot stops growing before significant lumen reduction (stenosis) or even a complete obstruction of the blood vessel (embolism) occurs. Thus, self-regulation mechanisms are necessary [16].

Human body presents different processes that limit the clot formation and allow its dissolution [19]. These go in parallel with clot formation, although they only become visible at a larger timescale, since it has to dissolve slowly and gradually, in order to allow the repair of the tissue, without releasing fragments into the bloodstream [16].

Before the lysis of the clot, three main mechanisms act to limit the formation of the clot, since they reduce the generation of fibrin. These are also called natural anticoagulant mechanisms [19, 33] and are mainly controlled by antithrombin III, protein C, TFPI (**Figure 3.9**) [31].

The first mechanism is performed by TF pathway inhibitor (TFPI), a plasma protein secreted by endothelial cells. It acts during the initiation phase of blood coagulation, binding to TF-FVIIa complex, which will inhibit the generation of FXa [19, 33]. For this reason, the extrinsic pathway can only form a small quantity of thrombin by itself. Though, when extrinsic pathway is inhibited, the intrinsic pathway continuous the formation of clot by the feedback mechanism of thrombin [33, 42].

After the formation of thrombin, it can bind to thrombomodulin (TM), an endothelial cell receptor that eliminates clot-producing effects of thrombin. Besides that, in this circumstances, thrombin also bind to protein C (PC), another plasma protein that will inactivate FVIIIa and FVa by proteolysis [19, 31, 33]. Therefore, this second mechanism is triggered by thrombin that, in this case, acts like an anticoagulant.

Finally, the third mechanism uses the plasma protein Antithrombin III (ATIII). It can bind to heparin (present in endothelial cells) and inactivates thrombin and some clotting factors, such as FIXa, Xa, and XIa [19, 37, 38]. This inhibition is slow, allowing the generation of fibrin at the beginning of clotting process [33].

Thus, similar to blood coagulation, the main inhibitors are proteins that circulate in plasma [40]. Moreover, it is important to highlight that the trap of thrombin in the fibrin matrix also allows the suppress of coagulation, and defects in these mechanisms are associated with high risk of clotting [19, 33]. Besides the mentioned functions of thrombin, it also activate the carboxypeptidase B, also known as thrombin-activatable fibrinolysis inhibitor (TAFI), which inhibits the reactions that involve TF and FVIIa [29, 42].

It was proved that, in extreme situations, when the concentration of procoagulants is higher (comparatively to their mean physiological values) and the concentration anticoagulants is smaller, the quantity of thrombin generated is higher. If the opposite scenario is verified, the result is the inverse (**Figure 3.10**) [31].

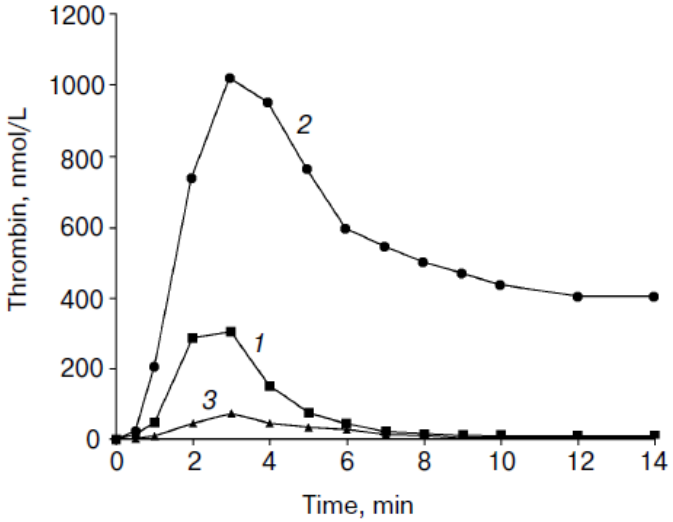

Figure 3.10 – Different scenarios that influence thrombin concentration: 1- normal concentration of procoagulants and anticoagulants; 2- high concentration of procoagulants and small concentration of anticoagulants; 3- small concentration of procoagulants and high concentration of anticoagulants. Adapted from [31].

When the repair of vessels begins, it is necessary to destroy the clot and to prevent the formation of thrombus healthy vessels. The mechanism that dissolves the formed clots is called Fibrinolysis (**Figure 3.11**) [32, 38]. As for coagulation, this process is made up of a plasma pro-enzyme, the plasminogen, which can be activated (through catalyse) to plasmin enzyme, via protein plasminogen activators [6, 16, 33]. Plasmin promote the destruction of fibrin, leading to the destruction of clot [16, 33].

Though, note that the fibrinolytic process is a complex system that involves various activators and inhibitors of plasminogen, and different pathways that lead to its formation [16]. The most common plasminogen activators presented in literature are the tissue plasminogen activator (t-PA), which is secreted by endothelial cells, and the urokinase plasminogen activator (u-PA) that is released by the kidney. Through the coagulation, plasminogen and t-PA (or u-PA) link to fibrin, becoming also incorporated in the clot [6, 16, 32].

Once again, similar to blood coagulation, this process also presents inhibitors that prevent the dissolution of the clot before the regeneration of the tissue. The principal inhibitor of t-PA and u-PA is plasminogen activator inhibitor-1 (PAI-1). Regarding plasmin, the main inhibitor is antiplasmin [6, 52].

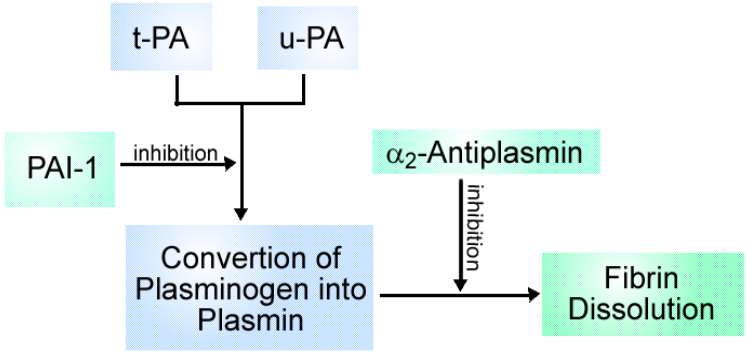

Figure 3.11 – Fibrinolysis process.

Concerning the platelet plug, the undamaged endothelial cells secrete the eicosanoid, also known as prostacyclin or prostaglandin I2 (PGI2), an inhibitor of platelet aggregation, and also nitric oxide, a vasodilator and platelet adhesion, activation, and aggregation inhibitor [19].

Such as coagulation factors, in normal conditions, anticoagulant factors also circulate in bloodstream, however, their main objective is to prevent unwanted clots. Thus, the normal concentrations of some of these factors are presented in the next table [25, 31, 48-50].

Table 3.5 - Normal Concentration in blood of anticoagulant factors. Adapted from [25, 31, 48-50].

Component	Concentration (nM)
TFPI	2.5
ATIII	3400/2410
Protein S	300
Protein C	60
t-PA	0.08

3.4 - Mechanical Properties

Flow influences the structure and destruction of the clot. The stresses that are applied during thrombus formation affect its strength, as well as its structure and organization [20, 26, 51]. For example, in a stagnant region the formed thrombus is gelatinous, with a low density of fibrin interlocking with platelets, when compared with a thrombus formed in areas where the quantity fluid is larger. In this last case, the formed thrombus is denser and it is structured in a pattern indicating the stresses applied during its formation [51]. Furthermore, blood protects the thrombus

through its yield stress, and it also support some pressure that tries to break thrombus, through its viscosity, avoiding embolization [26].

Disturbances in blood flow can affect the platelet adhesive function, nevertheless, it is not yet completely understood [7, 43]. As seen previously, blood is exposed to shear stress caused by the necessary force to produce flow, which alter the formation pattern of the clot since it acts like an agonist of adhesion and aggregation of platelets, [28, 43]. During this process, platelets may be exposed to shear stress values of several hundred dyn/cm^2, such as in small arteries and arterioles partially obstructed. Under high shear stress conditions (>108 dyn/cm^2), vWf is essential for clot formation process occurs, leading to a more stable aggregate, and it is the main support of induced aggregation, by shear forces above 81 dyn/cm^2. One the other hand, at low shear forces (<12 dyn/cm^2), reversible platelet aggregates are formed via fibrinogen [23, 53]. Besides that, high shear forces and rapid changes in flow, accelerate platelet accumulation on lesion site. One the other hand, decelerating low-shear zones, after thrombus region, lead to a progressive accumulation and aggregation [7]. Moreover, red blood cells motion and nonuniform platelet concentration can be related to the rate of platelet interaction with the lesion, since both of them increase this transport, with the increase of shear rate [20]. Red blood cells present transverse motion and rotation which relocates plasma and platelets, promoting their lateral transport [20]. Red blood cells usually flow in the centre of vessels, forcing the existence of a higher platelet concentration in the wall that increases with the increasing haematocrit, shear rate and platelet concentration. [20, 43, 53].

It is also important to highlight that platelets increase the dynamic rigidity modulus of the clot since they present crosslinking regions and exert a contractile force on clot network that leads to the reorientation of fibrin (**Figure 3.12**) [43].

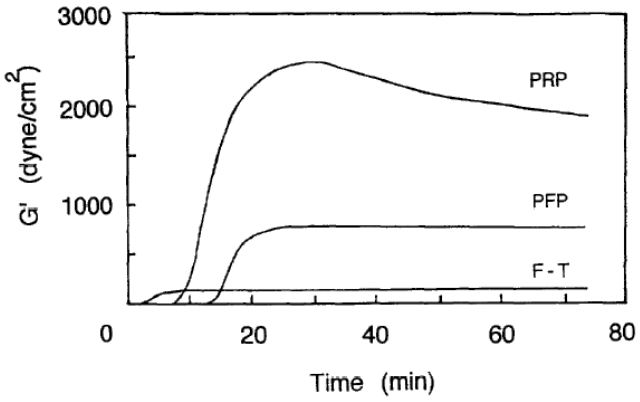

Figure 3.12 - Dynamic rigidity modulus (G') during clot formation in three different solutions: F-T - fibrinogen solution; PFP - platelet free plasma; PRP - platelet rich plasma. Adapted from [43].

Also, if the concentration of fibrinogen or thrombin increase, the number of crosslinks also increase, which lead to a decrease on the flexibility and on the lateral association of the fibres [43].

Regarding clot viscosity, it does not exist a constant value for this property since it depends on the type of clot and its features, as well as on the conditions of formation. However, the viscosity of blood clot is always higher than the viscosity of blood, and some assumptions can be found in literature. Anand M. *et al.*, assumed the clot viscosity as 16 times higher than the viscosity of blood and also determined the value of viscosity of the clot taking into account the shear rate. Thus, for a shear rate of 0.06 s^{-1}, the viscosity of clot was 2200 cP, and for 650 s^{-1}, the value was 84 cP, with the correspondent values of blood viscosity of 73.5 and 5 cP, respectively [50]. This correlation allowed to create a new phenomenological law to predict the clot viscosity with respect to the shear rate. This new phenomenological law can be adjusted to new data from the literature and it is fully presented in subsection **3.7**.

The viscosity value is also dependent on the concentration of fibrin, increasing with the increase of fibrin concentration [25, 49]. A model function base on that assumption is presented in the work of Bodnár T. *et al.*, and it can be seen in **Figure 3.13** [49].

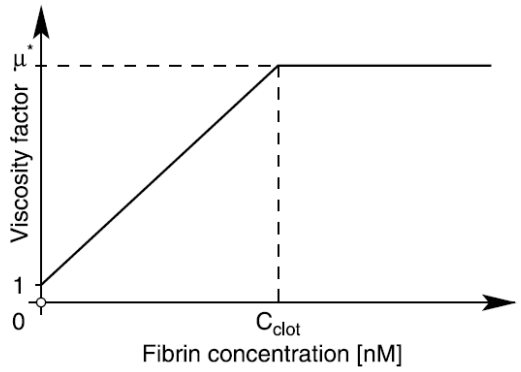

Figure 3.13 – Viscosity of clot as a function of fibrin concentration. Adapted from [49].

Concerning clot density, a density change between blood and the formed clot are usually neglected, since they present a similar density, being normally considered as the same value of blood plasma [50, 54]. Anand M. *et al*. describe the blood density as 1050 kg/m^3 and the clot density as 1030 kg/m^3 [50].

3.5 - Mathematical Models

Nowadays, the literature defines three main modelling approaches to study blood coagulation:

- **Continuous models**: this type of model is described by systems of partial differential equations (PDE's) that govern a physical event, as, for example, the concentrations of blood factors, being expressed by a strong form equations. Continuous models are capable to obtain exact analytical solutions. However, these can be difficult to solve, as in the case of use complex geometry. Concerning blood coagulation, these models are able to describe the diffusion of species in the blood flow. However, these do not consider interactions between cells, describing them just in terms of concentrations [55]. As an example, the model proposed by Leiderman and Fogelson is one of the most comprehensive continuum blood clotting model that modulates platelet aggregation and blood coagulation [56].
- **Discrete models**: contrary to the previous models, discrete models use the weak form of the PDE's, establishing a discrete system of equations that is stated for each integration point. This type of system presents lower consistency. However, the produced equations represent more stable algebraic systems. Regarding blood coagulation, discrete models pay attention on the description of individual cells, studying their interactions. However they lack in detail when describing the diffusion of blood factors [55].
- **Hybrid models**: these models emerged in the last decade and combined continuous and discrete methods in order to bypass their individual flaws. Thus, hybrid models allow for the association of the different features and mechanisms that each model can describe [55].

3.6 - Constitutive / Rheological Models

In the last two decades, mathematical modelling has become popular in the study of clot formation [57]. Advances in computational processing and in modelling of complex biological processes improved the treatment and diagnose of CVD [56]. Models concerning primary and secondary haemostasis, or even fibrinolysis, have emerged since the appearance of the 3-pathway cascade model and now, literature regarding mathematical models used to represent clot formation is huge [56]. However, due to the complexity of the process, many authors have assumed several simplifications, trying to stress only particular properties. The complexity of the models has increased over the years, and today clot formation models possess several interdependent differential equations requiring an excessive number of physiological parameters, which make them unrealistic and useless [16].

It is possible to find two main classes of models to describe coagulation process: the Ordinary Differential Equations (ODE's) and the Partial Differential Equations (PDE's) [16, 56]. In both, the

concentration of a specie C is normally represented by [C] and the reaction kinetics can follow one of these types of equations:

$$\begin{matrix} k[C] & First\ order\ kinetics \\ k[C_i][c_j] & Second\ order\ kinetics \\ k\ \frac{[C_i][c_j]}{k' + [C_i]} & Michaelis - Menten\ kinetics \end{matrix} \tag{3. 2}$$

Where k is the rate constant and k' the Michaelis-Menten constant [16].

3.6.1- ODE's Models

This type of system focus on the chemistry and on platelets, monitoring local evolution of the clot, and emphasizing some qualitative properties (like the existence of a threshold for clotting initiation) [16]. The first work was published in 1966, providing a scheme for a reaction cascade of the type zymogen-enzyme:

$$\begin{aligned} \frac{dy_{1a}}{dt} &= k_1\,[U(t) - U\,(t-a)] - H_1 y_{1a} \\ \frac{dy_{2a}}{dt} &= k_2 y_2 y_{1a} - H_2 y_{2a} \\ &\vdots \\ \frac{dy_{Na}}{dt} &= k_N y_N y_{(N-1)a} - H_N y_{Na} \end{aligned} \tag{3. 3}$$

Where y_i, y_{ia} ,for $i = \{1, \dots, N\}$, are the concentrations of the i^{th} zymogen-enzyme pair, H_i are the decay rates, and U(t) is a unit step function [16].

The TF-pathway was modelled in 1989, it was a simplified model (where a small number of factors were considered and [FVIIa] was taken as constant) with nonlinear dependence on the reaction terms of the concentrations. The system is represented by:

$$\begin{cases} \frac{d\,[VIIa]}{dt} = \alpha K_1 - H_1[VIIa] \\ \frac{d\,[Xa]}{dt} = K_2[VIIa] - H_2[Xa] \\ \frac{d\,[Va]}{dt} = K_3[IIa] - H_3[Va] \\ \frac{d\,[IIa]}{dt} = \frac{K_4[Xa][Va]}{K_a + [Va]} - H_4[IIa] \end{cases} \tag{3. 4}$$

This allows the identification of α, which can be an activation threshold [16].

More recently, in 2002, a more generalized work was proposed, with the same objective, but with a more complex system:

$$\begin{cases} \dfrac{d\,[VIIa-TF]}{dt} = [VIIa-TF]_0 - h'_1[VIIa-TF][TFPI][X_a]k_{14} \\ \dfrac{d\,[Xa]}{dt} = k_2[VIIa-TF] - k_{21}[IXa]\left(\dfrac{VIII_a}{d+VIII_a}\right)\left(c_0 + \dfrac{f([II_a])}{1+f([II_a])}\right) - h'_{21}[TFPI][X_a] - h'_{22}[ATIII][IX_a] \\ \dfrac{d\,[Va]}{dt} = K_3[VIIa-TF] - h'_3[ATIII][IX_a] \\ \dfrac{d\,[IIa]}{dt} = k_4[Xa]\left(\dfrac{[V_a]}{d_1+[V_a]}\right)\left(c_0 + \dfrac{f([II_a])}{1+f([II_a])}\right) - h'_4[ATIII][II_a] \\ \dfrac{d\,[Va]}{dt} = k_5[IIa][V] - h_5[Va] \\ \dfrac{d\,[VIIIa]}{dt} = k'_6[IIa][VIII] - h_6[VIII_a] \end{cases} \tag{3. 5}$$

Like in previous work, this empathize the existence of a threshold value for suitability, defined as “coagulation stimulus”. However, this new system involves more species, such as the FVIIa-TF complex, FIXa, FVIIIa, and also includes inactivated factors [16].

Moreover, some TF-pathway models were developed to find more threshold phenomenon. Although, the number of differential equations increased, having arrived at 20 ODE’s or even at 36 ODE’s. For example, the Hockin-Mann model present 34 ODE’s (with 42 rate constants). Besides that, it is possible to find in literature a list of reactions that are used as a standard by many authors [16].

These systems also can model the mechanical activation and aggregation of platelets, in conditions of high shear stress, and also can include an inhibitor of the activators of platelets. The model used to represent the previous mentioned is given by:

$$\begin{aligned} \tau\,\frac{dy}{dt} + y &= c(t)u(t) \\ c(t) &= \frac{c_0}{1 + e^{-c_1 P(t)}} \end{aligned} \tag{3. 6}$$

With $P(t)$ being the global platelet density, $c(t)$ the enhancing aggregation response, $u(t)$ the shear rate and $y(t)$ the thrombus size measured by its area [16].

A blood clotting model can be reduced to an initial value problem expressed by ODE’s, with the appropriated assumptions. Besides that, numerical techniques can be used, like the Backward Differentiation Formula Method (BDFM) and the Runge-Kutta method (RKM) to solve this type of

models [56]. One of the first ODE models of blood coagulation that has been solved by RKM was proposed by Alenitsyn *et al.*, which describes thrombus progression as a function of mean blood velocity, in an injured vessel. Another example was proposed by Kuharsky and Fogelson, who presented a powerful model of the extrinsic pathway, with this one being solved by BDFM [56].

Recently, a mathematical model based on ODE's, developed by Elizondo P. et al., described venous thrombosis as a consequence of slow flow and of activation of the endothelial cells, in the absence of an explicit mechanical disruption of them [39]. Another one predict the thrombin production in the presence of activated platelets, being governed by 25 equations [48].

3.6.2- PDE's Models

Contrary to the previous models, PDE's require a more sophisticated approach, being solved usually by mesh-based methods, such as, the Finite Difference (FD), the Finite Volume (FV), and the FE methods. Furthermore, regarding the meshless methods, the Smoothed Particle Hydrodynamics (SPH) method is a popular alternative to the mesh-based methods [56].

PDE's systems include, among others, spatial inhomogeneity, blood flow or clot mechanics, being considered some different modelling approaches that are classified according scales:

- **Nanoscale Models (Sub-cellular)**

This class studies the Molecular Dynamics, which is based on the motion of interacting molecules. One variant of this, is the Steered Molecular Dynamics, which has already been used in clot mechanics. In this variation, an external stimulus is used to analyse the response of some material [16].

- **Microscale Models (Cellular)**

The focus of these models is the motion and action of cells. The methods used to solve them are variants of the Euler-Lagrange Particle Tracking method, where fluid motion is studied with an Eulerian approach, and the Lagrangian tracking is applied to particles. However, the influence of the solid on the liquid component is neglected. Other methods, such as the Immersed Boundary method or the lattice Boltzmann implementation, are also used [16].

Another different class of methods describes the flow as an interaction between discrete particles and includes Dissipative Particle Dynamics (DPD), Fluid Particle Model and Moving Particles Semi-Implicit Method (MPS). These techniques are useful to study particle transport in blood and deposition on vessel walls, and the motion of leukocytes and of erythrocytes. It is possible to find in literature several works related to clot formation. An example of these models that use particles is the Cellular Potts Model. This model represents different types of cells and describes cell–cell and platelet-injury adhesion, platelet activation, cell movements, cell state changes, and

platelet aggregation [58]. One example where this model is used, is described in work of Xu Z. *et al*. [59].

- **Mesoscale Models (Statistical methods)**

These models are a mixed of the particle tracking and continuum models, where particles are not treated individually but by means of probability densities [16].

The Lattice Boltzmann Method (LBM) is one of the methods that are applied in computational fluid dynamics (CFD) and more particularly, to blood coagulation. It uses a discrete approximation of Boltzmann's equation and describe the probability density evolution at the nodes of a discrete lattice, where only discrete velocities are allowed [16, 56]. If $f(x, vi, t)$ is the distribution function defined on the lattice, it is possible to obtain the macroscopic density $\rho(x,t)$ and velocity field $u(x,t)$ by:

$$\begin{aligned} \rho(x,t) &= \sum_i f(x, vi, t) \\ \rho(x,t)u(x,t) &= \sum_i f(x, vi, t)\, vi \end{aligned} \tag{3. 7}$$

Statistical methods have been mainly applied to model aggregation processes, based on the Smoluchowski equation, being applied to blood coagulation models too. For example, a model of platelet aggregation under the action of a shear rate $\dot{\gamma}$ is defined as [16]:

$$K(a,b) = \frac{\dot{\gamma}}{\pi}\left[a^{\frac{1}{3}} + d^{\frac{1}{3}}\right]^3 \tag{3. 8}$$

This can be presented in a more complete form, allowing the application in platelet aggregation and disaggregation:

$$\int_0^{\infty} H(a,b) f(a,b) db - f(a,t) \int_0^{a} H(a-b,b) db \tag{3. 9}$$

With $H(a-b,b)$ being the fragmentation kernel expressing the probability of the decay of a particle of volume a into a pair $(a-b,b)$.

Moreover, it is important to stress that this two last models have discrete forms, which are also used to study platelets dynamics [16].

- **Macroscale Models (Continuum mechanics)**

Macroscopic Models describe the blood flow, based on the assumption that the system is a continuum medium, being dependent on the solution of the Navier-Stokes and Convection-Reaction–Diffusion (CRD) equations [16, 56]. CRD and CRD-like equations govern the thrombus formation and dissolution, as well as the cell behaviour described by means of macroscopic quantities [56].

The classic structure of a CRD system, involving N chemical species, is given by:

$$\frac{\partial C_i}{\partial \mathrm{t}} + \nabla \cdot \left(u\, C_i - D_{C_i} \nabla C_i \right) = R\,(C_1, C_2, \dots, C_N) \tag{3. 10}$$

Thus, the focus of the model is the specification of the reaction rates, however the presence of the diffusivities D_{C_i} requires the specification of boundary conditions, which makes the integration much more difficult [16].

One of the earliest models presents the concentration of the tenase $[Z]$ and prothrombinase $[W]$ complexes, and the inhibiting action of Protein C (APC), which are expressed by:

$$[Z] = k_{8,9}\, \frac{[VIII_a][IX_a]}{K_{8,9} + k_a\,[APC]'}$$

$$[W] = k_{5,10}\, \frac{[V_a][X_a]}{K_{5,10} + k_a\,[APC]'} \tag{3. 11}$$

Besides that, the reaction rates of the factors considered in the model are:

$$R_{IXa} = k_9[XIa] - K_9[IXa]$$

$$R_{Xa} = k_{10}\,[IXa] - K_{10}\,[Xa] - k_{10}\,[Z]$$

$$R_{IIa} = k_2\,[Xa][II] - K_2[II] + k_2\,\frac{[W][II]}{k_{2m} + [II]}$$

$$R_{II} = -k_2[Xa][II] - k_2\,\frac{[W][II]}{k_{2m} + [II]}$$

$$R_{VIIIa} = k_8[IIa] - K_8[VIIIa] - k_a[APC]([VIIIa] - [Z]) \tag{3. 12}$$

$$R_{Va} = k_5[IIa] - K_5[Va] - k_a[APC]([Va] + [\mathrm{W}])$$

$$R_{APC} = k_{APC}[IIa] - K_{APC}[APC]$$

$$R_{Ia} = k_1[IIa]$$

$$R_{XIa} = k_{11}$$

Being necessary a boundary conditions for all diffusing factors [16].

This model presents several species of the coagulation process, giving main importance to Z, W, APC.

Besides that, it is important to highlight that this model has evolved, having already incorporated the fibrinolysis process. However, the reaction rates have become more complicated and the number of differential equations has increased [16].

Another important model developed by Yasdani *et al.*, represents platelet motion and adhesion to the damaged endothelial wall that can be solved using an Eulerian-Lagrangian approach [16].

Moreover, the mechanical activation of platelets, as mentioned before, depends on the shear stress [16]. Thus, few models have been used to simulate platelet events with a continuous description, which can be viewed as extensions of the CRD equations [56]. In the model of David T. *et al.*, the deposition rate was assumed to depend linearly on the shear stress at the wall and it includes platelet diffusion-advection equations[16].

Finally, these models present lower computational costs, when compared to the other ones. Although, the analytical solution can be difficult to find due to a complex geometry, some solutions of basic aspects of the thrombus formation were found and demonstrated to be useful [56].

Since a fully mathematical model for blood coagulation is still inexistent, current models only use some elements or stages of the process, modelling just a sub-process [49, 56]. The most common sub-processes are, for example, Platelet signalling, Thrombin generation, Fibrin formation, Fibrinolysis, vWF mechanics, Platelet margination/Erythrocytes dynamics, each with several examples in the literature [27].

However, these models can be combined and form multiscale models, involving fluid mechanics, cell mechanics and biochemistry, these are already used to model platelet adhesion and thrombus formation [16]. A multiscale approach uses the simplicity and efficiency of the macroscopic model and, at the same time, the accuracy of the microscopic models, allowing the study of the macro–micro relationships of the flow, platelet and coagulation [59]. An example is the model developed by Xu Z. *et al.* [58], which describes the formation of the fibrin network through fibrin elements. It demonstrates the accumulation of fibrin on the surface of the clot, which limits its growth since it reduces thrombin concentrations on the surface and decreases adhesivity of nearby platelets. Several models have been developed to study thrombosis, but only a few simplified models are available for studying the effects of fibrin on blood clot formation [58].

3.7 – Phenomenological Laws for Clot formation

One of the main objectives of the present work is the creation of a new algorithm capable to predict clot formation in the blood flow. Additionally, the algorithm should be combined with advanced discretization techniques (such a meshless method) to allow the temporal-spatial progression of the clot. Thus, based on literature experimental data, two new distinct phenomenological mathematical laws were developed and implemented combined with a meshless method. The detailed description of the algorithm is shown in **Chapter 7**. This section focusses mainly in the presentation of the phenomenological mathematical laws.

As mentioned before, it is expected that the clot presents a higher viscosity, when compared to blood. Since a fixed value of this parameter does not exist, when it refers to clots, some correlations can be made with other parameters, namely the shear rate ($\dot{\gamma}$). For example, Anand M. *et al.*, as presented before, showed that, for a shear rate of 0.06 s^{-1}, the viscosity of clot was 2200 cP (or 2.2 Pa.s), and for 650 s^{-1}, the value was 84 cP (or 0.084 Pa.s) [50].

Thus, considering these values, it is possible to establish a simple phenomenological law (3.13), correlating the shear rate (locally) with the viscosity of the clot or the viscosity of the zone of formation of the clot, as seen in **Figure 3.14**.

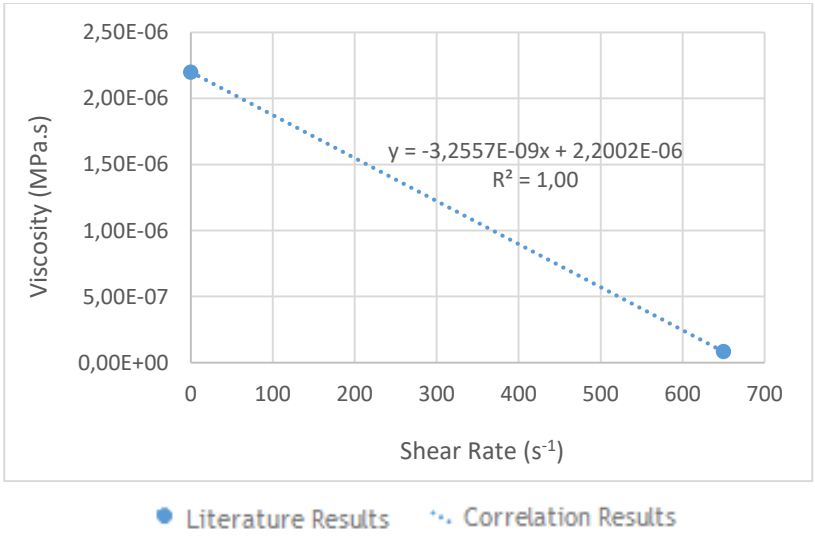

Figure 3.14 - Correlation obtained from the results obtained by Anand M. *et al.*.

$$\mu_{new} = -3.2557^{-9} \times |\dot{\gamma}| + 2.2002^{-6} \quad (3.14)$$

Since this work will resort to discrete numerical methods, each point has its value of shear rate, which make possible to calculate the expected value of viscosity in the respective point. Moreover, this is also an iterative/incremental process, so this value will be actualized in each

increment, allowing a variation of the viscosity of the domain, and consequently of the clot, over the increment (time steps).

Besides that, the clot growth can also be dependent on this parameter, as demonstrated by Casa L.D.C *et al*. [60].

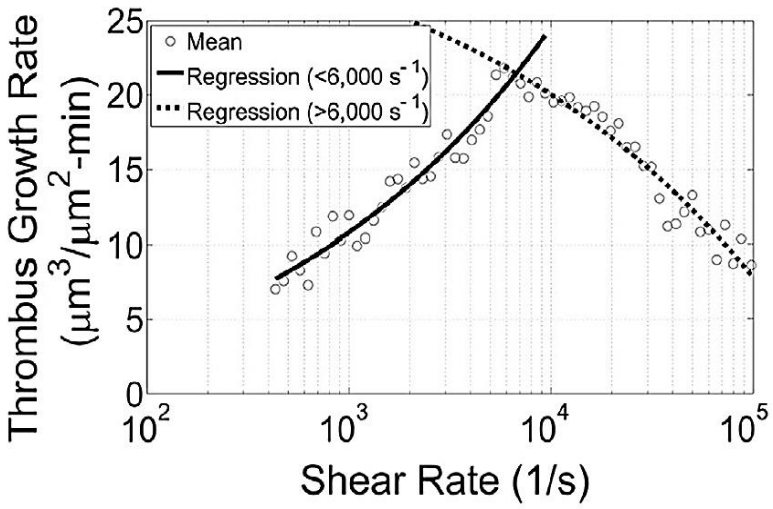

Figure 3.15 - Experimental results published in the work of Casa L.D.C. et al., relating the clot growth with the shear rate. Adapted from [60].

Figure 3.15 shows the experimental results published by Casa L.D.C. *et al.*, suggesting that the clot grows as a function of the shear rate. Notice that the curve seems to inflect around the value of 6000 for the shear rate. Thus, considered these experimental results, it was possible to create a new phenomenological law correlating the shear rate and with the clot growth. In this work, the clot growth will be translated by the Clot Growth Rate (CGR) variable, which is defined as $\mu m/min$.

Due to the curve inflection, it is necessary to develop two distinct curves to capture the experimental results (**Figure 3.16**). Thus, each equation is defined in a specific range, being the first applied if the shear rate is in the range of $[500;\ 6000]$, and the second if it is in the range of $]6000;\ 100000]$:

$$CGR = 0.8116 \times |\dot{\gamma}|^{0.3731} \tag{3. 15}$$

$$CGR = -2 \times 10^{-14} \times |\dot{\gamma}|^3 + 4 \times 10^{-9} \times |\dot{\gamma}|^2 - 0.0004 \times |\dot{\gamma}| + 23.805 \tag{3. 16}$$

The proposed phenomenological law allows to define the domain that will be affected by the clot.

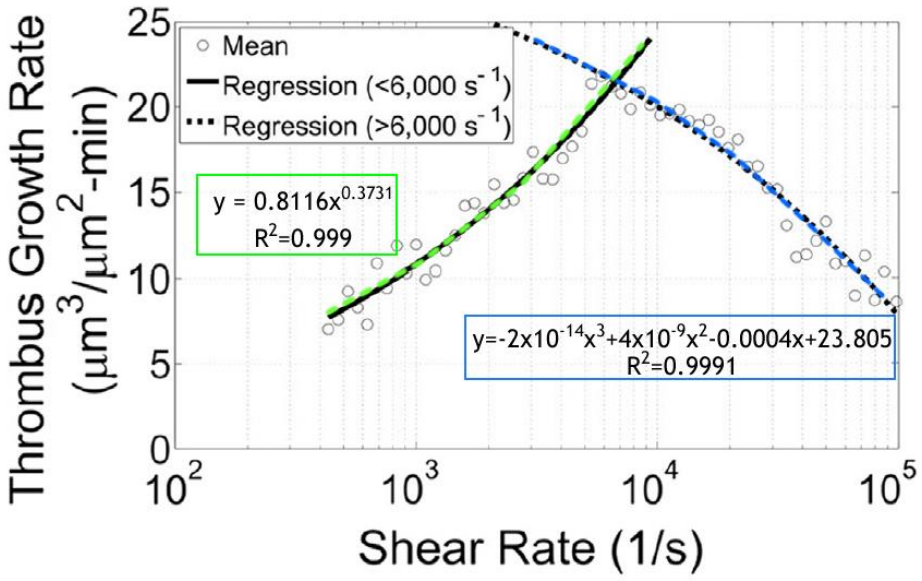

Figure 3.16 - Phenomenological law correlating the shear rate and with the clot growth taking into account the experimental results published in the work of Casa L.D.C. *et al*..

Since CGR depends on time ($\mu m/\mathrm{min}$), it is necessary to define a time step. In this work, it was defined a time step of 50 minutes. Thus, each increment will represent a time lapse of 50 minutes. The value of the time step was selected taking into account the spatial discretization (the mesh of nodes and integration points).

The clot growth algorithm will, in each increment, identify the integration points with a thrombin concentration higher than a threshold value (the basal concentration). Then, if those points (the interest points) possess a shear rate between 500 and 100000, then, the clot growth radius (R_{CGR}) will be calculated with CGR obtained with expression 3.17 or 3.18 multiplied by 50 minutes (the time step of each increment). Afterwards, all nodes and integration points closer to the interest point (which radial distance is smaller than the clot growth radius) will modify its viscosity based on equation 3.19. Thus, all those nodes or points inside the clot growth radius will become, virtually, clot domain for the next increment.

A more detailed and comprehensive view of the new developed algorithm will be presented further, in **Chapter 7**.

Chapter 4

Numerical Methods

Numerical methods became a recurrent tool in engineering science with the advance of computer applications, being an alternative to in vivo experiments [61]. Thus, computer simulation research in the medical field has increased exponentially in the last decades and emerged as an useful tool to supplement experimental data and analysis, helping in the development of clinical applications and device design [49, 57].

This chapter presents a brief overview of FEM and explains the two meshless methods that will be used in this work, RPIM and NNRPIM. Furthermore, the adopted fluid flow formulation is presented and explained.

4.1 – FEM

A mesh-dependent method is a method in which the solid domain is divided in partitions (elements, for examples) and each partition is connected to other partitions through common interfaces (without gaps), forming a mesh [62].

In the 1950's, FEM emerged as a powerful numerical tool, which facilitated the resolution of a large and complex system of equations. Originally, it was developed to be applied in aeronautics [63, 64], only becoming popular in 1980's [65].

At the moment, FEM is the most popular numerical method used in computation mechanics, being an effective tool to model systems in a large range of fields, such as, the biomedical engineering [63]. In 1972, it was applied in biomechanics for the first time, in the analysis of

mechanical behaviour of skeleton parts [66], and, in the same decade, it was also applied to fluid mechanics, for the Navier-Stokes equations [67].

FEM is a mesh-based approximation method that discretizes the continuum domain in finite elements, connected by nodes, with a pre-establish configuration, which creates smaller and simpler domains [68]. To these elements, linear functions (shape functions) are applied in order to acquire the approximated distribution of the variable under study, establishing the equations that represent the global system [66, 69]. Afterwards, FEM is able to solve the global equation system and the field variables are obtained in every cycle, over the entire mesh, until a converged value is achieved [69, 70]. Thus, it allows for an approximate solution, preserving the properties of the original domain [68].

To perform this type of analysis, it is important to define the virtual model in terms of geometry, properties of the materials and boundary conditions, with all these parameters in accordance with the type of analysis, which will lead to a more or less realistic model. After that, a mesh may be created, where the number of nodes and elements is defined [66, 71]. However, it is important to stress that, the problem's geometry, its mesh configuration and boundary conditions influence the computational time of the analysis and the accuracy of the results [70, 71].

The main advantage of FEM is its simple discretization concept, low computational cost and facility to program [63]. Besides that, it allows for an easy analysis of irregular surfaces and it permits to deal with different materials and boundary conditions in the same body. Additionally, the obtained FEM results present a reasonable degree of accuracy [72].

However, it can also present some disadvantages, such as the large deformation problems, in which the mesh distortion decreases the accuracy and the solution stability of FEM. Besides that, in fluid flow analysis, the mesh update increases the computational cost [63].

4.2 - Meshless Methods

Another class of discrete methods is called meshless methods. However, these methods can be divided into two different approaches: the continuum meshless methods (commonly known as meshless methods) and the particle meshless methods (commonly known as particle methods). In particle methods each node is an independent entity – a particle – that discretizes the continuum. The interaction between particles is imposed by force-reaction law [73]. In continuum meshless methods, each node represents a partition (a sub-volume) of the global domain. The interaction between nodes is established by compatibility strain equations, assuring the integrity of the continuum.

Nevertheless, this work presents the formulation of two continuum meshless methods for continuum mechanics in detail, the RPIM and the NNRPIM. However, only RPIM is used in this work.

4.2.1 – Meshless Methods: State of the Art

Computational mechanics is continuously evolving, becoming more challenging over time. Thus, with the objective of overcoming the weaknesses of mesh based methods, meshless methods appeared in the 1990's [63, 74, 75]. Meshless methods are usually used to analyse more complex domains and can be applied to solve (virtually) any physical problem, such as solid mechanics, fluid dynamics and heat transfer [76].

Contrary to FEM, a generic meshless formulation discretizes the problem domain with an unstructured nodal distribution, without a pre-established relation between the nodes [63, 77]. Besides that, it is from a flexible set of nodes (also called influence-domain) that the shape functions are obtained [63]. The influence-domain creates the nodal connectivity, instead of elements, with the field functions being, in this case, approximated by it. Furthermore, the influence domains may and must overlap [61, 77].

Thus, when compared with FEM, these methods present significant advantages: the shape functions present virtually a higher order, allowing for a higher continuity and reproducibility, they have compact support, deal with a transient geometry, can achieve more accurate approximation and also add/remove nodes easily, which allows for the refinement of the process [63].

Yet, meshless methods can also be divided into two classes: approximation meshless methods and interpolation meshless methods [63].

The approximation methods were the first to appear. The Diffuse Element Method is considered one of the first meshless methods, which constructs the approximation of the shape functions via moving least square approximants. Another example is the SPH, which is based on the kernel estimation and usually used in flow problems [63, 74, 75]. Moreover, these methods have been improved, leading to the appearance of new ones, such as the element free Galerkin method (EFGM), from DEM, or the meshless local Petrov–Galerkin method (MLPG), from SPH [63]. These methods obtain a smoother solution since they use approximation functions and the influence-domains are obtained through fixed radial searches. Besides that, the integration mesh is independent of the nodal distribution and constructed through integration cells [78]. However, they cannot produce shape functions with delta Kronecker property, which hinders the imposition of boundary conditions [63]. For this reason, meshless method community developed interpolation meshless methods. Some examples are the natural element method (NEM) [79-81], the Point Interpolation Method (PIM) [82], the Radial Point Interpolation Method (RPIM) [61, 83] and, more recently, the natural neighbour radial point interpolation method (NNRPIM) [61, 63].

RPIM and NNRPIM will be the meshless methods used in the present work so, the next topics will focus on their formulation.

4.2.1 - Generic Procedure of Meshless Method

Similar to FEM and other numerical methods, first it is important to define the geometry of the problem, to establish the solid domain and its limits, and its boundary conditions. After that, the domain is discretized by a nodal set, with regular or irregular distribution, which will affect the problem resolution (**Figure 4.1**) [77].

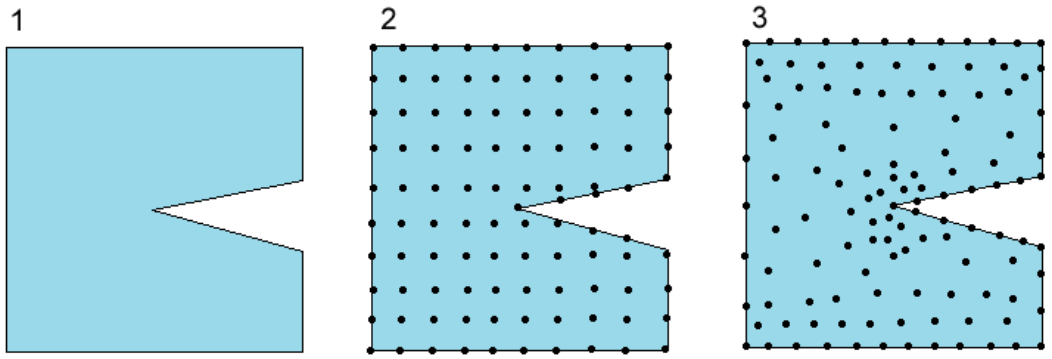

Figure 4.1 – 1) Problem domain; 2) Regular nodal discretization; 3) Irregular nodal discretization.

Since meshless methods do not require a mesh to construct the interpolation or approximation functions, it is not necessary a relation between the nodes, being just important to know the spatial location of each discrete node in the problem domain. This spatial distribution influences the performance of the method, as well as the computational cost [77].

To impose the nodal connectivity, after the discretization of the domain have been done, a background integration mesh (the numerical integration scheme) need to be created to integrate the weak form equations that govern the physical phenomenon. This process is usually performed by Gaussian integration meshes, as in FEM and RPIM. However, other techniques, like the Voronoï diagrams, can also be used, to obtain the integration points [77].

As mentioned before, in FEM, the nodal connectivity is achieved by elements where the nodes of the same element interact between them. In meshless methods, the nodal connectivity is enforced by concentric areas or volumes formed by the nodes inside them. These area or volume form the influence-domain (or influence-cell in NNRPIM) of an interest point. The nodal connectivity achieved by overlapping the influence-domains (or influence-cells) [77].

Then, using approximation or interpolation shape functions, the field variables are obtained in order to find the equation system. In the case of RPIM and NNRPIM, interpolation functions are used, being based on the combination of the radial basis functions (RBF) with the polynomial basis functions. Besides that, the interpolation functions present the delta Kronecker property, which

assures that the obtained function passes through all nodes inside the influence-domain/influence-cell and allows the use of direct imposition techniques to impose boundary conditions [77].

Briefly, meshless methods require the construction of: influence-domains/influence-cells (to establish the nodal connectivity), background integration points (to integrate the integro-differential equations), and on shape functions (to build the local system of equations). Thus, the next points will explain these main steps for RPIM and NNRPIM formulations [77].

4.2.2 - Nodal Connectivity

4.2.2.1 – RPIM

Nodal connectivity is imposed after the discretization of the domain. In RPIM, the nodal connectivity is acquired with the overlap of the influence-domain of the nodes. An influence-domain, as seen before, it is an area (2D) or volume (3D) that encompass some number of nodes of the domain, which can present a fixed/variable size and different shapes, leading to a different nodal connectivity (**Figure 4.2**) [77].

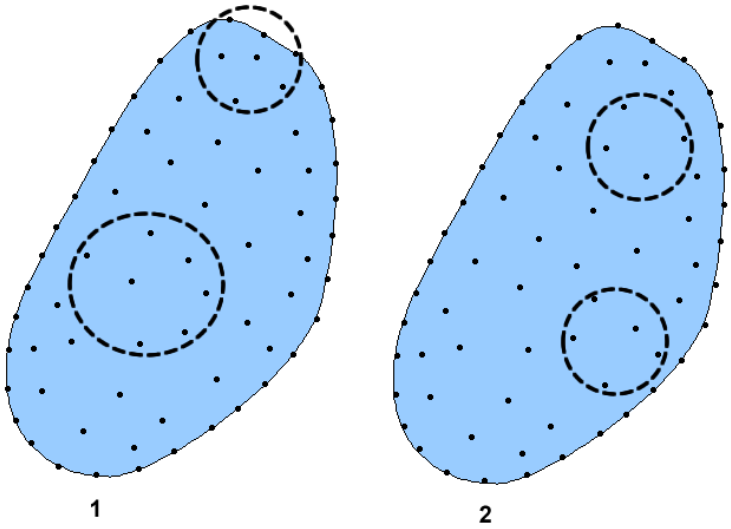

Figure 4.2 - Circular influence domain: 1) with variable size; 2) with fixed size.

However, influence-domains with fixed and regular shape can imply a loss of accuracy since the nodal distribution may not be the same in all the domain (leading to influence domains with distinct number of nodes inside them, as **Figure 4.2** shows). So, to avoid that, RPIM use variable influence-domains, centred in the interest point x_I, which will perform the radial search of the n closest nodes, leading to influence-domains with the same n number of nodes [77].

4.2.2.2 – NNRPIM

The nodal connectivity in this meshless formulation is done by flexible influence-domains completely dependent on the nodal mesh arrangement, also called influence-cells since they are obtained by the geometric relation of the Voronoï cells from the Voronoï diagram, instead of radial distances [77, 84]. This diagram uses the concept of the natural neighbours and is applied to the nodal distribution in order to create the influence-cells [84].

The problem domain $\Omega \subset \mathbb{R}^2$ is discretized by the nodal set $\boldsymbol{N} = \{n_0, n_1, \ldots, n_N\} \in \mathbb{R}^2$ with $\boldsymbol{X} = \{\boldsymbol{x}_0, \boldsymbol{x}_1, \ldots, \boldsymbol{x}_N\}$ coordinates. Thus, the Voronoï diagram of $\boldsymbol{N}$ corresponds to the division of the domain in the sub-regions V_i (called Voronoï cells), which can be closed or convex, and are associated with a node n_i so that all points inside V_i are closer to n_i than any other node $n_j \in \mathbf{N} \wedge i \neq j$ [77]. Thus, the Voronoï cell is given by:

$$\boldsymbol{V}_i = \left\{ x_I \in \Omega \subset R^d : \|x_I - x_i\| < \left\|x_I - x_j\right\|, \quad \forall\, i \neq j \right\} \tag{4. 1}$$

With $\boldsymbol{x}_I$ being the interest point and $\|.\|$ the Euclidian metric norm (that is the distance between the interest point and the nodes defined by $\boldsymbol{x}_i$ and $\boldsymbol{x}_j$). **Figure 4.3** illustrates a generic way to obtain a two-dimensional (2D) Voronoï diagram [77].

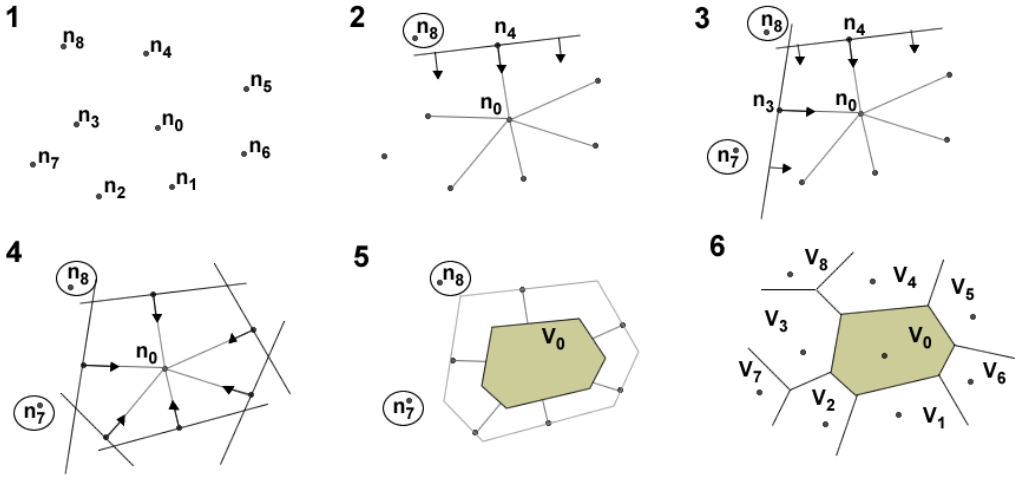

Figure 4.3 – Creation of Voronoï diagram: 1) initial node set; 2) first trial plane; 3) second trial plane; 4) provisional Voronoï cell; 5) Voronoï cell of $n0$; and 6) Voronoï diagram.

From the nodal set of **Figure 4.3** (1), the Voronoï cell of node n_0 is selected. It is intended to find the neighbouring nodes that need to be chosen, and exclude all the others. Thus, it is selected one node as the potential neighbour **Figure 4.3** (2), notice that nodes of n_1 to n_6 were chosen as potentials neighbouring nodes. Then, one of them, in this case, the node n_4, is selected.

Thereafter, vector $\boldsymbol{u}_{40}$ is written as:

$$\boldsymbol{u}_{40} = \frac{(x_0 - x_4)}{\|x_0 - x_4\|} \tag{4. 2}$$

With $\boldsymbol{u}_{40} = \{u_{40}, v_{40}, w_{40}\}$. From this, it is possible define a plane:

$$u_{40}x + v_{40}y + w_{40}z \geq (u_{40}\, x_4 + v_{40}\, y_4 + w_{40}\, z_4) \tag{4. 3}$$

Then, all the other nodes of the domain are tested with the previous equation, substituting their nodal coordinates into the equation. If the equation is not satisfied, the tested node is definitively removed as neighbour node of node n_0. This process is repeated for all nodes in the problem domain, **Figure 4.3** (3-4). In end, only the neighbour nodes will remain, **Figure 4.3** (5). Repeating this process (1-6) for each node discretizing the problem domain, it is possible to achieve the final Voronoï diagram. Using the Voronoï diagram, two types of influence-cells can be established (Fig. 4.4), taking into account the level of nodal connectivity: the first-degree influence-cells (a) and the second-degree influence-cells (b) [77].

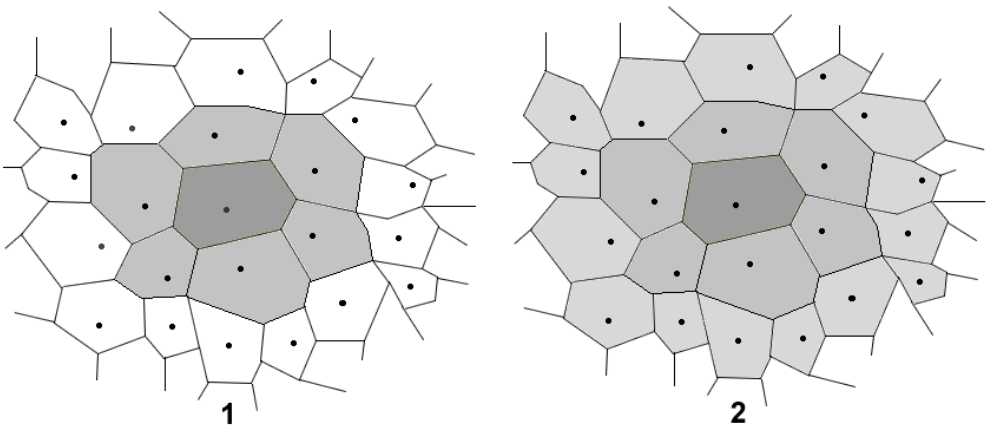

Figure 4.4 – Types of influence-cells: 1) first-degree influence-cell; 2) second-degree influence-cell.

The first-degree influence cell only considers the natural neighbours of the interest point. On the other hand, the second-degree influence cell considers the natural neighbours of the interest point and, in addition, the natural neighbours of those first natural neighbours. Since it present larger influence-domains, the results obtained with second-degree influence-cells are better when compared to the first one [77].

4.2.3 - Numerical Integration

4.2.3.1 – RPIM

The Gauss-Legendre quadrature scheme is used in RPIM for numerical integration (**Figure 4.5**). After the background mesh is created, the initial grid-cell must be transformed into an isometric square, in order to distribute the Gauss-Legendre quadrature points inside it. Using **Figure 4.5** as an example, a cell is selected **Figure 4.5** (1) and it is transformed into the isoparametric square **Figure 4.5** (2), in this case, a 2x2 quadrature [77].

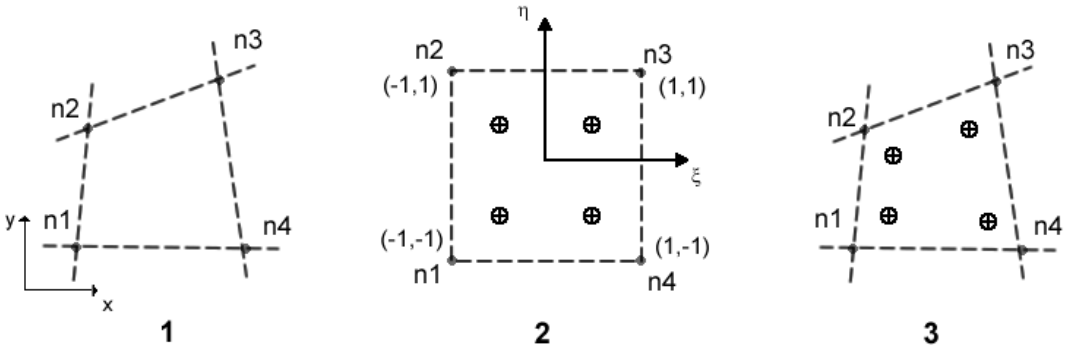

Figure 4.5 - Gauss-Legendre quadrature scheme: 1) Initial quadrilateral; 2) Isoparametric square; and 3) Initial shape.

After that, the isoparametric interpolation functions, N_i, are defined for this case as:

$$\begin{aligned} N_1(\xi,\eta) &= \frac{1}{4}(1-\xi)(1-\eta) \\ N_2(\xi,\eta) &= \frac{1}{4}(1-\xi)(1+\eta) \\ N_3(\xi,\eta) &= \frac{1}{4}(1+\xi)(1+\eta) \\ N_4(\xi,\eta) &= \frac{1}{4}(1+\xi)(1-\eta) \end{aligned} \tag{4. 4}$$

Note that triangles also can be used, being just necessary to adapt the equations. From this, it is possible to obtain the Cartesian coordinates of the quadrature points through the integration weight of the quadrature point [77].

$$x = \sum_{i=1}^{m} N_i(\xi, \eta) \cdot x_i$$
$$y = \sum_{i=1}^{m} N_i(\xi, \eta) \cdot y_i \qquad (4.\ 5)$$

With m being the number of nodes inside the grid-cell and x_i and y_i the Cartesian coordinates. The weights of the isoparametric integration points are fixed values and can be found both for quadrilaterals and triangles [77].

Note that, if the cell grid that discretize the domain is larger than it, the integration points that do not belong to it, must be eliminated. This procedure is recurrent in meshless methods since it is preferable use regular integration mesh in order to reduce the computational cost of the analysis (**Figure 4.6**) [77].

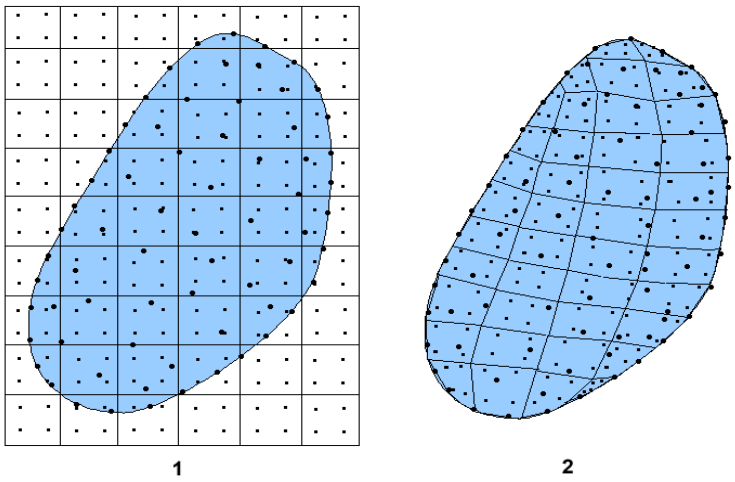

Figure 4.6 - Cell grid to discretize the domain 1) Regular grid integration mesh; 2) Fitted background mesh.

4.2.3.2 – NNRPIM

After Voronoï diagram be built, with nodal distribution, it is obtained the integration mesh. For such, it is necessary use the Delaunay triangulation, which is the geometrical dual of the Voronoï diagram. The Delaunay triangulation is used to construct the nodal dependent background integration mesh (**Figure 4.7**). The Delaunay triangulation subdivided the Voronoï cells, by connecting the nodes to the ones that have common boundaries. Overlapping the Delaunay triangulations with the influence-cell boundaries, smaller sub-cell are obtained [77].

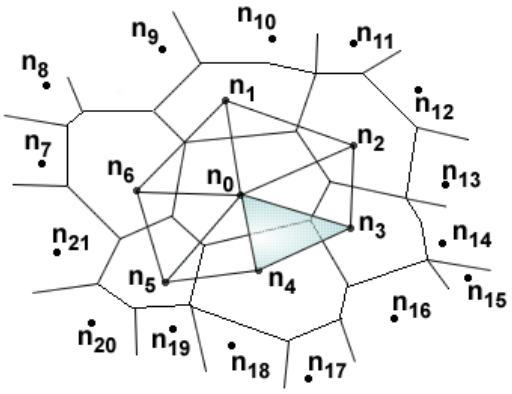

Figure 4.7 - Delaunay triangulation taking into account the initial Voronoï diagram.

The number of sub-cells (k) of each cell is equal to number of neighbour nodes of its central node n_I, being the cell area, A_{V_I}, equal to the sum of the areas of the sub-cells, $A_{S_{Ii}}$ [77]:

$$A_{V_I} = \sum_{i=1}^{k} A_{S_{Ii}}, \qquad \forall A_{S_{Ii}} \geq 0 \tag{4. 6}$$

The Voronoï cell is identified by the corners of the polygon, P_{Ii}, and its middle points, M_{Ii} . If the nodes of the cell are arranged irregularly, the corresponding sub-cells will present a quadrilateral form (**Figure 4.8**) [77].

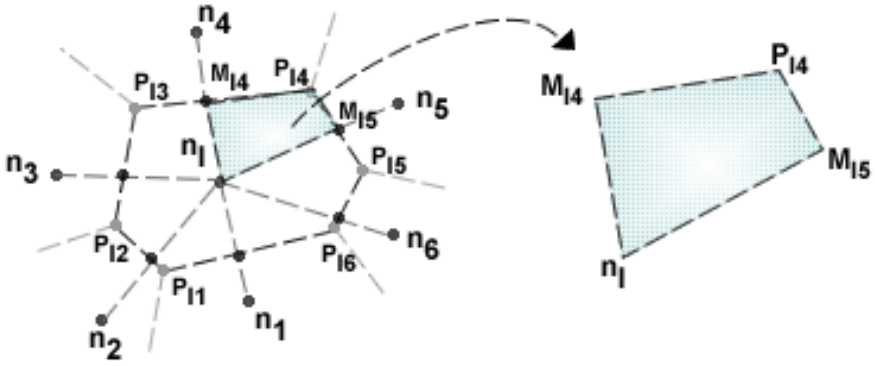

Figure 4.8 - Voronoï cell with intersection points (P_{Ii}) and middle points (M_{Ii}) and the generated quadrilaterals.

On the other hand, if the nodes are regularly arranged, the sub-cells will present a triangular form (**Figure 4.9**).

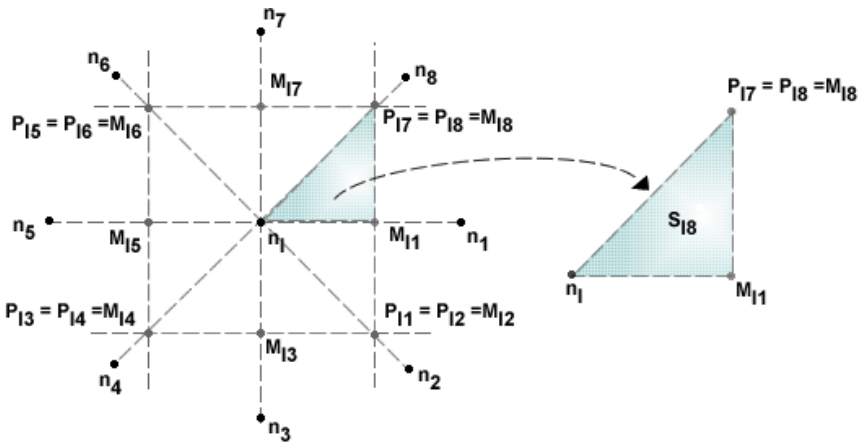

Figure 4.9 - Voronoï cell with intersection points (P_{Ii}) and middle points (M_{Ii}) and the generated triangles.

Thereafter, it is used the Gauss-Legendre numerical integration in order to establish the numerical integration. Thus, integration points are placed on the barycentre of sub-cells and their location is determined in each sub-cell [77].

In the literature various integration schemes are available, with different numbers of integration points. However, the simplest presents only a single point in the centre of each sub-cells and the integration weight is the area of the corresponding sub-cell. Thus, the use of one integration point is sufficient in order to obtain a precise integration (**Figure 4.10**) [77].

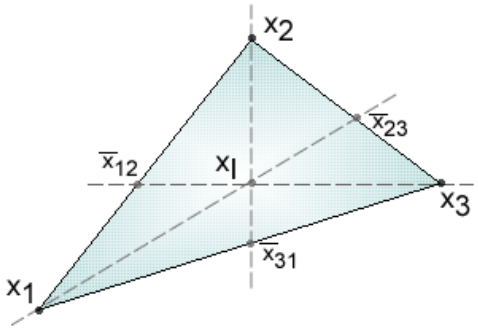

Figure 4.10 – Representation of one integration point x_I.

If more integration points are required, the sub-cell need to be divided again, taking into account the centre point and the middle points of the edges (**Figure 4.11**) [77].

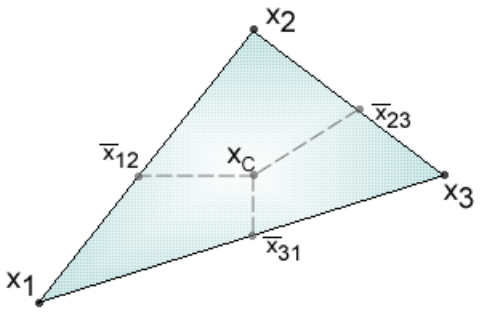

Figure 4.11 - Division of the sub-cells in quadrilaterals.

To obtain the integration mesh, this process is repeated for all Voronoï cells, which will compose the Voronoï diagram.

4.2.4 - Interpolation Shape Functions

Shape functions, as mentioned before, allow to interpolate the unknown field functions, obtaining thus, the numerical solution. RPIM and NNRPIM use the same procedure to construct the interpolation functions – the radial point interpolation (RPI) technique. Generally, shape functions constructed with the RPI technique possess the delta Kronecker property. If delta Kronecker property exists, the essential boundary conditions can be imposed using simple imposition techniques, as the ones used in FEM [77].

Thus, both methods use the RPI technique to construct the interpolation function $u(\boldsymbol{x})$, combining a RBF $R_i(\boldsymbol{x})$ and a polynomial base function $p_j(\boldsymbol{x})$ [61].

So, considering the function $u(\boldsymbol{x})$ at a point of interest $\boldsymbol{x}_I$, defined in the domain Ω, and discretized by a set of n nodes inside the influence domain or the influence-cell:

$$u(\boldsymbol{x}_I) = \sum_{i=1}^{n} \boldsymbol{R}_i(\boldsymbol{x}_I) \cdot \boldsymbol{a}_i(\boldsymbol{x}_I) + \sum_{j=1}^{m} \boldsymbol{p}_j(\boldsymbol{x}_I) \cdot \boldsymbol{b}_j(\boldsymbol{x}_I) = \boldsymbol{R}^T(\boldsymbol{x}_I)\boldsymbol{a}(\boldsymbol{x}_I) + \boldsymbol{p}^T(\boldsymbol{x}_I)\boldsymbol{b}(\boldsymbol{x}_I) \quad (4.\ 7)$$

Such function $u(\boldsymbol{x})$ can be written as:

$$u(\boldsymbol{x}_I) = \{\boldsymbol{R}(\boldsymbol{x}_I)^{\mathrm{T}}, \boldsymbol{p}(\boldsymbol{x}_I)^T\} \begin{Bmatrix} \boldsymbol{a}(\boldsymbol{x}_I) \\ \boldsymbol{b}(\boldsymbol{x}_I) \end{Bmatrix} \quad (4.\ 8)$$

With $\boldsymbol{a}_i(\boldsymbol{x}_I)$ and $\boldsymbol{b}_i(\boldsymbol{x}_I)$ being the non-constant coefficients associated with the respective functions, which need to be determined [77]. Usually, it is considered that $m < n$, to assure a stable function and the vectors presented above can be written as:

$$\boldsymbol{R}(\boldsymbol{x}_I) = [R_1(\boldsymbol{x}_I)\ R_2(\boldsymbol{x}_I) \dots R_n(\boldsymbol{x}_I)]^{\mathrm{T}} \quad (4.\ 9)$$

$$\boldsymbol{P}(\boldsymbol{x}_I) = [p_1(\boldsymbol{x}_I)\ p_2(\boldsymbol{x}_I) \dots p_m(\boldsymbol{x}_I)]^{\mathrm{T}} \quad (4.\ 10)$$

$$\boldsymbol{a}^{\mathrm{T}}(\boldsymbol{x}_I) = [a_1(\boldsymbol{x}_I)\ a_2(\boldsymbol{x}_I) \dots a_n(\boldsymbol{x}_I)] \quad (4.\ 11)$$

$$\boldsymbol{b}^{\mathrm{T}}(\boldsymbol{x}_I) = [b_1(\boldsymbol{x}_I)\ b_2(\boldsymbol{x}_I) \dots b_m(\boldsymbol{x}_I)] \quad (4.\ 12)$$

The RPIM and the NNRPIM use the Multiquadrics (MQ) radial basis function, which is defined by the general form:

$$R(r_{Ii}) = (d_{Ii}^2 + c^2)^p \quad (4.\ 13)$$

With d_{Ii}, the Euclidian norm, as the distance between the relevant node $\boldsymbol{x}_I$ and the neighbour node $\boldsymbol{x}_i$, which can be given by $d_{Ii} = \sqrt{(x_i - x_I)^2 + (y_i - y_I)^2}$. Besides that, c and p represent two shape parameters that, to obtain accurate results, they must be defined as 0.0001 and 1.0001, respectively [77].

The literature allows several forms for the polynomial basis functions for 2D problems (null basis, constant basis, linear basis, quadratic basis, etc.) [77] Its general form is:

$$\boldsymbol{p}(\boldsymbol{x})^T = [1, x, y, x^2, xy, y^2, \dots] \quad (4.\ 14)$$

To assure a single solution [63, 77], it is defined an extra equation:

$$\sum_{i=1}^{n} p_j(\boldsymbol{x}_i) a_i(\boldsymbol{x}_i) = 0 \quad (4.\ 15)$$

Considering the equation (4. 8) and the previous assumptions, the equation can be reformulated in the next system:

$$\begin{Bmatrix} \mathbf{u}_s \\ \mathbf{0} \end{Bmatrix} = \begin{bmatrix} \boldsymbol{R} & \boldsymbol{P} \\ \boldsymbol{P}^T & \mathbf{0} \end{bmatrix} \begin{Bmatrix} \boldsymbol{a} \\ \boldsymbol{b} \end{Bmatrix} = \boldsymbol{M} \begin{Bmatrix} \boldsymbol{a} \\ \boldsymbol{b} \end{Bmatrix} \quad (4.\ 16)$$

In which $\boldsymbol{u}_s$, $\boldsymbol{R}$ and $\boldsymbol{P}$ (polynomial basis), considering a 2D problem, can be defined as:

$$\boldsymbol{u}_s = \{u_1, u_2, \dots u_n\}^T \quad (4.\ 17)$$

$$\boldsymbol{R} = \begin{bmatrix} R(r_{11}) & R(r_{21}) & \dots & R(r_{n1}) \\ R(r_{21}) & R(r_{22}) & \dots & R(r_{n2}) \\ \vdots & \vdots & & \vdots \\ R(r_{1n}) & R(r_{2n}) & \dots & R(r_{nm}) \end{bmatrix} \tag{4. 18}$$

$$\boldsymbol{P} = \begin{bmatrix} 1 & x_1 & y_1 & z_1 \\ 1 & x_2 & y_2 & z_2 \\ \vdots & \vdots & \ddots & \vdots \\ 1 & x_n & y_n & z_n \end{bmatrix} \tag{4. 19}$$

Thus, equation (4. 16) can be solve in order to determine the non-constant coefficients $\boldsymbol{a}$ and $\boldsymbol{b}$ through the resolution of the following equation:

$$\begin{Bmatrix} \boldsymbol{a} \\ \boldsymbol{b} \end{Bmatrix} = \boldsymbol{M}^{-1} \begin{Bmatrix} \boldsymbol{u}_s \\ 0 \end{Bmatrix} \tag{4. 20}$$

$$\boldsymbol{M}^{-1} = \begin{bmatrix} \boldsymbol{R} & \boldsymbol{P} \\ \boldsymbol{P}^T & 0 \end{bmatrix}^{-1} \tag{4. 21}$$

Such can be replaced in the equation (4. 8) and the shape function can be now defined as:

$$\boldsymbol{u}(\boldsymbol{x}_I) = \{\boldsymbol{R}^{\mathrm{T}}(\boldsymbol{x}_I)\, \boldsymbol{p}^{\mathrm{T}}(\boldsymbol{x}_I)\}\, \boldsymbol{M}^{-1} \begin{Bmatrix} \mathbf{u}_s \\ 0 \end{Bmatrix} = \{\Phi(\boldsymbol{x}_I), \Psi(\boldsymbol{x}_I)\} \begin{Bmatrix} \boldsymbol{u}_s \\ 0 \end{Bmatrix} \tag{4. 22}$$

Where vector $\Psi(\boldsymbol{x}_I)$, which do not possess a significant physical meaning, comes from the imposition equation: $\sum_{i=1}^{n} p_j(\boldsymbol{x}_i) a_i(\boldsymbol{x}_i) = 0$. Besides that, the interpolation functions $\Phi(\boldsymbol{x}_I)$, as mentioned before, possess the delta Kronecker property δ_{ij}:

$$\varphi_i(x_j) = \delta_{ij} \tag{4. 23}$$

For which:

$$\delta_{ij} = \begin{cases} 1 & if \quad i = j \\ 0 & if \quad i \neq j \end{cases} = 1 \ and \ \delta_{ij} = 0. \tag{4. 24}$$

This property allows to use direct imposition techniques to numerically apply the essential boundary conditions in the stiffness matrix, passing through all the nodes of the influence-domain/influence-cell [77]. Thus, the RPI shape function, $\Phi(\boldsymbol{x}_I)$, can be defined as $\Phi(\boldsymbol{x}_I) = \{\varphi_1(\boldsymbol{x}_I), \varphi_2(\boldsymbol{x}_I), \dots, \varphi_n(\boldsymbol{x}_I)\}$:

$$\{\Phi(\boldsymbol{x}_I), \Psi(\boldsymbol{x}_I)\} = \{\boldsymbol{R}(\boldsymbol{x}_I)^{\mathrm{T}}\, \boldsymbol{p}(\boldsymbol{x}_I)^{\mathrm{T}}\}\, \boldsymbol{M}^{-1} = \{\varphi_1(\boldsymbol{x}_I), \varphi_2(\boldsymbol{x}_I), \dots, \varphi_n(\boldsymbol{x}_I), \psi_1(\boldsymbol{x}_I), \dots, \psi_m(\boldsymbol{x}_I)\} \tag{4. 25}$$

Where n is the number of nodes inside the influence domain, and m the number of monomials of the polynomial basis [77].

4.3 - Fluid Flow Formulation

The formulation used in the present work is based on the flow theory proposed initially by Zienkiewicz, suitable for viscoplastic materials [85-87]. Contrary to solid formulations, the parameter of interest here is the velocity, and not the displacement.

Assuming a problem with a velocity $\boldsymbol{u}$, defined by $\boldsymbol{u} = \{v_x\ v_y\ v_z\}^T$, it is possible to define the strain rate $\dot{\boldsymbol{\varepsilon}}$, the primary cause of stress rate, through the next expression [86, 87]:

$$\dot{\boldsymbol{\varepsilon}} = \boldsymbol{S}\boldsymbol{u} \qquad or \qquad \dot{\boldsymbol{\varepsilon}}_{ij} = \frac{u_{i,j} + u_{j,i}}{2} \tag{4. 26}$$

Being $\boldsymbol{S}$ the strain operator matrix, defined by:

$$\boldsymbol{S} = \begin{bmatrix} \frac{d\varphi_1}{dx} & 0 & 0 & & \frac{d\varphi_n}{dx} & 0 & 0 \\ 0 & \frac{d\varphi_1}{dy} & 0 & & 0 & \frac{d\varphi_n}{dy} & 0 \\ 0 & 0 & \frac{d\varphi_1}{dz} & & 0 & 0 & \frac{d\varphi_n}{dz} \\ \frac{d\varphi_1}{dy} & \frac{d\varphi_1}{dx} & 0 & \dots & \frac{d\varphi_n}{dy} & \frac{d\varphi_n}{dx} & 0 \\ 0 & \frac{d\varphi_1}{dz} & \frac{d\varphi_1}{dy} & & 0 & \frac{d\varphi_n}{dz} & \frac{d\varphi_n}{dy} \\ \frac{d\varphi_1}{dz} & 0 & \frac{d\varphi_1}{dx} & & \frac{d\varphi_n}{dz} & 0 & \frac{d\varphi_n}{dx} \end{bmatrix} \tag{4. 27}$$

With φ being the shape function, and n the number of nodes of the studied element (or inside the influence-domain) [86, 87].

Stress tensor, $\boldsymbol{\sigma}$, can be written as sum of two contributions:

$$\boldsymbol{\sigma} = \boldsymbol{\sigma}_m + \boldsymbol{\sigma}_d = \{\sigma_{xx}\ \sigma_{yy}\ \sigma_{zz}\ \tau_{xy}\ \tau_{yz}\ \tau_{zx}\}^T \tag{4. 28}$$

Where $\boldsymbol{\sigma}_d$ is the deviatory stress tensor and $\boldsymbol{\sigma}_m$ is the mean stress tensor, characterized by a hydrostatic stress state [86, 87]. Note that the same can be assumed to $\dot{\boldsymbol{\varepsilon}}$:

$$\dot{\varepsilon} = \dot{\varepsilon}_m + \dot{\varepsilon}_d = \{\dot{\varepsilon}_{xx}\ \dot{\varepsilon}_{yy}\ \dot{\varepsilon}_{zz}\ \dot{\gamma}_{xy}\ \dot{\gamma}_{yz}\ \dot{\gamma}_{zx}\}^T \tag{4. 29}$$

Assuming vector $\boldsymbol{m} = \{1\ 1\ 1\ 0\ 0\ 0\}^T$ and knowing that the mean stress is equal to the pressure $\boldsymbol{p}$ associated with that hydrostatic stress state, it is possible to define $\boldsymbol{\sigma}$ using the following constitutive law:

$$\boldsymbol{\sigma} = \mu\, \boldsymbol{D_0}\, \dot{\boldsymbol{\varepsilon}} + \boldsymbol{m}p = \boldsymbol{C_D}\dot{\boldsymbol{\varepsilon}} + \boldsymbol{m}p \qquad or \qquad \sigma_{ij} = 2\mu \left(\dot{\varepsilon}_{ij} - \frac{\delta_{ij}\, \dot{\varepsilon}_{kk}}{3}\right) - \delta_{ij}p \tag{4. 30}$$

With μ being the viscosity, $\boldsymbol{\sigma}$ the stress, δij the delta Kronecker and $\mathbf{C_{D,}}$ for a 3D problem, defined as:

$$\boldsymbol{C}_D = \frac{1}{3}\begin{bmatrix} 4\mu & -2\mu & -2\mu & 0 & 0 & 0 \\ -2\mu & 4\mu & -2\mu & 0 & 0 & 0 \\ -2\mu & -2\mu & 4\mu & 0 & 0 & 0 \\ 0 & 0 & 0 & \mu & 0 & 0 \\ 0 & 0 & 0 & 0 & \mu & 0 \\ 0 & 0 & 0 & 0 & 0 & \mu \end{bmatrix} \tag{4. 31}$$

One the other hand, $\dot{\boldsymbol{\varepsilon}}$ can also be written as:

$$\dot{\boldsymbol{\varepsilon}} = \frac{1}{\mu}\boldsymbol{D}^{-1}(\boldsymbol{\sigma} - \boldsymbol{m}p) \tag{4. 32}$$

And $\boldsymbol{D^{-1}}$ is:

$$\boldsymbol{D}^{-1} = \begin{bmatrix} 2 & 0 & 0 & 0 & 0 & 0 \\ 0 & 2 & 0 & 0 & 0 & 0 \\ 0 & 0 & 2 & 0 & 0 & 0 \\ 0 & 0 & 0 & 1 & 0 & 0 \\ 0 & 0 & 0 & 0 & 1 & 0 \\ 0 & 0 & 0 & 0 & 0 & 1 \end{bmatrix} \tag{4. 33}$$

This formulation allows to use the regular displacement-based methodology, changing the nodal displacements for nodal velocities [86, 87]. Thus, the velocity and pressure in an interest point given by:

$$\boldsymbol{u} = \boldsymbol{N}_u\overline{\boldsymbol{u}} \qquad and \qquad p = \boldsymbol{N}_p\overline{\boldsymbol{p}} \tag{4. 34}$$

With $\boldsymbol{N}_u$ being the shape functions of velocity and $\boldsymbol{N}_p$ of pressure, and $\overline{\boldsymbol{u}}$ e $\overline{\boldsymbol{p}}$ the vectors with nodal values [86, 87].

Taking the first and the (4. 30) equation s, these can be rewritten as:

$$\dot{\boldsymbol{\varepsilon}} = \boldsymbol{S}\boldsymbol{u} = \boldsymbol{S}\boldsymbol{N}_u\overline{\boldsymbol{u}} = \boldsymbol{B}\overline{\boldsymbol{u}} \tag{4. 35}$$

$$\boldsymbol{\sigma} = \mu\, \boldsymbol{D_0}\, \dot{\boldsymbol{\varepsilon}} + \boldsymbol{m}p = \boldsymbol{C_D}\, \boldsymbol{B}\overline{\boldsymbol{u}} + \boldsymbol{m}p \tag{4. 36}$$

Furthermore, as previous mentioned, for a Newtonian fluid, μ is constant however, in general viscoplastic materials, μ can be dependent on the strain rate and on the total accumulated strain, which introduced non-linearity to the problem [86, 87]. Thus, the μ of some viscoplastic materials can be defined as:

$$\mu = \frac{\sigma_y + \gamma \dot{\bar{\varepsilon}}^{\,m}}{3\dot{\bar{\varepsilon}}} \tag{4. 37}$$

With $\dot{\bar{\varepsilon}}$ being the second strain invariant, γ the fluidity parameter, and σ_y the uniaxial yield stress, which can be defined, for a strain hardening, as a function of a temperature T [86, 87].

$$\sigma_y = \sigma_y\,(\check{\varepsilon}, T) \tag{4. 38}$$

$$\dot{\bar{\varepsilon}} = \left(\frac{2}{3}\dot{\varepsilon}_{ij} \cdot \dot{\varepsilon}_{ij}\right)^{\frac{1}{2}} \tag{4. 39}$$

If pure elasticity is assumed, thus γ = 0 and the strain hardening can be omitted. Therefore, exists momentum conservation (4. 40) and incompressibility (4. 41), so the governing equations can be written as:

$$\boldsymbol{S}^T\boldsymbol{\sigma} + \boldsymbol{b} = 0 \qquad or \qquad \sigma_{ij,i} + b_i = 0 \tag{4. 40}$$

$$\boldsymbol{m}^T\boldsymbol{S}\boldsymbol{u} = 0 \qquad or \qquad \frac{du}{dx} + \frac{dv}{dy} = 0 \tag{4. 41}$$

Where $\boldsymbol{b}$ is the body force (defined as $\rho\boldsymbol{f}$) and $\boldsymbol{S}$ the strain operator, defined above. Note that, in an incompressible fluid, the dynamic forces are neglected [86, 87].

To omit the pressure from the problem resolution, penalty formulation is used in order to eliminate pressure variables at element level. The penalty is given by p/α, being α the penalty number, which is defined as $\alpha = 10^{7\sim10}\mu$ [86, 87].

Taking this into account, it is possible to rewrite the equation (4. 41):

$$\boldsymbol{m}^T\boldsymbol{S}\boldsymbol{u} = 0 \;\rightarrow\; \boldsymbol{m}^T\boldsymbol{S}\boldsymbol{u} - \frac{p}{\alpha} = 0 \;\leftrightarrow p = \alpha\boldsymbol{m}^T\boldsymbol{S}\boldsymbol{u} \tag{4. 42}$$

Thus, it is possible to substitute p in the equation (4. 40):

$$\boldsymbol{S^T C_D S u} - p\boldsymbol{\nabla} \; + \; \rho \boldsymbol{f} = 0 \; \leftrightarrow \; \boldsymbol{S^T C_D S u} - \; \boldsymbol{S^T \, m \, \alpha m^T S u} = - \, \rho \boldsymbol{f} \tag{4. 43}$$

With $\boldsymbol{\nabla} = \left\{\frac{d}{dx}, \frac{d}{dy}\right\}^T$ and ρ being the density of the fluid. Thus, it is possible to resolve the problem without the term of pressure [86, 87].

To use discrete methods, such as FEM, it is necessary to determine the weak form of the previous equation so, it is considered the virtual work principal, which considered a virtual displacement. Thus, the standard Galerkin discretization process leads to:

$$\int_{\Omega} \boldsymbol{B}^T \, \boldsymbol{C_D} \; \boldsymbol{B} \; d\Omega \, . \, \overline{\boldsymbol{u}} - \int_{\Omega} \boldsymbol{H}^T \, \boldsymbol{G} \; d\Omega \, . \, \overline{\mathbf{p}} = \; - \int_{\Omega} \boldsymbol{H}^T \, \boldsymbol{f} \; \rho \; d\Omega \tag{4. 44}$$

With $\boldsymbol{B}$, $\boldsymbol{H}$ and $\boldsymbol{G}$ defined as:

$$\boldsymbol{B} = \begin{bmatrix} \dfrac{\boldsymbol{d\varphi_i(x_I)}}{\boldsymbol{dx}} & 0 \\ 0 & \dfrac{\boldsymbol{d\varphi_i(x_I)}}{\boldsymbol{dy}} \\ \dfrac{\boldsymbol{d\varphi_i(x_I)}}{\boldsymbol{dy}} & \dfrac{\boldsymbol{d\varphi_i(x_I)}}{\boldsymbol{dx}} \end{bmatrix} \tag{4. 45}$$

$$\boldsymbol{H} = \boldsymbol{\varphi_i(x_I)} \begin{bmatrix} 1 & 0 \\ 0 & 1 \end{bmatrix} \tag{4. 46}$$

$$\boldsymbol{G} = \begin{bmatrix} \dfrac{dN_i(\boldsymbol{x}_I)}{dx} \\ \dfrac{dN_i(\boldsymbol{x}_I)}{dy} \end{bmatrix} \tag{4. 47}$$

The equation (4. 44) can also be written as:

$$\begin{bmatrix} \boldsymbol{K} & \boldsymbol{Q} \\ \boldsymbol{Q^T} & 0 \end{bmatrix} \begin{bmatrix} \overline{\boldsymbol{u}} \\ \overline{\boldsymbol{p}} \end{bmatrix} = \begin{bmatrix} \boldsymbol{f} \\ \mathbf{0} \end{bmatrix} \tag{4. 48}$$

Where

$$\boldsymbol{K} = \int_{\Omega} \boldsymbol{B}^T \, \boldsymbol{C_D} \; \boldsymbol{B} \; d\Omega \tag{4. 49}$$

$$\boldsymbol{Q} = \int_{\Omega} \boldsymbol{B}^T \, \boldsymbol{m} \, \boldsymbol{N}_p \; d\Omega \tag{4. 50}$$

$$\boldsymbol{f} = \int_{\Omega} \boldsymbol{N}_u^T \, \boldsymbol{b} \; d\Omega + \int_{\Gamma \, t} \boldsymbol{N}_u^T \, \boldsymbol{t} \; d\Gamma \tag{4. 51}$$

Which $\boldsymbol{K}$ being the stiffness matrix, $\boldsymbol{Q}$ the matrix that impose the incompressible condition and $\boldsymbol{f}$ the force [86, 87]. If the penalty condition is considered, then the previous system is defined as:

$$\begin{bmatrix} \boldsymbol{K} & \boldsymbol{Q} \\ \boldsymbol{Q^T} & \frac{\boldsymbol{I}}{\alpha} \end{bmatrix} \begin{bmatrix} \overline{\boldsymbol{u}} \\ \overline{\boldsymbol{p}} \end{bmatrix} = \begin{bmatrix} \boldsymbol{f} \\ \boldsymbol{0} \end{bmatrix} \tag{4. 52}$$

With $\boldsymbol{I}$ as the identity matrix. This leads to a single matrix element stiffness matrix given by:

$$\overline{\boldsymbol{K}}\overline{\boldsymbol{u}} = (\boldsymbol{k} - \boldsymbol{Q}\,\gamma\,\boldsymbol{Q^T})\,\overline{\boldsymbol{u}} = \boldsymbol{f} \tag{4. 53}$$

Which allows to obtain the final assembled non-linear equations that are given by:

$$\overline{\boldsymbol{K}}\,\overline{\boldsymbol{u}} = \boldsymbol{f} \rightarrow\ \overline{\boldsymbol{u}} = \overline{\boldsymbol{K}}^{-1}\,\boldsymbol{f} \tag{4. 54}$$

$$\overline{\boldsymbol{K}} = \ \overline{\boldsymbol{K}}\,(\boldsymbol{u}) \tag{4. 55}$$

$$\mu(\dot{\boldsymbol{\varepsilon}}) = \mu(\boldsymbol{u}) \tag{4. 56}$$

Which can be solved iteratively [86, 87].

Chapter 5

Discrete Numerical Methods for Blood Flow and Clot Formation

The complexity of the processes associated with the formation, growth and dissolution of thrombus leads to a complex analysis of the mathematical models associated with them. Thus, it is necessary to use computer simulations to solve them [57].

Numerical tests provide new ideas and allow for the creation of new biological hypothesis that can be first tested numerically, avoiding laboratory experiments and saving time [25]. Numerous computer simulations have been performed to study blood and blood coagulation. For this, several numerical methods have been proposed. These computational simulations are a powerful tool. However, the models used so far are still too simple, given the complexity involved in this specific field [88].

This chapter presents relevant numerical works done in the field of fluids, focusing mainly on the ones that analyse blood and blood coagulation. Thus, and taking into account the numerical methods selected in this present work, chapter 5 was divided in the works where FEM and Meshless methods were used.

5.1 - Discrete Methods

Mesh-based methods became popular to analyse fluids, such as blood. Finite Volume Method (FVM) is the most currently used, being the most popular used in this field, due to its simple implementation [70]. Regarding blood coagulation, the principal focus of this work, Finite Difference Method (FDM) solves blood clotting models in simple 2D geometries with structured

grids, and is the oldest and the simplest numerical method used for solving PDEs, mainly in simple and regular geometrical domains [56]. For example, Wang N. *et al*. study mathematical continuum models of platelet aggregation in vessels, with size of the coronary arteries or larger, through the FDM, being the fluid described by the Navier–Stokes equations [45]. However, the computational grid has to be sufficiently smooth, to maintain high accuracy on nonuniform meshes when FVM is used [70]. Besides that, when the domain becomes more complex, it cannot be used, so other alternative discrete methods need to be considered (such as FVM and FEM) to overcome the previous disadvantages [56, 70].

FVM is often implemented in commercial Computational Fluid Dynamics (CFD) codes [56]. For example, Sorensen E. *et al*. create a continuum 2D model to simulate the platelet-mediated thrombogenesis, sorting out the reaction rates for resting platelet surface, activated platelet-surface and activated platelet-platelet adhesion, and solve it by FVM [89]. After that, it has been calibrated against several sets of experimental results for platelet deposition on collagen, demonstrating good agreement with them [90]. Another example is the work done by Bodnár T. *et al*. that used a simplified version of an advanced model of clot growth and lysis to obtain preliminary numerical results of 3D simulations using a FVM, using a straight vessel with a circular cross-section. They suggest that fibrin concentration increase significantly in the clotting area and, due to advection, it is transported downstream in the injured wall region, as expected [49].

FEM is another alternative to FDM, although, in the past, it was mainly used for structural analysis, while FVM was preferred for the studying of fluid dynamics problems. Thus, the use of FEM applied to CFD only started in the 1980s, and was applied to thrombus formation much later [56].

Regarding Meshless methods, also discrete techniques, they are more recent when compared to the previous ones. So, their application in CFD as only occurred lately. SPH, for example, is a particle meshless formulation appropriate for simulating non-Newtonian flow, in simple or complex geometries and is the most popular methods used to study flow. For example, Chui and Heng used this method in adhesion and aggregation of platelets activated by low shear stress [56].

The number of studies that used Meshless methods is smaller when compared to the ones that used Mesh-based methods, however, it is important to stress that they also present good results when used, particularly concerning coagulation process.

5.1.1 – FEM

5.1.1.1 - FEM: Fluids

In the 1950's, modern FEM appeared with the advance of digital computer. FEM is a basic tool to solve ODEs and PDEs, being the first work published in this field in 1956, in the Aeronautical

Science Journal, being related to aircraft stress analysis [91, 92]. After that, FEM has been extensively used in fluid dynamics, heat transfer, and related areas [91].

In the 1960's, the principal focus of CFD, using numerical techniques, was aeronautic and nuclear industries, and, in the 1970's, the first implementation of FEM for the potential equation and the Navier-Stokes equations occurs [67], which was much later, when compared with its use in solid mechanics [93].

At the time of FEM development, simple flow problems were used, starting with the studies done by Zienkiewicz and Cheung [91]. In 1966, it was considered a simple case of anisotropy seepage, and a solution to a hypothetical problem using water was obtained by FEM [94]. After that, Martin H.C., use FEM in a potential flow problem [95, 96], and important problems in fluid mechanics, as applications of FEM, were reported in the following years [96-98]. Until the mid of 1970's, FEM was already applied to viscous and compressible flows, wave and stability phenomena, diffusion, dispersion and convection problems, lubrication, estuary flows, creeping flows, flows in porous media and a variety of other applications [93].

For example, in 1972, Oden and Wellford studied arbitrary fluids using FEM, demonstrating that this method presents great potential when applied to flow problems, in particular, viscous flows [91, 96]. Previously, they have also done some works to study unsteady compressible and incompressible flow, emphasizing, in this last case, isotropic Newtonian fluids with constant viscosities [96, 99-101]. Already in 1976, Eidelberg B.E. *et al.*, used FEM to analyse squeeze films between porous surfaces with a fluid film region. First, a simple example with uniform properties was used and then more complex examples demonstrated the power and versatility of FEM. Their work confirmed the extension of FEM to analyse lubrication of porous surfaces [102].

Regarding the 1980's, 1990's and to the following years, the number of studies that used FEM in CFD increased, as well as the development of faster algorithms for the treatment of 3D flows and the solution of more complex problems, such as the compressible Navier-Stokes equations with the interaction of shock-boundary layers [67, 103]. As example, Bathe KJ. and Zhang H. presented some solutions for fluid flow structural interaction analyses, considering some different materials (oil, steel and rubber), and assumed laminar and turbulent flow. They also presented an 'ideal' solution scheme for the laminar Navier-Stokes equations [13].

5.1.1.2 - FEM: Blood

The interest in modelling blood flow emerged long time ago. However, the development of realistic models has only started recently, in 1957. FEM just start to be used in the study of blood flow about 30 years [104]. Before that, numerous studies have been solved using only some types of numerical schemes and different types of vessels, in order to understand the mechanics of blood flow in the human vascular system [104, 105].

Two of the first studies using FEM were performed by Ray G. *et al.*, which provide velocity and shear stress profiles at the vessel walls, under laminar flow, considering a straight cylindrical tube [106]. The other one was performed by Porenta G. *et al.*, in order to investigate pulsatile flow in a segment of the femoral artery with arterial taper, branches and stenoses. The equations of the model were transformed into a system of algebraic equations by FEM, which was solved quickly, to obtain pressure and volume rates of flow, as functions of time and arterial position. With this study, they conclude that flow and pressure waveforms are significantly affected by moderate and severe stenoses [104].

In the 1990's, the use of computational techniques to understand vascular haemodynamics has increased. A huge number of 2D analyses have been performed in branched channels, as an approximation for vessels, emerging as a first step in the development of the computational framework. Baaijens J.P.W. *et al.*, studied the stationary blood flow in a 2D bifurcation model of the carotid artery, concluding that a steady generalized Newtonian blood flow can be well numerically solved using FEM [107]. Another common example used in literature, concerning vessel branches, is the 2D aortic bifurcation model. As example, it is possible to find in the literature the work of Chakravarty S. *et al.* (**Figure 5.1**) [108].

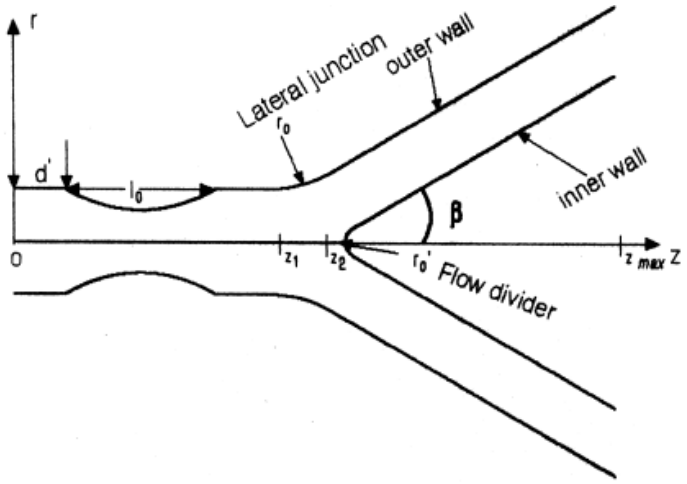

Figure 5.1 – Schematic draw of a stenosed bifurcated model. Adapted from [108].

On the other hand, some 3D analyses were also performed, such as the case of the work done by Perktold *et al.* and the work of Ethier *et al.*, who analyse the pulsatile flow in 3D models of bifurcations and bypass grafts [12]. Another example is presented by Parker D. *et al.* which created complex 3D patient-specific vessel models for numerical blood flow simulations through Computer Aided Design and Computer Aided Engineering technologies (**Figure 5.2**). To determine the exact blood flow conditions in clinical diagnoses or in surgical plan, it is important to re-create the real

characteristics of blood vessels, which can be done using real data and patient-specific vessel models (although, this is error-prone and time consuming) [105].

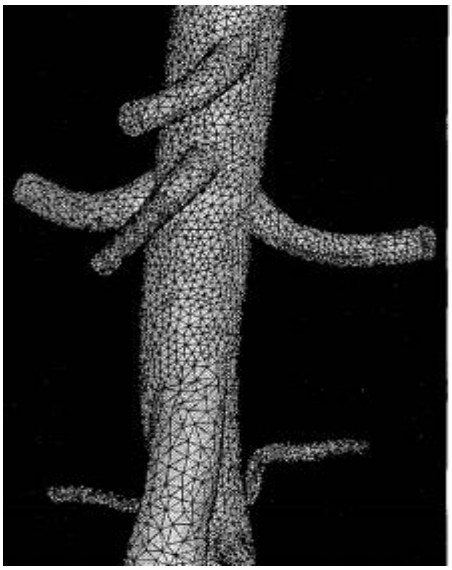

Figure 5.2 - Obtained model of a human artery and the respective mesh. Adapted from [105].

Numerical methods are useful to support experimental procedures and to allow the determination of flow variables that are normally difficult to obtain experimentally, such as, the wall shear stress. In 1995, a 3D numerical model of blood flow in the carotid artery bifurcation was developed and studied by Perktold K. *et al.*. They analysed the wall displacement and stress using FEM, obtaining their profiles during a pulse cycle [109].

Over the years, to make models more realistic, flexible vessels wall and pulsatile flow began to be considered. Lee S. H. *et al.*, investigate the effect of a flexible artery wall on the flow field to determine the wall shear stresses in the carotid artery wall, through numerical simulations using FEM in a straight flexible tube. Ku *et al.*, also studied the pulsatile flow in a flexible carotid bifurcation using FEM, taking into account the velocity profiles and the wall shear stress distributions, which allowed the comparison with experimental results [110].

Although, these previous assumptions make the analysis more complex and with higher computational cost, which make various authors choose to use steady fluid flow in rigid compartments. This can be acceptable in some parts of the vascular system, where the pulsatility of the flow is reduced, due to the compliance of the major arteries. A fixed geometry can also be reasonable, depending on the type of analysis, vessel and available data. Smaller vessels present smaller relative movement when compared to larger vessels. However, even in the last ones, the main characteristics of the flow were already acquired by a fixed model [11]. One example of this type of analyse is the work done by Hoogstraten H. *et al.*, which considerer a steady fluid flow in

a rigid tube of constant circular cross-section bent with shape of S, as a specific part of the femoral artery, to study the velocity of blood flow [111].

It is also important to emphasise that software and hardware technologies allowed the creation of idealized and patient-specific vascular models more easily and quickly. Another important advance was the development of noninvasive imaging techniques capable to obtain geometric solid models, by extracting anatomical surfaces or features from medical imaging data via CT, MRI, or other sources. Besides that, automatic mesh generation strategies, which operate directly on the model, save time in discretizing the continuous problem domain. Taylor C. A. *et al*. consider a finite element discretization of patient-specific abdominal aorta models, acquire from MRI, to conduct computational vascular research. Besides, it was possible to analyse a patient-specific aneurysmal abdominal aorta model, which allows, for the first time, the possibility of introducing predictive computational methods into vascular surgery planning [12]. Another example is the work done by Milner J.S. *et al.*, which also use MRI images of two normal volunteers, to create a 3D carotid bifurcation geometry in order to compute the wall shear stress [112]. Using CT images, the work performed by Oshima M. *et al*. is a good example, where a 3D model of a cerebral artery was constructed (**Figure 5.3**) to study the haemodynamics of blood flow (such as the flow patterns), under real flow conditions (**Figure 5.4**) [113].

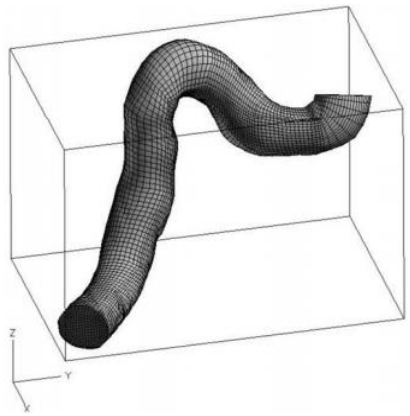

Figure 5.3 - Cerebral artery model obtained from CT images. Adapted from [113].

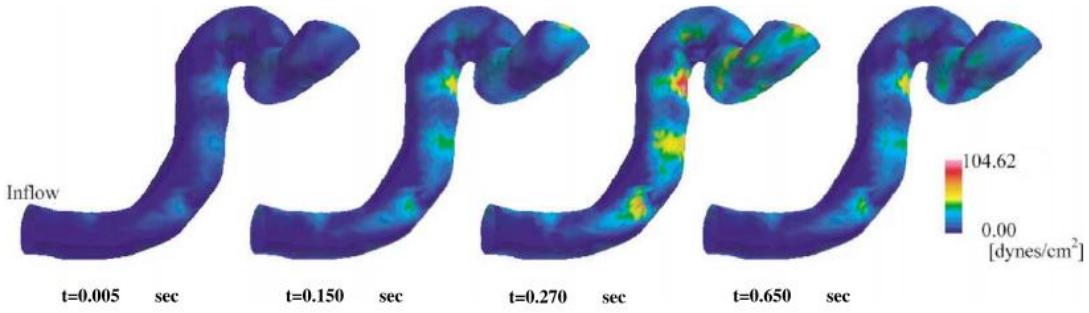

Figure 5.4 - Results of the surface traction obtained during the cardiac cycle. Adapted from [113].

Besides 2D and 3D, it also exists one dimensional (1D) blood flow simulation, which were proved to be an efficient tool to describe the characteristics of blood flow in the circulatory system. Nithiarasu P. *et al*. used a physical model that consists in a network of 63 elastic tubes representing blood flow in large arteries, including bifurcations and cross sectional discontinuities. In the end, they presented results, for example, of the pressure and flow for the thoracic and abdominal aorta [114]. Besides that, these models can be used as an alternative to 3D models, such as the work accomplished by Formaggia L. *et al.*, which presented lower complexity 1D models to compute the blood flow and pressure-wave propagation in the human vascular system [115]. 3D models of the whole arterial tree are not feasible, due to the elevate computation costs and the complexity to obtain and to manage all the geometric and physiologic information related with them. So, the idea of combine different dimensional models emerged. These types of models can be found in literature and, in some cases, can also be solved by FEM. Urquiza S. *et al.*, used a multidimensional 3D–1D model of the whole arterial tree, being a 3D model of a carotid bifurcation coupled with a 1D model for the remaining part of the arterial tree, in order to appropriately set inflow and outflow boundary conditions for the previous ones. The main objective was the evaluation of the computational requirements for an accurate representation of the phenomena, being obtained the flow patterns for an entire cardiac period (**Figure 5.5**), which were coherent with the general flow patterns reported in the literature [116].

Figure 5.5 – Volume difference between the systole and diastole. Adapted from [116].

Finally, it is also important to highlight that FEM was also used to support some surgical procedures, to study the influence of some vascular problems or even to understand the influence

of introducing an artificial body into the cardiovascular system. A recurrent example in literature is the study of stenose, which can be related to heart attack and stroke. Tang D. proposed a model with symmetric and asymmetric stenoses, assuming tube wall as hyperelastic, homogeneous, isotropic and incompressible. With this, Tang conclude that severe stenosis promotes significant compressive stress in the wall, which can cause atherosclerotic plaque rupture. Although, it was also possible to study the wall deformation, flow, pressure, velocity and shear stress fields [117].

Regarding surgical procedures, it is noted that bypass procedures are quite present in literature works, where FEM is applied. As last examples, the work done by Inzoli F. *et al*. has studied the fluid dynamics in a 3D model of an aortocoronary bypass (**Figure 5.6**) using a FEM approach [118], and the work of Bertolotti and Deplano analysed the flow patterns on the anastomosis of a stenosed coronary bypass (**Figure 5.7**) [119].

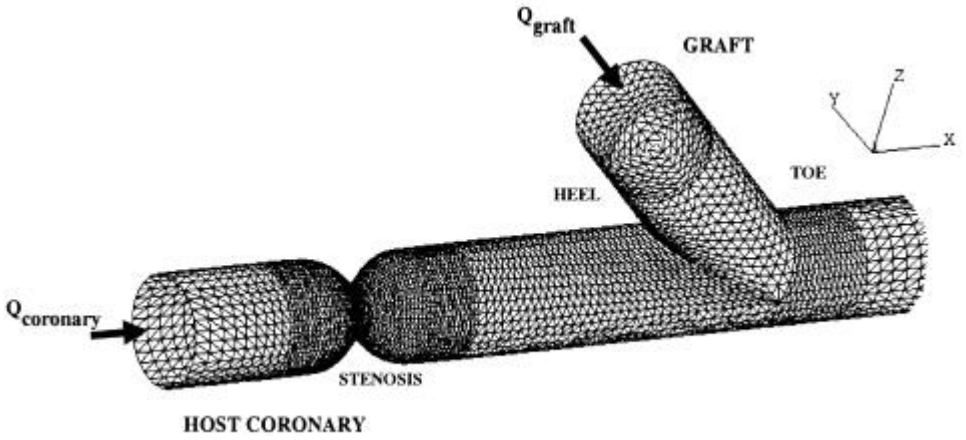

Figure 5.6 - Geometrical model used by Bertolotti and Deplano. Adapted from [119].

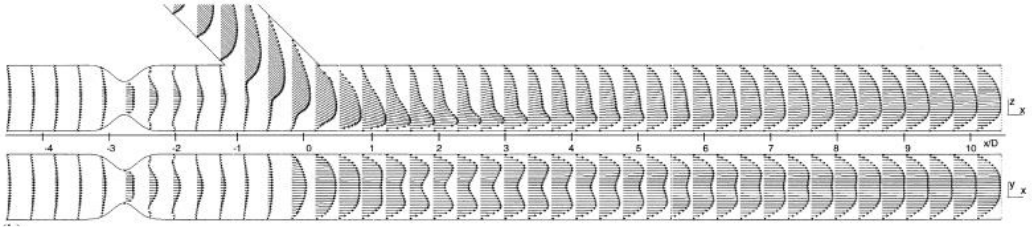

Figure 5.7 - Example of the velocity vectors obtained. Adapted from [119].

Although, several other interventions can be found in literature.

5.2.1.3 - FEM: Clots

As previous mentioned, FEM only started to be used in blood flow analysis in the 1980's, which conditioned the number of works dealing with blood coagulation and using this method. Thus, the number of works in this field using FEM is not vast, when compared with other themes.

In the 1990's, the interaction of flow in thrombus formation was a critical point for medical and engineering fields, since this was not totally understood at that time, and the quantitative data from well-defined experimental conditions was not common to find [120].

As said before, numerical studies can be used to understand fluid dynamics mechanisms. The first ones regarding blood haemostasis were related to measurements of blood platelet deposition, which allowed to obtain useful information, for example, of platelet deposition curves [121].

Affeld K., one of the pioneers in this theme, used a flow chamber as a model to study flow conditions by CFD, which allowed to assess to the platelet flow along the wall and the distribution of the shear rate in the chamber. The obtained results indicated that platelets were deposited at a defined shear rate, which could be compared with experimental results [120].

Another related work was performed by Bluestein D. *et al.*, which presented an aneurysm model to study the fluid dynamic mechanisms that characterize aneurysm deterioration, and its correlation with platelet deposition. This study showed that the recirculation zone formed inside the aneurysm cavity creates conditions that promote thrombus formation, being the obtained results correlated with experimental and in vivo results [121].

Aneurysm models used in numerical simulations are often found in literature due to their relevance for clinical field. However, they can also be related to thrombus formation, as seen in the previous work, and therefore some studies are directed for it.

Intraluminal thrombus can be found in abdominal aortic aneurysm. Mower W. R. *et al.*, examined how intraluminal thrombus affects abdominal aortic aneurysm wall stresses, through FEM, studying how the size, shape and material properties of the thrombus influence the same properties in aneurysm, which consequently influence the wall stress distributions [122]. A similar work was performed by Wang D. H. *et al*. [123].

A more recent and relevant work about this problem was performed by Li ZY. *et al*.. The main aim was to evaluate the impact of the calcification and intraluminal thrombus on abdominal aortic aneurysm (two factors that increase the risk of aneurism rupture), computing the wall stress distribution in 3D models constructed from CT images (**Figure 5.8**) [124].

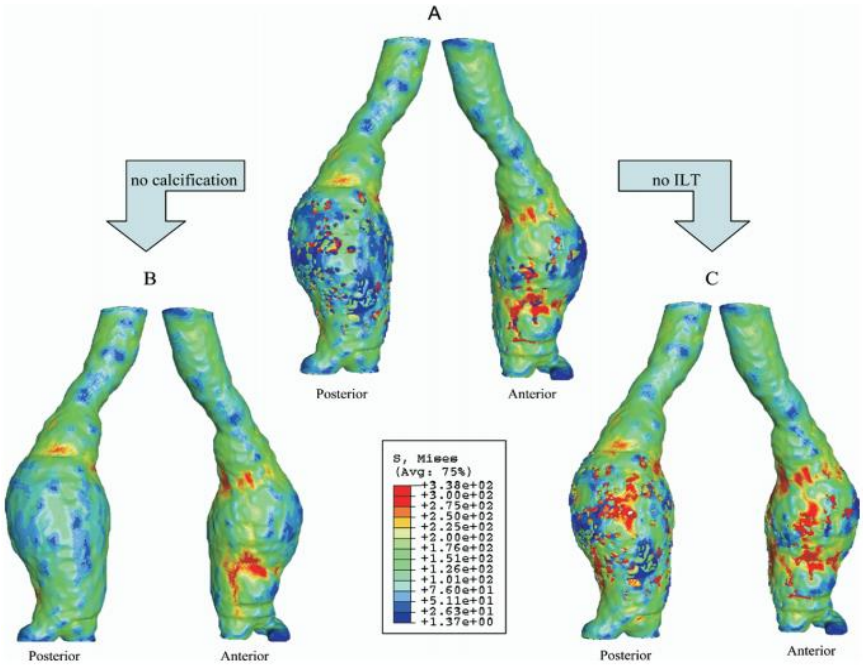

Figure 5.8 - Obtained results of wall shear distribution. Adapted from [124].

Regarding intraluminal thrombus, Wang J. *et al*. characterized it as an inhomogeneous and possibly isotropic material [123].

Due to the increase in the numbers associated with CVD, the interest in haemostasis and blood coagulation increased over the years. Arterial coronary stenoses can be associated with mural thrombosis and embolization, which can lead to myocardial infarction and sudden ischemic death [125]. Consequently, numerical studies emerged as a useful tool to understand the changes in normal behaviour of blood flow. For example, Bluestein D. *et al*. analysed the blood flow in a stenosis model and resorted to numerical predictions to describe the fluid dynamics that lead to platelet deposition, being confirmed by digital particle image velocimetry. With this, it was possible to verify that the deposition was dependent on the wall shear stress distribution, increasing in areas of flow recirculation and reattachment [125]. Another example was the work done by Karner G. *et al*. that used a 3D model with a mural microthrombus, modelled as a semisphere attached to a plane surface. The aim was to study numerically the flow effect on the concentration of platelet active substances, taking into account the shear stress at the inlet. For this, they analysed local concentrations of thrombogenic substances in the vicinity of the clot, with three different diameters, concluding that thrombin is the most important substance in the process of platelet activation [126].

In the 2000's, there was an increase of the number of papers regarding haemostasis and blood coagulation, which can also be related with the development of new mathematical models of the clot formation process, as well as the improvement in the knowledge of this subject.

A relevant work was performed Wootton *et al.*, in 2002, which analysed the mechanisms of formation and lysis of mural thrombus, under the influence of flow rate. For this, they used the model of Diamond and Anand and solved numerically the corresponding transport equation using FEM [56, 127].

After that, Weller propose a continuum model of platelet adhesion that is influenced by shear and by surface reactivity [56, 128], which he after improved to model the interaction between the platelet aggregates and the fluid flow, in order to make it a more realistic process [56, 129].

Besides that, Tokarev A. *et al.*, proposed a new PDE-based model to clot formation, solved by FEM, which considered erythrocytes, platelets and the processes of activation, secretion, and aggregation of platelets. This model can be easily extended to other mechanisms and integrated in other continuous blood flow models. However, this is a sufficiently complete quantitative model to study haemostasis mechanisms and regulation, and to considered pathologic processes, such as haemorrhage and thrombosis [130].

More recently, these models also allowed to predict some different disorder cases in coagulation process, such as, for example, the effects of abnormal values of antithrombin. Pavlova J. *et al.*, worked with a complex mathematical model, which incorporates the action of the biochemical and cellular components of blood, as well as the effects of the flow. Besides that, they also considered three different cases that can be related to some blood disorders: anticoagulant dominance (**Figure 5.9**), hypercoagulation and platelets deficiency. Furthermore, the numerical resolution was done using FEM and the results showed the clot evolution within the blood flow, during the propagation and fibrinolysis phases, in the different cases [25].

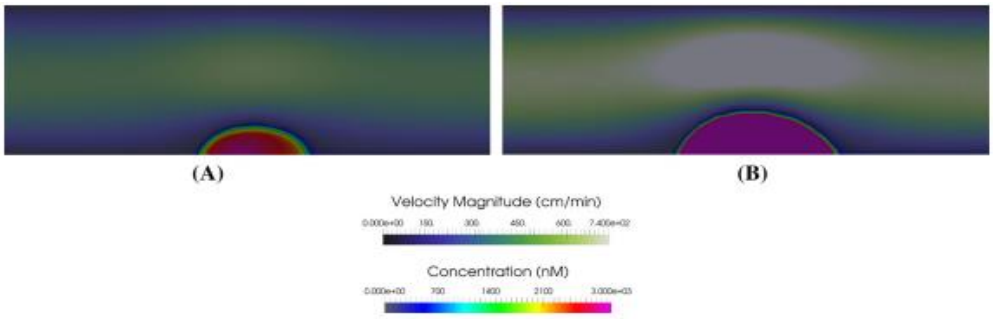

Figure 5.9 – Fibrin concentration and blood clot size: a) normal case; and b) ATIII excess. Adapted from [25].

With the advance of technology, more realist blood clot structures were possible to obtain through image-based modelling. Voronov R.S. *et al.* used a 3D clot structure to quantify transport within and around the clot, in order to define physical processes during thrombosis and limitations for drug delivery to the thrombus. For this, it was done a combination of in vivo experiments, biomedical imaging and computer simulations, to quantify the intrathrombic environment, which

is better than to use typical simulations that create mathematically the clot. In this case, FEM was used to validate the obtained results, which simulated an idealized homogeneous porous model of a thrombus in a blood vessel [131].

Once again, the construction of anatomically precise geometries is a progress in numerical studies, although, it is also costly, time consuming and, therefore, it is important to considerer the relevance of its use in each study [132].

When it comes up with blood clot formation, it is also important to consider the inhibitors that intervene in clotting process. Also, the recently use of multiscale approaches helps patient-specific simulation of this process under haemodynamic and pharmacological conditions.

As previous mentioned, during coagulation process, the platelets can activate and release some factors, such as ADP and thromboxane. Lu Y. *et al*. performed a patient-specific simulation of thrombosis using a multiscale approach to predict dynamic platelet deposition. In this, it was considered the wall-generated thrombin and platelet-released ADP/thromboxane convection-diffusion that were solved by FEM. Regarding the results, they were validated by comparison with real data and are clinical useful to understand how to use direct thrombin inhibitors and antiplatelet agents [133].

It is also important to highlight that exist few information available about the hemodynamic factors that influence the path taken by the clot in bloodstream, due to complexity of the phenomenon associated with the motion of a clot in a vessel network. However, predict its route would be an important step to understand and prevent, for example, strokes. One of the groups that cared about this lack of information was the Abolfazli E. *et al*.. They focused on the motion of a blood clot in a 3D human carotid artery bifurcation model, measuring the shear stress magnitudes in the inner wall and analysing the clot trajectory (**Figure 5.10**). Besides that, they also investigate the clot size and density, since it influences the motion velocity. In a previous work, they also studied this problem in a stenosed artery, taking into account the stenosis severity and the diameter of the clot. These studies were an important achievement, since they provide a framework for the prediction of embolic strokes in any patient-specific artery [132].

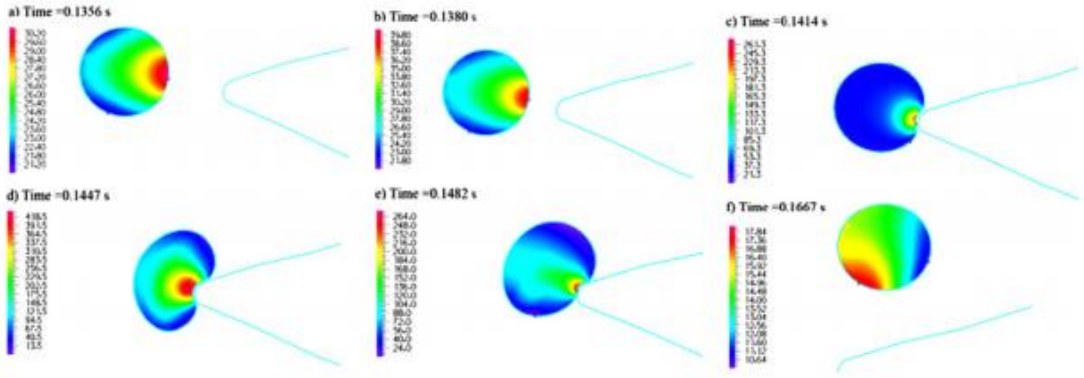

Figure 5.10 – Example of shear stress distribution in different positions of the clot. Adapted from [132].

Lastly, blood coagulation and haemostasis are not exclusively studied in cases of poor health or diseases, it is possible to find, in the literature, works that highlight the importance of the formation of blood clots to maintain the normal behaviour of the body. An interesting example is the work done by Vanegas-Acosta and Garzón-Alvarado, which regards the insertion of a dental implant. It is known that the healing process of injured tissues, after the insertion of this type of implants, initiates with the formation of a fibrin clot since it stops blood loss and favours osseointegration. However, it is important that there is an adequate formation, for the implant process to occur correctly. Therefore, the aim of their work was to introduce a mathematical model of the coagulation in the bone–dental implant interface, which was solved by FEM. With this, it was possible to obtain the distribution of spatial–temporal patterns in the bone–dental implant interface and to verify that they are in accordance with previous experimental results, in terms of reaction mechanisms and fibrin concentration needed [134].

5.1.2 - Meshless Methods

5.1.2.1 - Meshless Methods: Fluids

Meshless methods emerged as an alternative to the traditional methods like FEM [135] however, only recently, were they used in CFD in order to avoid mesh generation by discretizing the governing PDE's on dispersed clouds of points. Thus, very different approaches have been applied to a diversity of fields [136].

One of the firsts meshless methods used in CFD was the Finite Point Method (FPM) and the Boundary Element Method (BEM) [137]. In 1989, Grilli *et al*. presented a computational model for highly nonlinear 2D water waves solved by BEM [138]. In the same year, Kikani also used the BEM to analyse streamline generation in odd shaped reservoirs with multiple walls, which presents a good agreement for the classical methods in terms of accuracy and consistency [137, 139].

FPM was used in 1996 by Onate *et al*. [140], in solving 1D and 2D convection-diffusion and fluid flow type problems, obtaining excellent results in all cases. Before that, it was also used by Lohner *et al*. to study compressible flow problems, presenting similar accuracy when compared to equivalent mesh-based FVM or FEM. [137, 141].

SPH method, one of the most popular meshless methods in this filed, was used to analyse fluid flow in porous media, such as in the work performed by Holmes *et al*. which concluded that the obtained friction coefficient and permeability are in agreement with the existing benchmarks [137, 140]. This method was also applied to compressible viscous conductive flow problems, as in the work done by Chaniotis *et al*., or even to simulate fluids with free surfaces, as in the work done by Muller *et al*. or even to simulated the fluid droplets [137]. More recently, Noutcheuwa and Owens

developed a truly incompressible SPH method for application in the discretization of incompressible Navier-Stokes equations [137, 142].

EFGM or MLPGM method appeared in CFD in the 2000's. In 2000, Lin and Atluri solved 1D and 2D steady state convection-diffusion problems using MLPG, which has been further extended to solve steady-state 1D incompressible Navier-Stokes equation [137, 143]. Besides that, it was also used to study steady, non-isothermal fluid flow problems and to solve non-study 2D incompressible Navier-Stokes equations for different flow field problems and to simulate unsteady incompressible fluid flow problems [137]. Regarding EFG, it was used to examine 2D transient and steady state fluid flow problems in the work performed by Singh, in 2014, and to model incompressible fluid flow, as in the work done by Vlastelica *et al*.. In this last work, it was established that an increased number of free points per cell with increased number of integration points brings about more accurate results [137, 144]. More recently, Bhargava and Singh explored unsteady magneto-hydrodynamic flow of a non-Newtonian second grade viscoelastic fluid. It is important to stress that in both methods there is convergence and good agreement with FEM and other mesh-based methods [137, 145].

Also, it is important to emphasise that other methods, such as Reproducing Kernel Particle, Local Boundary Integral Equation and Singular Boundary method, can also be used in the referred field, and some works can be found in the literature [137].

Regarding RPIM, one of the methods that will be used in the present work, it is not common for it to be used in CFD, as in one of the first works published in 2003 by Liu *et al*.. They used this new method for solving coupled hydro-mechanical problems (1D and 2D) and showed that the obtained results presented good agreement with the classical methods [137]. RPIM was also used by Mužík, J., to analyse incompressible fluid flow, where the method constructs the shape functions, in combination with MLPG method to solve the incompressible Navier-Stokes equations [146].

5.1.2.2 - Meshless Methods: Blood

Blood flow is not very explored by meshless methods and it is difficult to find works done related to it. Recently, meshless methods using discrete particles were proposed to understand the behaviour of blood cells in the blood flow, such as the interactions among monocytes or the adhesive dynamics of rolling cell. For example, in the work performed by Tsubota, K. *et al*. in 2006, the moving-particle semi-implicit method was used to study the motion of a deformable 2D red blood cell in the blood flow, which allowed to demonstrated the capability of the proposed method to simulate this blood flow phenomena taking into account the size and deformability of red blood cells [147].

These methods also allow the reconstruction of vessel models through CT or MRI images. For example, Qin Y. *et al*., simulated blood flow in a stenosed artery with SPH method, using 3D straight

and curved arterial models acquired from CT images (**Figure 5.11**). This study showed the potential of SPH in virtual surgery system and in the use of the simulation results output in surgical procedures [148].

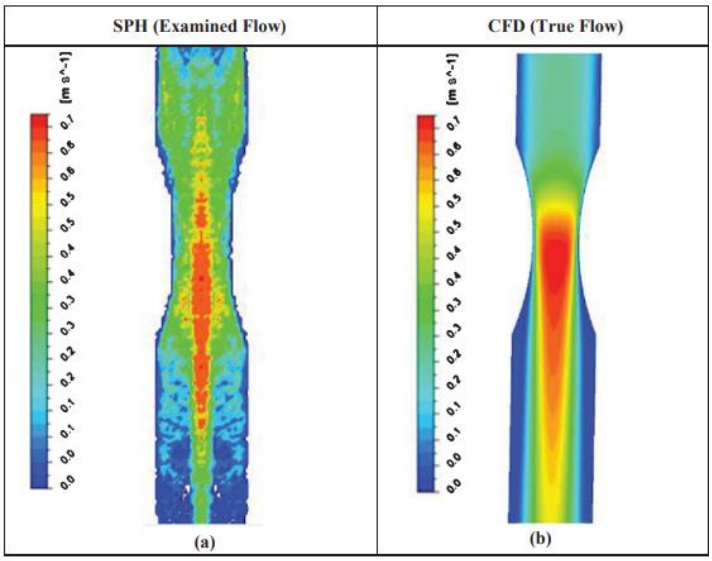

Figure 5.11 – Velocity profile obtained with SPH method and its comparison with the true flow profile. Adapted from [148].

Regarding models obtained from MRI images, the work presented by Caballero A. *et al.*, also using SPH method, is an example where they are used. In this, they try to understand the capability of the used method to simulate the blood flow dynamics in two realistic left ventricular models obtained by MRI and CT (**Figure 5.12**). In the end, it was possible to conclude that SPH is a promising tool for clinical predictions [149].

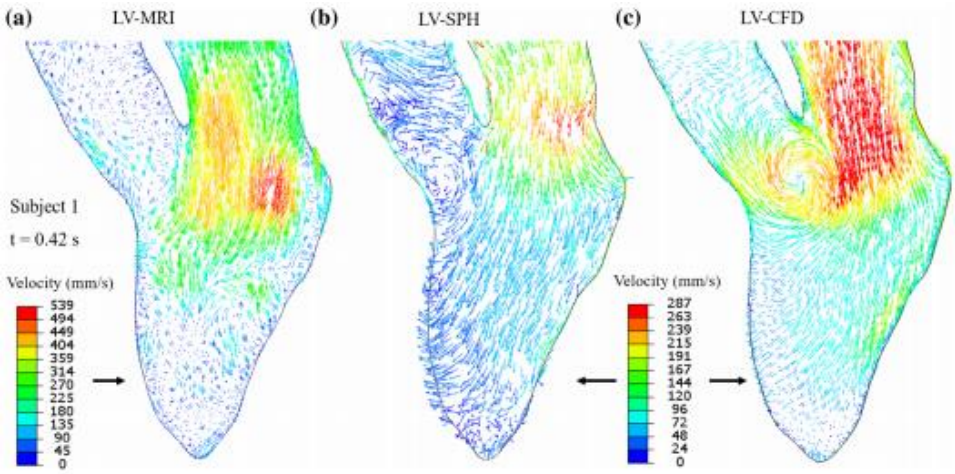

Figure 5.12 – Example of velocity vectors obtained by Caballero A. *et al.*. Adapted from [141].

Recently, in 2018, Karimi and Razaghi used SPH combined with FEM to simulate the blood as a fluid with free surfaces, to determine the vulnerable plaque on a basis of the induced stresses and deformations due to the interaction of the red blood cells, white blood cells and plasma, where the stress in the plaque, necrotic core and arterial layers were calculated and compared. With this work, it was possible to understand the role of red and white blood cells and plasma in providing useful information for the prediction of plaque vulnerability for medical and biomechanical experts, making it a novel approach in these blood numerical analyses [150].

5.1.2.3 - Meshless Methods: Clots

Computational and mechanical approach can also complement the experimental data, creating a new vision of the mechanisms that lead to thrombus formation, contributing to the development of future treatments. Considering just the primary haemostasis, Mori D. *et al*. used a computational analysis to study the influence of red blood cells in the transport, interaction and diffusivity of platelets when occur thrombus formation, by the Stokesian Dynamics method (**Figure 5.13**). They concluded that red blood cells play a significant role in primary thrombus formation and it also increases the number of platelets involved in the aggregate and accelerates the horizontal spread of the thrombus, while inhibiting the vertical growth. Thus, the importance of considering the presence of red blood cells when investigating the mechanism of thrombus formation is stressed [151].

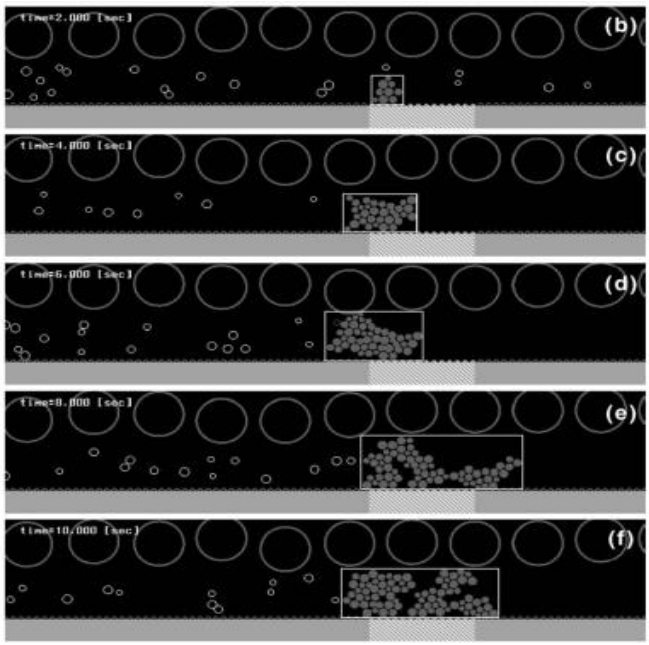

Figure 5.13 – Obtained results from clot formation. Adapted from [151].

Stokesian Dynamics Method is a particle method that uses the stoke equations to determine the interaction forces between particles in the fluid continuum combined with a discrete particle formulation. In another work, Mori D. *et al.*, using the same method, simulated thrombus formation under simple shear flow while taking into account the distinct behaviours of vWF and fibrinogen. Their results suggest that the consideration of the distinct roles of these different plasma proteins is essential in investigating the physiological and pathophysiological mechanisms of thrombus formation using a computational approach since, in these two cases, the adhered platelets subsequently recruited additional platelets, leading to platelet aggregation that built up a thrombus. So, the model has the potential to answer questions such as why does a thrombus progress at sites of disease and obstructs the vessel lumen, but does not develop to the point of obstruction in physiological haemostasis [88].

Recently, a Lagrangian-based CFD technique was introduced to analyse the behaviour of corpuscles and their interactions in blood flow where mesh generation is unnecessary. Significant difference were found when compared with the conventional Eulerian-based methods [73].

Kamada H. *et al*. used the Moving Particle Semi-implicit method, a particle method, to simulate the clot formation due to platelet aggregation under the influence of fluid. Thus, a 3D computer simulation in a rectangular channel was performed (**Figure 5.14**). It was possible to demonstrate that the growth rate of a thrombus, its height and time required from formation to its collapse, are dependent on the flow rate, which has an important role in thrombus formation [73].

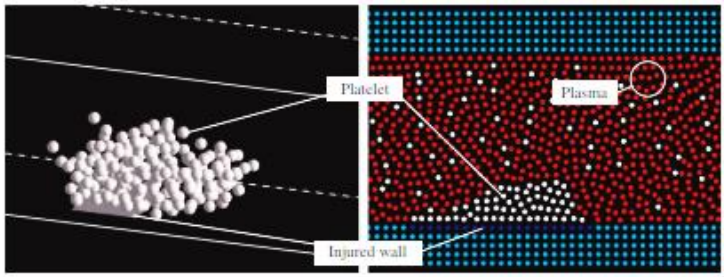

Figure 5.14 - Comparison between a 3D and a 2D clot formation model. Adapted from [73].

Haemodynamics are affected by alterations in geometry of the vessel, such as the ones that occur in atherosclerosis, which leads to the formation of stenoses. Kamada H. *et al*. attempted to evaluate the effects of stenosis geometry on primary haemostasis with a Particle Semi-implicit method. For this, they created a 2D model to simulate the clot formation in stenosed vessels (**Figure 5.15**). It was possible to verify that the presence of a stenosis induced changes in blood flow and, besides that, modified the formation, growth, and destruction of the clot. Moreover, they concluded that the number of platelets that adhered to the lesion increased with the severity of the stenosis as well as the shear stress, which influences the size of the clot and is coherent with experimental studies [152].

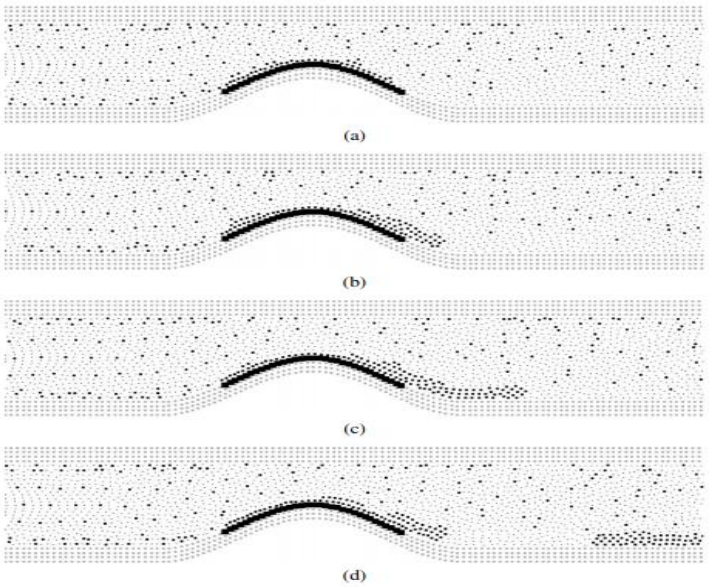

Figure 5.15 – Platelet aggregation in a stenosed model. Adapted from [152].

Another interesting example using meshless methods is the work performed by Tosenberger A. *et al.*, which developed a 2D hybrid model of a suspension of platelets in the plasma flow. This model was solved by DPD method with the aim of proposing a new possible mechanism of clot growth and growth arrest in normal healthy flow. As other models, it allows for the study of qualitative aspects of blood coagulation and it was used to investigate the influence of initial fibrinogen levels and of the fibrin production rate in the flow [55].

In a more specific case, simulations can help to evaluate and to predict some surgical approaches in order to make them more efficient and to minimize the occurrence of thrombogenesis. Sughimoto K. *et al.* analysed the mechanism of thrombus formation in the Fontan route through 2D computer haemodynamic simulation, using a particle method. They suggested that the local flow is dependent on the geometry of the vessel, which is a main factor in thrombus formation. Furthermore, it is also suggested that patients with reduced cardiac output are more likely to form a thrombus [153].

Finally, it is important to highlight that, normally, red blood cells and 3D models are not considered in these types of analyses, in order to reduce the complexity of the model and the simulation [55].

Regarding surgical procedures, endovascular intervention is one of the mainly used in interventional radiology. However, due to limited visual perception during the procedures, training is difficult. Thus, numerical simulation can be helpful for this specific case as well as other ones. For example, Chui and Heng, proposed a particle based rheological modelling method for medical simulation of vascular procedures, as virtual catheterization training applications. Blood was simulated as a non-Newtonian flow and a flow-related thrombus aggregation-dissolution scheme

was proposed, solved by SPH method (**Figure 5.16**). It was concluded that the presented model demonstrated the necessary feasibility in order to be used in endovascular simulations and very similar predictions in the clotting scheme were shown with the experimental results [154].

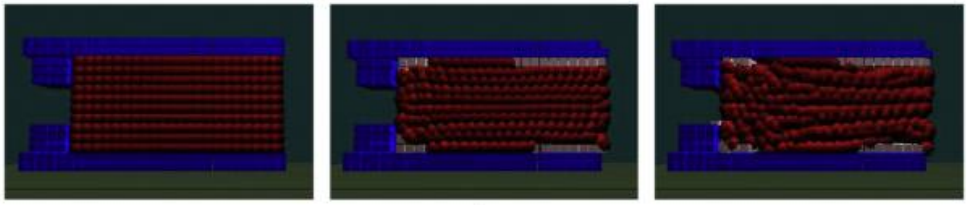

Figure 5.16 – Results of clotting. Adapted from [154].

Chapter 6

Preliminary Research Work

This chapter aims to present the work developed by the author during an initial research phase. The objective was to acquire the competences required for the successful development of the dissertation, such as autonomy in the use of the proposed software and becoming familiar with the distinct numerical methods selected and with the type of analysis intended. The main software's used were FEMAP (Siemens PLM Software, student version), which provides drawing tools to create a model and to construct the respective mesh, and FEMAS®, a Finite Element and Meshless Analysis Software (cmech.webs.com), which is a freeware academic software capable to analyse models using either the FEM or meshless methods (combined with several linear and non-linear formulations, such as the fluid flow proposed for this work). In addition, FEMAS allows the user to import an input file (INP file) such as the ones created in FEMAP. Besides that, this initial research phase also allowed to understand how the viscosity modify/affect the studied domain with the presence of blood clots.

6.1 – Analyse of Blood Flow

In order to acquire the knowledge previously mentioned, three 2D models representing a tubular straight artery and a 2D bifurcation artery model were created and discretized with different meshes with FEMAP (**Figure 6.1** and **Figure 6.2**) and one 2D bifurcation artery model with FEMAS (**Figure 6.4**). Only one of the tubular straight models does not possess a clot, such as the bifurcation artery model created by FEMAP. Besides that, different sizes for the clot were plotted

in the same model. Thus, it was possible to study the influence of the clot in the blood flow and how the flux is affected by the growth of the clot.

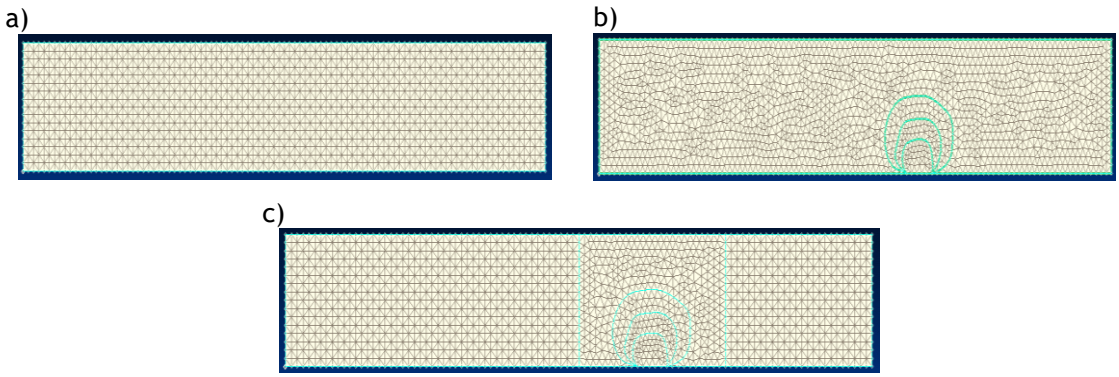

Figure 6.1 -Different meshes of the tubular model, obtain in FEMAP program: a) Regular, b) Irregular and c) Mixed mesh.

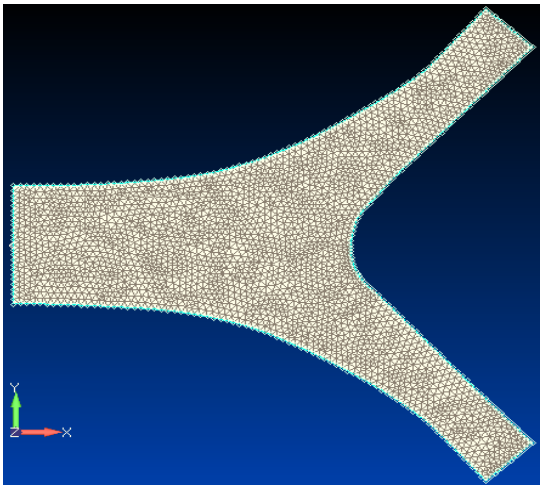

Figure 6.2 - Mesh of the bifurcated model, obtain in FEMAP software.

Besides that, for the models in **Figure 6.1** a) and **Figure 6.2**, a patch (which is a part of the domain) was defined to represent the blood. For the models presented in **Figure 6.1**b) and c), four patches were defined. Patch one was defined as blood and the other three, in a first analysis, were defined as blood as well (thus, all the domain was blood). Afterwards, for the model of figure 6.1 c), these three circular patches were defined as clot sequentially, in order to simulate a clot growth (**Figure 6.3**).

Thus, first, only the inner patch is defined as clot, then the inner and the middle clot is defined as clot and, finally, the three clot patches are defined as clot.

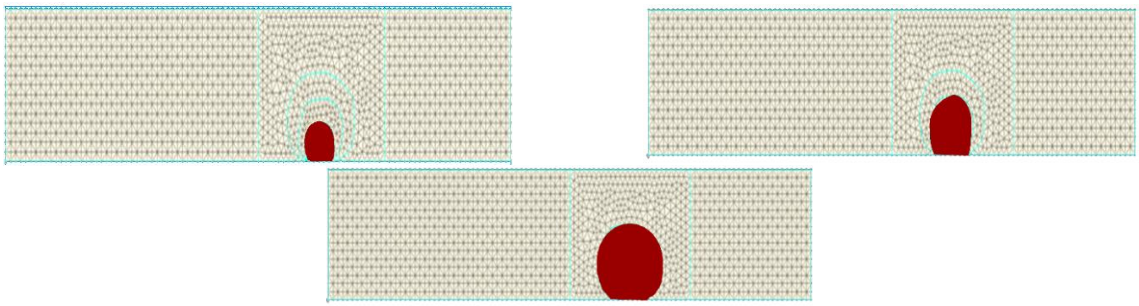

Figure 6.3 – Schematic representation of the different simulations of the clot: a) one patch defined as clot; b) two patches defined as clot; and c) three patches defined as clot.

For the bifurcation, a script was written in MATLAB to define a clot directly in the mesh (**Figure 6.4**).

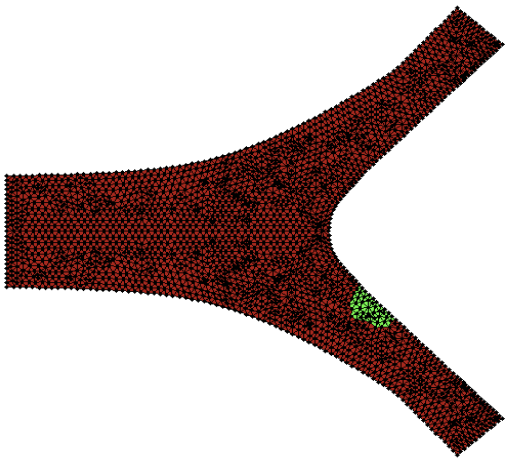

Figure 6.4 – Bifurcation model with clot, obtained with FEMAS software.

The fluid flow formulation encoded in FEMAS requires two parameters to define viscous fluids: the density and the viscosity. Accordingly to the literature, the value for the blood's density is 1050 kg/m^3 and the viscosity 3.5×10^{-9} Pa.s. These were the values used for this work and assumed as constants. Besides that, it was assumed that the blood was isotropic.

Blood possesses a complex rheology, however in this work it was considered a homogeneous flow.

The blood clot is considered as a homogenous viscous fluid, with the same density of blood, but with upper viscosity. The viscosity was assumed as 3.5 Pa.s.

For all models, it was imposed that the artery's wall is fixed over its length, in u and v directions, preventing its movement/slipping (**Figure 6.6**). This condition leads to a velocity of 0 along the wall. Besides that, assuming a laminar flow, a parabolic velocity profile was used for the

inlet (**Figure 6.5**), with a maximum velocity at the centre point of the parabola. The general equation of a parabola is given by:

$$v(y) = a_0 + a_1 x + a_2 x^2 \quad (6.\ 1)$$

Taking into account the previous assumptions (velocity in the walls is 0 and in the center of the artery is maximum) and knowing that x varies from 0 to 16 mm, it is possible to obtain the parameters a_0, a_1 and a_2, for a given velocity.

In this work, an initial velocity of 0.18 mm/s was selected and imposed to the model, as observed in **Figure 6.6**.

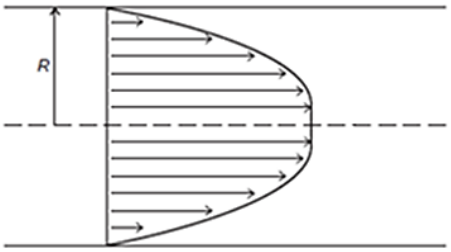

Figure 6.5 - Schematic representation of the parabolic velocity profile on the artery. Adapted from [155].

Also, it was assumed that the artery's wall is rigid since the duration of the simulation is short.

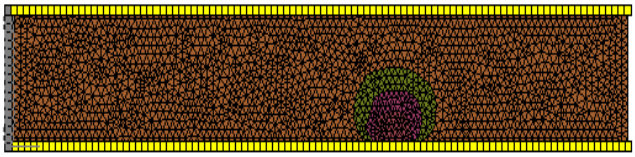

Figure 6.6 - Illustrative example of the boundary conditions imposed in the artery's wall and as initial velocity.

In order to simplify the analysis of the different models and shapes, the results were divided into two sections (tubular straight model and bifurcated model). The velocity maps, which can be observed in this work, present a colour gradient that varies from blue to red, being the blue colour the lower velocity locations and the red colour the highest velocity locations.

6.1.1.1 - Tubular Model

The next figure (**Figure 6.7**) represent the velocity maps of the different tubular models that were used, taking into account the chosen velocity and using FEM and RPIM.

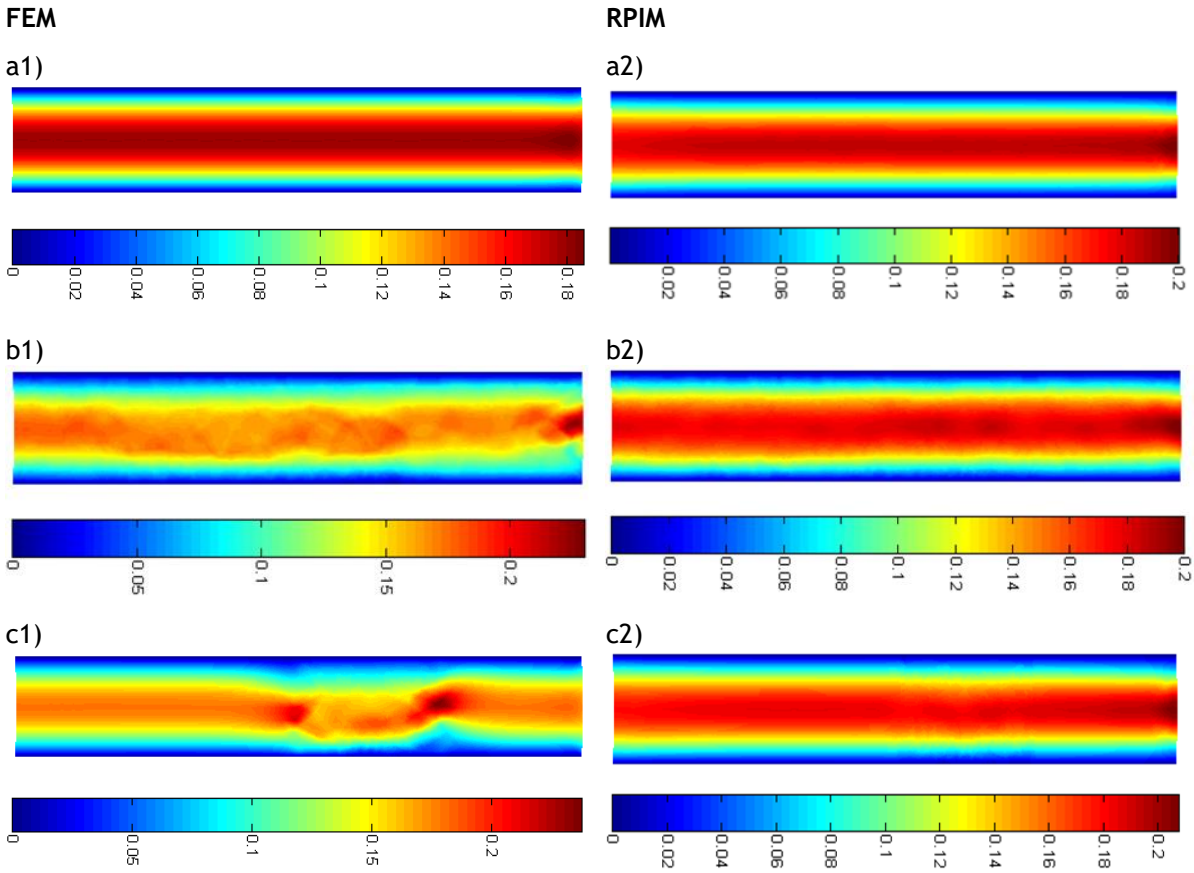

Figure 6.7 - Colour maps of the velocity profile obtained for the tubular models with the two methods: a) Regular mesh, b) Irregular mesh, c) Mixed mesh without clot.

Analysing the shown images, it is possible to verify the behaviour of the flow and the differences of the velocity along the artery.

On **Figure 6.7** a1), it is possible to verify that the model with the regular mesh exhibits a uniform flow, with a maximum velocity of 0.18 mm/s, as it was initially defined with both methods. Comparing with the irregular mesh using FEM (**Figure 6.7** b1)), it is apparent that there is a disturbance on the flow, which causes a non-uniform flow. However, with RPIM, this disturbance is reduced, presenting a more uniform flow.

On the other hand, **Figure 6.7** c1) shows a regular flow up until and after the clot area. An unexpected perturbation is visible in the clot area (notice that in this model, there is no clot, all domain is blood). Moreover, the maximum velocity is around 0.20 mm/s, in the area where the mesh changes, but, in the regular mesh area, the velocity is 0.18 mm/s. With RPIM, once again, this disturbance does not exist, with the flow being almost uniform in all its length.

In **Figure 6.8**, the results obtained considering a clot are shown. As already mentioned, three clots are studied a smallest one, medium one and a largest one.

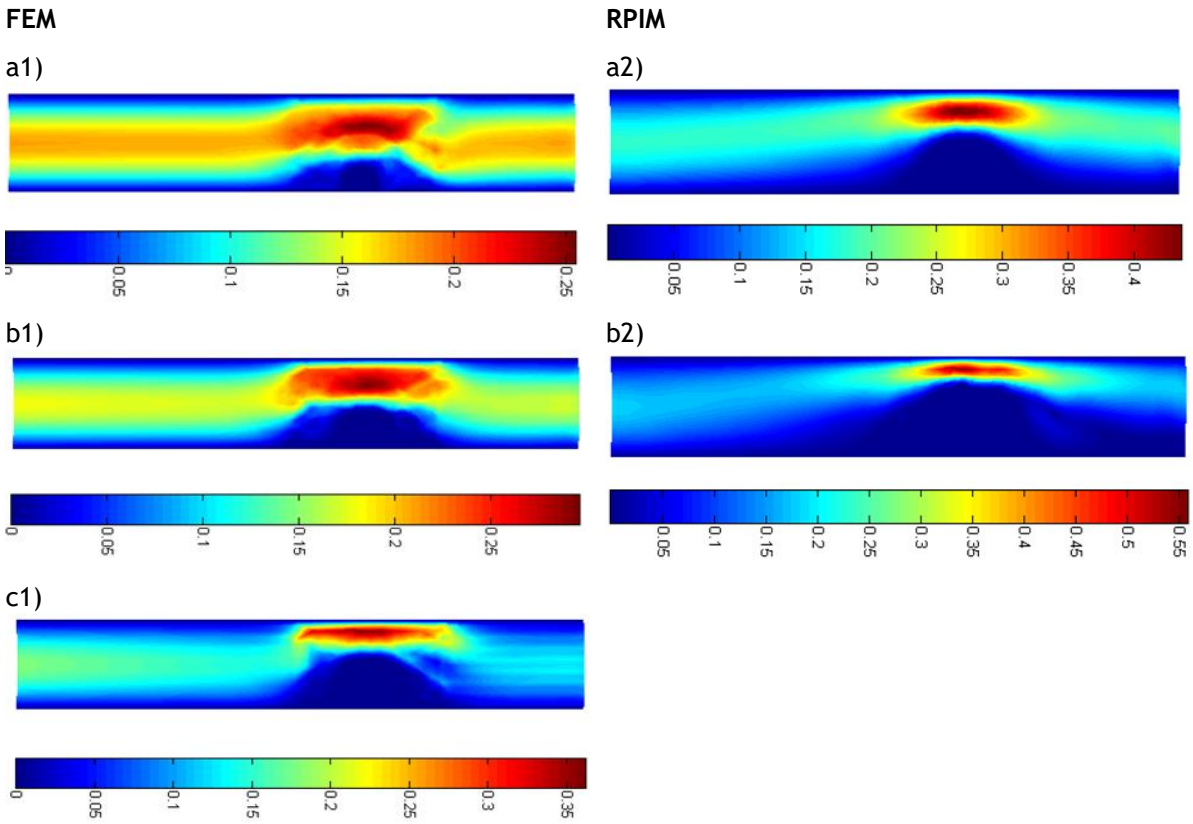

Figure 6.8 -Colour maps of the velocity profile obtained for the tubular models with mixed mesh and with the two methods: a) Smallest clot b) Medium clot and c) Largest clot

In all of the velocity maps of **Figure 6.8**, the velocity increases in the clot area with the decrease of the area that allows the passage of the fluid. The maximum velocities that were achieved using FEM are 0.25, 0.30 and 0.35 mm/s, respectively. In the regular region (before the clot), the flow is almost uniform and with a velocity around 0.18 mm/s.

Regarding RPIM, it is possible to verify that the flow is smother and more uniform however, the presence of the clot becomes more prominent, which promotes a blockage in the model with the largest clot and, for this reason, the results of RPIM with the largest clot are not shown.

To simplify the analysis of the previous figure, and to verify the behaviour of the flow, five sections were selected along the model. These correspond to $x = \{24, 49, 62, 75\,, 90\,\}\,\mathrm{mm}$, in order to obtain the velocity profile in different points of interest. These points represent the velocity in the inlet, immediately before the clot, in the clot area, immediately after the clot and in the outlet. The graphics shown in **Figure 6.9** represent the results obtained for the five selected sections, first with FEM.

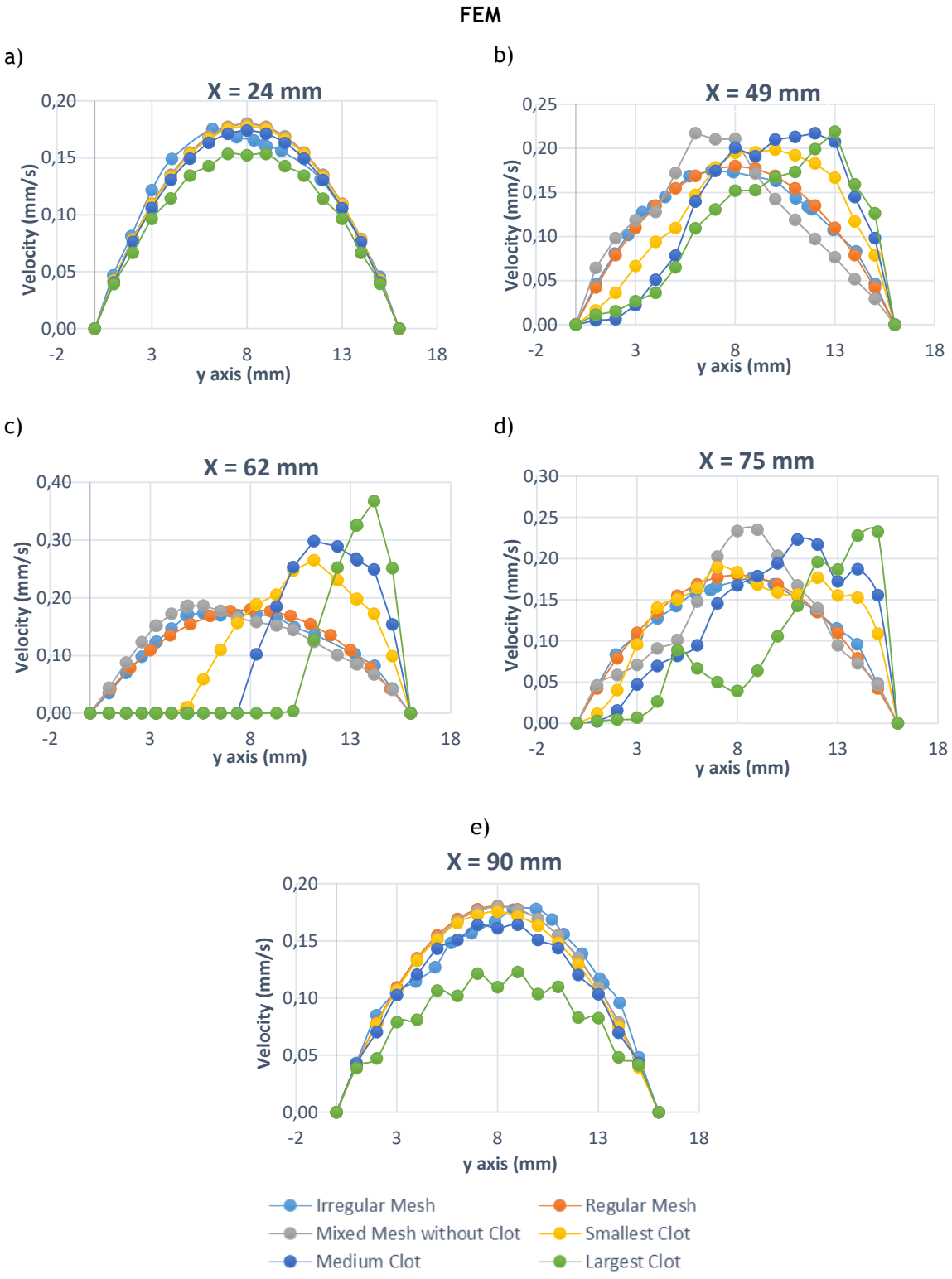

Figure 6.9 -Velocity profile for all the tubular meshes in the section of: a) $x = 24\ mm$, b) $x = 49\ mm$ c) $x = 62\ mm$ d) $x = 75\ mm$ and e) $x = 90\ mm$.

After analysing **Figure 6.9** a), which corresponds to the section of $x = 24\,mm$ (inlet), it is possible to see that all the curves present a parabolic profile. However, it is observed a slight disturbance in the irregular mesh and in the model with the largest clot.

Regarding the second graphic (**Figure 6.9** b)), which corresponds to the section of $x = 49\,mm$ (immediately before the clot), it is possible to observe that the models corresponding to the regular and the irregular mesh kept the parabolic profile, while the other ones present more disturbance on the flow when comparing to the first graphic.

In the section corresponding to the clot ($x = 62\,mm$, (**Figure 6.9** c)), it is possible to notice that the models with a defined clot, presented a velocity equal to 0 at its location and an increased velocity in the area where blood was able to flow, but with a tendency to maintain the parabolic profile. The other models tend to have a parabolic profile: the regular mesh maintained a well-defined parabola, although the irregular and the mixed mesh presented some disturbance on the velocity profile.

Analysing section $x = 75\,mm$ (**Figure 6.9** d)), it is noticeable that the velocity profile of the models with a defined clot presents a major disturbance. However, they tend to return to a parabolic profile. The models that correspond to regular and irregular mesh show similar results to the previous graphic, although the mixed mesh stepped slightly away from the parabolic profile.

In the last one ($x = 90\,mm$, (**Figure 6.9** e)) the velocity profiles of the models are similar to the first graphic. The velocity of all models tends to a parabolic profile. Nevertheless, the models corresponding to the largest clot, the medium clot and to the irregular mesh present a higher disturbance when compared to the first graphic.

The results obtained with RPIM, for the five selected sections, are shown in **Figure 6.10**.

RPIM

a)

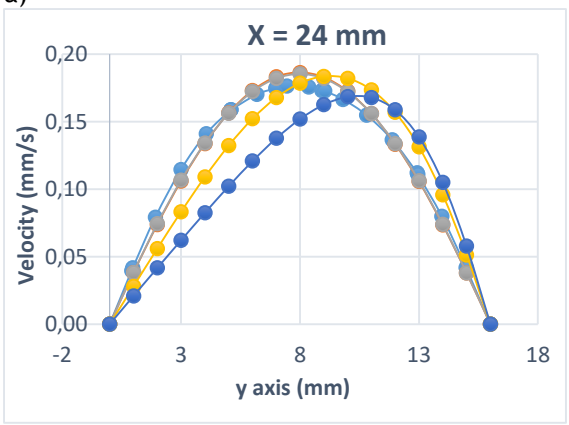

b)

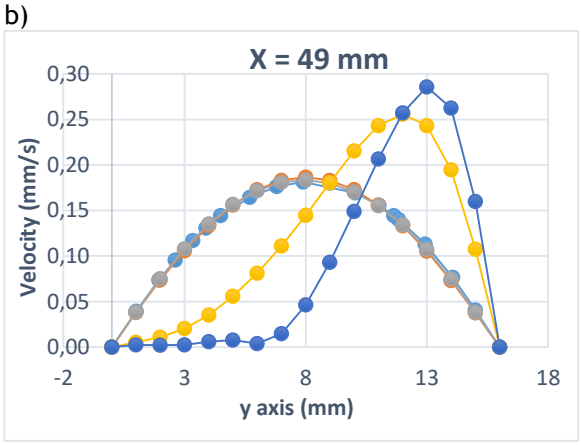

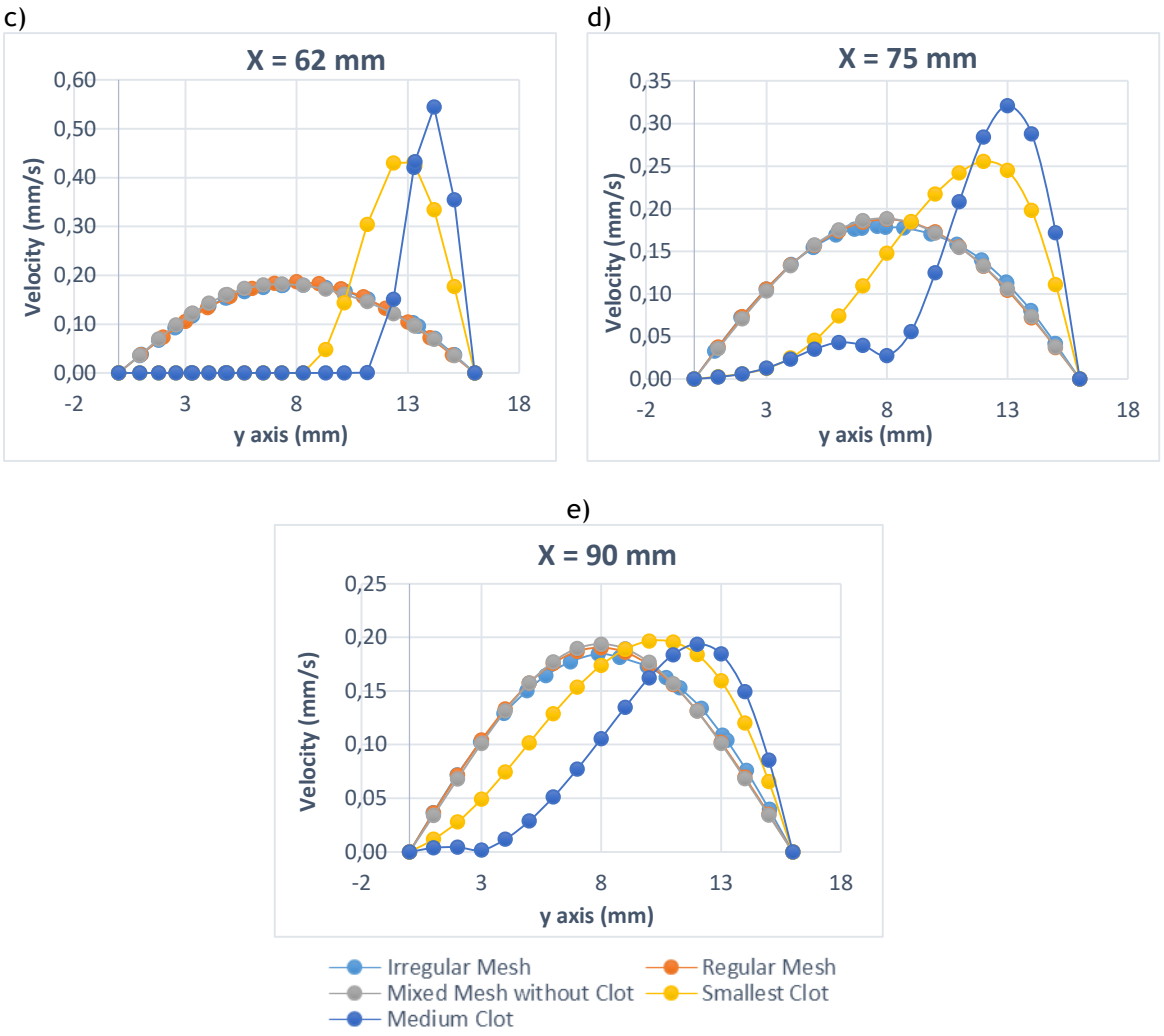

Figure 6.10 -Velocity profile obtained from RPIM for all the tubular meshes in the section of: a) $x = 24\ mm$, b) $x = 49\ mm$ c) $x = 62\ mm$ d) $x = 75\ mm$ and e) $x = 90\ mm$

Comparing the previous FEM results (**Figure 6.9**) with the ones obtained with RPIM (**Figure 6.10**), it is possible to verify that they are similar. However, in irregular and mixed meshes the RPIM results were better since they do not present disturbance in the parabolic profile. Concerning the models with clot, the results were more uniform, in spite of being influenced by the magnitude of the clot, as seen in the colour maps.

6.1.1.2 - Bifurcated Model

First, it was constructed in FEMAP a model containing a clot, as occur for the previous models presented. However, the obtained results were not satisfying, and for this reason, they are not extensively shown in this work. Thus, it was necessary to resort to another strategy: a MALTAB script was written to impose the clot in a regular mesh of the bifurcated model. In order to show effects of non-suitable mesh, in **Figure 6.11** it is shown the velocity maps obtained with a non-suitable mesh, i.e., the first FEMAP model containing a well-defined clot area. It is possible to visualize the obtained velocity map in **Figure 6.11**, showing a severe numerical perturbation at the lower branch, caused by the presence of the clot.

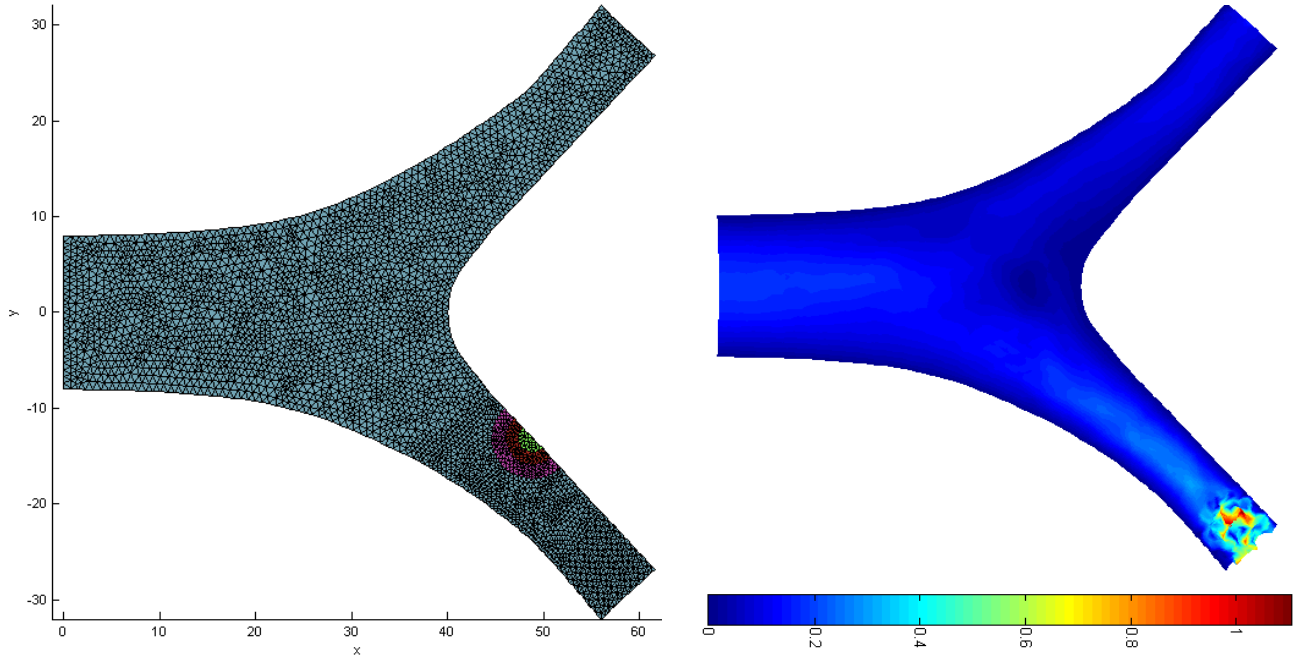

Figure 6.11 – Mesh and colour map of the velocity profile of the bifurcated model with a clot drawn.

As already mentioned, the strategy was to build a regular mesh of the bifurcated model, and afterwards, using a MATLAB script, the domain intended to be clot was declared as clot domain. **Figure 6.13** a) shows the nodal mesh used and the blood and clot domain.

The results shown in **Figure 6.12** represent the velocity colour maps of the two bifurcated models discretized with a regular mesh: one without clot and the other with a clot (defined afterwards using the developed script).

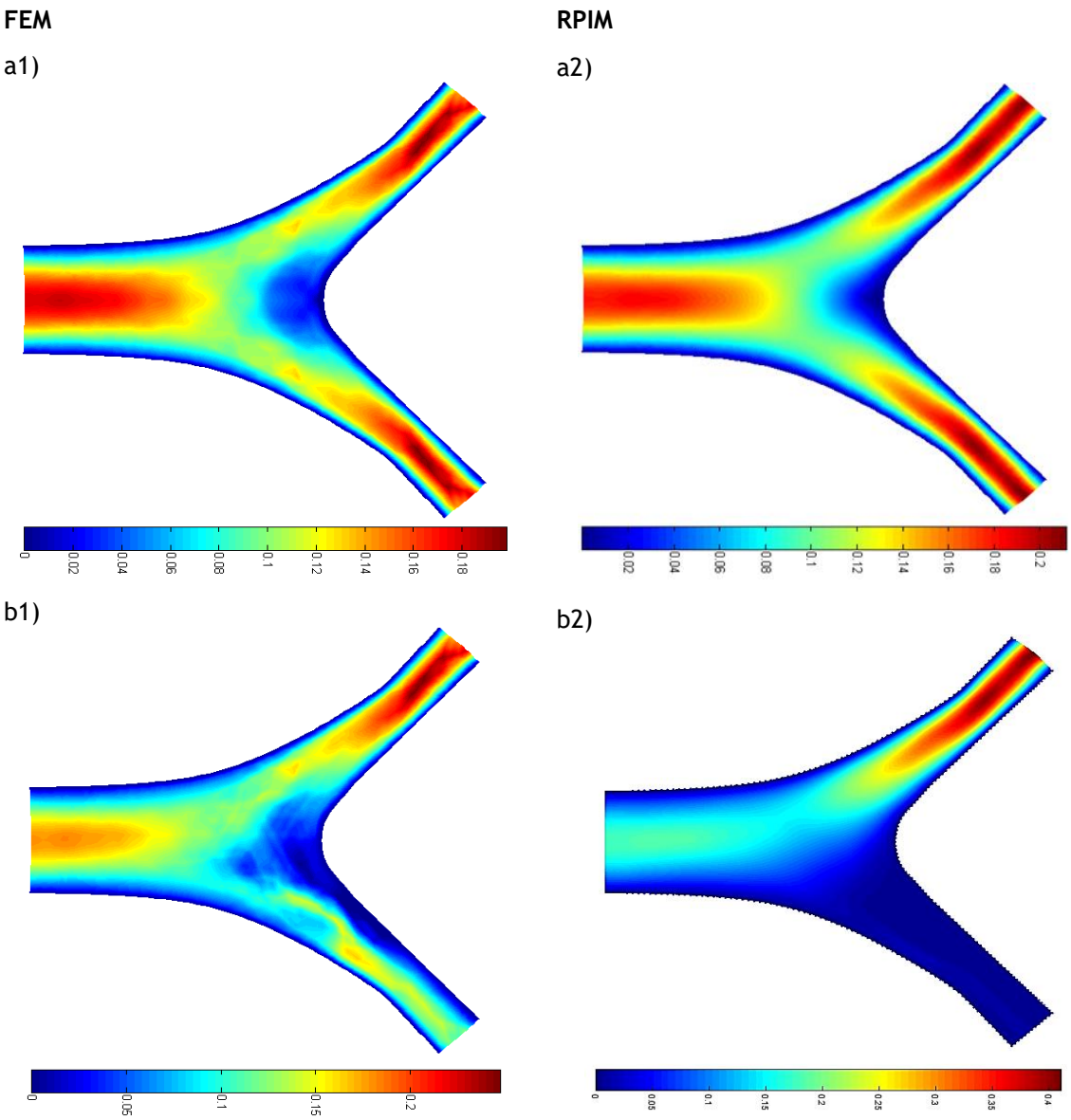

Figure 6.12 - Colour map of the velocity profile of the bifurcated model: a) without clot and b) with clot.

On **Figure 6.12** a1), it is possible to verify that the bifurcated model without clot exhibits a uniform flow in the tubular areas and a reduction of the velocity in the junction area. Besides that, this model presents a maximum velocity of around 0.18 mm/s, in the tubular areas. Furthermore, the two small branches present an identical profile (there is symmetry in the solution, as expected). Regarding the results of RPIM (**Figure 6.12** a2)), it is possible to verify, once again, that the results are similar, but better since the flow is more uniform.

On the other hand, in **Figure 6.12** b1), it is noticeable that the flow experiences some changes and became less uniform. The main modification is in the branch that contains the clot where the velocity is 0. Besides that, there is a difference in the velocity of the two branches and

consequently, these no longer present a similar profile, as seen in the previous model. The achieved maximum velocity is of around 0.22 mm/s, a higher value than the one found in the previous model. Regarding the results of RPIM (**Figure 6.12** b2)), it is possible to verify that the results are unexpected. Although the velocity in the branch without clot presents a similar profile to the one obtained in **Figure 6.12** b1), the branch with the clot presents an unexpected lower velocity in the area where the flow is allowed to pass. That way, this can be due to the fact that better fluid flow formulation are necessary when more complex domains are used. This is something which will be studied in this work. Such formulations are presented in the next chapters, however, since they are quite recent, they have not yet been implemented in FEMAS®.

Similar to what was previously mentioned, three regions of interest were defined in the model. These correspond to $x = 10\ mm$, the line that passes through the middle of the clot (in the lowest branch) and in the symmetric line (in the highest branch), as seen in **Figure 6.12** a).

The **Figure 6.13** shows the obtained FEM results for each section.

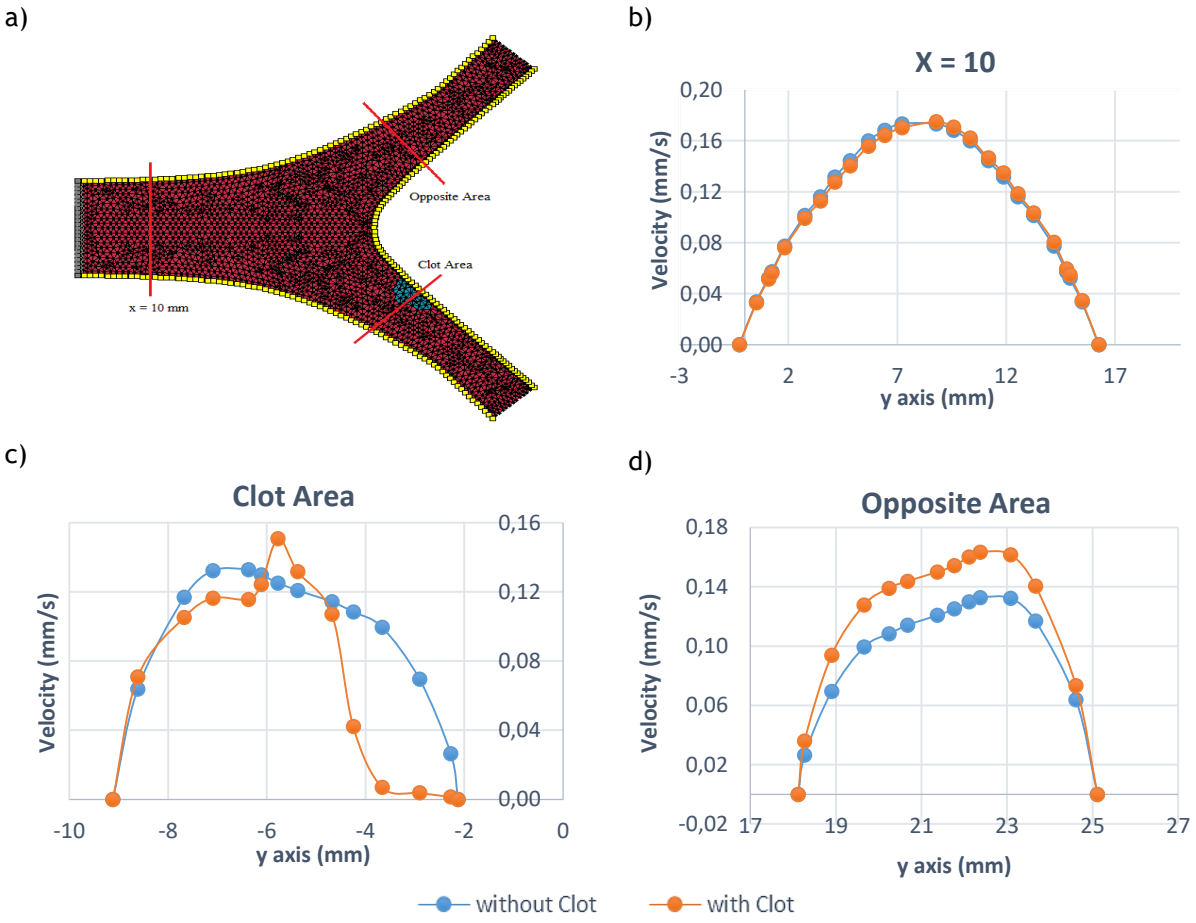

Figure 6.13 – FEM results: Regions of interest defined in the bifurcated model in a) and velocity profiles for the bifurcated models in the section of: b) $x = 10\ mm$ c) clot area and d) opposite area to clot.

When analysing the first graphic ($x = 10\ mm$ (**Figure 6.13** b)), it is possible to observe that the two curves display a parabolic profile.

In the section corresponding to the clot area (**Figure 6.13** c)), it is possible to visualize that the model with the clot presented a velocity equal to 0 in the clot and an increased velocity in the area where blood would flow, but with a tendency to maintain the parabolic profile. The other model tended to have a parabolic profile.

In the last section (symmetric to the clot area (**Figure 6.13** d)), it is possible to notice that the model without a clot presented a similar profile to the previous section. The model with a clot is similar to the other model. However, as expected, it exhibits a higher velocity.

Figure 6.14 shows the velocity profiles obtained with the RPIM. The results were obtained in the same locations of previous analysis (as **Figure 6.14** a) shows).

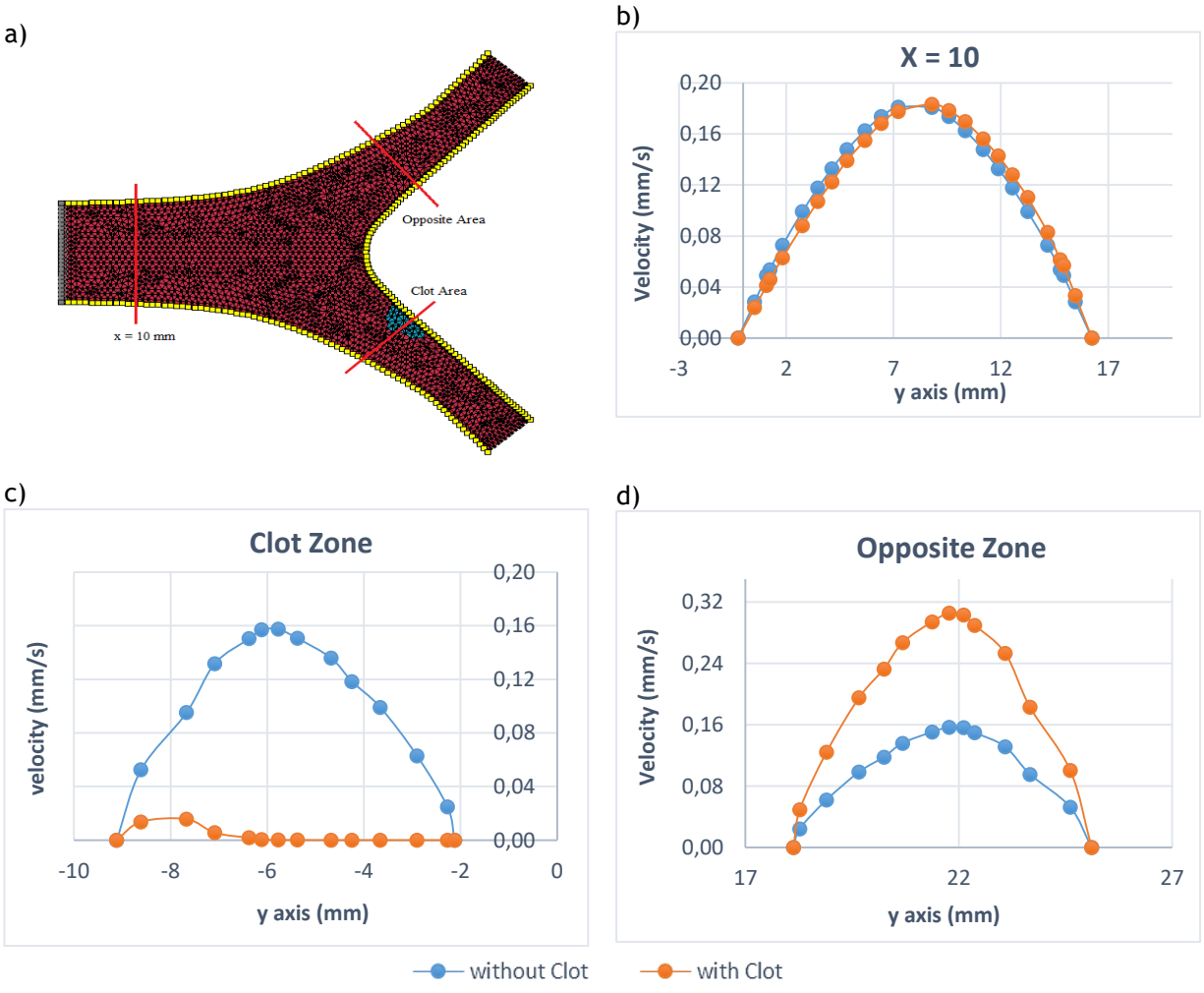

Figure 6.14 – RPIM results: Regions of interest defined in the bifurcated model in a) and velocity profiles for the bifurcated models in the section of: b) $x = 10\ mm$ c) clot area and d) opposite area to clot.

With RPIM, an identical result was obtained when the clot is not defined in the domain but, once more, it is possible to observe that the results are closer to parabolic profile, in particularly in the two branches of the bifurcation.

Regarding the results with clot, it is possible to see that they are coherent with the velocity profile, presenting low velocity in the branch with clot. However, it is possible to see that the curve is similar to the ones obtained for the tubular models. Analysing the other two section, it is possible to see that they present a similar profile, when compared to the curves without clot, while also being similar to the results obtained with FEM. However, as seen in the velocity profile, the velocity in the branch without clot unexpectedly presents higher velocity. The flow tends to shift to this branch because of the low velocity that the other branch presents, due to the presence of the clot. Therefore it is possible to conclude that the clot affects the results obtained with RPIM.

It was expected that the models would present a parabolic constant velocity profile, as mentioned previously, along its length, in the absence of obstacles. For example, in the work of M. W. Siebert *et al*. [156], a tubular model was presented with a parabolic profile, similar to those obtained in this work. Taking into account the results presented in the previous section, it is possible to verify that all the models tend to have this characteristic.

Comparing the tubular models with the regular mesh, the irregular mesh and the mixed mesh, it is noticeable that different meshes presented different results. Though similar, the regular mesh allows to achieve better results, with a uniform flow and a perfect parabolic graphic in all the five sections. Besides that, it showed a maximum velocity of 0.18 mm/s in the centre, as expected, taking into account the initial velocity defined for the FEM analysis. The other two models exhibit some disturbance in sections two, three and four, for the mixed mesh, and in all sections, for the irregular mesh, due to the presence of the mesh disturbance (in the zone of the clot domain).

When it comes to the models that presented a defined clot, they manifested different profiles along the artery and in the different sections that were selected. The clot was defined as a highly viscous body, in order to ensure that it would act as a barrier to the blood flow. The first and the last section showed a parabolic profile, as expected, since these correspond to normal blood flow. In the clot area, the velocity was zero since the blood flow could not pass under the clot. In the area where blood could flow, the velocity increased, and this can be explained according to the equation of flow rate. This can be translated $m = v \cdot \rho \cdot A \cdot \cos\theta$, being m the flow rate, v the velocity, ρ the density of the fluid, A the area where blood flows and θ the angle between the unit normal and the velocity of mass elements. Thereby, if the section area decreases, to maintain the flow rate, the velocity needs to increase. Therefore, the results related to the defined clot are coherent with what was to be expected. The model with the smallest showed a maximum velocity of around 0.25 mm/s, the one with medium clot had a velocity around 0.30 mm/s and the model with the largest clot had a maximum velocity of around 0.35 mm/s, which confirms what was

previously mentioned. Besides that, it is important to note that, as in the models that were previously analysed, this models present an irregular mesh, which influences the velocity profile. Therefore, a full regular mesh is more suitable, even in the presence of a clot domain, in order to obtain better results.

Regarding the bifurcated models, it is possible to verify some similarity to the tubular shape. In the bifurcated model without a clot, the main branch presents uniform flow and a maximum velocity in the centre, as expected, such as in the regular mesh of the tubular straight model. In the area of bifurcation, the velocity decreases and the blood tends to flows to the smaller branches. However, in the small branches, the flow tends to restore the parabolic profile, following the laminar flow initially defined. When establishing a comparison with the model with the clot, as expected, the velocity in the clot area is zero, as it was the case with the tubular straight models with clot. It should be noted that, the velocity profile in the upper branch was similar to the model without a clot since the introduction of the clot did not influence the mesh, similar to results observed for the tubular straight model.

Chapter 7

Blood Coagulation Algorithm

Blood coagulation is a complex non-linear phenomenon and, for this reason, it can only be solved iteratively. Thus, an iterative algorithm to simulate this process was designed, in order to obtain an approximated solution of the clot growth and its final configuration after formation.

In this section, a detailed description of the proposed algorithm is presented, and the generic procedure, the key points of the code, and the key variables used are described.

7.1 - Code Description

The proposed blood coagulation algorithm developed in the scope of this dissertation is a program made up by four main blocks (Fluid Flow Formulation, Thrombin, Clot Formation and Clot Growth Block), as can be seen in **Figure 7.1**.

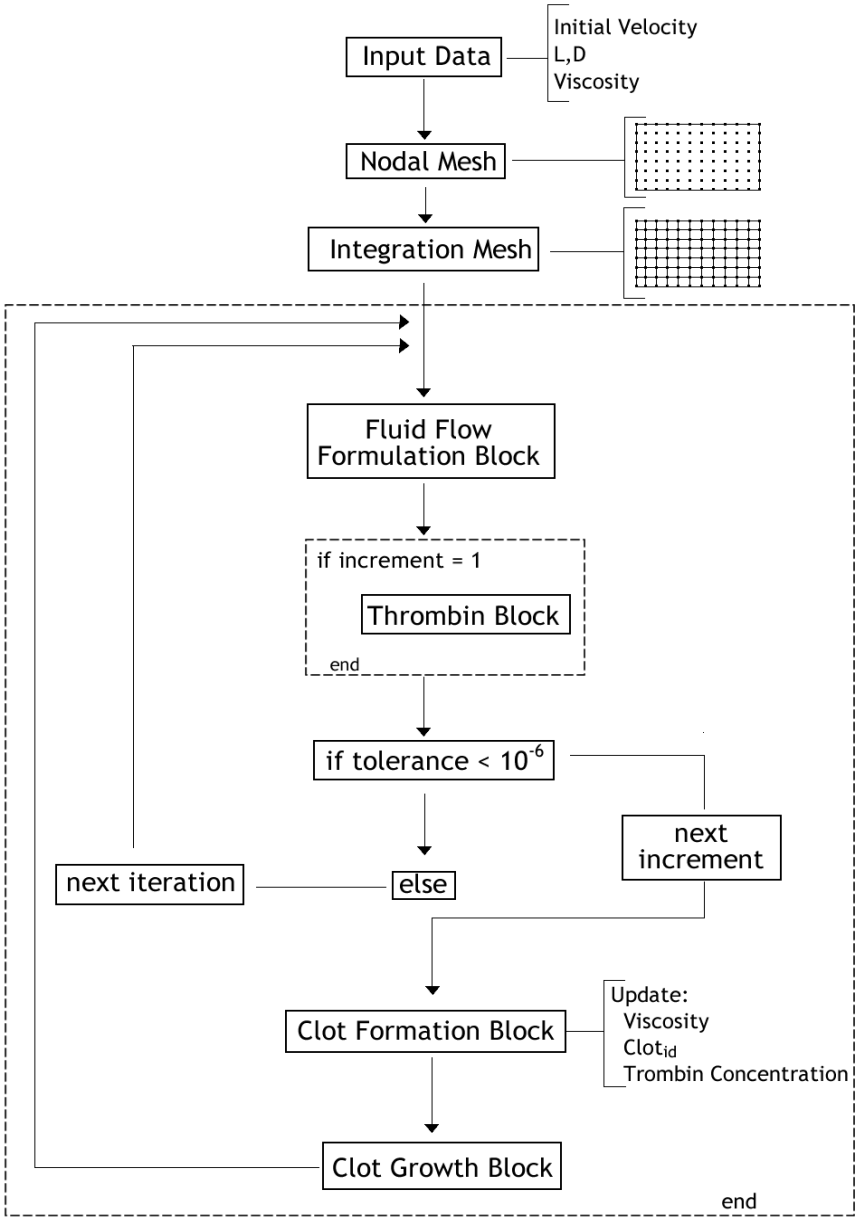

Figure 7.1 -Generic procedure of the created program.

Briefly, this code allows to verify the evolution of the growth of a clot, according to the conditions that are initially defined inside the several blocks.

First, the nodal mesh and the integration mesh is created, using the information of an input file containing all the initial conditions. Then, the shape functions are constructed and the stiffness matrix is built assuming an initial viscosity for each integration point using the information of the input file. Afterwards, the essential boundary conditions declared in the input file are imposed and the velocity field is obtained: $\dot{\boldsymbol{u}} = \boldsymbol{K}^{-1}\boldsymbol{f}$, allowing to calculate the strain rate on each integration point.

Thus, the “Fluid Flow Formulation Block” comprises the stiffness matrix construction, the essential boundary conditions imposition and the calculation of the velocity and strain rate fields.

Afterwards, only in the first iteration of the first increment, the “Thrombin Block” is called. This block sets the initial thrombin concentration in the entire domain, i.e., it sets the initial thrombin concentration of each integration point. In this block, the spatial distribution of the thrombin concentration is defined by means of a smooth quadratic surface function. The user can declare its maximum and minimum values, and also define the basal thrombin concentration. The basal thrombin concentration defines the value from which the clot formation is initiated.

After that, and, if some physiological conditions are satisfied, some points can turn into clot due to the “Clot Formation Block”, leading to the rise of the clot in the domain. Thus, in this block the viscosity of the integration points newly declared as clot, or of the integration point already declared as clot in previous increment, is modified accordingly with the phenomenological laws already presented in section **3.7**.

Furthermore, in this block, the thrombin concentration is modified in the integration points already declared as clot. In fact, the thrombin concentration of this integration points is increased, following the idea that the presence of the clot increases the local concentration of thrombin [16]. Thus, in this block, two different parameters are defined ($Magnitude$ and R_{action}), which will control the variation of thrombin concentration in those integration points.

Lastly, “Clot Growth Block” is responsible for the growth of the clot, by performing a radial search of the integration points inside a specific radius, which is defined based on the phenomenological law presented in section **3.7**. If a point is inside this radius, it becomes part of the clot, promoting its increase in each increment.

In the next subsections, a more detailed description of each block is done, with the main steps performed by the code being presented along the text.

7.1.1 - Fluid Flow Formulation Block

Taking into account the mathematical basis used in the fluid flow formulation of Zienkiewicz, an already developed program for fluid flow analysis of viscous fluids was used to implement the clot growth algorithm. The already develop code, in which the clot growth algorithm was included, considers the RPIM to solve the numerical problem.

Briefly, the already developed meshless code for fluid flow formulation can be divided into some key steps, which allow to obtain the flow profile on the studied domain. Thus, the generic procedure of this block is described as:

1. Reading the data file, in which the input variables and the material properties are declared;
2. Creating the nodal discretization based on the input data;

3. Creating the integration mesh following the isoparametric formulation and the Gaussian quadrature scheme;
4. Constructing the influence domains of each integration points performing a radial search;
5. Calculating the shape functions and respective derivatives;
6. Building the stiffness matrix with the equation:

$$\int_{\Omega} \boldsymbol{B}^T \mu \, \boldsymbol{I_0 B} \, d\Omega \, \overline{\boldsymbol{u}} - \int_{\Omega} \boldsymbol{B}^T \boldsymbol{m} \boldsymbol{N} p \, d\Omega \, \overline{\boldsymbol{p}} + \int_{\Omega} \boldsymbol{N}_v^T \, \boldsymbol{b} \, d\Omega + \int_{\Gamma} N_v^T \, t \, d\Gamma = 0 \tag{7. 1}$$

Resorting to the initial value of viscosity that is provided by the input data (if it is the first iteration). In the end, the global system matrix is obtained through the assembly of the local stiffness matrixes:

$$\begin{bmatrix} \boldsymbol{K}_v & \boldsymbol{Q} \\ \boldsymbol{Q} & -\frac{h^2}{\alpha} \boldsymbol{I} \end{bmatrix} \begin{bmatrix} \overline{\boldsymbol{u}} \\ \overline{\boldsymbol{p}} \end{bmatrix} = \begin{bmatrix} \boldsymbol{f} \\ \boldsymbol{0} \end{bmatrix} \tag{7. 2}$$

7. Imposing boundary conditions based on input data;
8. Solving the algebraic system of equations to obtain the nodal velocities and pressures:

$$\begin{bmatrix} \widetilde{\boldsymbol{u}} \\ \widetilde{\boldsymbol{p}} \end{bmatrix} = \begin{bmatrix} \boldsymbol{K}_v & \boldsymbol{Q} \\ \boldsymbol{Q} & -\frac{h^2}{\alpha} \boldsymbol{I} \end{bmatrix}^{-1} \begin{bmatrix} \boldsymbol{f} \\ \boldsymbol{0} \end{bmatrix} \tag{7. 3}$$

9. Computing the strain rate at the integration point to prepare for the next iterations:

$$\dot{\varepsilon} = \boldsymbol{L u} = \boldsymbol{L N}_v \tilde{u} = \boldsymbol{B} \widetilde{\boldsymbol{u}} \tag{7. 4}$$

10. Interpolating the velocity of the integration points based on the nodal values:

$$u = \begin{bmatrix} u_x \\ v_y \end{bmatrix} = \boldsymbol{N}_v \widetilde{\boldsymbol{u}} \tag{7. 5}$$

11. Calculating the average velocities and pressure values of the domain and storing them. In the first iteration of the first increment/step, the process returns to point 6 and repeats, because the first iteration is just to obtain a trial velocity, so estimated viscosities (depending on the velocity) can be obtained. In the other iterations (within the same increment/step), the program verifies if the process converged (the viscosities of the previous iteration are equal to the viscosities of the present iteration). In this case, it skips to the next increment/step (point 12), otherwise, the process returns to point 6 and repeats (enters an iterative loop until the viscosities of the previous iteration are equal to the viscosities of the present iteration).

12. In the end of each step/increment, the nodal spatial coordinates and integration point coordinates are updated based on their velocity (the discretization mesh moves):

$$x_{new} = x_{old} + \tilde{v}_x \Delta t \quad (7.6)$$

$$y_{new} = y_{old} + \tilde{v}_y \Delta t \quad (7.7)$$

13. With the new nodal spatial coordinates, the process moves to point 4 in order to compute the next time step and repeat each sequential step until the desired time step is reached.

A schematic representation of this block is presented below (**Figure 7.2**):

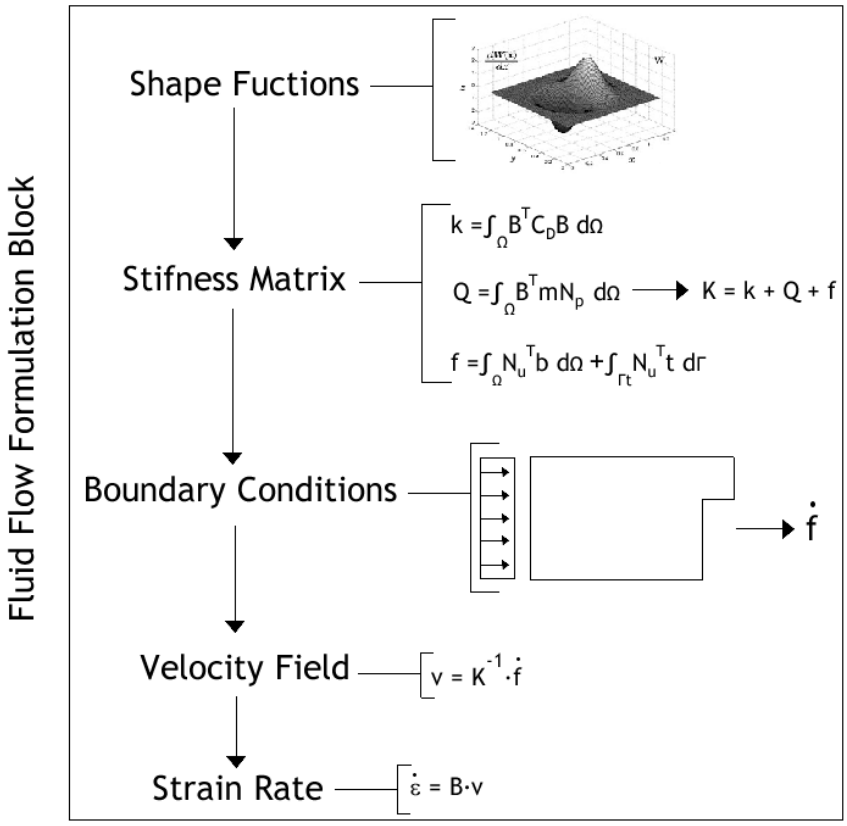

Figure 7.2 - Schematic representation of the main steps of the Fluid Flow Formulation Block.

Thus, after these steps, the blood coagulation algorithm starts running, leading to clot formation and growth, if some conditions are fulfilled. Furthermore, note that this program resorts to some variables, which are also used in the new algorithm, being listed next:

- $\boldsymbol{x}$ - Vector of spatial coordinates for velocity and pressure nodes;
- L - Total length of the model in the x direction;
- D- Total length of the model in the y direction;
- d_L - Number of mesh divisions created along the x direction;

- d_D - Number of mesh divisions created along the y direction;
- n_{dom} - Number of nodes inside a particular influence domain;

7.1.2 - Thrombin Concentration Block

After obtaining the velocity field (with the Fluid Flow Formulation Block), a thrombin concentration is generated resorting to a surface function. In normal conditions, the basal concentration of thrombin is around 0.14 nM. However, under some pathological conditions and during the process of blood coagulation, this concentration can increase, which can promote the formation of a clot.

This component of the coagulation was chosen since it is one of the main products of the coagulation cascade, one of the process that leads to the formation of clots. Besides that, thrombin is presented in the clot structure in the end of the process. Note that only this concentration was considered in the algorithm, in order to simplify its implementation and analysis.

Thus, a surface function $Ct(x,y)$ is established. The surface function is a polynomial function, as defined in equation (7. 8).

$$\begin{aligned} Ct = a_1 + a_2 \cdot x + a_3 \cdot y + a_4 \cdot x^2 + a_5 \cdot y^2 + a_6 \cdot xy + a_7 \cdot x^2y + a_8 \cdot xy^2 + a_9 \\ \cdot x^2y^2 \\ = \{1, x, y, x^2, xy, y^2, x^2y, xy^2, x^2y^2\}^T \{a_1, a_2, a_3, a_4, a_5, a_6, a_7, a_8, a_9\} \\ = \boldsymbol{p}(\boldsymbol{x}_i)^T \boldsymbol{a} \end{aligned} \tag{7. 8}$$

Applying this equation to nine known points, and setting for those points the thrombin concentration, it is possible to obtain the following set of equations:

$$\begin{cases} Ct(\boldsymbol{x}_1) = \boldsymbol{p}(\boldsymbol{x}_1)^T \boldsymbol{a} \\ Ct(\boldsymbol{x}_2) = \boldsymbol{p}(\boldsymbol{x}_2)^T \boldsymbol{a} \\ \dots \\ Ct(\boldsymbol{x}_9) = \boldsymbol{p}(\boldsymbol{x}_9)^T \boldsymbol{a} \end{cases} \Leftrightarrow \begin{Bmatrix} Ct(\boldsymbol{x}_1) \\ Ct(\boldsymbol{x}_2) \\ \dots \\ Ct(\boldsymbol{x}_9) \end{Bmatrix} = \begin{bmatrix} \boldsymbol{p}(\boldsymbol{x}_1) \\ \boldsymbol{p}(\boldsymbol{x}_2) \\ \dots \\ \boldsymbol{p}(\boldsymbol{x}_9) \end{bmatrix}^T \boldsymbol{a} \Leftrightarrow \boldsymbol{Ct} = \boldsymbol{P} \cdot \boldsymbol{a} \tag{7. 9}$$

The constant parameters of the surface function are obtained with: $\boldsymbol{a} = \boldsymbol{P^{-1}} \cdot \boldsymbol{Ct}$. Substituting back into equation $\boldsymbol{Ct} = \boldsymbol{P} \cdot \boldsymbol{a}$, it will allow to obtain the value of thrombin concentration in any point $\boldsymbol{x}_I$ belonging to the domain. Thus, $Ct(\boldsymbol{x}_I) = \boldsymbol{p}(\boldsymbol{x}_I)^T \boldsymbol{a} = \boldsymbol{p}(\boldsymbol{x}_I)^T \boldsymbol{P^{-1}} \cdot \boldsymbol{Ct}$.

Thus, by setting the values $\{Ct(\boldsymbol{x}_1), Ct(\boldsymbol{x}_2), \dots, Ct(\boldsymbol{x}_9)\}$ in points $\{\boldsymbol{x_1}, \boldsymbol{x}_2, \dots, \boldsymbol{x}_9\}$ it is possible to set a surface function $Ct(\boldsymbol{x}_I)$, representing the thrombin concentration at any point $\boldsymbol{x}_I$ of the domain (node or integration point). Also, it is possible to set the maximum value of thrombin concentration, $Magnitude_{Ct}$, which allows to control the higher value of the imposed thrombin concentration.

A schematic figure of the thrombin concentration block is presented below (**Figure 7.3**):

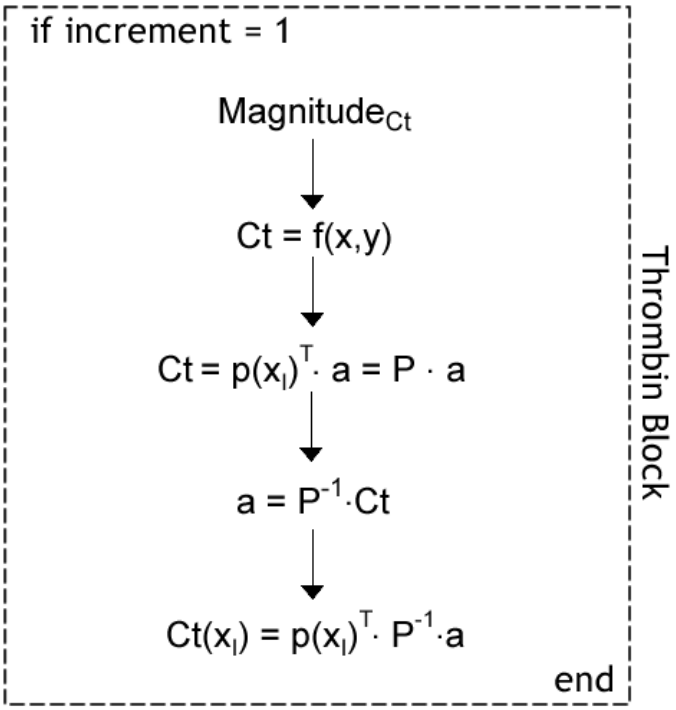

Figure 7.3 - Schematic representation of the main steps of the Thrombin Block.

7.1.3 - Clot Formation Block

This block is the one responsible for generating clot points. As previous stated, the process that leads to the formation of a clot is complex, implying a huge number of components, interactions and behaviours.

A concentration of thrombin was imposed in the previous block, in order to be one of the triggers that initiate the formation of a clot. However, other factors need to be considered when a clot is formed. In some circumstances, shear rate is one of the main triggers to the formation of clots and, for this reason, shear rate was also considered in this algorithm as a promoter of blood coagulation.

Thus, this block checks the points that present a concentration of thrombin and an absolute shear rate in a specific range, in order to modify them to clot. For such purpose, the viscosity of these points is modify, as a function of the absolute shear rate of this point (as seen in **3.7**), in each increment, promoting the appearance and growth of the clot, which consequently promote an alteration in the velocity profile of the domain.

Moreover, if a point is considered clot, a radius (R_{CGR}) is generated according to an expression dependent on the absolute shear rate (the one presented in **3.7**), and on a step time, which was define as 50 minutes, in order to promote the clot growth in the next block.

This block also analyse the points that already are clot ($clot_{id} = 1$) in order to increase the concentration of thrombin of the points near to the clot that present a $clot_{id} = 0$ (non-clot points/nodes). For points that present a $clot_{id} = 1$, a radius (R_{action}) is created taking into account the dimension L and the number of divisions d_L. This is compared with the distance between the integration point that present a $clot_{id}$ equal to 1 and all others points that present a $clot_{id}$ equal to 0. If this distance is lower than the R_{action}, then the concentration of thrombin in the correspondent integration point with a $clot_{id}$ equal to 0 is increased, taking into account the value of the $Magnitude$ defined for this purpose. Lastly, note that this concentration cannot pass from the 400 nM (a physiological value for normal higher concentrations of thrombin in the coagulation process [16]) and for this reason a condition to prevent concentration higher than this value was imposed.

By steps, this block can be presented as:

1. Verifying the $clot_{id}$ (in the first increment, all integration points present a $clot_{id} = 0$);
2. For each integration point $\boldsymbol{x_I}$: checking if the concentration of thrombin (C_t) is higher than the basal concentration (C_{t_b}) and if its shear rate ($\dot{\gamma}$) is in the range of $[500;\ 6000]$ or of $]6000;\ 100000]$. If this occurs, then for that integration point $\boldsymbol{x_I}$:
   a) Defining a $clot_{id} = 1$, if $clot_{id} = 0$;
   b) Calculating the clot growth rate (CGR), for each range, using the effective shear rate obtained in that integration point $\boldsymbol{x_I}$ using the equations created in **3.7**, respectively:

$$CGR = 0.8116 \times |\dot{\gamma}|^{0.3731},\ if\ \ \dot{\gamma}_{ff} \epsilon [500;\ 6000] \tag{7. 10}$$

$$CGR = -2 \times 10^{-14}\ |\dot{\gamma}|^3 + 4 \times 10^{-9}\ |\dot{\gamma}|^2 - 4 \times 10^{-4} |\dot{\gamma}| + 23.805,\ if\ \ \dot{\gamma}_{eff} \epsilon\ ]6000;\ 100000] \tag{7. 11}$$

   c) Calculating the R_{CGR} for the respective integration point, using the following equation:

$$R_{CGR} = 50 \times CGR \times 10^{-3} \tag{7. 12}$$

   Note that 50 (minutes) is the step time and R_{CGR} is defined in millimetres since the domain is defined in this unit (and the phenomenological law of CGR in μm).

   d) Determining the new viscosity on each integration point, using the expression already developed in the subsection **3.7**:

$$\mu_{new} = -3.2557^{-9} \times |\dot{\gamma}| + 2.2002^{-6} \tag{7. 13}$$

3. Else, calculating the viscosity of each integration point ($\mu(\boldsymbol{x}_I)$) resorting to:

$$\mu(\boldsymbol{x}_I) = \frac{\mu_0 \times \dot{\varepsilon}_{eff}{}^{m}}{3 \times \dot{\varepsilon}_{eff}} \quad (7.\ 14)$$

Being μ_0 the initial viscosity, m a material parameter (defined in previous experimental works) and $\dot{\varepsilon}_{eff}$ is the effective strain rate, $\dot{\varepsilon}_{eff} = \left(\left(\frac{2}{3}\right)\boldsymbol{\varepsilon}^{\boldsymbol{T}}\boldsymbol{\varepsilon}\right)^{\frac{1}{2}}$.

Regarding the part of the code to increase the concentration of thrombin, the next steps were created:

1. Calculate the R_{Action}:

$$R_{Action} = Magnitude_{RA} \times \frac{L}{d_l} \quad (7.\ 15)$$

2. Identify the integration points with a concentration of thrombin higher than the basal thrombin concentration;
3. Calculate the distance ($Dist$) between the integration points that present $clot_{id} = 1$ and the other all integration points that are defined as blood ($clot_{id} = 0$);
4. Calculate the new concentration of thrombin (Ct_{new}), for each integration points, if the condition $Dist < R_{Action}$ is satisfied:

$$Ct_{new} = Ct \times \left(1 + Magnitude \times \left(1 - \frac{Dist}{R_{action}}\right)\right) \quad (7.\ 16)$$

5. If the new concentration of thrombin is higher than 400 nM in some integration points, then this concentration is changed to 400 nM.

Note that this part of the block only is used when exist an integration points with a $clot_{id} = 1$.

The next figure (**Figure 7.4**) presents a schema of Clot Formation block:

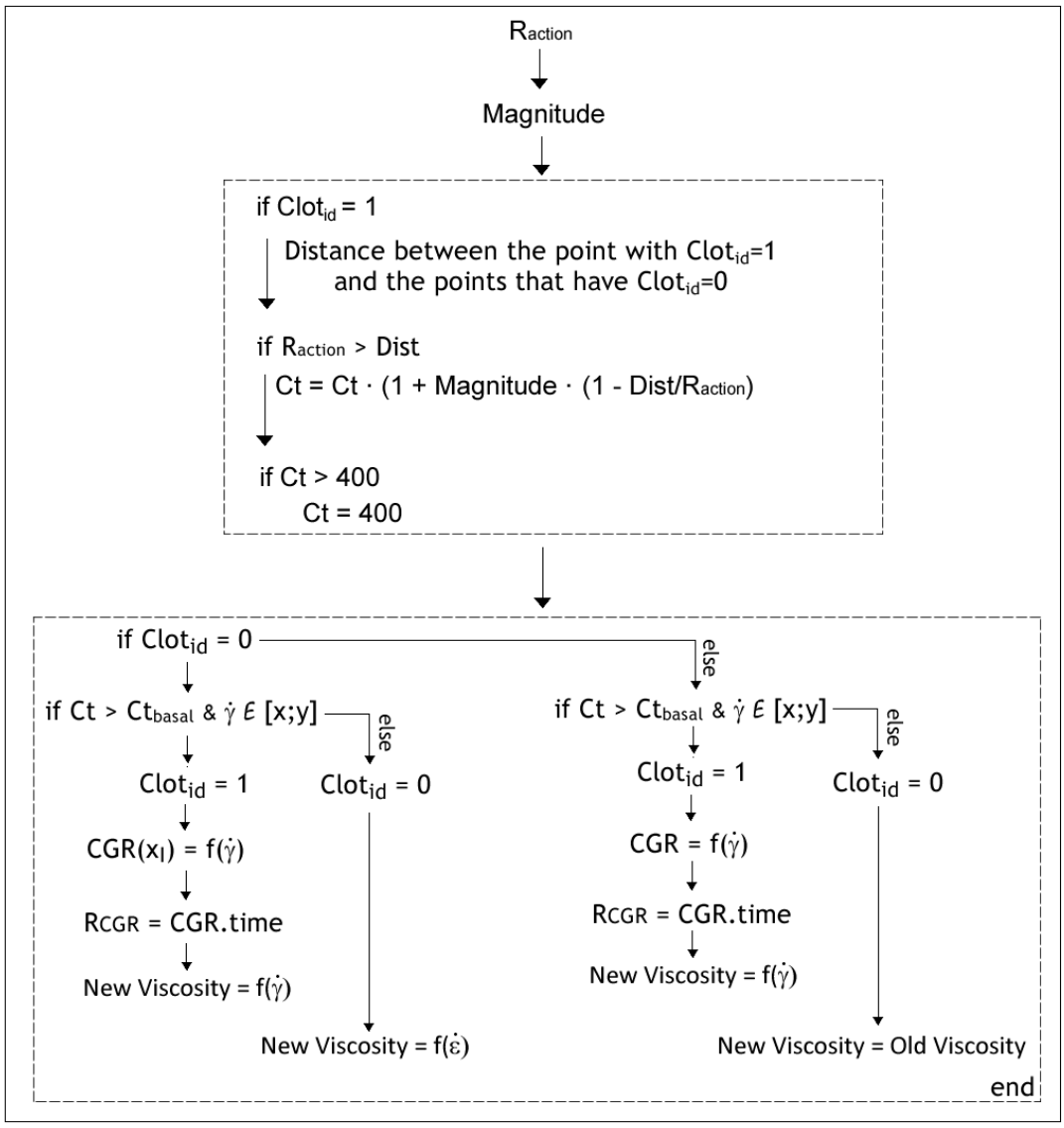

Figure 7.4 - Schematic representation of the main steps of the Clot Formation Block.

7.1.4 - Clot Growth Block

When a point became clot, a radial search is performed, considering the clot growth rate radius (R_{CGR}) define in the previous block. Thus, if an integration point with a $clot_{id} = 0$ is within the area defined by this radius, it becomes clot by changing its $clot_{id}$ to 2, and changing its viscosity.

In this block, the $clot_{id}$ of the new points that became clot is considered 2, in order to differentiate the points that correspond to the clot growth and the points that already are clot from the previous block. However, to advance to the next increment, this $clot_{id}$ is modify to 1 with the aim of analyse the clot growth throughout each increment.

Therefore, the key steps and the generic procedure of this block are:

1. For each integration point that became clot (which implies a $clot_{id} = 1$), checking the integration points that are inside a specific radius:
   a) Calculating the distance between the integration point and all the other points;
   b) If the distance between the integration point and other point is lower than the R_{CGR}, the point that presents $clot_{id} = 0$ becomes clot:
      a. The $clot_{id}$ is modify to 2.
      b. Calculating a new viscosity for the new clot point, resorting to the expression already created in **3.7**:

$$\mu_{new} = -3.2557^{-9} \times |\dot{\gamma}| + 2.2002^{-6} \quad (7.17)$$

   Note that the $\dot{\gamma}$ corresponds to the shear rate of the integration point that already is clot. The other points that do not satisfy the condition in 3., maintain their previous viscosity.
   c) Modifying the $clot_{id}$ of the new clot points ($clot_{id} = 2$) to 1, ($clot_{id} = 1$).

A schematic representation of this block is presented in **Figure 7.5**.

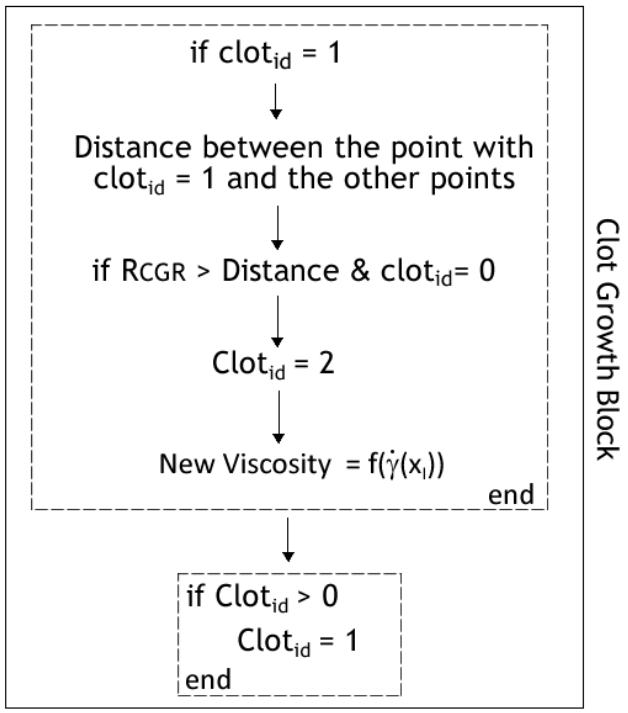

Figure 7.5 - Schematic representation of the main steps of the Clot Growth Block.

Chapter 8

Validation Results

In order to validate the algorithm created, two different parameters of the code were considered (Magnitude and the Action Radius). For such purpose, different values for both variables were tested and combined, in order to understand the viability of the algorithm and to define the combination of parameters that promote better results for this analysis. Besides that, for the two better combinations of parameters, the colour maps were presented and analysed.

Thus, this chapter will present the preliminary results obtained using the created algorithm, as well as, their analysis.

8.1 - Description of the Domain

The domain was defined with a geometry of a square, with a L and a D equal to $14\ mm$, being that L represents a generic diameter for the Iliac arteries [157]. In the left, the flow is allowed to pass along all the border, being imposed a velocity (v) of $1300\ mm/s$ in the inlet, a reference value for the peak velocity of the Iliac arteries [157]. Besides that, the walls are constrained in the top and in the bottom borders in the direction v (Oy). In the right border, the wall is also constrained in the bottom part (in u direction - Ox), however, an opening of $3D/8$ was defined in the top, in order to allow the exit of the flow and to simulates a bifurcation of a vessel. In **Figure 8.1**, it is possible to observe a schematic representation of the domain and its boundary conditions:

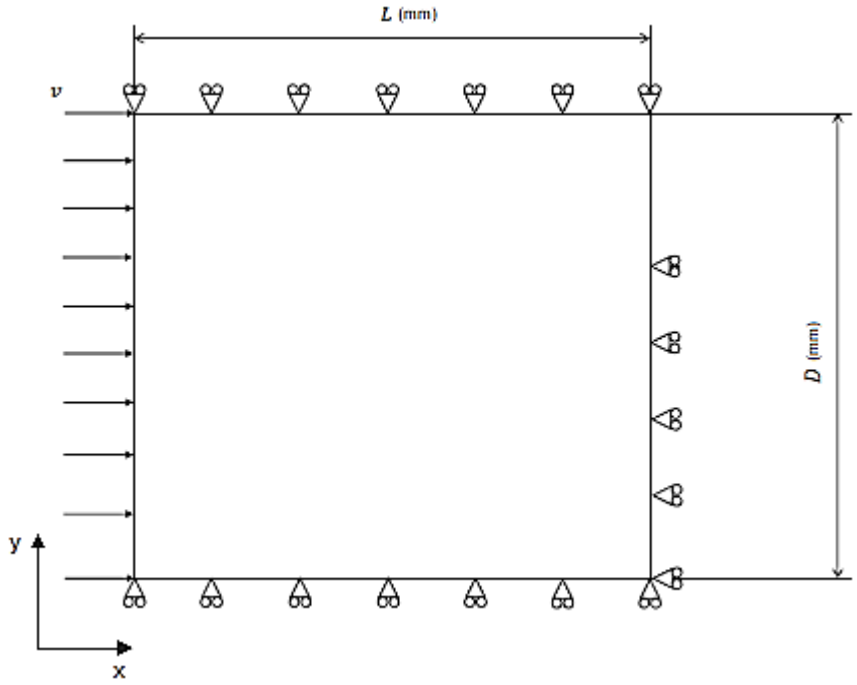

Figure 8.1 – Representation of the domain with boundary conditions.

Besides that, the blood initial viscosity was define as $\mu_O = 3.5 \times 10^{-9}$ Pa.s, the reference value of the blood.

Regarding the nodal mesh, the number of the divisions d_L and d_V were defined as 48 (allowing to build a $49 \times 49 = 2401$ nodal mesh) and the influence domain presents a n_{dom} of 18.

Furthermore, the focus of the concentration of the thrombin was defined in the bottom right corner since this area corresponds to a region of lower velocities of the flow, being known as the zones that present a higher concentration of the coagulation factors, such as the thrombin.

In **Figure 8.2**, it is possible visualize the initial distribution of the concentration of thrombin.

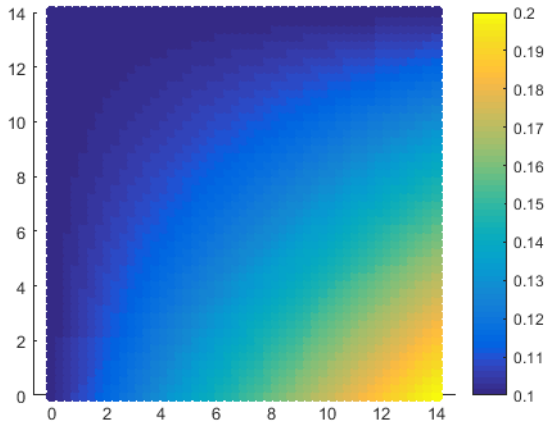

Figure 8.2 – Color map of the distribution of the concentration of thrombin (nM).

8.2 - Initial Results

After run the algorithm in Matlab, several results were obtained. First, the parameters $Magnitude$ and the $Action\ Radius\ (R_{Action})$ were analysed. After that, and according to the obtained results of the previous analysis, two different combinations of the mentioned parameters were selected, being presented the respective colour maps in order to analyse the influence of the appearance and growth of the clot in the blood flow. For such, the colour maps of the clot, the viscosity, the velocity, the concentration of thrombin and the shear rate, were obtained, and then analysed.

In the next figure (**Figure 8.3**), it is possible to observe what is expected to obtain as a result when the designed algorithm is applied:

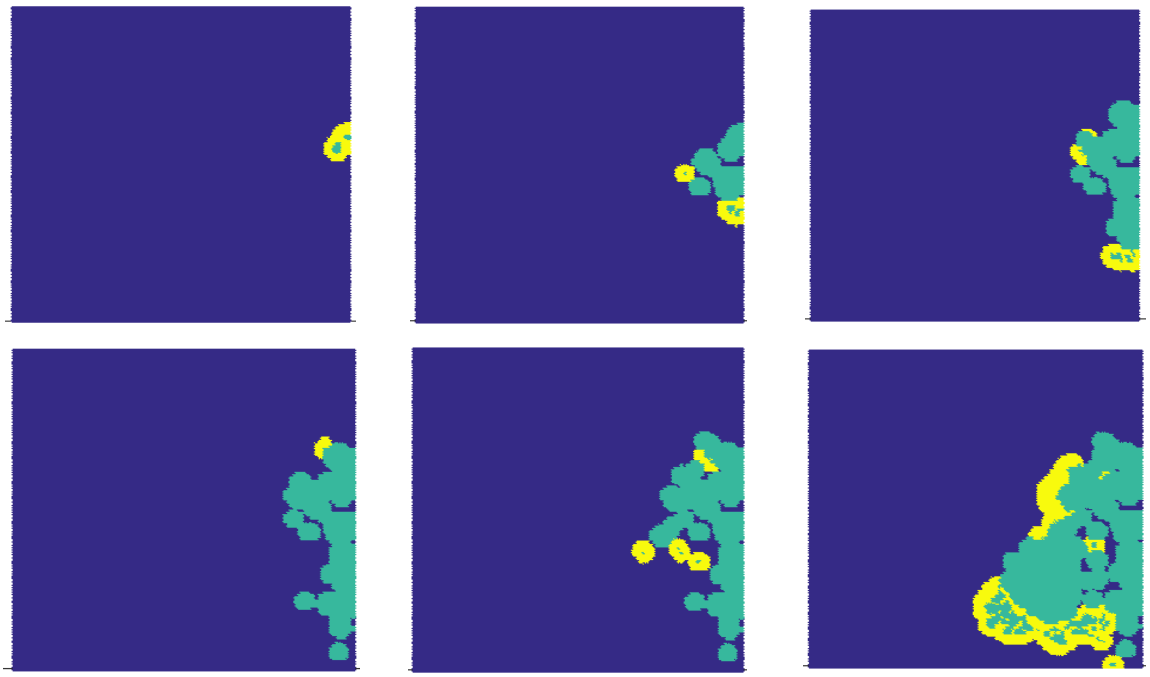

Figure 8.3 – Example of clot growth results. Blue: blood; Green: old clot; Yellow: new clot

It is possible to observe the evolution of the clot along the increments (time steps). Note that the representation of the previous figures do not correspond to consecutive increments.

8.2.1 - Variation of the Magnitude

As mentioned before, thrombin was defined as one of the triggers of the formation of the clot in this algorithm. Thus, the variation of its concentration will influence the growth of the clot, being expected a higher growth when the concentration is higher, which can be obtain by increasing

the value of $Magnitude$. When this parameter increase, the concentration of thrombin in the integration point in a given $Action\ Radius$ will increase, which can affect the number of points that are modify to become clot.

In this section, the parameter $Magnitude$ is altered in order to verify how the growth of the clot is affected, when the parameter $Action\ Radius$ is maintain constant. For such, the $Magnitude$ was defined as 0.01, 0.025, 0.05, 0.075 and 0.1, being also analysed for four different $Action\ Radius$ (0.5, 1.0, 1.5 and 2.0 mm). Thus, the parameter $Magnitude$ was evaluated through the variation of the clot growth over the time and, for this, four graphics were done for each $Action\ Radius$ (**Figure 8.4**), being presented five curves that correspond to the five different $Magnitude$ that were selected.

Note that, the Clot Fraction corresponds to the percentage of the number of integration points (num_{gp}) that are clot : $Clot_{id} = 1$, after running the Clot Growth Block. Such is calculated by:

$$Clot\ Fraction\ \% = \frac{\sum Clot_{id} \neq 0}{num_{gp}} \times 100 \qquad (8.\ 1)$$

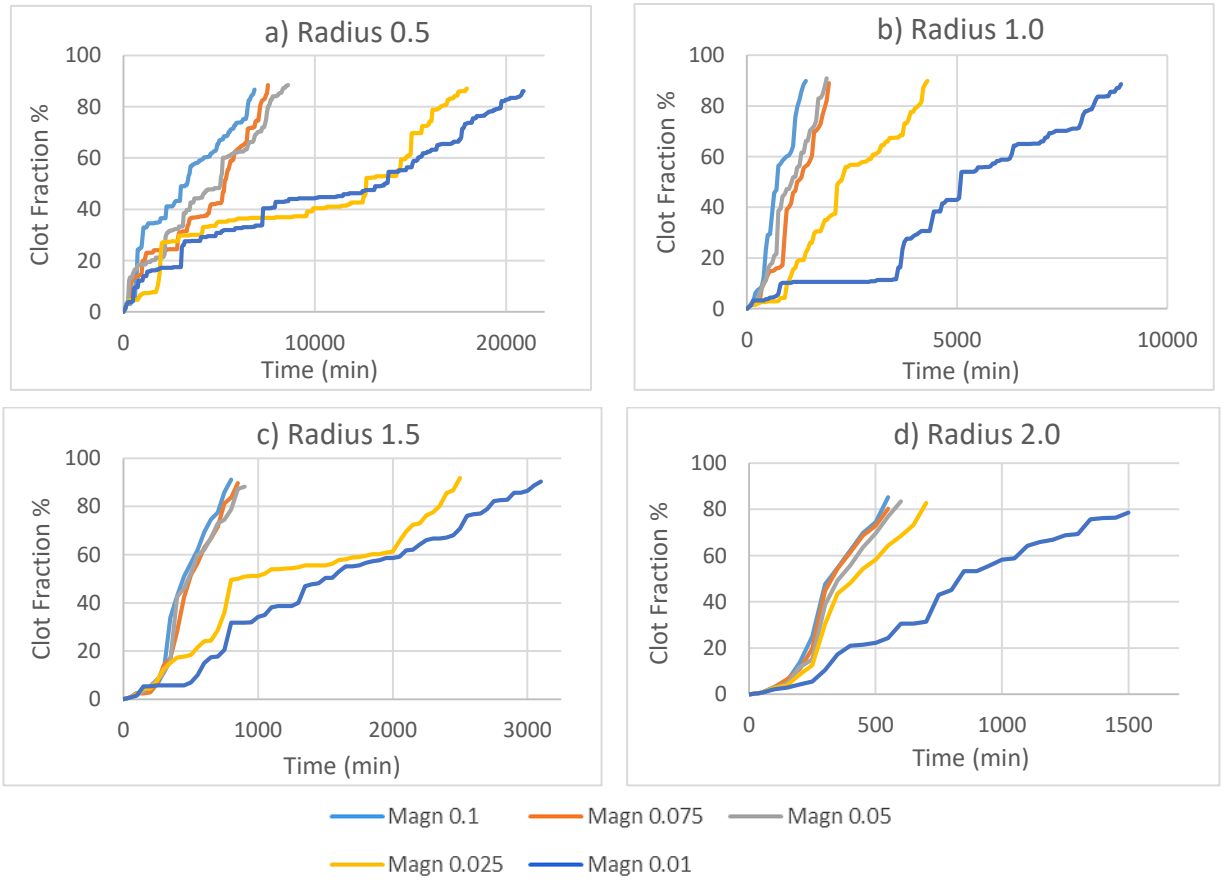

Figure 8.4 – Evolution of the Clot Fraction over the time, for five different values of Magnitude, using the Action Radius: a) 0.5 mm; b) 1.0 mm; c) 1.5 mm and d) 2.0 mm.

Analysing the results, it is possible to see that higher $Magnitude$ lead to a faster growth of the clot, being clear that the $Magnitude$ of 0.1, 0.075 and 0.05 promote a faster growth in all cases when compared with the $Magnitude$ of 0.025 and 0.01. Such is coherent with the expected, since the $Magnitude$ influence the concentration of thrombin of the integration points of the domain that are defined as blood, if they are inside a specific defined radius. This way, the concentration of thrombin in these points increase, which allow them to become clot if the conditions of concentration and shear rate are satisfied. So, if higher values of $Magnitude$ are used, then more quickly the conditions of the concentration are achieved. Thus, the same clot fraction is acquired with less increments, as seen in the obtained results.

Besides that, it is possible to see that some curves present a constant clot fraction in some time steps, as occur in the curve of $Action\ Radius$ 1.0 and $Magnitude$ 0.01 (for example, between the 1100 and the 3050 minutes). Such can be explain by the fact that the increase in the concentration of thrombin cannot be sufficient to reach the basal concentration so, the integration points remain as blood. Note that this behaviour is more visible when lower $Magnitudes$ are used.

8.2.2 - Variation of the Action Radius

The $Action\ Radius$ affects the number of integration points that are not clot, majoring their concentration of thrombin. Thus, if a higher radius is used, then the number of points that will have its concentration increased is higher, which will influence the number of points that can become clot if their concentration is higher than the basal concentration of thrombin.

Similar to the previous results, the same was performed for the $Action\ Radius$. In this case, the $Magnitude$ was maintained constant in order to analyse how the growth of clot is affected when the parameter $Action\ Radius$ is altered. As previously, the $Action\ Radius$ were defined as 0.5, 1.0, 1.5 and 2.0 mm, and the $Magnitude$ as 0.01, 0.025, 0.05, 0.075 and 0.1

Once again, similar to **Figure 8.4**, the parameter $Action\ Radius$ was evaluated through the variation of the clot growth over the time and, for this, five graphics were construct for each $Magnitude$ (**Figure 8.5**), being presented four curves, which correspond to the four different $Action\ Radius$ that were selected.

Note that, the Clot Fractions was obtained in the same way as in the previous section.

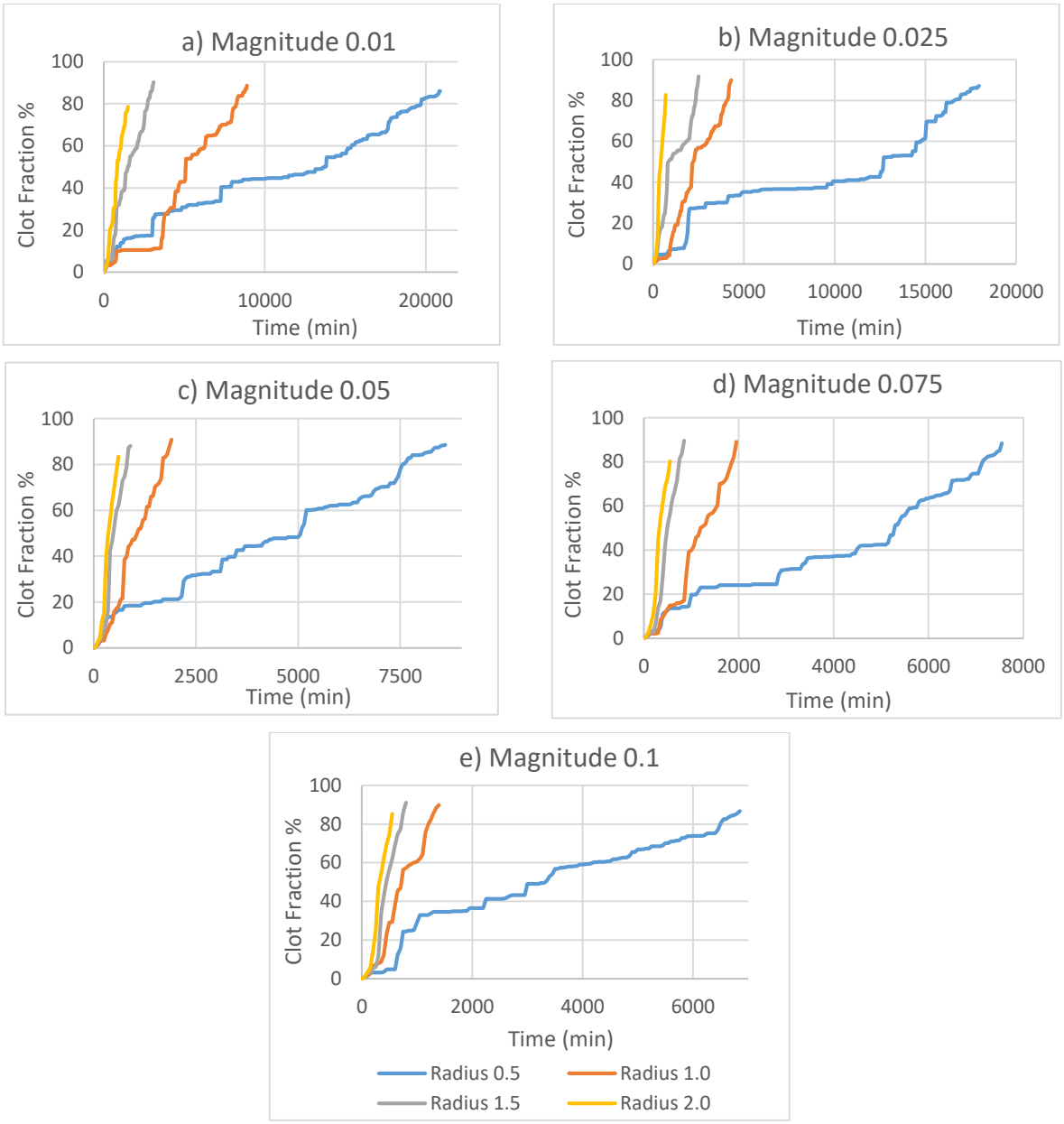

Figure 8.5 - Evolution of the Clot Fraction over the time, for four different values of Action Radius, using the Magnitude: a) 0.01; b) 0.025; c) 0.05; d) 0.075 and e) 0.1.

Performing a similar analysis of the results, but now varying the $Action\ Radius$, it is possible to see that a higher radius leads to a faster growth of the clot in all cases. In other words, the same clot fraction is acquired with less increments. These results were according to what was expected since the use of a larger $Action\ Radius$ is supposed to imply that more integration points are found, which leads to a larger number of points with increased thrombin concentration.

Furthermore, it is possible to see that, with the increase of the value of the $Magnitude$, this growth is faster, being in agreement with the results presented previously.

8.2.3 - Clot Fraction Analysis

Through the previous results and aiming to evaluate the time taken to obtain the results of each combination of the two parameters, the clot growth fraction was also individually analysed. For such purpose, four different percentages of Clot Fraction (12.5, 25, 37.5 and 50%) were defined and, four tables were construct for each percentage (***Table 8.1***, **Table 8.2**, **Table 8.3** and **Table 8.4**), in order to analyse specific points of the evolution of the growth of the clot. The tables present the time, in minutes, that every combination of parameters took to reach the respective percentage of Clot Fraction and, for each table, a 3D graphic was construct to simplify the analyses (**Figure 8.6**, **Figure 8.7**, **Figure 8.8** and **Figure 8.9**).

Table 8.1 – Time to reach 12.5% of Clot Fraction, for the different combination of parameters.

		Action Radius (mm)			
		0.5	1.0	1.5	2.0
Magnitude	0.01	1009	3560	575	315
	0.025	1845	1034	300	250
	0.05	310	466	316	211
	0.075	483	478	291	209
	0.1	650	401	303	192

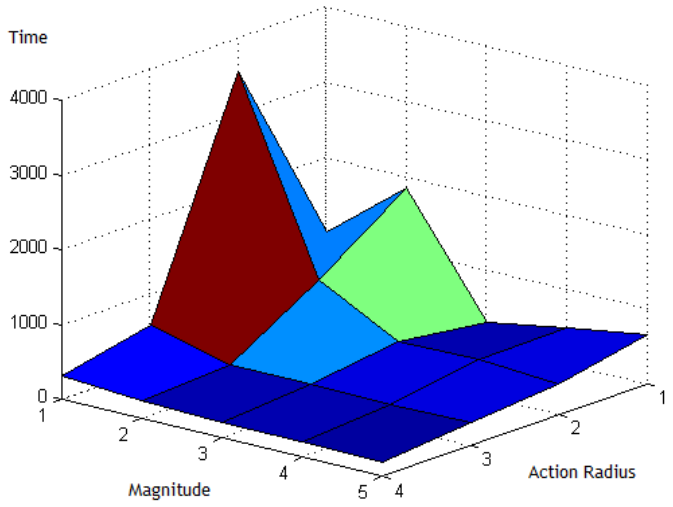

Figure 8.6 – 3D distribution of the **Table 8.1**.

Analysing the Clot Fraction of 12.5%, it is possible to see that the previously stated is also verified when specific points are studied. With the increase of the $Action\ Radius$ and the $Magnitude$, in general, it is possible to see that the number of increments to achieve the same Clot Fraction is lower, being in agreement with the previous results. However, in some cases, this increase do not affect the results as expected. For example, analysing the $Magnitude$ 0.01 and the $Action\ Radius$ of 0.5 and 1.0, it noticeable that the increase of the $Action\ Radius$ took much more time to reach the same Clot Fraction, being noticeable the difference between the peaks in the 3D graphic. Although, this is not the expected, but can be justify by the fact that the use of different parameters leads to different geometries of the clot, which influences the behaviour of the flow in the next increment. That way, the growth of the clot can be delayed when specific Clot Fractions are compared. However, when the overall result is analysed, it is possible to see that the run using a $Magnitude$ of 0.01 and an $Action\ Radius$ of 0.5 is the one that takes longer to reach higher percentages of Clot Fraction.

This difference is also noticeable when the $Magnitude$ 0.01 and 0.025, for the $Action\ Radius$ 0.5, are compared. It was expected that a higher $Magnitude$ leads to a shorter time of growth, which do not occur in this case. Such can be explain by the same reason presented above. However, when the overall result is analysed, although the $Magnitude$ 0.025 leads to a faster global run, it is possible to see that both combinations present similar curves.

Table 8.2 - Time to reach 25% of Clot Fraction, for the different combination of parameters.

		Action Radius (mm)			
		0.5	1.0	1.5	2.0
Magnitude	0.01	3050	3724	770	556
	0.025	2976	1481	657	285
	0.05	2170	710	367	271
	0.075	2806	881	384	260
	0.1	950	464	330	250

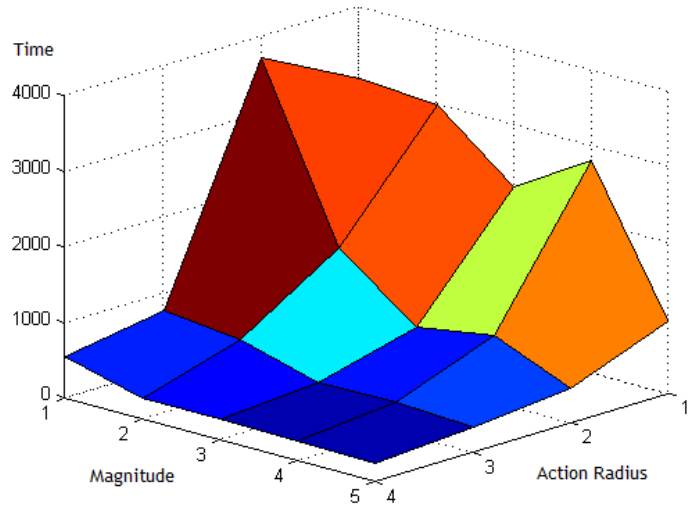

Figure 8.7 - 3D distribution of the **Table 8.2**.

Regarding the Clot Fraction of 25%, it is possible to see that the results are similar to the ones obtained previously, being noticeable a decrease in the time necessary to reach the mentioned Clot Fraction when the value of the $Action\ Radius$ or of the $Magnitude$ increase.

Also, once again, analysing the same combination of parameters referred in the Clot Fraction of 12.5% ($Magnitude$ 0.01 and the $Action\ Radius$ of 0.5 and 1.0), it is possible to see that, although the increase of the radius do not lead to the expected results, the results tend to converge, presenting now a more similar result, which can also be seen in the 3D graphic since the difference between the peaks obtained is now softer.

On the other hand, analysing the $Magnitude$ of 0.05 and 0.075, for all $Action\ Radius$, the same is verified. With the increase of the $Magnitude$, the time to reach the 25% of the Clot Fraction also increase. Once again, and similar to the other example, this can also be justified by the fact that the use of different parameters leads to different geometries of the clot, which influences the behaviour of the flow in the next increment. However, again, when the global result is analysed, it is possible to see that the $Magnitude$ 0.075 leads to a faster increase of the Clot Fraction. Moreover, note that this difference is more clear when lower $Action\ Radius$ are used.

Regarding the $Magnitude$ of 0.01 and of 0.025, for the $Action\ Radius$ 0.5, note that now the time which led to this percentage, decreased with the increase of the parameter $Magnitude$, being dependent, once again, of the evolution of the clot, over the increments.

Table 8.3 - Time to reach 37.5% of Clot Fraction, for the different combination of parameters.

		Action Radius (mm)			
		0.5	1.0	1.5	2.0
Magnitude	0.01	7279	4438	1089	726
	0.025	9550	2100	756	327
	0.05	3141	747	391	289
	0.075	4250	941	433	285
	0.1	2211	596	370	278

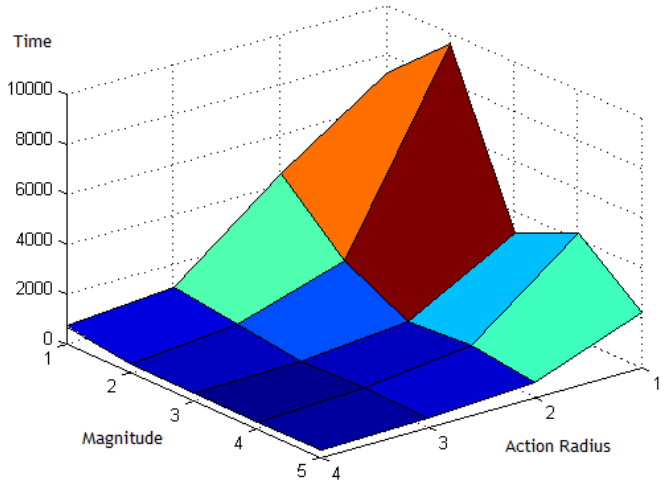

Figure 8.8 - 3D distribution of the **Table 8.3**.

The results of the Clot Fraction of 37.5% are very similar to the ones obtained for the previous Clot Fraction percentages. Once again, analysing the $Magnitude$ 0.01 and 0.025, for the $Action\ Radius$ 0.5, and the $Magnitude$ of 0.05 and 0.075, for all $Action\ Radius$, it is possible to see that the previous behaviours are presented. For both, the time to achieve this Clot Fraction is higher when the $Magnitude$ presents a higher value.

In the remaining results, the opposite occurs, being that, the higher $Action\ Radius$ (2.0 mm) combined with the higher $Magnitude$ (0.1) reach the Clot Fraction of 37.5% in a lower time, as expected.

Table 8.4 - Time to reach 50% of Clot Fraction, for the different combination of parameters.

		Action Radius (mm)			
		0.5	1.0	1.5	2.0
Magnitude	0.01	13650	5080	1500	830
	0.025	12677	2200	850	416
	0.05	5059	1062	481	362
	0.075	5283	1200	492	327
	0.1	3321	717	444	317

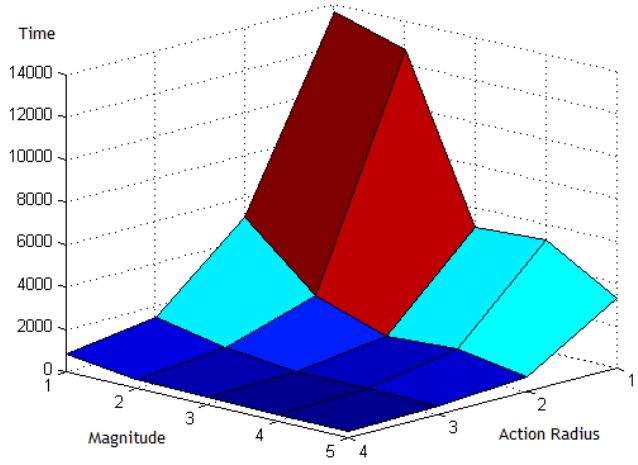

Figure 8.9 - 3D distribution of the **Table 8.4**.

Lastly, analysing the results for the Clot Fraction equal to 50%, it is possible to see that they are the ones that are more coherent with what is expected. In this case, only in the *Magnitudes* of 0.05 and 0.075, for the first three *Action Radius*, exist an increase in the time to reach the 50% of the Clot Fraction when the *Magnitude* defined is higher. However, these curves tend to converge and, when the global time curve is analysed, it is possible to see that the results of the *Magnitude* 0.075 tend to reach a faster growth of the clot in a final phase.

Summing up, it is possible to conclude that, for all percentages, the results are similar, having only unexpected oscillations in a few results. Thus, once again, it was possible to verify that higher *Magnitude* and/or *Action Radius* lead to a lower time to reach a specific Clot Fraction.

That way, and also assuming the results of the sections **8.2.1** and **8.2.2**, the author defines that the *Action Radius* of 1.0 mm combined with a *Magnitude* between 0.05 and 0.1, were the

ones that lead to more accurate and equilibrated results. Lower $Magnitude$ and lower $Action\ Radius$ are time consuming and, for this reason, inefficient. One the other hand, higher $Action\ Radius$, mainly when combined with higher $Magnitude$, promote a fast growth of the clot and also a fast blockage of the outlet, which make the process less realistic and inaccurate. One the other hand, the results obtained with the $Action\ Radius$ of 1.0 mm combined with a $Magnitude$ between 0.05 and 0.1 lead to a more coherent growth over the time, presenting the most suitable growth results. Thus, the results that will be presented next only will considered these combinations of parameters.

8.2.4 - Colour Maps

After studying how the growth of the clot is affected by the two parameters analysed, one $Action\ Radius$ and two $Magnitude$ were selected as the better combinations to calibrate the algorithm. For these, sequential colour maps were obtained in order to verify the viability of the code, as well as to verify the influence of the growth of the clot in the domain, over the increments.

Thus, five different colour maps (Clot Growth, Concentration of Thrombin, Velocity, Shear Rate and Viscosity) are presented along this section, in different 12 time steps.

The colour maps are presented for the $Action\ Radius$ 1.0 combined with the $Magnitude$ 0.1, and for the $Action\ Radius$ 1.0 with $Magnitude$.5 and can be seen in the next points. Note that the $Magnitude$ of 0.075 was not used, since it promote a similar result to the $Magnitude$ of 0.05 and for this reason, the author opted for two more distant values of $Magnitude$.

8.2.4.1 - Parameters: Action Radius 1.0 and Magnitude 0.1

a) Clot Growth

In the next figures (**Figure 8.10**) it is possible to see the evolution of the growth of the clot, over 12 selected time steps, which will allow to analyse the other colour maps presented next. Besides that, for each image, the respective Clot Fraction (in percentage) is presented.

a) 0.66% b) 1.85% c) 2.35%

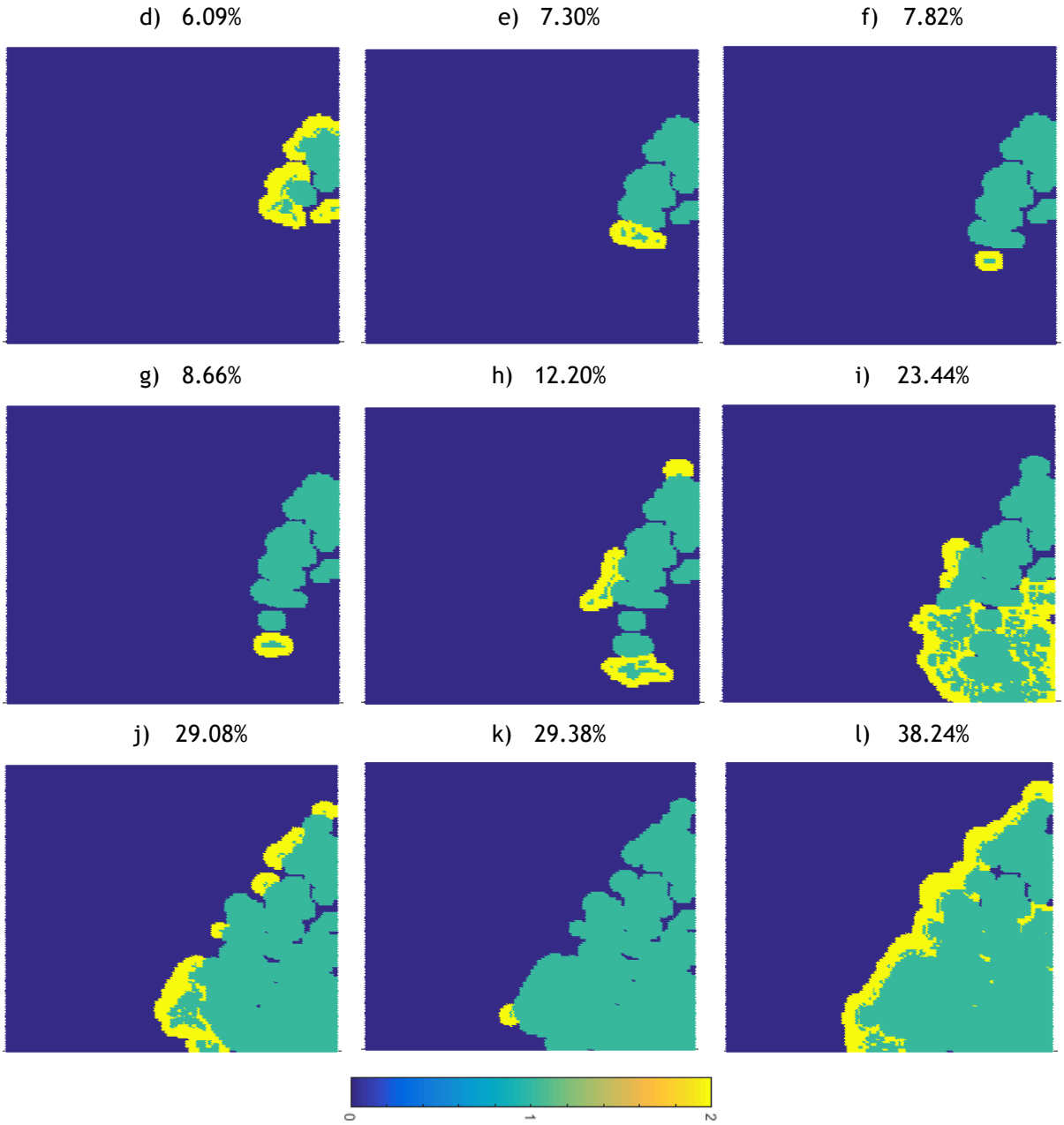

Figure 8.10 – Colour maps of the growth of the clot, using an Action Radius of 1.0 and a Magnitude of 0.1. Blue: blood; Green: old clot; Yellow: new clot.

Since a clot is an agglomerate of blood components, it is expected that it has an appearance without a specific form. Such feature can be seen in the previous colours maps, being a preliminary indicator of suitable results. Besides that, the growth is random, that is, it does not follow a pattern of growth. Initially, the clot tends to grow mainly for the zone of higher concentration of thrombin and, in the last increment, to the zone of the outlet, promoting its occlusion. Thus, the growth is strongly dependent on the conditions of the domain, namely, the concentration of thrombin, and also not homogeneous over the time.

b) Concentration of Thrombin

Since the concentration of thrombin is one of the main factors that affect the growth of the clot, it is important to verify its variation along the growth. So, the variation of the concentration of thrombin due to the growth of the clot is presented in the next colour maps (**Figure 8.11**).

Note that the results are presented in a logarithmic scale in order to present more noticeable results. In the **Figure 8.2**, it is possible to see the original distribution of thrombin, being represented here in a logarithmic scale in the first colour map.

a) Initial Concentration

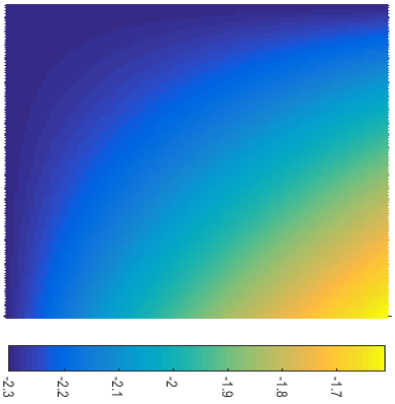

b) 0.66%

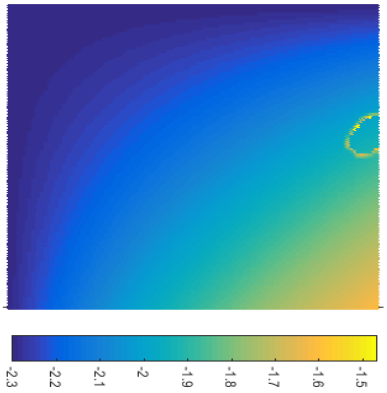

c) 1.85%

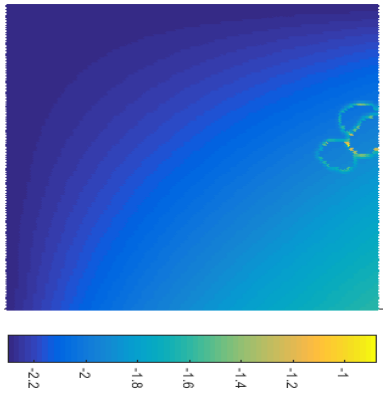

d) 2.35%

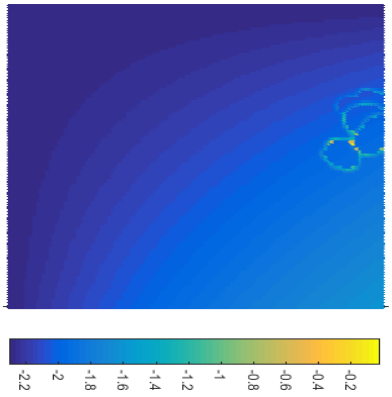

e) 6.09%

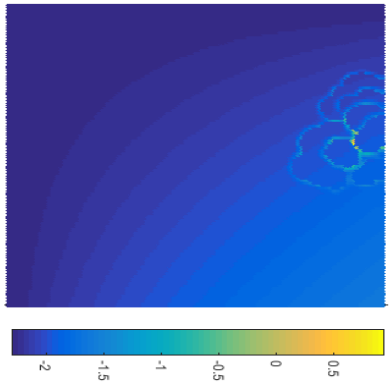

f) 7.30%

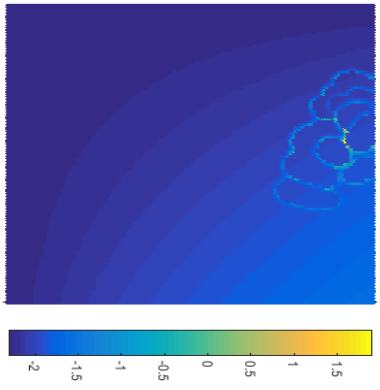

g) 7.82%

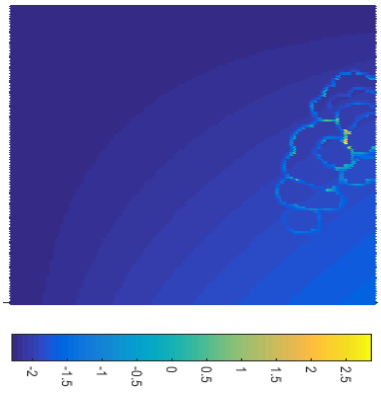

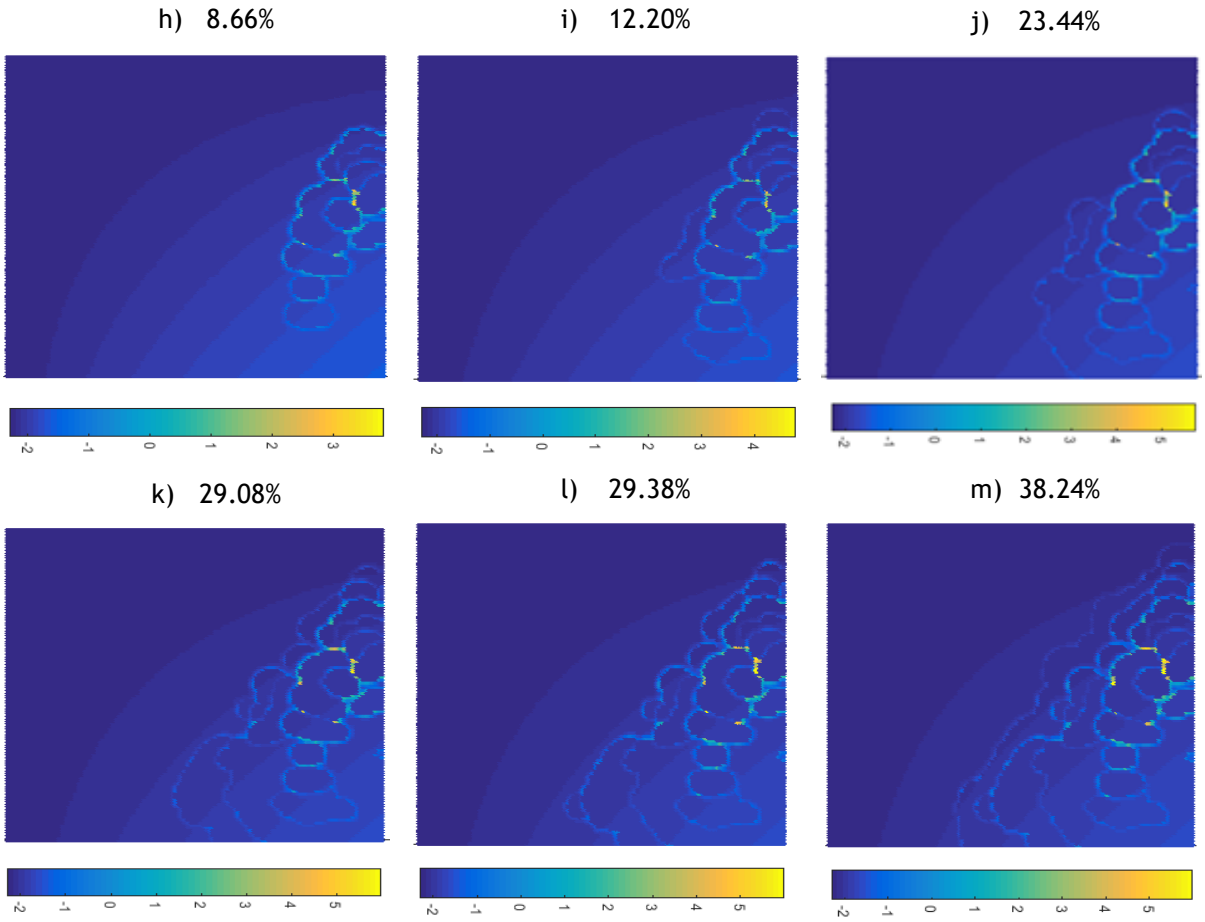

Figure 8.11 - Colour maps of the distribution of the concentration of thrombin, using an Action Radius of 1.0 and a Magnitude of 0.1.

As mentioned before, the concentration of the thrombin is one of the triggers that promote the growth of the clot, being dependent on the two parameters that were previous analysed: the $Magnitude$ and the $Action\ Radius$. The algorithm was design in order to increase the concentration of this in all the points that are in the $Action\ Radius$, at each increment, with a define $Magnitude$ of increase. Thus, over the time, it is expected that the concentration of the thrombin increase in the integration points near to the clot, and that it is maintained at the integration points that already are clot. Such behaviour is possible to see in the previous colour maps. As mentioned, over the figures, it is possible to see an increase in the concentration of the thrombin in the points near to the one that already are clot, being that increase responsible for the clot growth in upper zones of the domain, since the concentration of the points in this zone are lower than the basal concentration in the first increment.

c) Velocity

Similar to the previous colour maps, the next figures (**Figure 8.12**) correspond to the colour maps of the variation of the velocity of the domain, over the 12 time steps selected, being that the first colour map represents the distribution of the velocity without the clot.

a) Initial Velocity

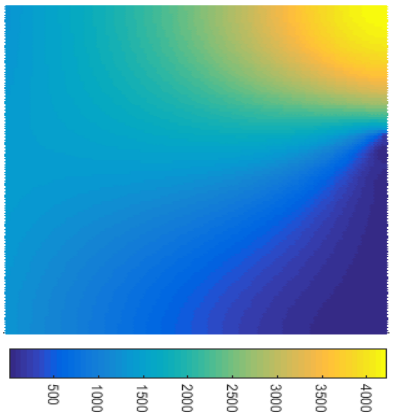

b) 0.66%

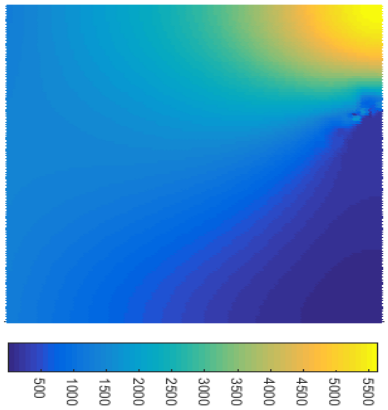

c) 1.85%

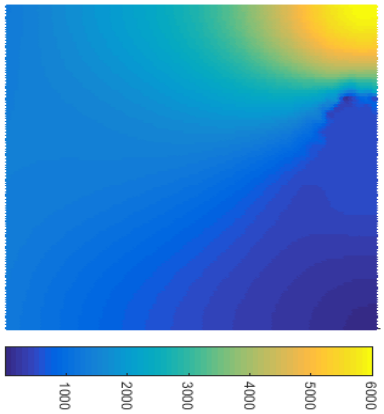

d) 2.35%

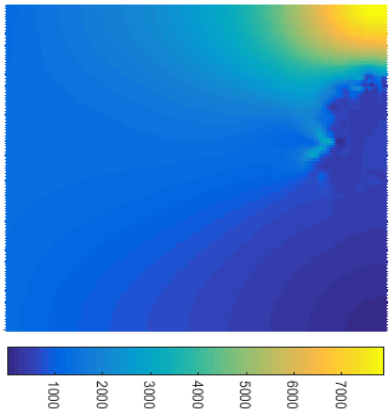

e) 6.09%

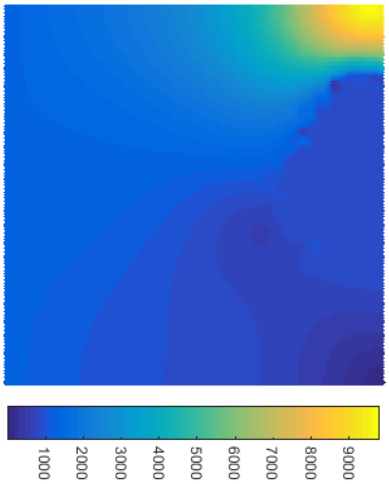

f) 7.30%

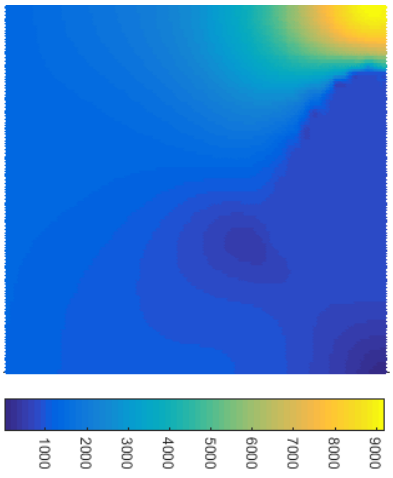

g) 7.82%

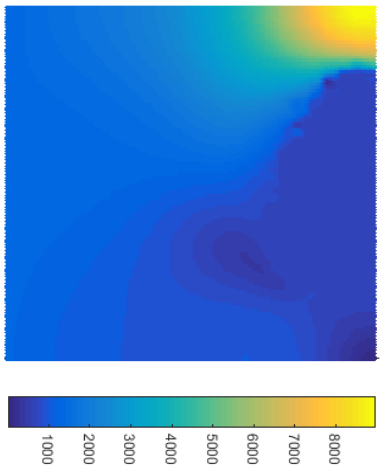

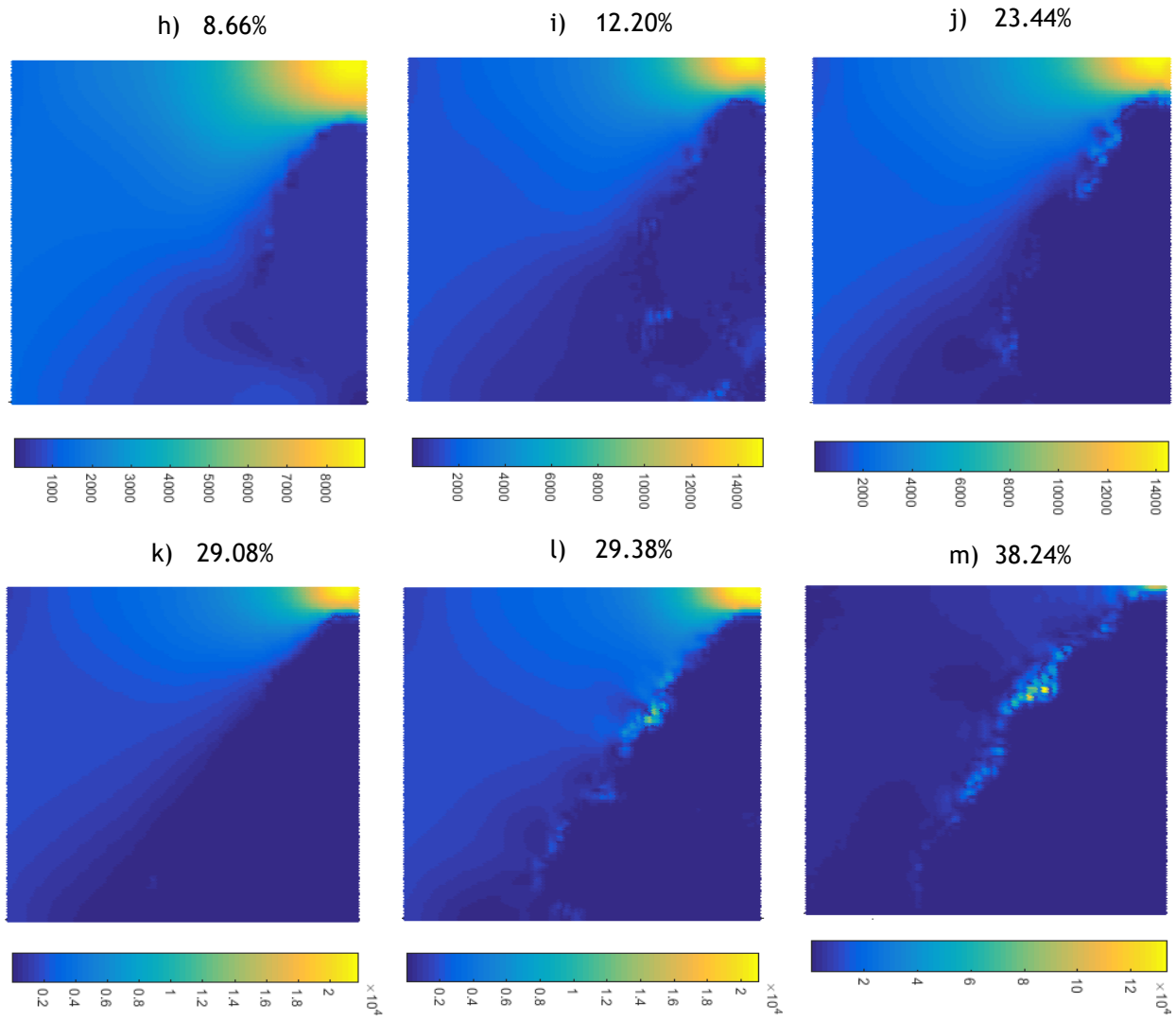

Figure 8.12 - Colour maps of the velocity profiles, using an Action Radius of 1.0 and a Magnitude of 0.1.

Usually, a clot is a viscous body that acts as a barrier to the blood flow so, when a clot starts to appear, the velocity profile tend to change. In the clot area, it is expected that the velocity tends to be lower and near to zero, since the blood flow cannot pass through the clot.

In the area where the leak exists, it is expected for the value of the velocity to increase, if the clot grows in that direction, promoting the occlusion of the outlet. In this last case, the velocity tend to increase since the section area that allows the flow to pass decrease. So, as seen in Chapter 6, to maintain the flow rate, the velocity needs to increase, which is demonstrated by the equation of Flow Rate ($m = v \cdot \rho \cdot A \cdot cos\theta$, being m the flow rate, v the velocity, ρ the density of the fluid, A the area where blood flows and θ the angle between the unit normal and the velocity of mass elements).

Analysing the colour maps, it is possible to see that the velocity variation is coherent with what is expected. With the clot growth exist an increase of the velocity in the outlet that tends to intensify over the increments. Besides that, since the clot tends to block the passage of the blood, the velocity in that zone tend to 0, which is also possible to see with the growth of the clot.

d) Shear Rate

Regarding now the shear rate and its variation over the time, the respective colour maps are presented in **Figure 8.13**.

Note that the first colour map (**Figure 8.13** a)) corresponds to the Shear Rate profile when all the domain is define as blood.

a) Initial Shear Rate

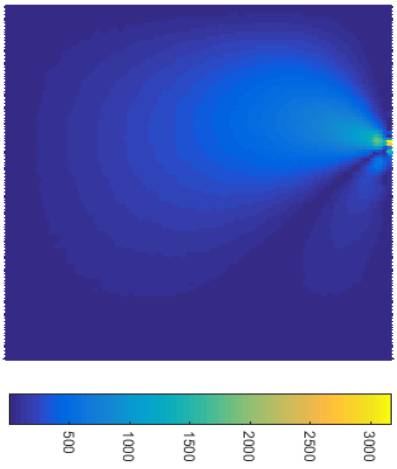

b) 0.66%

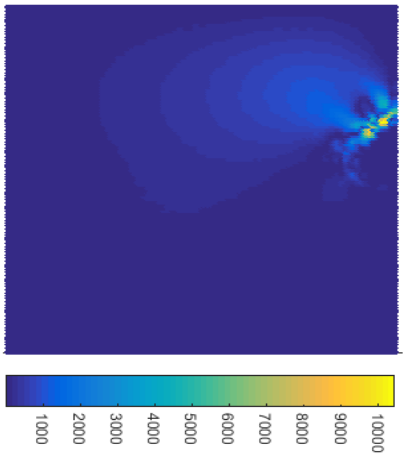

c) 1.85%

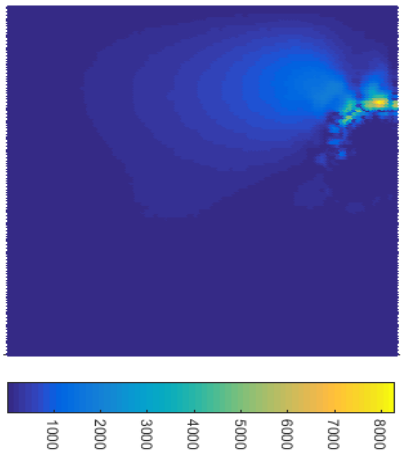

d) 2.35%

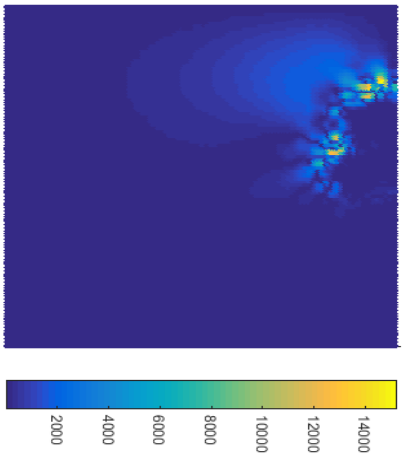

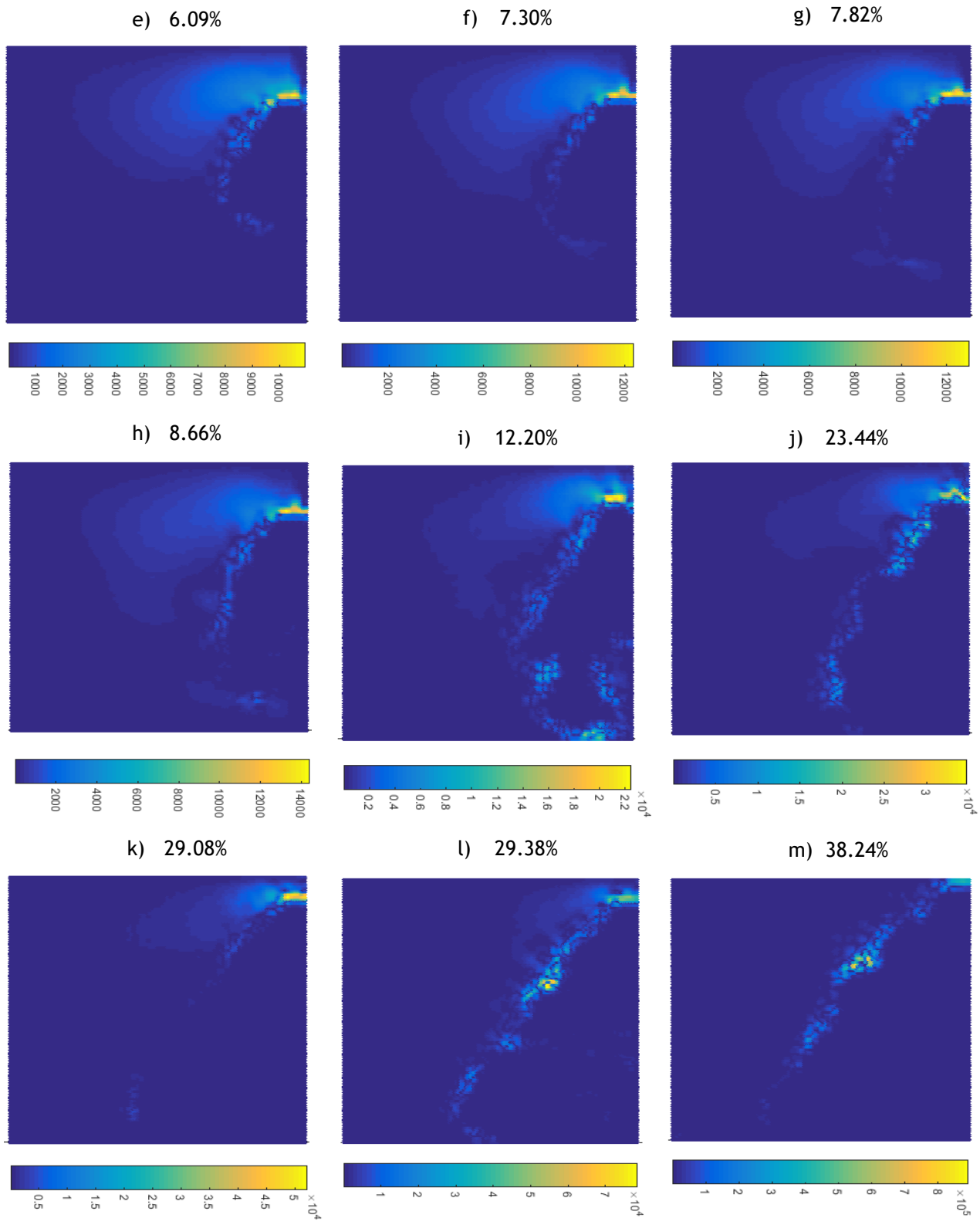

Figure 8.13 - Colour maps of the shear profiles, using an Action Radius of 1.0 and a Magnitude of 0.1.

The shear rate is the deformation of a material, over the time, which can be directly related with the velocity of the domain. So, and analogous to the velocity, with the growth of the clot the shear rate tend to increase, mainly in the zone of the outlet.

Moreover, it is possible to see that the shear rate also increase in the border of the clot. As mentioned, the shear rate is the other trigger defined in this algorithm to promote the appearance and the growth of the clot. Thus, for this reason, it is expected that, in the zones where the clot grows, it exists a value of shear rate within the intervals ($[500;\ 6000]$ or $]6000;\ 100000]$) defined as limits for a point to be modified as clot. Note that in the zones of growth, the values of shear rate are in that ranges, which allows the growth of the clot in the next increment.

e) Viscosity

Finally, the variation of the viscosity of the domain due to the growth of the clot is represented in the colour maps that are presented below (**Figure 8.14**).

Note that the results are in a logarithmic scale and, besides that, all images correspond to the difference between the increment under study and the first increment.

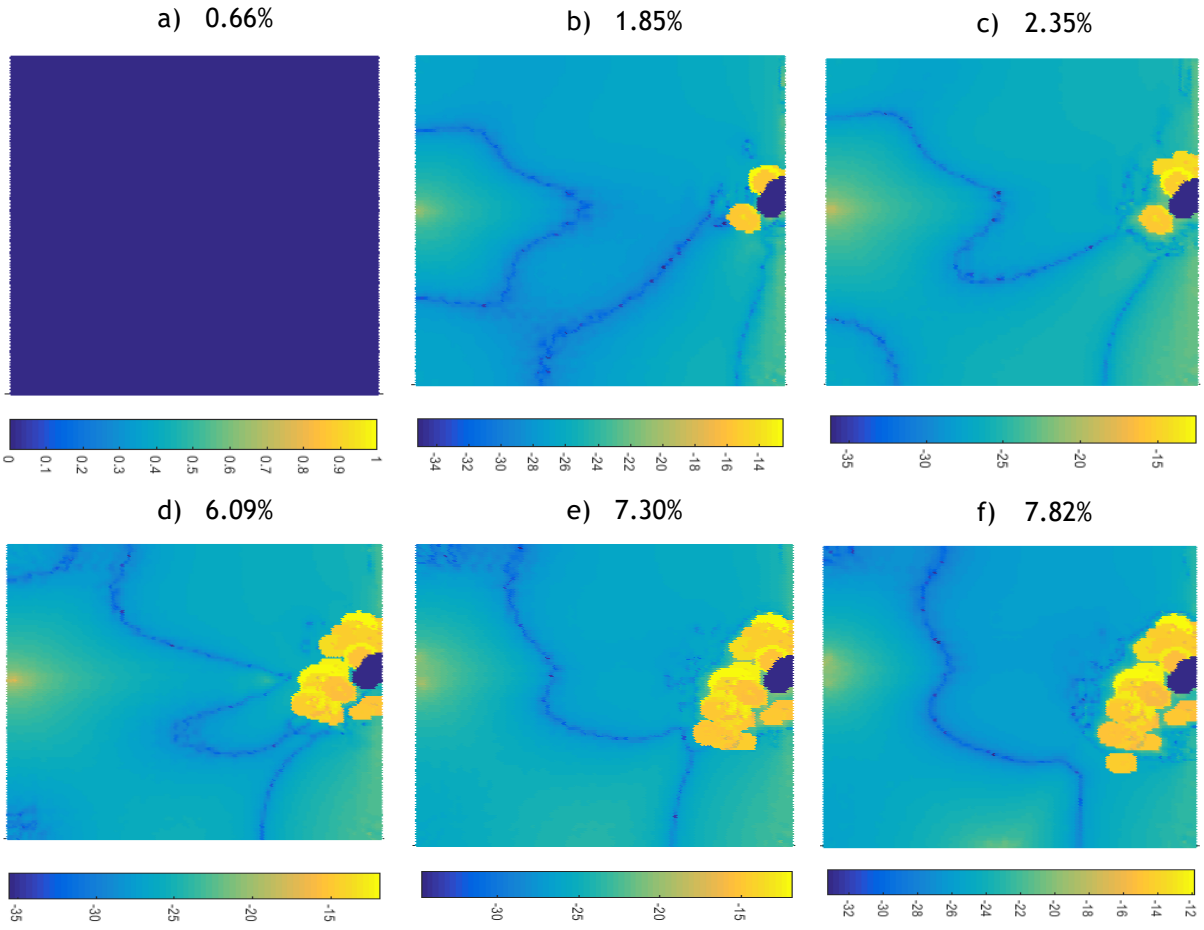

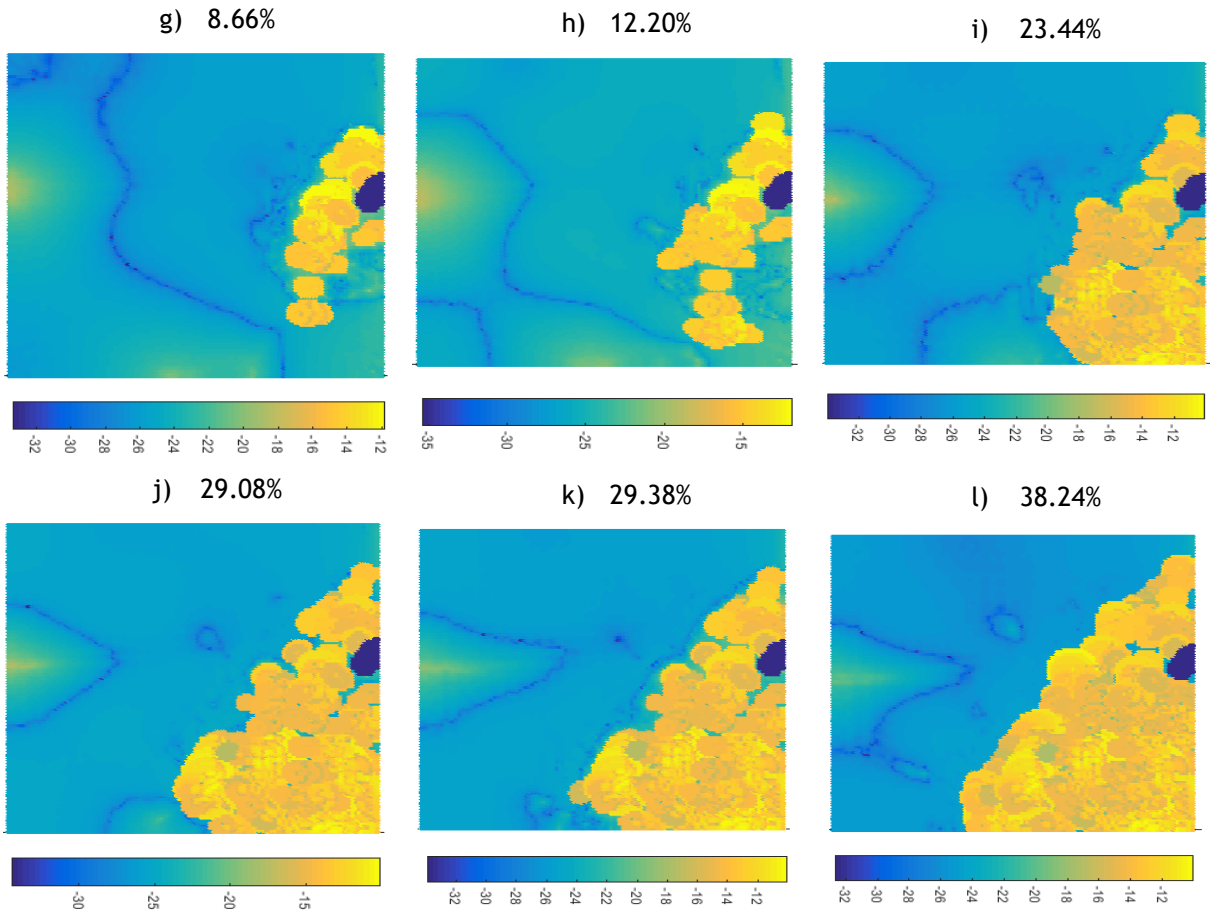

Figure 8.14 - Colour maps of the variation of the viscosity of the clot, using an Action Radius of 1.0 and a Magnitude of 0.1.

When a clot is formed, the viscosity of that zone tend to increase since the formation of agglomerates of coagulation components occurs and, the blood in that vicinity can also have its viscosity change due to the alterations of the blood flow pattern, promoted by the growth of the clot.

In the case of this algorithm, the viscosity of the domain is dependent on the shear rate so, the higher the shear rate at an integration points, the higher the viscosity at that integration point. Analysing the colour maps of the Shear Rate, it was possible to conclude that this variable alters with the clot growth. That variation is also visible in this case, since the viscosity of the domain changes along the colour maps, which demonstrate the coherence of the results.

Moreover, it is possible to see that the viscosity of the clot is different of the rest of the domain, proving that the algorithm can efficiently alter the properties of the domain over the increment in order to create an obstacle to the passage of flow.

Lastly, in the clot, it is possible to verify that exist different viscosity values, which is coherent with the expected. Such is justified by the fact that this parameter depends on the shear rate and each point presents its own value.

8.2.4.2 - Parameters: Action Radius 1.0 and Magnitude 0.05

Similar to what was presented for the first example, the same colour maps are presented in this section. That way, it is possible to compare the results and verify in a visual way the influence of the $Magnitude$ in the growth of the clot and, consequently, in the other parameters that were analysed in the section above.

Thus, the colour maps were organized in the same way, being the same correspondent 12 increments were selected.

a) Clot Growth

As in the previous section, the colour maps and the respective Clot Fraction are presented in **Figure 8.15**.

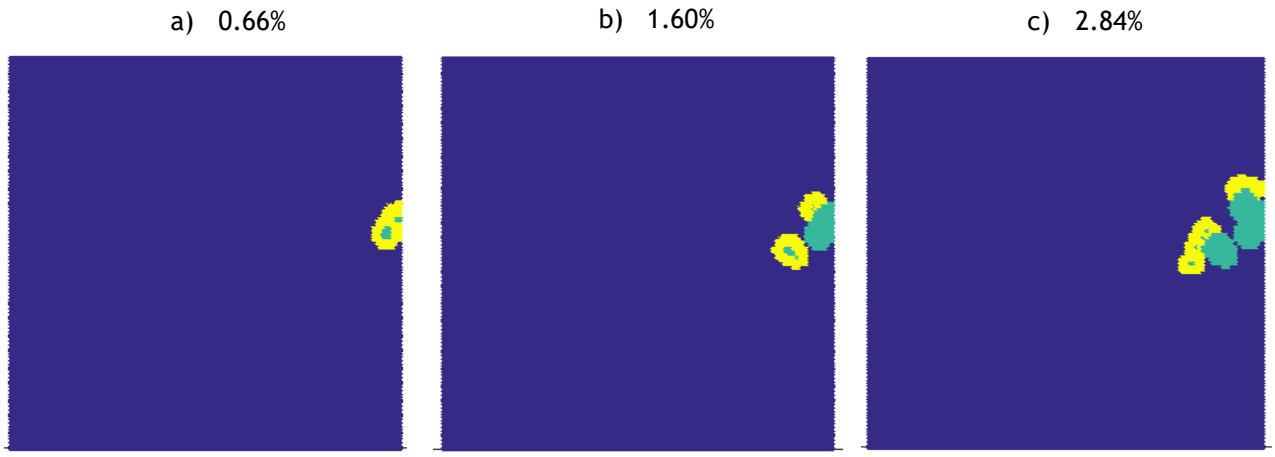

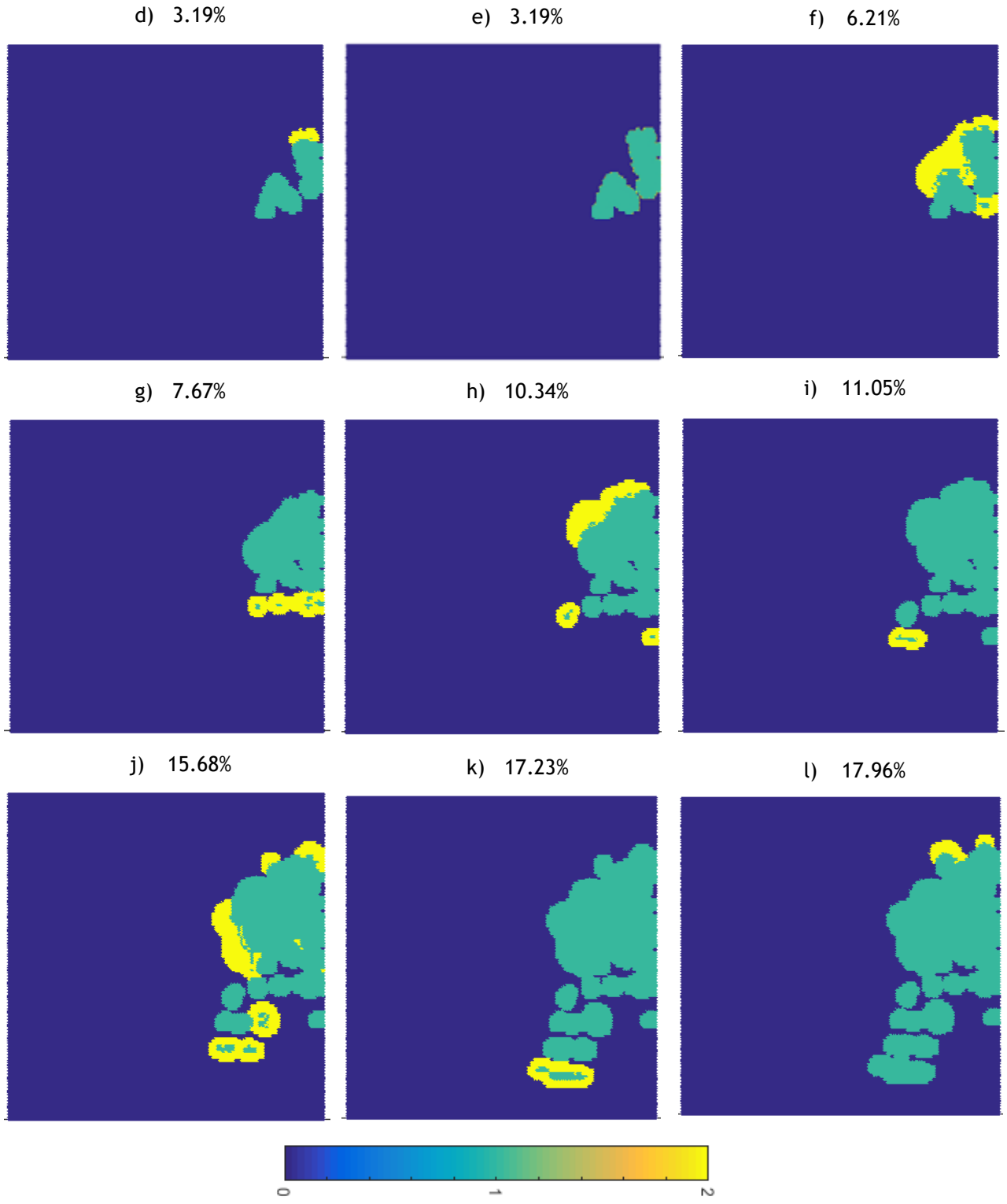

Figure 8.15 – Colour maps of the growth of the clot using an Action Radius of 1.0 and a Magnitude of 0.1. Blue: blood; Green: old clot; Yellow: new clot.

It is possible to see that the growth of the clot presents the same behaviour of the previous example, that is, a growth towards the focus of concentration of thrombin and towards the outlet, without a specific pattern.

However, as expected, the growth is slower, being reached a lower Clot Fraction. Such can be explain by the use of a lower $Magnitude$, which is in concordance with the conclusion taken in **8.2.1**, **8.2.2** and **8.2.3**.

b) Concentration of Thrombin

The colour maps regarding thrombin are presented below, in logarithmic scale (**Figure 8.16**). The first colour map, **Figure 8.16** a), correspond to the initial concentration of thrombin, without clot.

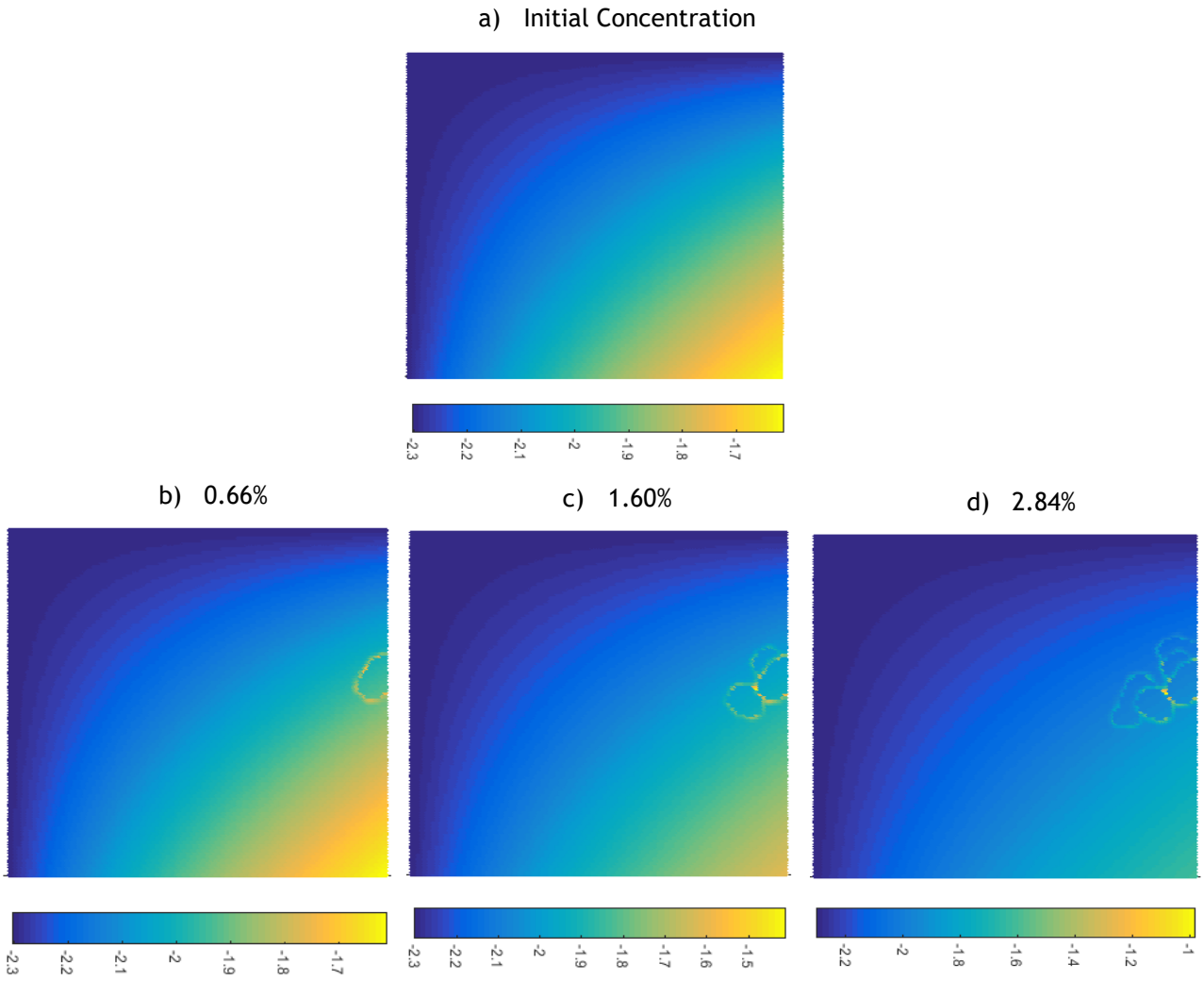

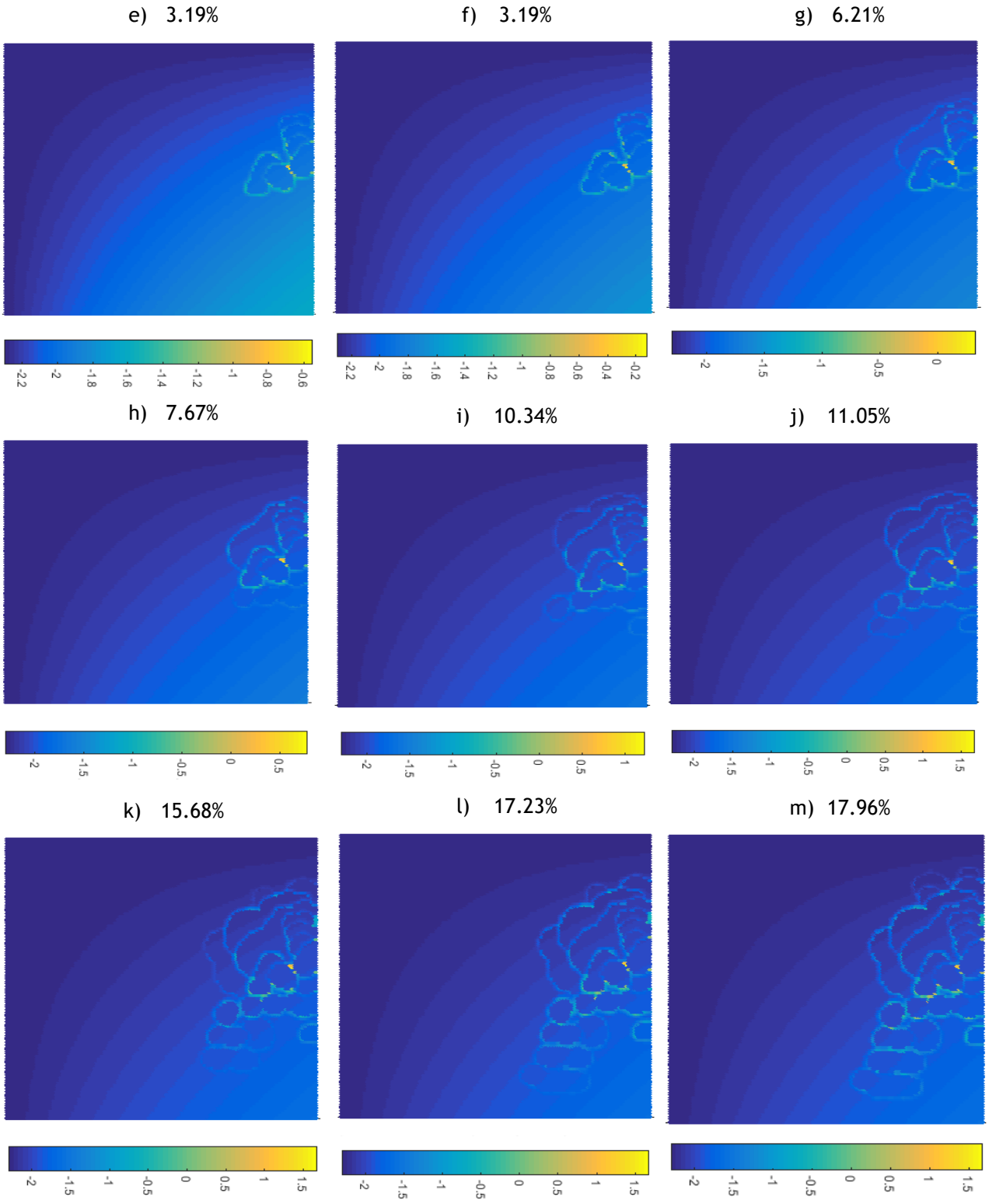

Figure 8.16 - Colour maps of the distribution of the concentration of thrombin, using an Action Radius of 1.0 and a Magnitude of 0.05.

As the previous results, these colour maps are similar to the ones obtain with the $Magnitude$ of 0.1, presenting a similar profile of concentration. Besides that, it is also possible to observe the increase in the concentration of thrombin, over the increments, in the zones near to the clot. Such are coherent with what is intended by the algorithm, presenting satisfactory results.

c) Velocity

The next colour maps show the variation of the velocity along the 12 selected increments (**Figure 8.17**). Note that the first one correspond to the velocity profile without the clot (**Figure 8.17** a)).

a) Initial Velocity

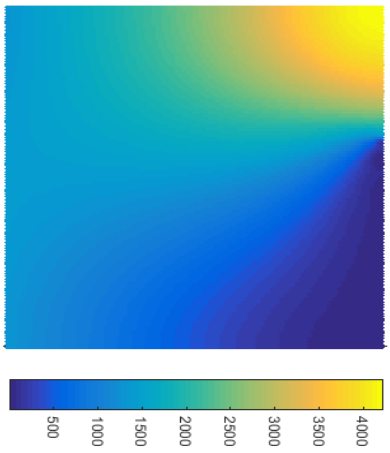

b) 0.66%

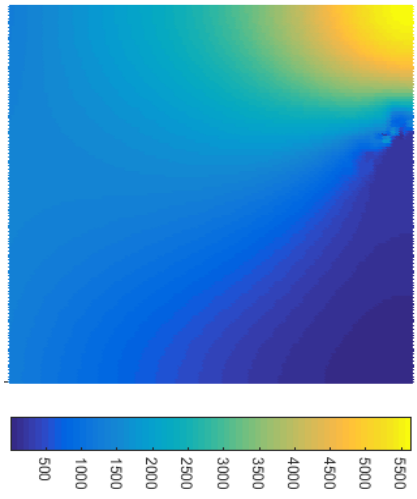

c) 1.60%

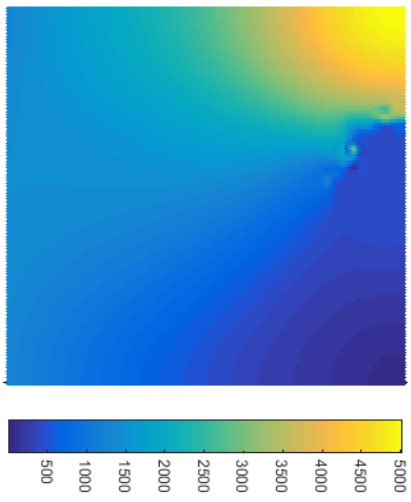

d) 2.84%

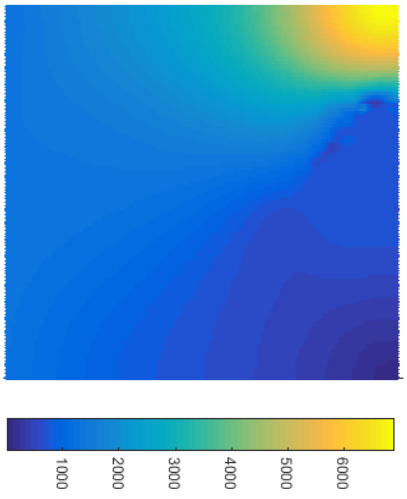

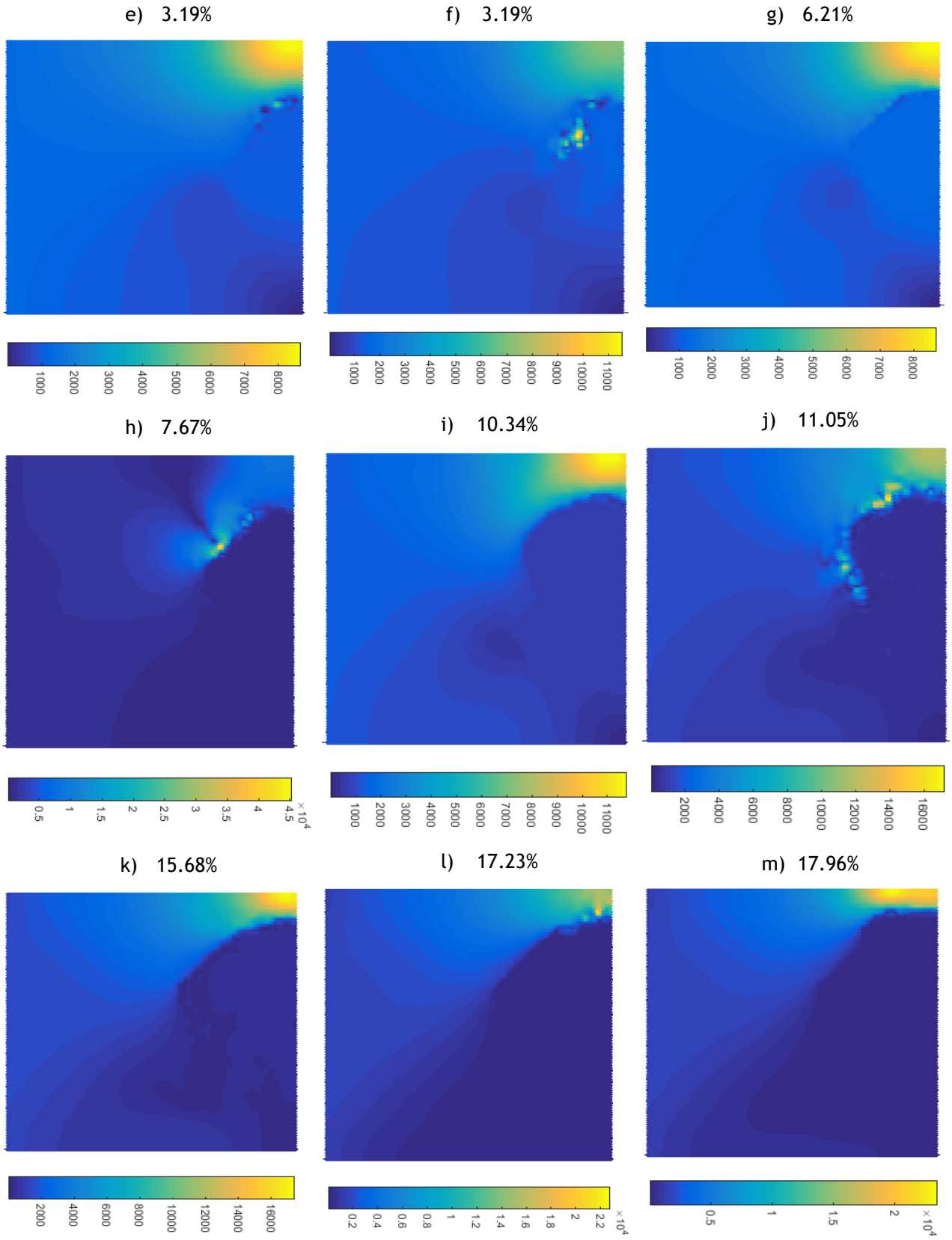

Figure 8.17 - Colour maps of the velocity profiles, using an Action Radius of 1.0 and a Magnitude of 0.05.

Analysing the results, it is possible to verify that, once again, they are similar to the obtained in the previous example, being also coherent with what is expected.

The main difference is increment 7 (**Figure 8.17** h)) that presents a point with an unexpected higher value of velocity. However, if the whole domain is analysed, it is possible to see that the velocity profile is similar to the other colour maps. Thus, this unexpected result can be caused by a numerical error in that specific set of points.

d) Shear Rate

Similar, the next colour maps show the variation of the shear rate along the 12 selected increments (**Figure 8.18**). Note that the first figure correspond to the shear rate profile without the clot (**Figure 8.18** a)).

a) Initial Shear Rate

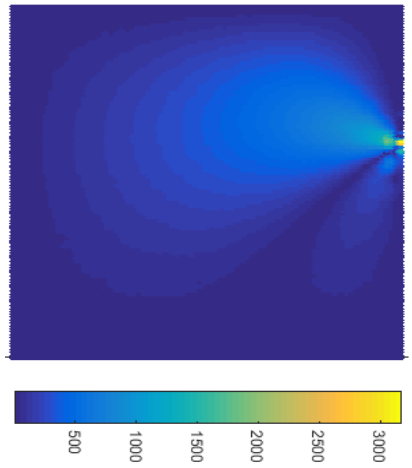

b) 0.66%

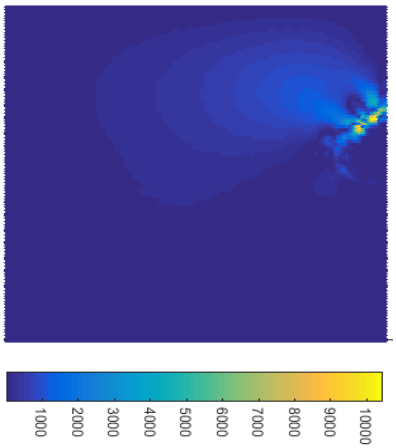

c) 1.60%

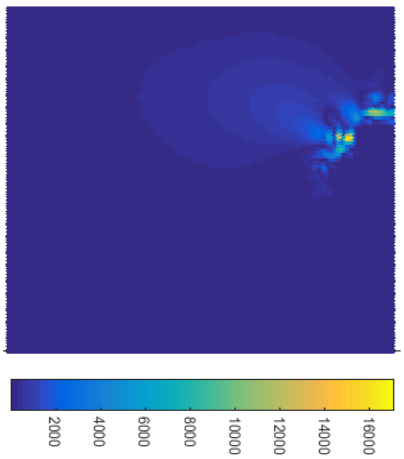

d) 2.84%

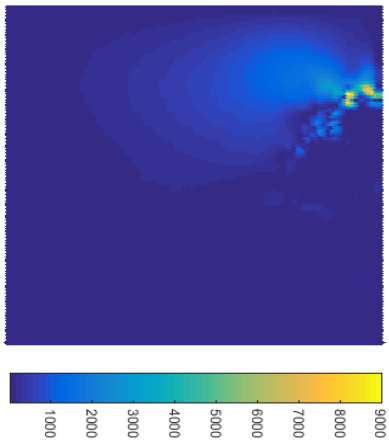

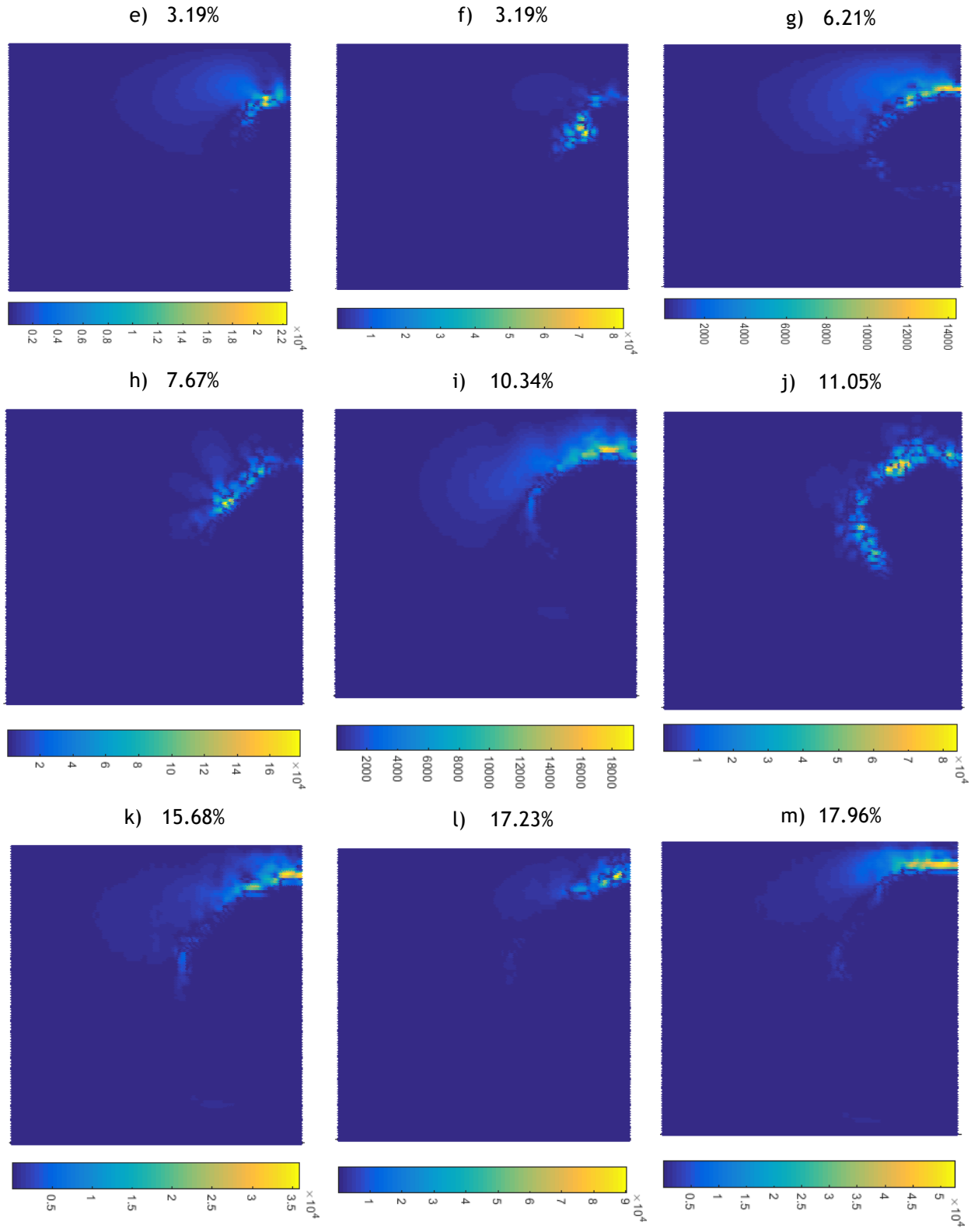

Figure 8.18 - Colour maps of the shear profiles, using an Action Radius of 1.0 and a Magnitude of 0.05.

Once more, the obtained results are similar to the ones in **Figure 8.13**. Here, it is possible to visualize the same increase in the shear rate, which can also be related with the increase of the velocity, as it was shown in the **Figure 8.17**. Moreover, the shear rate tends to increase in the zone of the clot, promoting its growth, as occurred previously. Thus, the results are in accordance with the expected.

e) Viscosity

The variation of the viscosity of the combination $Action\ Radius$ 1.0/$Magnitude$ 0.05 is represented in the colour maps of **Figure 8.19**. The representation assumed in the previous viscosity colour maps was also assumed here.

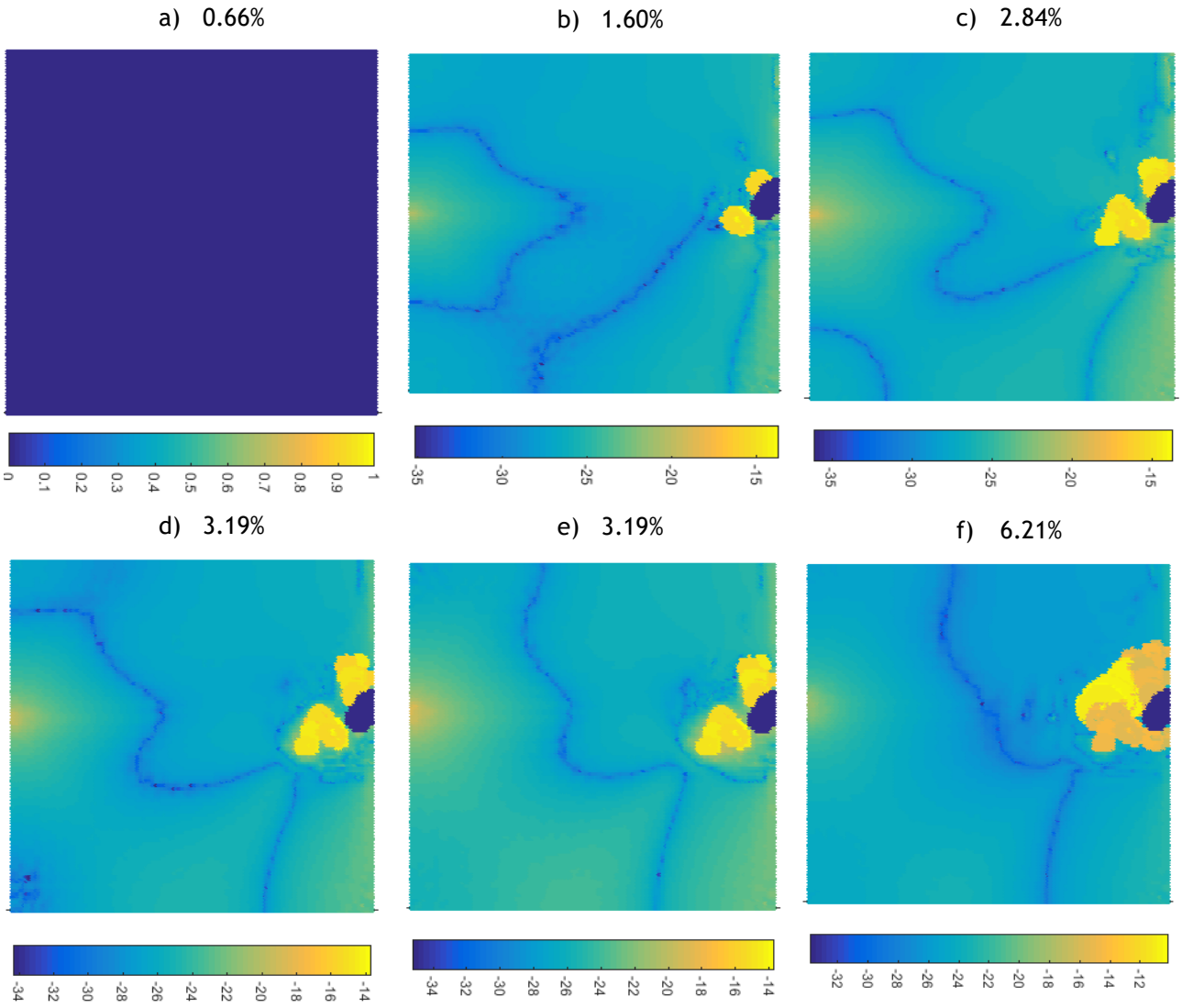

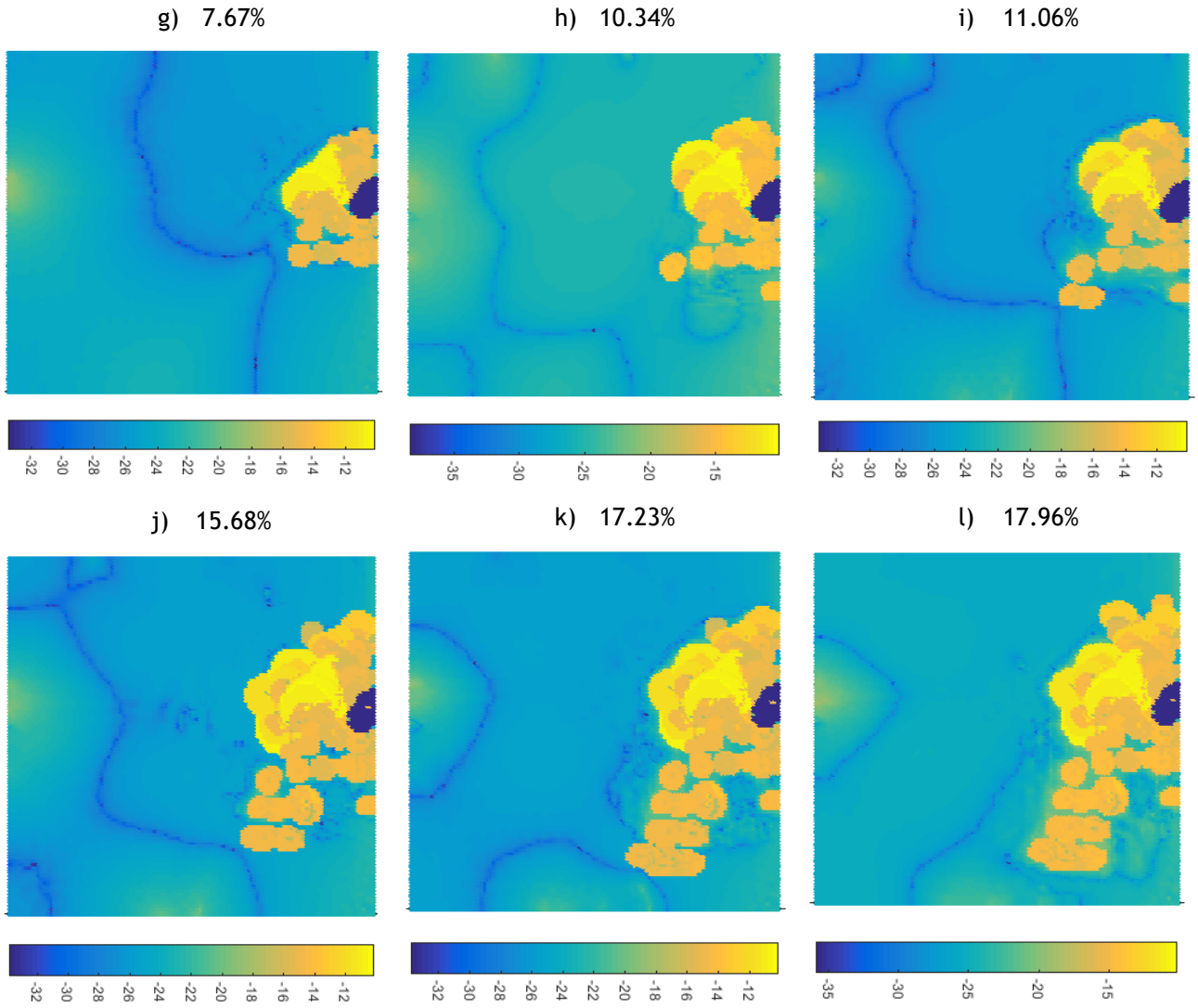

Figure 8.19 - Colour maps of the variation of the viscosity, using an Action Radius of 1.0 and a Magnitude of 0.05.

The colour maps resemble the previous ones, since they present the same features, which were previously mentioned. This shows, once more, that the algorithm is changing the viscosity as expected, presenting suitable results.

To sum up, it was possible to verify that both cases were in accordance to what was expected, presenting adequate profiles to the characteristics of the domain in each increment (time step). Also, it was possible to show that the algorithm performs as intended, namely the increase of the concentration of thrombin in the points near to clot or the alteration of the viscosity, being clearly visible in the colour maps. Besides that, the results that were obtained are in compliance with the ones obtained in section **8.2.1**, showing that lower magnitudes promote slower growth.

Considering both cases and their respective results, as well as the growth obtained in each of them, the combination of parameters used in the first case was assumed as the initial calibration combination of the algorithm. This combination of parameters will be used to simulate more complex situations, a topic that will be explored in the next chapter.

Chapter 9

Benchmark Results

After verify the viability of the algorithm with a simple and controlled scenario, different situations were created in order to verify the behaviour and robustness of the algorithm. Thus, two different scenarios were assumed:

(1) variation of the initial distribution of the concentration of thrombin and

(2) variation of the essential boundary conditions.

In the first case, the focus of thrombin was alter to the top corner and to the middle of the top wall. Additionally, two simultaneous focuses of concentration were defined in domain. That way, it was possible understand the influence of the distribution of the concentration of the thrombin in the growth of the clot in the domain.

In the other case, the size of the inlet and the position of the outlet were modify in three different ways, in order to test the algorithm in different configurations, and also to verify the influence of the flow in the growth of the clot.

For such purpose, the values of $Magnitude$ and of $Action\ Radius$ used are the ones that were establish as the ones that calibrate the algorithm, which were defined in the previous section as: $Action\ Radius = 1.0$ and $Magnitude = 0.1$.

9.1 - Variation of the Distribution of Thrombin

The distribution of thrombin present a focus that was initial define in the bottom right corner, as previous shown. However, this distribution can be modify in order to have other values of

concentration or to have the focus in other zone of the domain. Besides that, it is also possible to define multiple zones with focus, which can makes the simulation more complex.

As has been demonstrated, the concentration of thrombin influence the appearance and the growth of the clot, being critical the localization of the higher concentration of thrombin.

So, the distribution of the concentration of the thrombin was modify in three different cases: focus of thrombin in the top corner, focus of thrombin in the middle of the top wall, and two simultaneous focus of concentration. For each case, five different colour maps (Clot Growth, Concentration of Thrombin, Velocity, Shear Rate and Viscosity) were presented. Moreover, the results were compared evaluating the variation of the Clot Fraction over the time. All the initially defined conditions were fixed, namely the initial velocity, boundary conditions, etc. (as **Figure 8.1** shows).

9.1.1 – Thrombin Distribution Case 1

In the following figure (**Figure 9.1**) the new distribution of thrombin is represented.

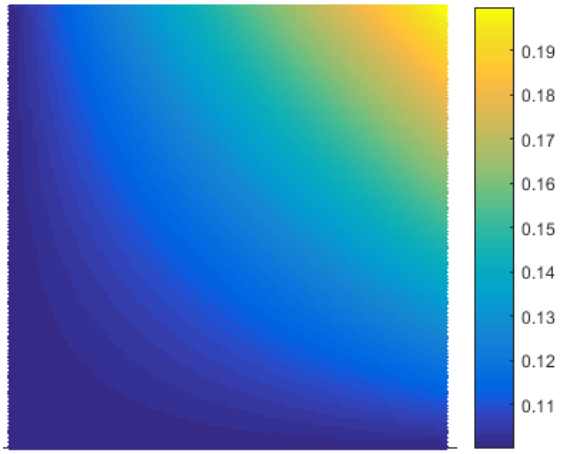

Figure 9.1 – Distribution of the thrombin concentration (nM) in case 1.

Analogous to what was previously presented, in the following points, the colour maps will be presented, in the same order. Note that, in this case, only two increments are shown since the clot growth led rapidly to the occlusion of the outlet (in only two time steps).

a) Clot Growth

The following figures present the clot growth, along the increments (**Figure 9.2**).

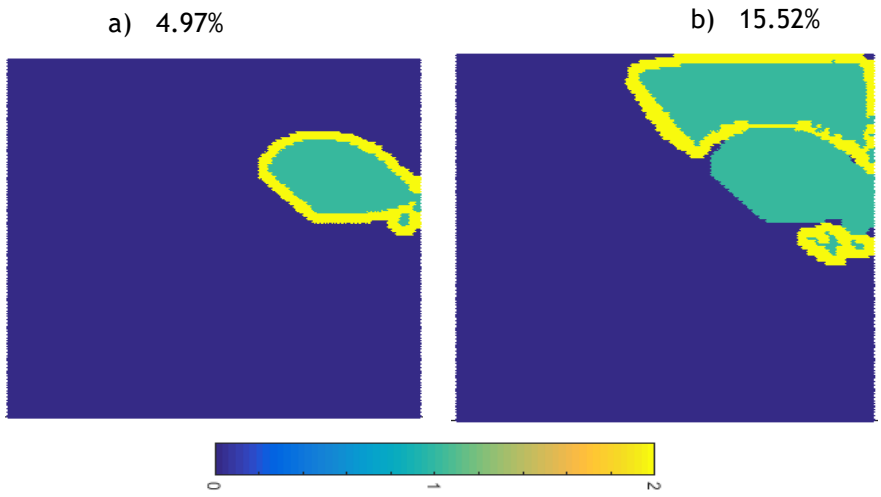

Figure 9.2 - Colour maps of the growth of the clot - thrombin concentration case 1. Blue: blood; Green: old clot; Yellow: new clot.

Analysing the results it is possible to conclude that the change in the thrombin concentration focus led to an abrupt growth of the clot, when compared to **Figure 8.10**. Since the focus is located at the area of fluid exit, it possesses the necessary conditions of thrombin and shear rate to promote clot growth. This leads to an increased and faster growth.

b) Concentration of Thrombin

The following figures represent the colour maps of the variation of the thrombin concentration in a logarithmic scale (**Figure 9.3**).

The first picture (**Figure 9.3** a)) corresponds to the thrombin concentration when the clot is absent.

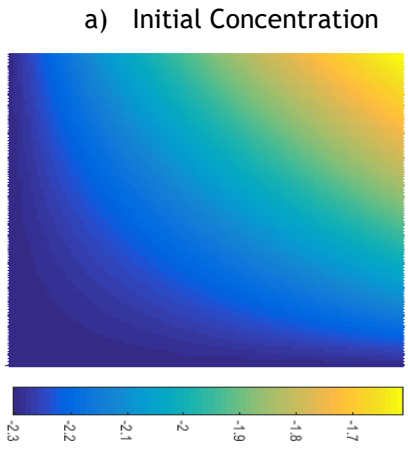

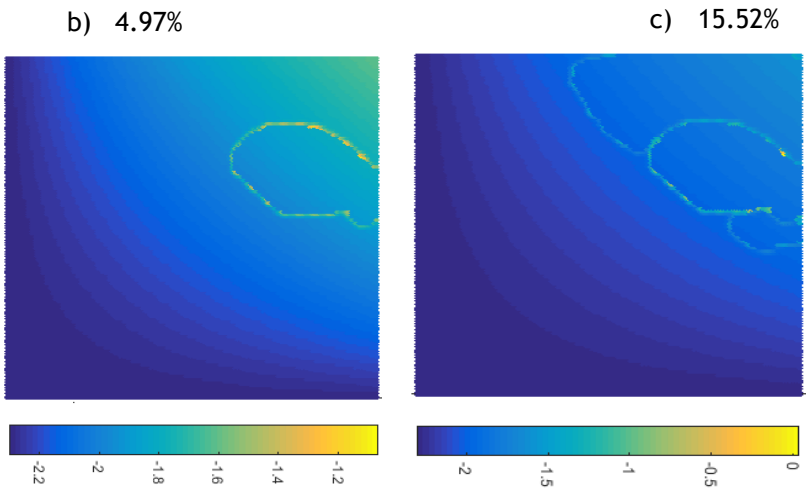

Figure 9.3 - Colour maps of the concentration of the thrombin - thrombin concentration case 1.

With respect to the example of **Chapter 8**, the only change was the thrombin concentration distribution. Since the highest value of thrombin is now located at the extrusion area, the maximum concentrations values are also located in the same area. Thus, more integration points are found above the basal concentration, which, in turn, caused them to be transformed into a clot. Regarding the variation of thrombin along all increments, it is possible to verify that the behaviour maintained.

c) Velocity

The following pictures (**Figure 9.4**) show the variation in the velocity during the process of clot growth.

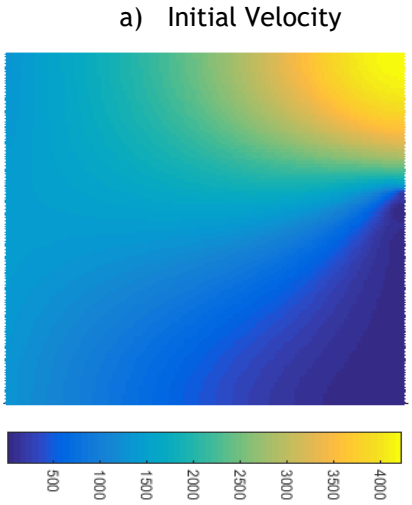

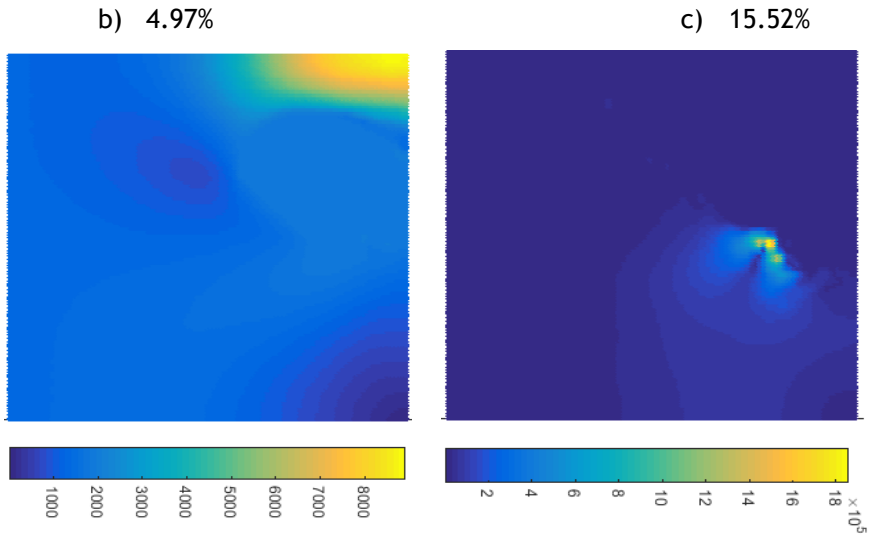

Figure 9.4 - Colour maps of the velocity profile - thrombin concentration case 1.

Since only the thrombin distribution was altered in comparison with the previous results, it was expected that the velocity profile would not change, which is possible to verify in **Figure 9.4** a). Regarding the remaining figures, it is noticeable that there was a more sudden increase in the velocity of the exit area. This is due to the fact that the clot grows in a faster way to that area. Besides that, when looking at **Figure 9.4** c), it is possible to see that nearly all the domain presents a velocity equal to 0, which is caused by the exit occlusion attributed to the clot.

d) Shear Rate

The following figure (**Figure 9.5**) represents the colour maps of the shear rate variation along the different increments.

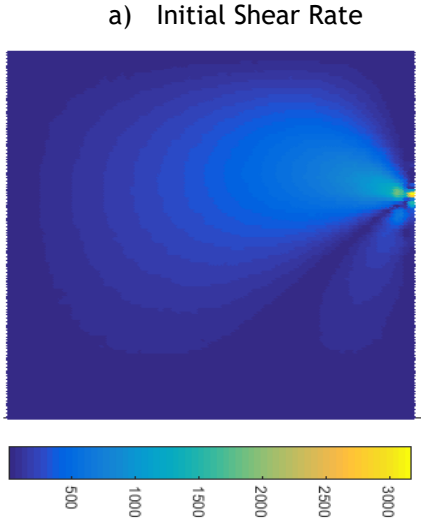

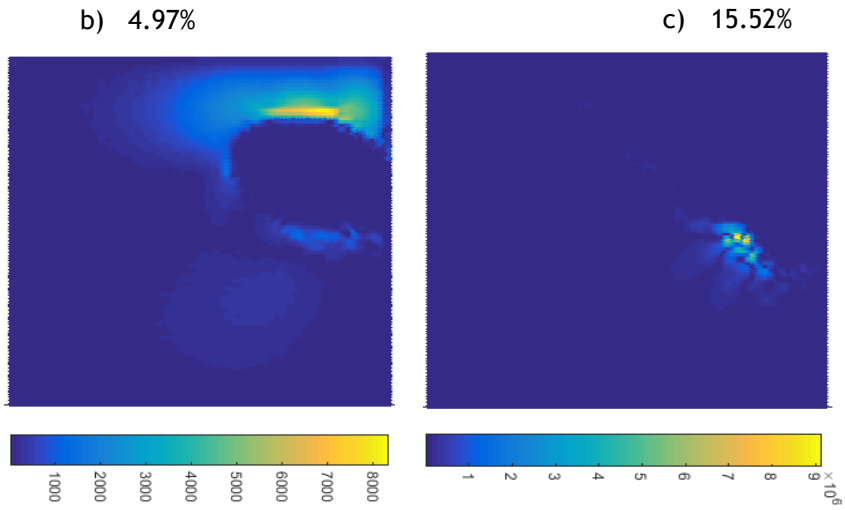

Figure 9.5 - Colour maps of the shear rate profiles - thrombin concentration case 1.

Similarly to what occurred in the velocity profile, the initial profile of the shear rate distribution in the domain (**Figure 9.5** a)) resembles the profile which was previously presented. When the clot is present, the areas with the highest shear are also the areas of higher velocity, namely in the exit areas (areas that are not blocked by the clot). When it comes to the last increment, the shear rate values are close to 0 (in the majority of the domain), which is in accordance with the profile which was previously presented.

e) Viscosity

The following image (**Figure 9.6**) represents the difference in the viscosities between the increment in question and the first one, at a logarithmic scale.

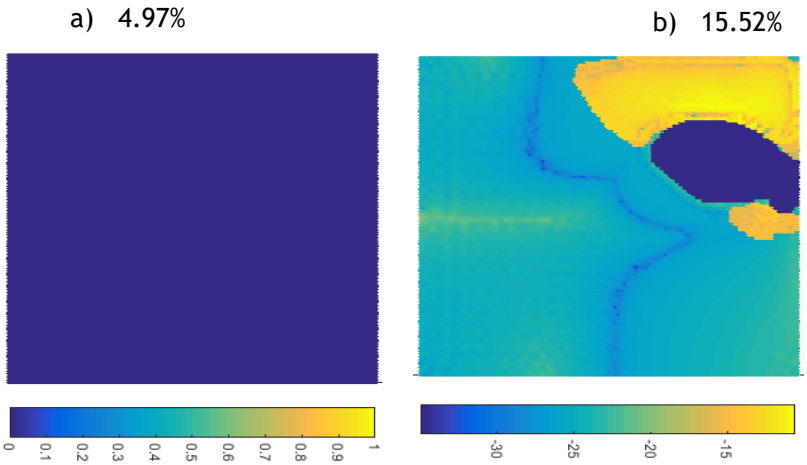

Figure 9.6 - Colour maps of the variation of the viscosity - thrombin concentration case 1.

As in previous results, there is a difference in the viscosity between the points defined as clot and the remaining domain, which is, once again, in accordance to what was expected.

9.1.2 - Thrombin Distribution Case 2

In order to analyse the influence of the thrombin focus, it was defined to be at the middle of the upper wall, which is noticeable in the following figure (**Figure 9.7**). This way, it is possible to compare the differences in the growth of the clot, caused by this distribution and the previous one.

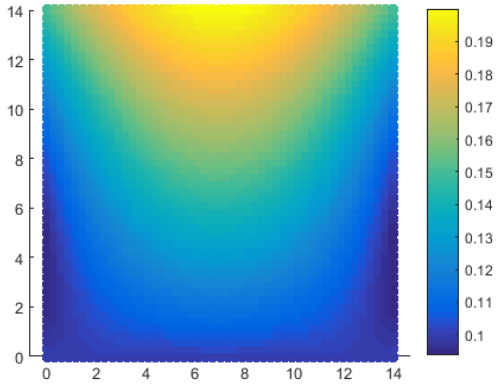

Figure 9.7 - Distribution of the thrombin concentration (nM) in case 2.

a) Clot Growth

The following image represents the growth of the clot for the presented thrombin distribution (**Figure 9.8**).

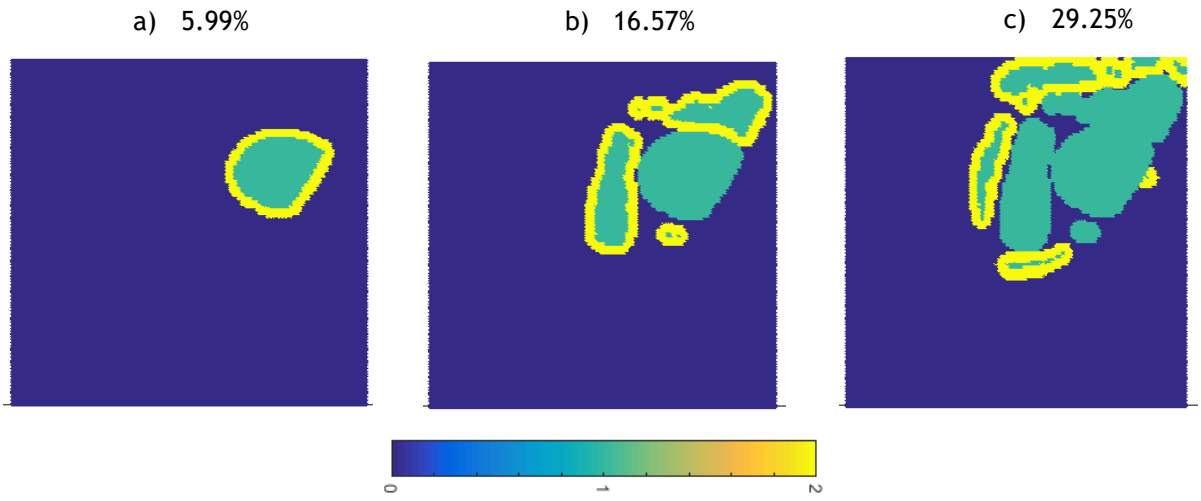

Figure 9.8 - Colour maps of the growth of the clot - thrombin concentration case 2. Blue: blood; Green: old clot; Yellow: new clot.

Once again it is noticeable that there is a faster and larger growth when compared to the example in section **8.2.4.1**, which was expected due to the change in the focus of distribution of thrombin. However, the change of the focus from the upper right corner to the middle of the wall caused a different type of growth, which is noticeable when comparing the shape of these images and the images in the previous example. It is also possible to conclude that, the further away the points of maximum thrombin concentration, the longer it takes for the blockage of the exit area to occur.

b) Concentration of Thrombin

The following figure represents the colour maps of the concentration of thrombin along the clot growth (**Figure 9.9**).

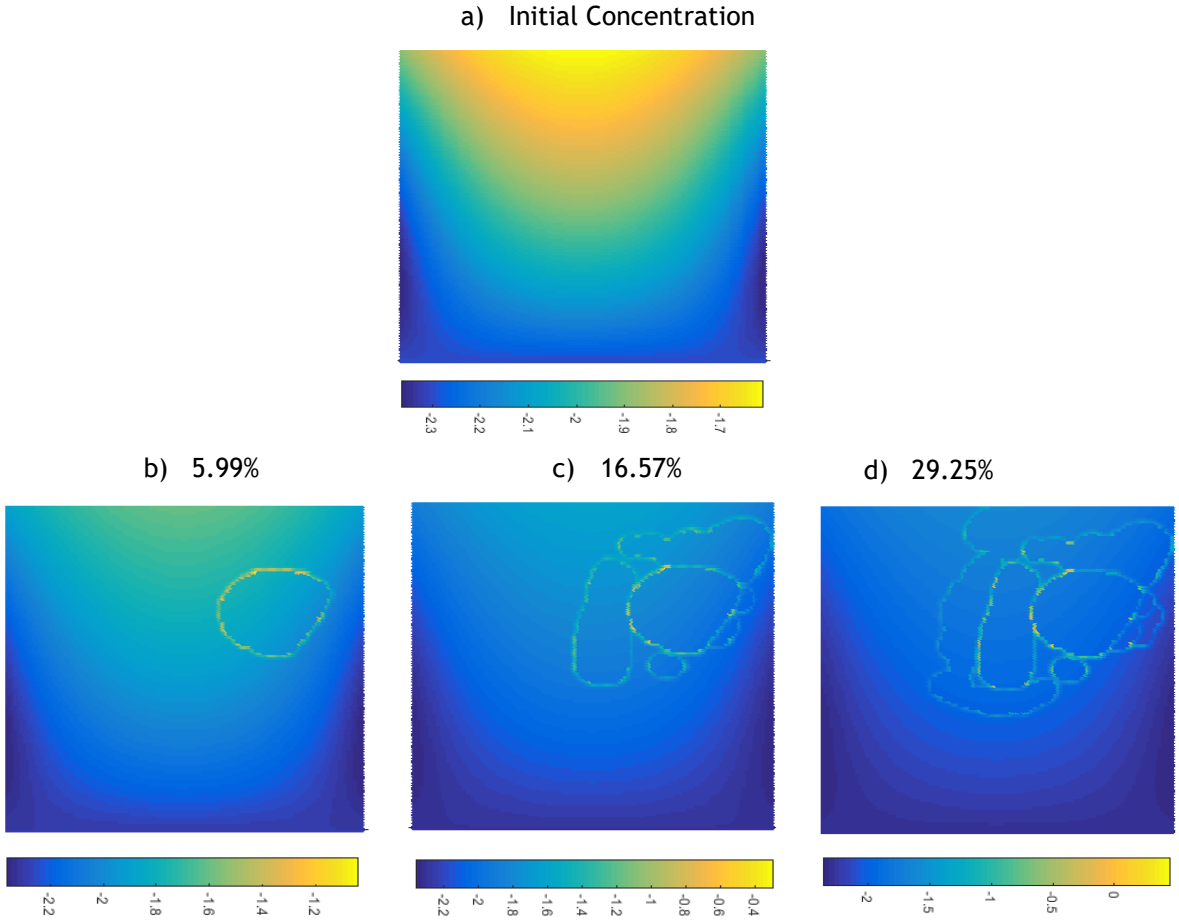

Figure 9.9 - Colour maps of the concentration of the thrombin - thrombin concentration case 2.

It is possible to conclude, from these images, that there is an increase of the thrombin concentration in the areas close to the clot like what was defined by the algorithm and what was shown in previous results.

c) Velocity

The following figures show the velocity variation caused by the clot growth along each increment (**Figure 9.10**).

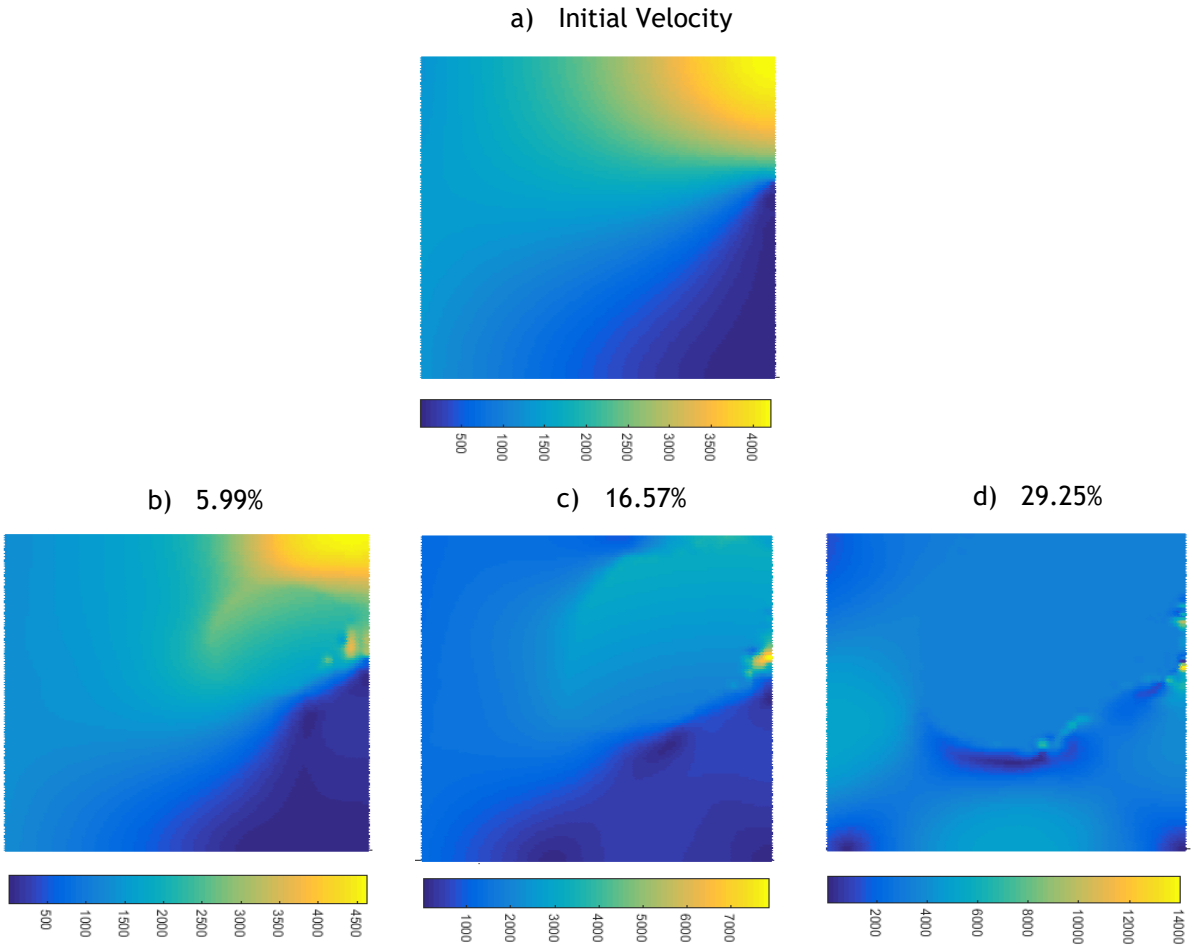

Figure 9.10 - Colour maps of the velocity profile - thrombin concentration case 2.

As in the previous results there is an increase in the velocity with the clot growth. However, in this instance, the upper area of the exit area, is the one which tends to be blocked, causing an area of high velocities at a place which previously appeared as blocked (see **Figure 9.10** b)). Like what happened in the previous example, due to the blockage of the exit area, the velocities along the domain tend to 0.

d) Shear Rate

The following figure represents the colour maps of the shear rate variation along the different increments (**Figure 9.11**).

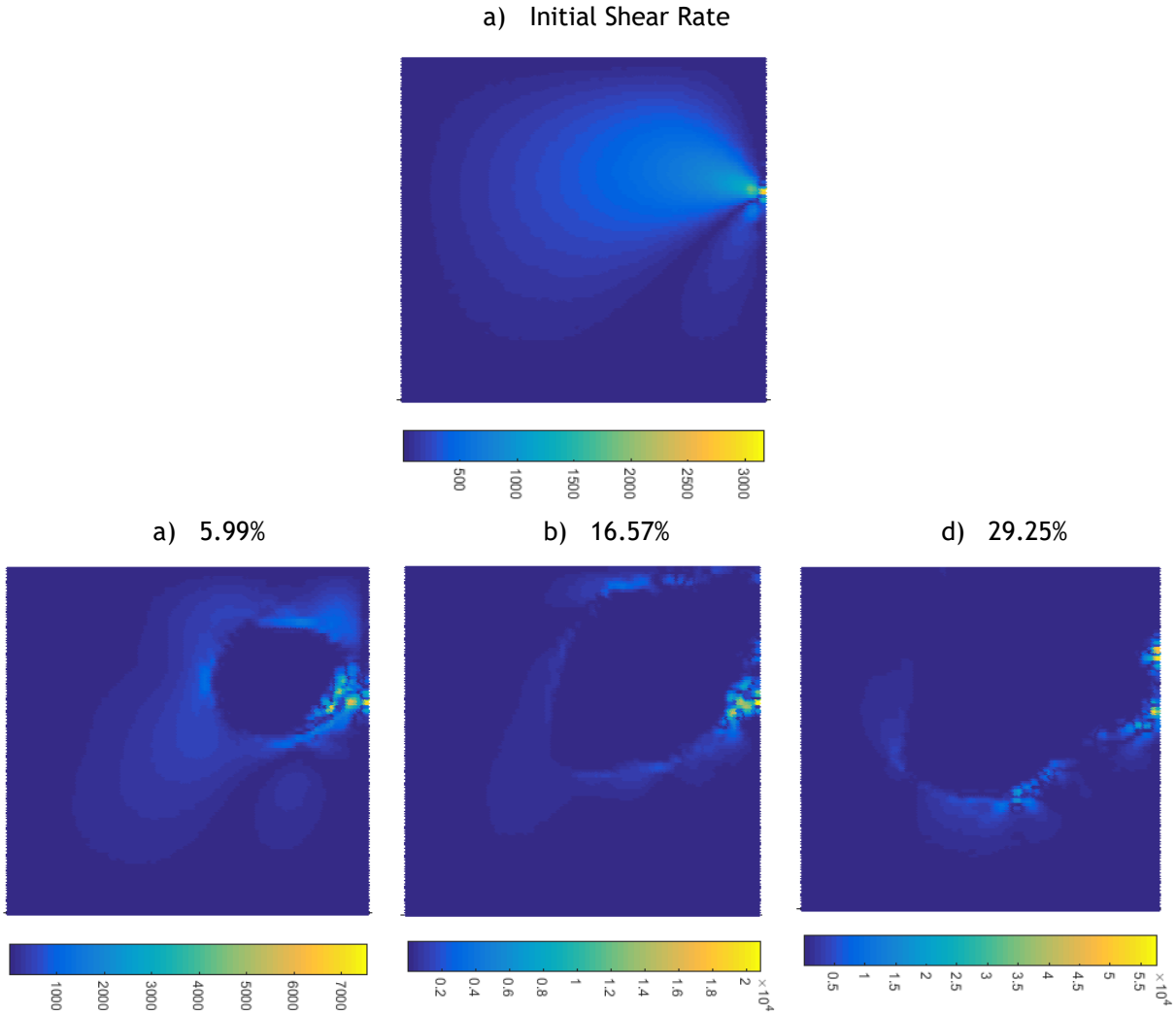

Figure 9.11 - Colour maps of the shear rate profiles - thrombin concentration case 2.

Analysing the colour maps, the results are in accordance with what was expected considering the velocity profiles which were previously presented and, once again, show the characteristics of shear rate variation, of clot growth and seen in the previous examples.

e) Viscosity

The following figures represent the colour maps of the viscosity variation along the different increments (**Figure 9.12**).

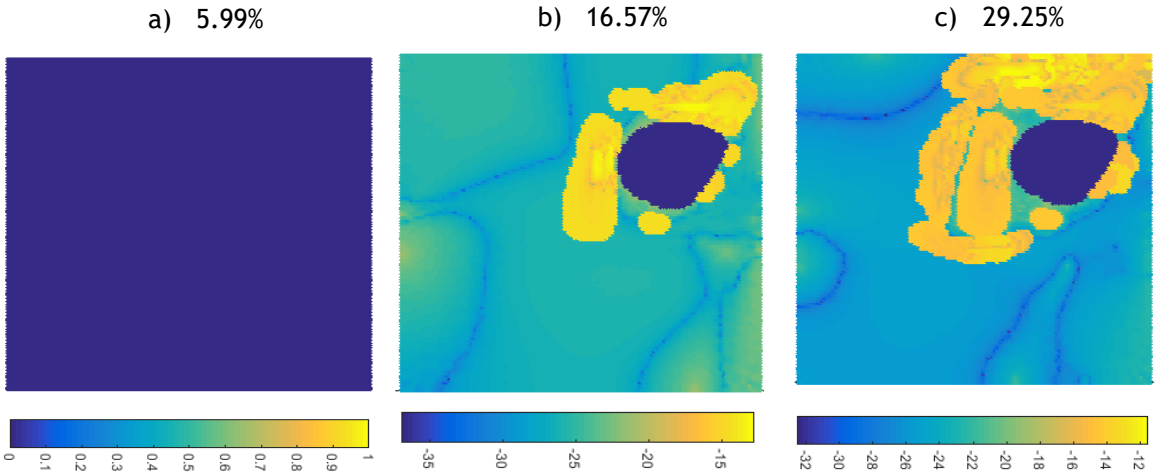

Figure 9.12 - Colour maps of the variation of the viscosity - thrombin concentration case 2.

The presented colour maps are in accordance to previous results, being quite similar in the viscosity distribution.

9.1.3 - Thrombin Distribution Case 3

In order to make the thrombin distribution more complex, two thrombin focuses were created, and this distribution is presented in the following figure (**Figure 9.13**). One of these focuses correspond to the standard thrombin distribution (**Figure 8.2**) and the other one to the distribution presented in case 2 (**Figure 9.7**).

Note that both present the same maximum concentration, which is also the same presented in the previous results.

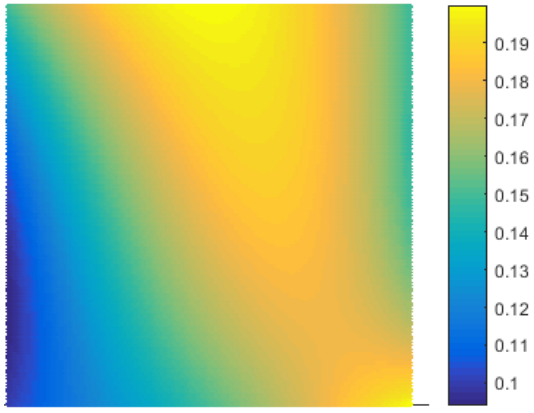

Figure 9.13 - Distribution of the thrombin concentration (nM) in case 3.

a) Clot Growth

As in the previous examples, in the next figures the colour maps that represent the growth of the clot of the case 3 are presented (**Figure 9.14**).

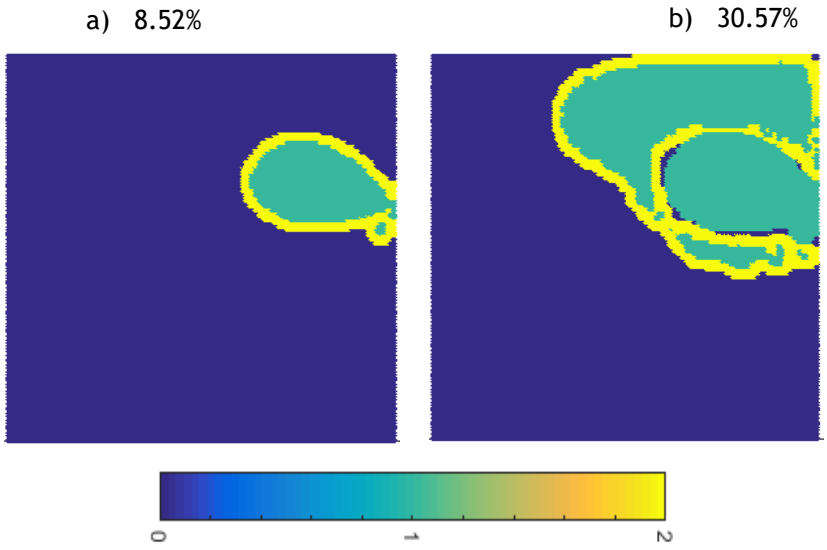

Figure 9.14 - Colour maps of the growth of the clot - thrombin concentration case 3. Blue: blood; Green: old clot; Yellow: new clot.

Once again, it is possible to see a faster and more prominent growth of the clot since one of the focus is in upper part of the domain, which is coherent with the previous cases. However, when compared with the same figures of case 2, the increase is more accentuate, which can be justified by the fact that almost all the domain presents a higher concentration of thrombin than the basal concentration. Moreover, the growth of the clot tends to migrate to lower areas due to the focus of thrombin in the lower portion of the domain.

b) Concentration of Thrombin

The variation of the concentration of thrombin, in logarithmic scale, is presented in the following colour maps (**Figure 9.15**).

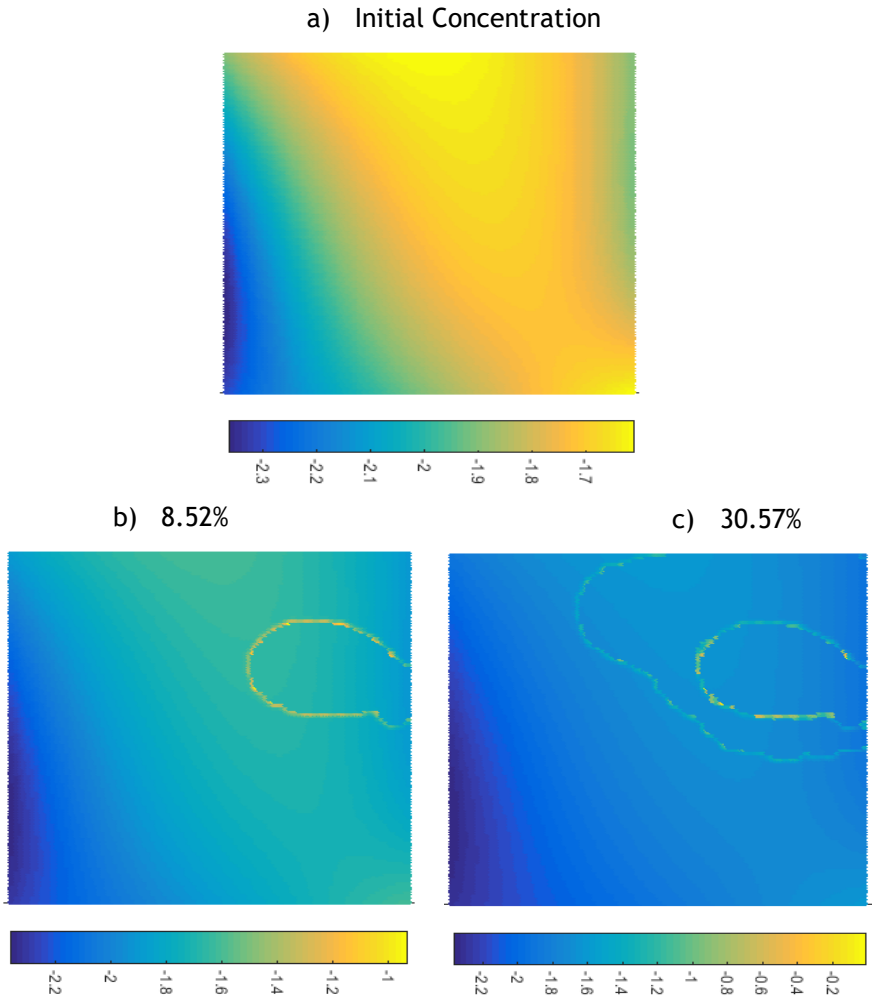

Figure 9.15 - Colour maps of the concentration of the thrombin - thrombin concentration case 3.

The first colour map shows the distribution of the concentration of thrombin. In these, it is possible to see that there is an increase of the concentration in all the domain, mainly in the middle section. That way, almost all the domain presents a concentration higher than the basal concentration, due to the presence of the two focus.

Regarding the colour maps with clot, the increase of the concentration of thrombin is visible at the border of the clot, presenting a similar pattern to the cases presented previously.

c) Velocity

The colour maps of the variation of the velocity, due to the growth of the clot, are presented in the next figure (**Figure 9.16**):

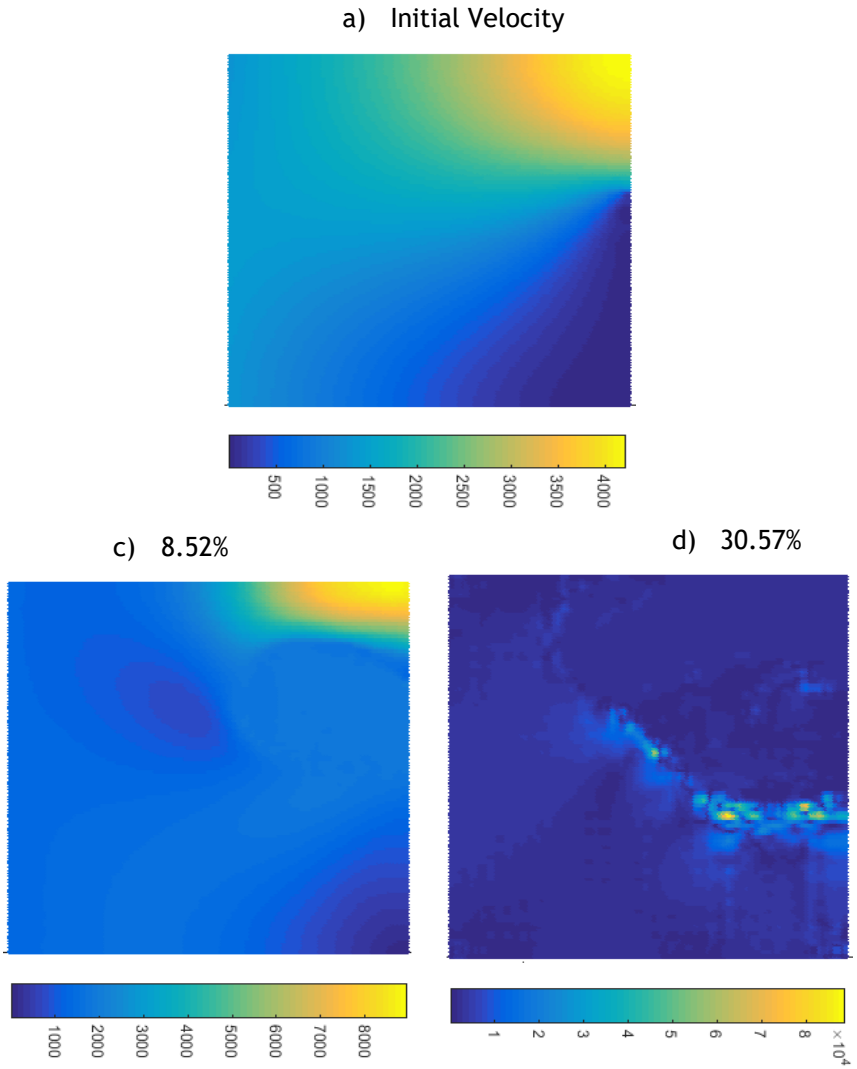

Figure 9.16 - Colour maps of the velocity profiles - thrombin concentration case 3.

Analysing the figures above, it is visible that they present a similar profile to the ones presented in case 1. First, an increase of the velocity occurs in the outlet, due to the growth of the clot, and then, due to the blockage of the same area, the velocity of the domain tends to 0 in the whole domain.

d) Shear Rate

The following figure presents the colour maps of the shear rate in each increments (**Figure 9.17**).

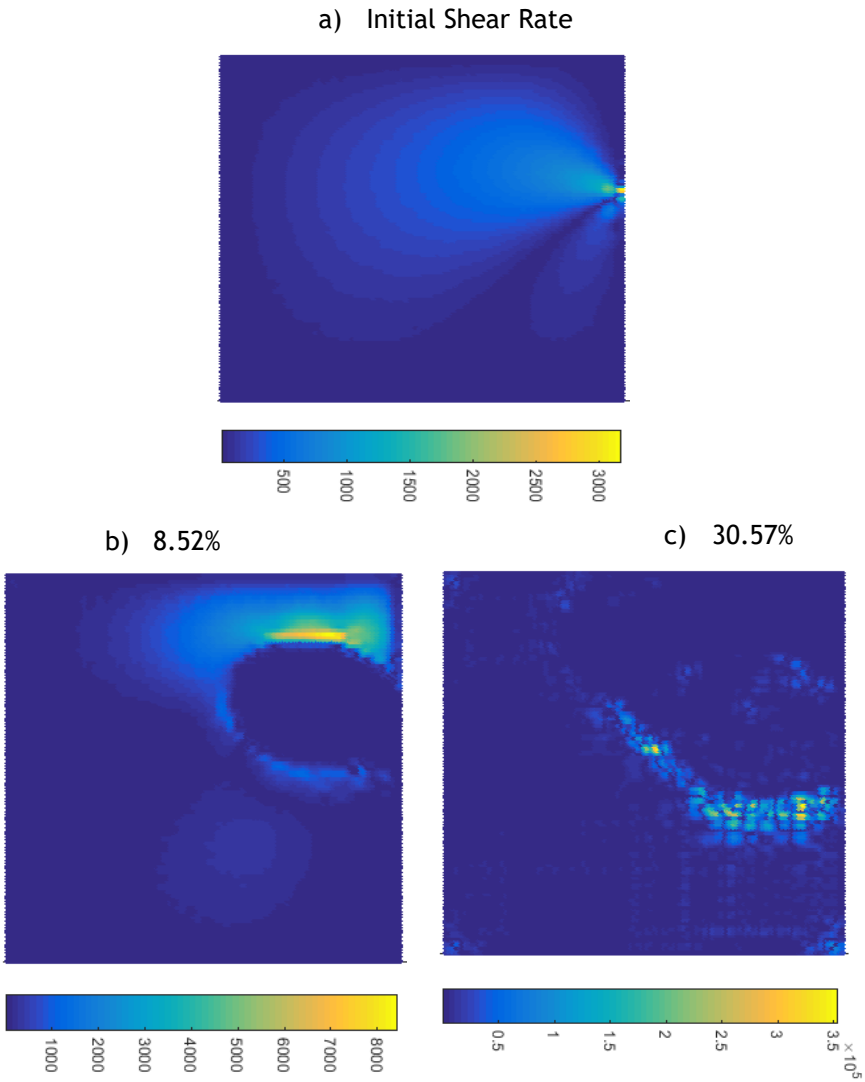

Figure 9.17 - Colour maps of the velocity profiles - thrombin concentration case 3.

As in the velocities profiles, these colour maps are similar to the ones presented in case 1. Besides that, they are coherent with the previous results, presenting the same features that were already mentioned.

e) Viscosity

Lastly, the colour maps of the variation of the viscosity is presenting in the following figure (**Figure 9.18**). Once again, the results are presented through the difference between each increments and the first, in a logarithmic scale.

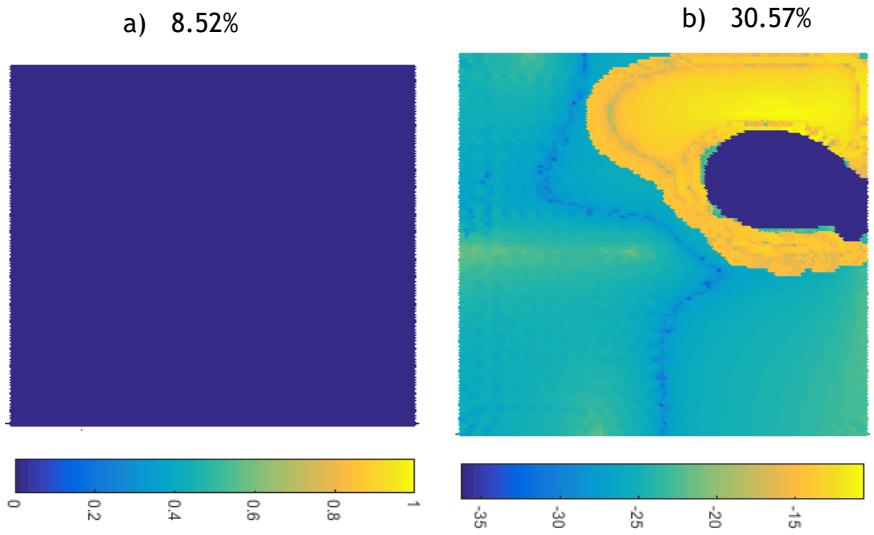

Figure 9.18 - Colour maps of the variation of the viscosity - thrombin concentration case 3.

Clearly, a difference in the viscosity between the clot and the rest of the domain is visible. Thus, the results are coherent with the expected and with the previous results.

Summing up, the alteration of the distribution of the concentration of thrombin influences the obtained results and can cause a faster and larger clot growth, which influences the velocity and shear profiles. This is visible in the comparison of the results in section **8.2.4.1** (termed "standard case") and the ones from this section ("case 1", "case 2" and "case 3")..

Lastly, a comparison between the Clot Fraction obtained in each case (including the ones found in section **8.2.4.1**), over the time, is performed next, resorting to the graphic in **Figure 9.19**.

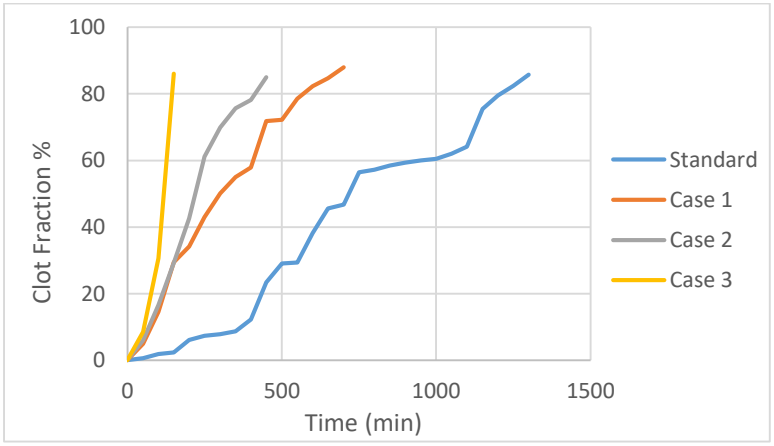

Figure 9.19 - Variation of the Clot Fraction due to the alteration of the distribution of the thrombin concentration.

Comparing all the curves, it is possible to see that when the thrombin focus is further from the extrusion are, the clot growth is delayed. This is proved by the colour maps of the shear rate, since it is in this area that has the highest values.

It is also possible to note that case 3 is one which presents the fastest growth, a fact that is explained by the presence of two focuses of thrombin concentration. These lead to an increase of the general concentration of the domain, which stimulates the growth process.

When analysing cases 1 and 2, even though they are similar, since case 2 presents a better distributed thrombin concentration along its domain, the clot growth is faster reaching a higher clot fraction in less time.

9.2 - Variation of Boundary Conditions

The haemodynamics is strongly dependent on the geometry and the computational boundary conditions of the domain [158]. Therefore, an alteration in the boundary conditions affects the final obtained velocity profile, being expected as alteration in the formation of the clot.

In this section, the aim is to analyse the influence of the boundary conditions in the clot and the viability of the results when these are modified. For this, three different cases were designed. Similar to the previous results, for each case, five different colour maps (Clot Growth, Viscosity, Velocity, Concentration of Thrombin and Shear Rate) were presented, and, in the end, the results were compared through the variation of the Clot Fraction over the time.

Note that the rest of the initially defined parameters were maintained, and the results presented in section **8.2.4.1** were assumed as a comparison.

9.2.1 - Boundary Conditions Case 1

In this case, the area of entry of the flow was reduced for it to have the same length as the exit area and was defined in such a way that it is symmetric to it. This is seen in the following picture (**Figure 9.20**).

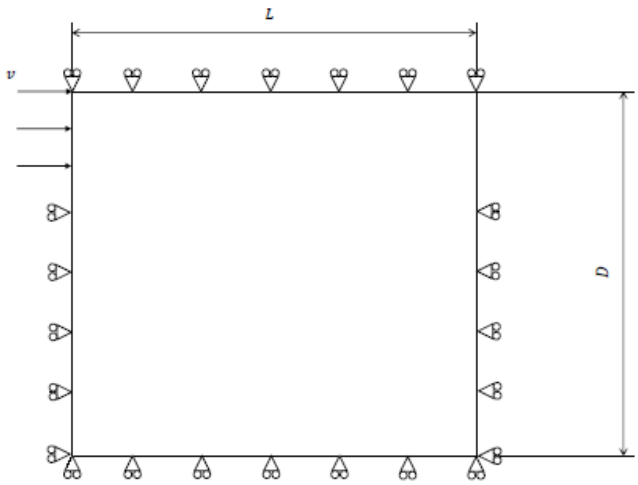

Figure 9.20 – Representation of the boundary conditions of case 1.

a) Clot Growth

The following figure represents the clot growth along 12 increments (**Figure 9.21**), which correspond to the same temporal moment as the ones presented in section **8.2.4.1**.

a) 0.50% b) 1.36% c) 2.44%

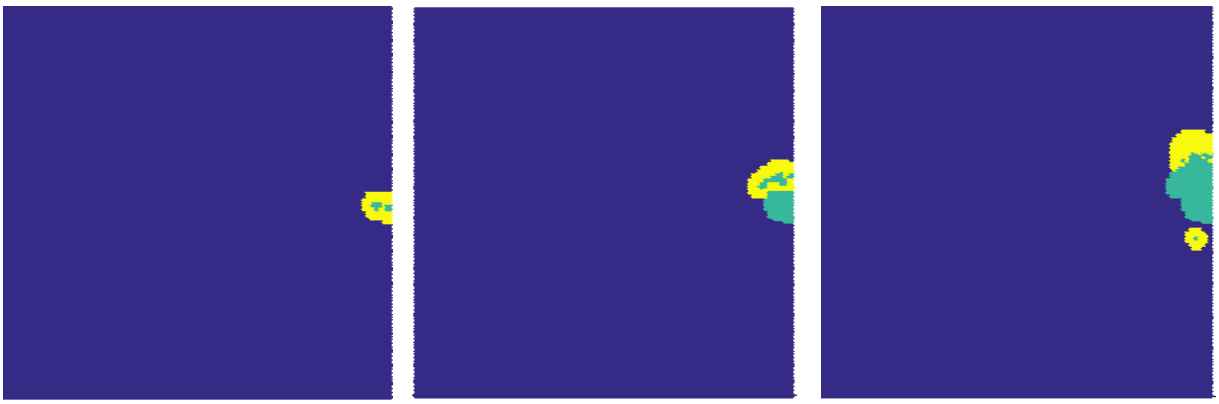

a) 2.44% a) 2.44% f) 2.44%

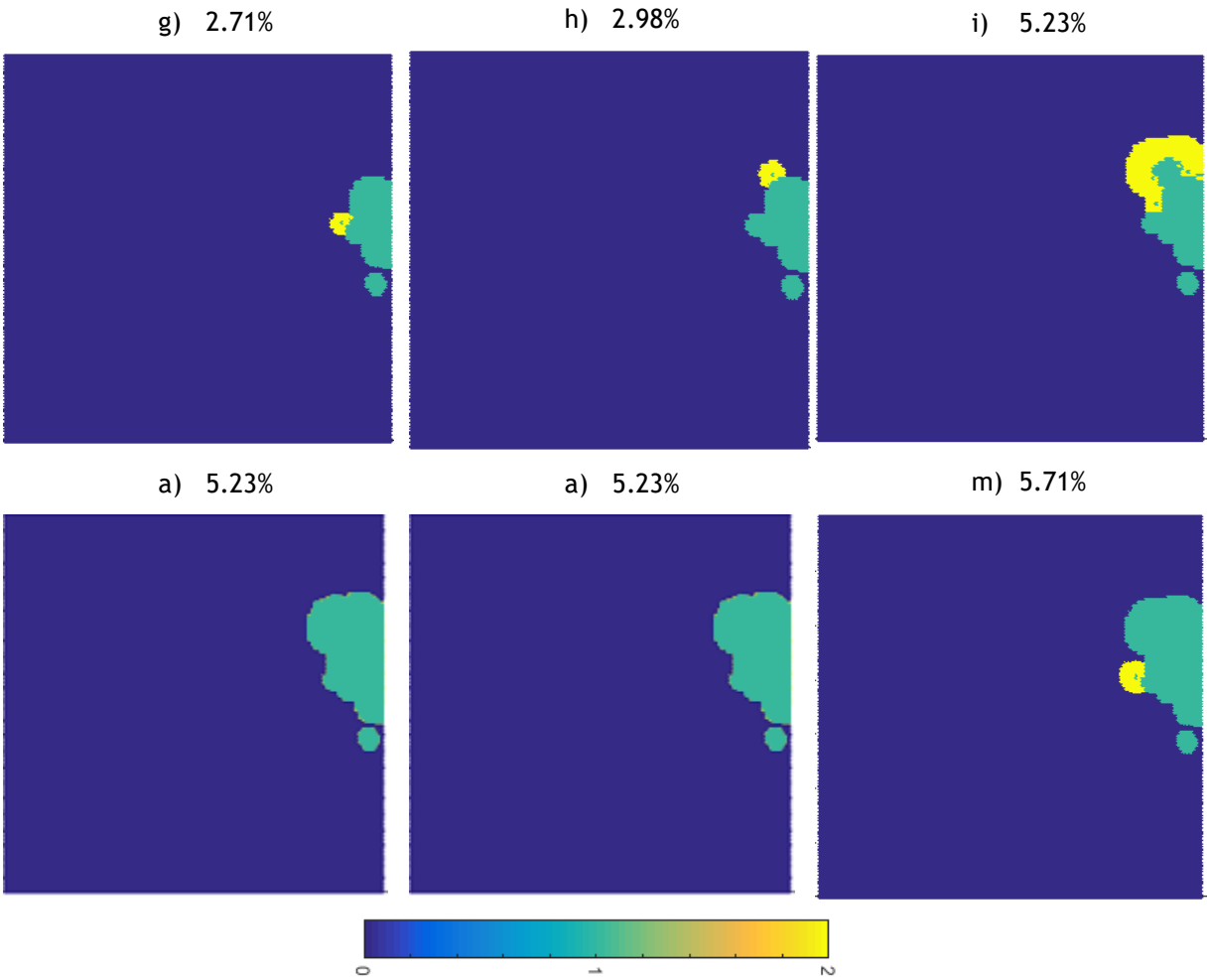

Figure 9.21 - Colour maps of the growth of the clot – boundary conditions case 1. Blue: blood; Green: old clot; Yellow: new clot.

When analysing the images it is possible to note that the growth occurred in the same area as in the previous results (**Figure 8.10**). However, with the modification of the boundary condition of the area which allows for the flux entry, the growth is slower and smaller and there are some time steps when there is no growth.

b) Concentration of Thrombin

The following figure represents the thrombin concentration along 12 increments, in a logarithmic scale (**Figure 9.22**).

a) Initial Concentration

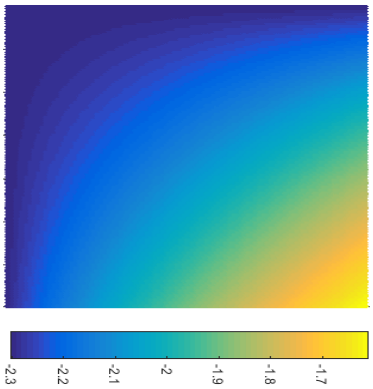

b) 0.50%

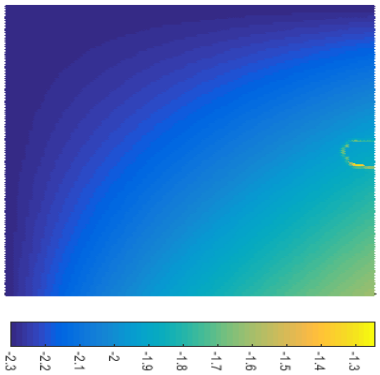

c) 1.35%

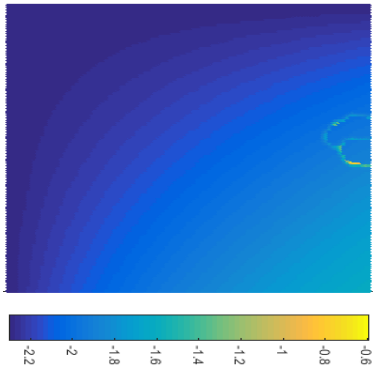

d) 2.45%

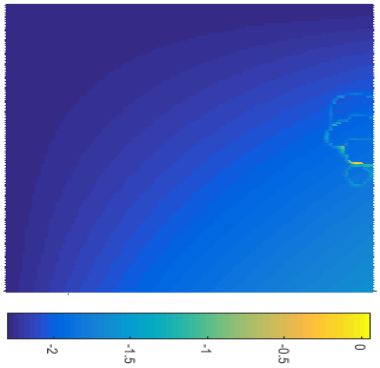

e) 2.45%

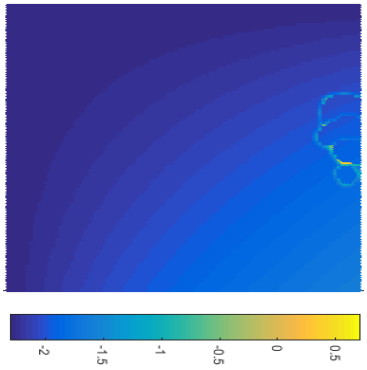

f) 2.45%

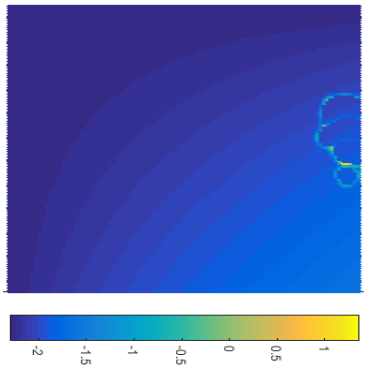

g) 2.45%

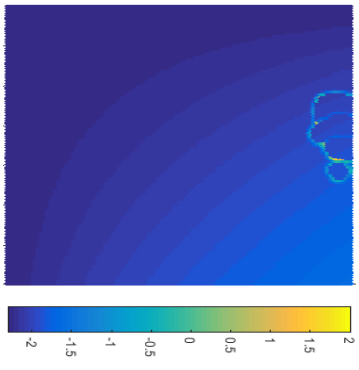

h) 2.71%

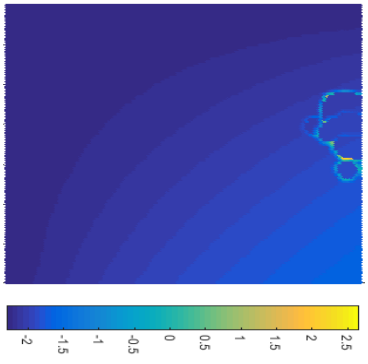

i) 2.98%

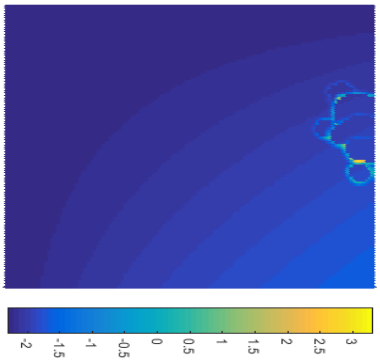

j) 5.23%

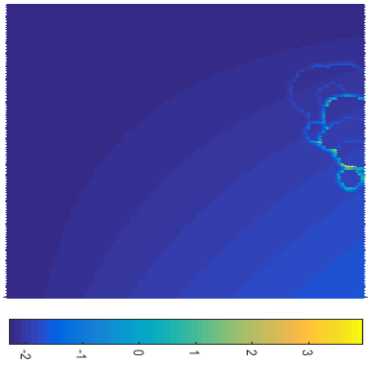

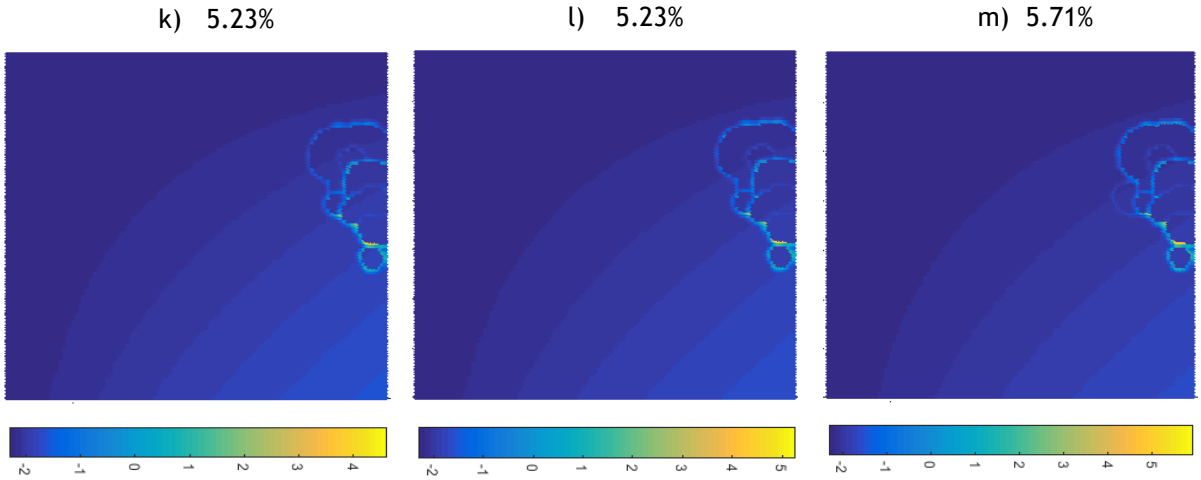

Figure 9.22 - Colour maps of the concentration of the thrombin – boundary conditions case 1.

As in the previous results, there is an increase in the thrombin concentration at the edges of the clot capable of promoting its growth along increments, presenting a similar profile to the ones that were previously shown. Besides that, an increase of the concentration is visible between increments where there is no clot growth, showing that the growth is dependent on this parameter.

c) Velocity

The following figure represents the velocity profile along 12 increments (**Figure 9.23**).

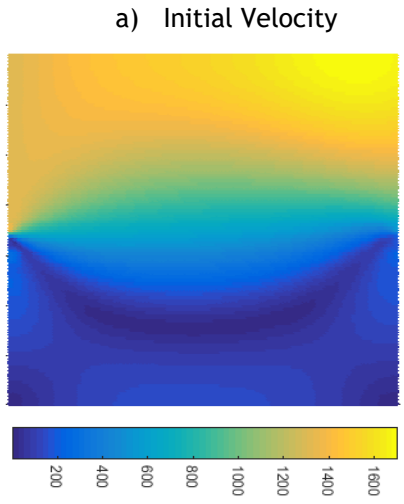

b) 0.50%

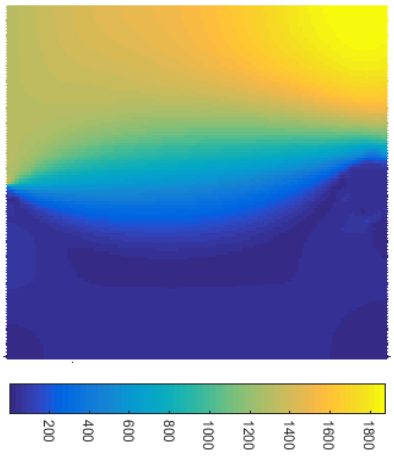

c) 1.36%

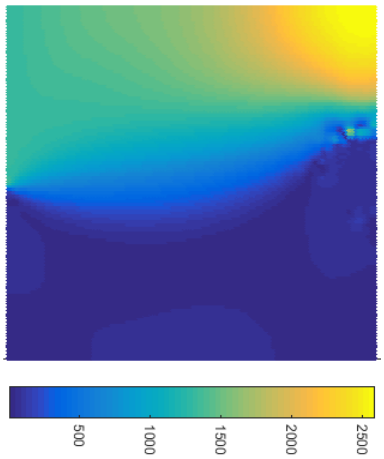

d) 2.45%

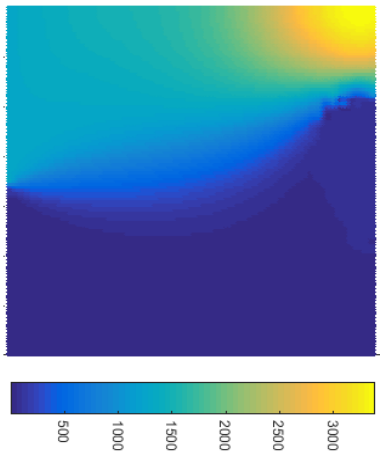

e) 2.45%

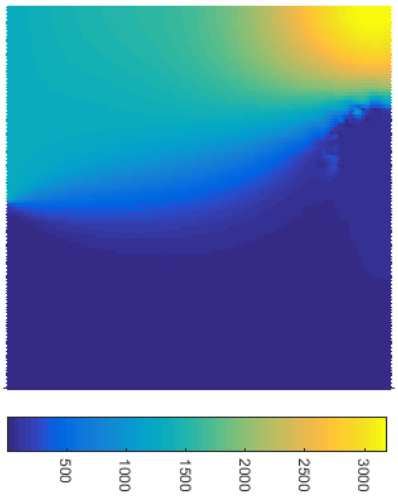

f) 2.45%

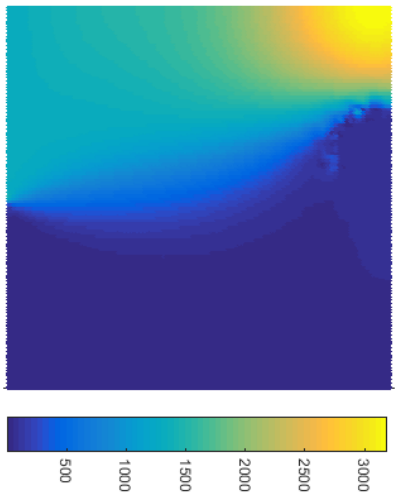

g) 2.45%

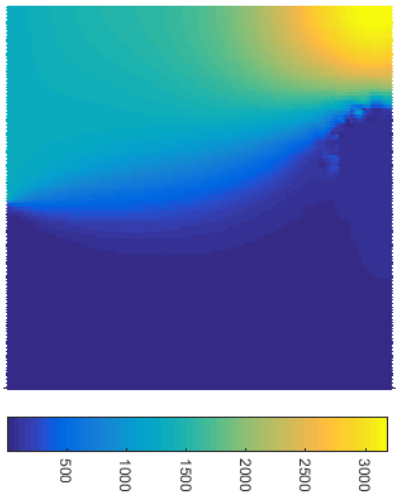

h) 2.71%

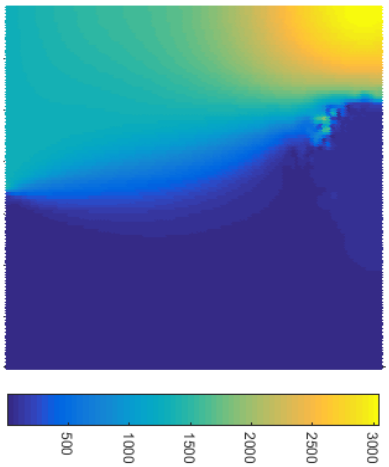

i) 2.98%

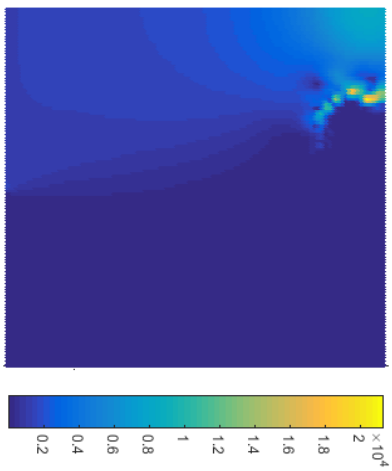

j) 5.23%

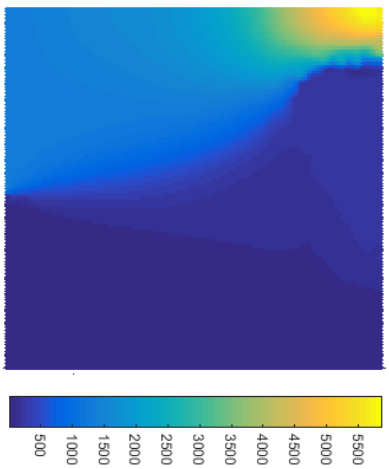

k) 5.23% l) 5.23% m) 5.71%

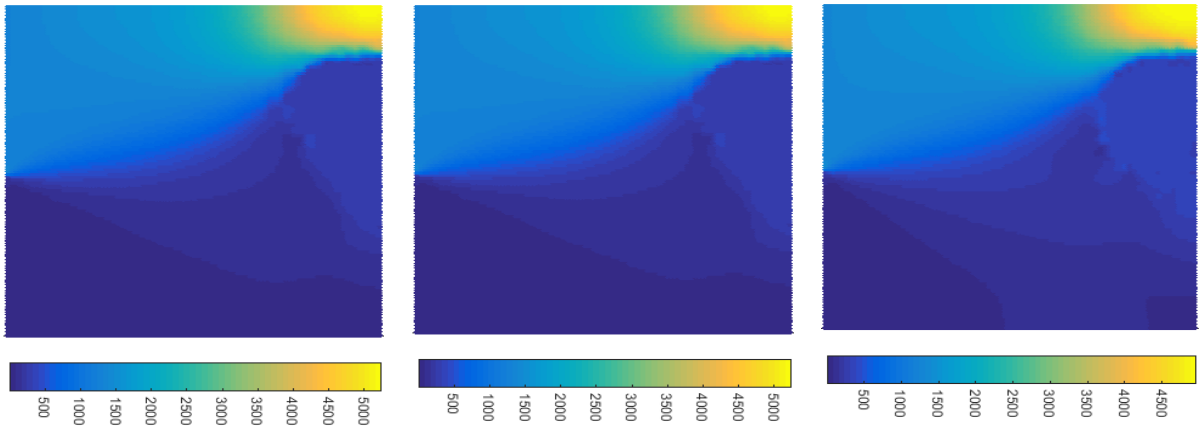

Figure 9.23 - Colour maps of the velocity profiles – boundary conditions case 1.

With the changing of the boundary condition, the main difference is the presence of low velocities in the lower half of the domain. When it comes to the velocity variation, the profile tends to be the same since the clot is formed in the same area, and its growth tends to block the exit area of the flow, which causes an increase in the velocity in that area along the increments (time steps), such as what happened in the results presented in **Figure 8.12**. It should be noted that in increment 8, the velocity profile is not what was expected, since it presents a small area with high velocities, probably due to numeric difficulties during the computation of the algorithm. However, if that area is ignored and the rest of the domain is analysed along with its respective velocities, it is possible to note that it tends to present a similar profile to the remaining increments.

d) Shear Rate

The following figure represents the variation of the shear rate, along 12 increments, in colour maps (**Figure 9.24**).

a) Initial Shear Rate

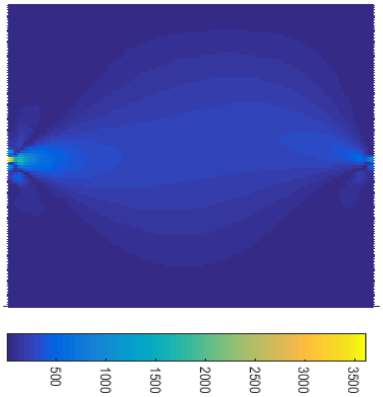

b) 0.50%

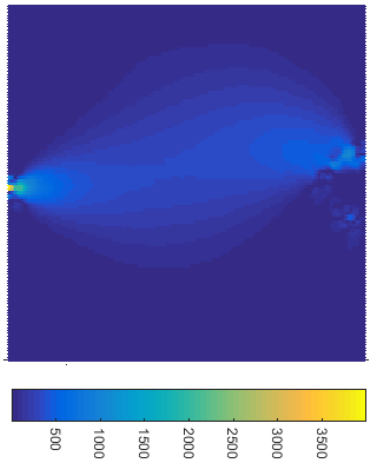

c) 1.36%

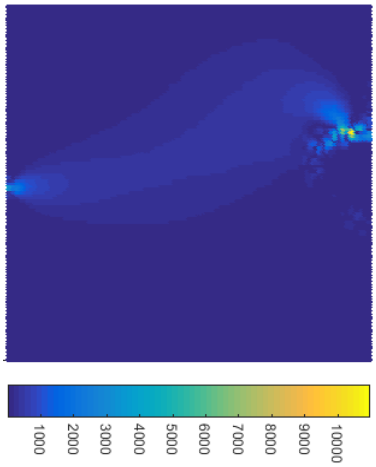

d) 2.45%

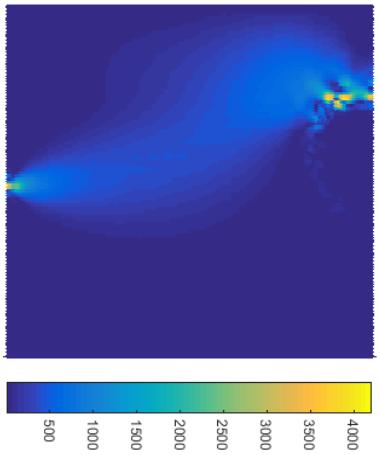

e) 2.45%

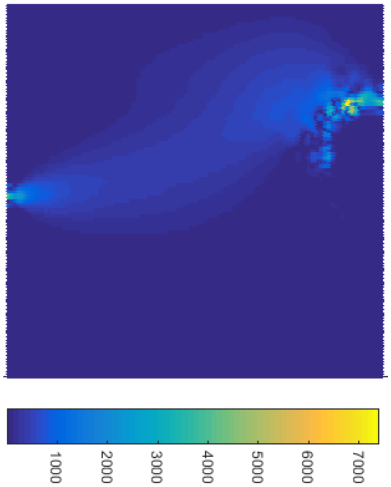

f) 2.45%

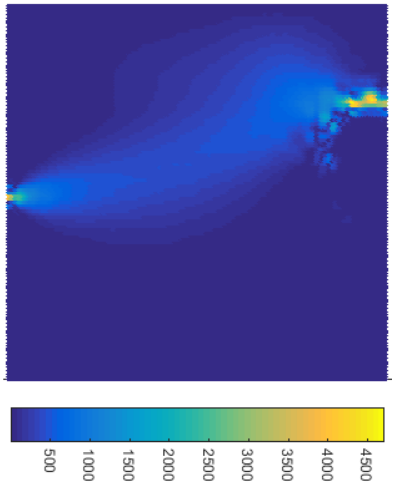

g) 2.45%

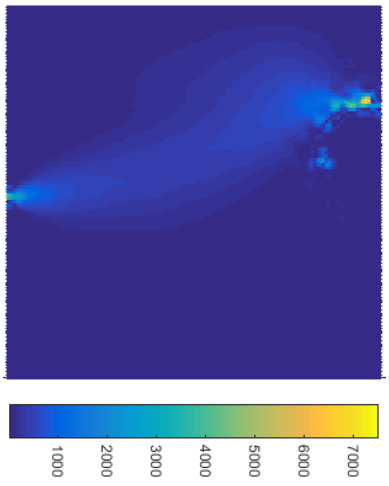

h) 2.71%

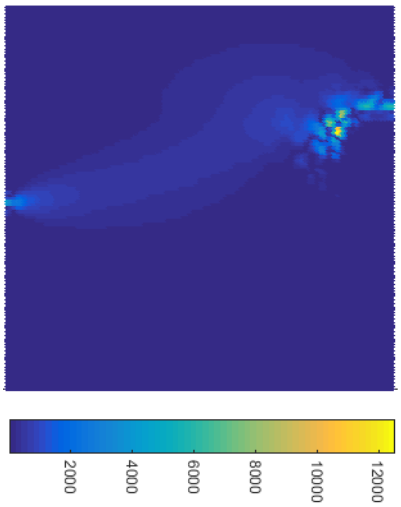

i) 2.98%

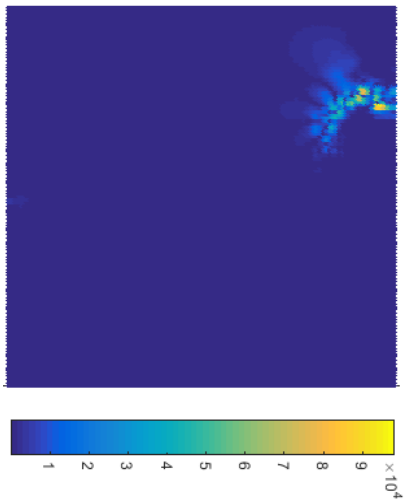

j) 5.23%

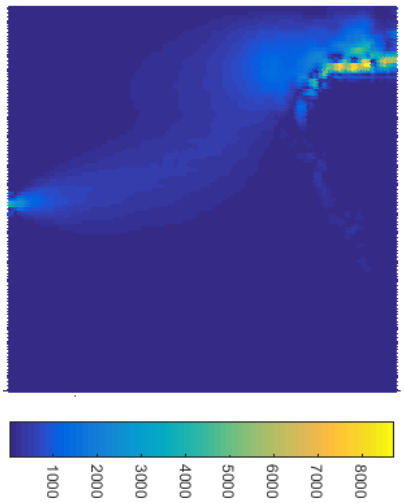

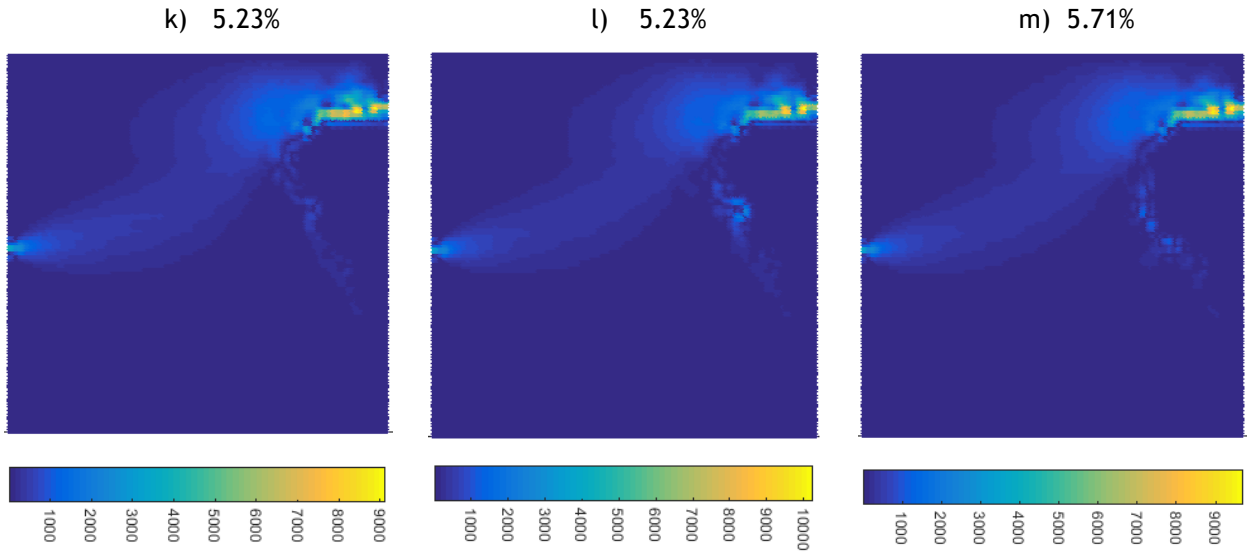

Figure 9.24 - Colour maps of the shear rate profiles – boundary conditions case 1.

Regarding the initial profile, it is possible to see that with the modification of the boundary condition, the initial profile also modified, presenting an area with a larger shear rate on the side of the flow entry.

When it comes to the following figures, these tend to maintain the behaviour presented in the previous examples and to maintain accordance with the velocity profiles. Therefore, with an increase of the velocity, the shear rate tends to increase as well, in the same area.

e) Viscosity

The following figures represent the variation of the viscosity, along 12 increment, due to clot growth (**Figure 9.25**). The scale is defined in the same way as in all the previous results.

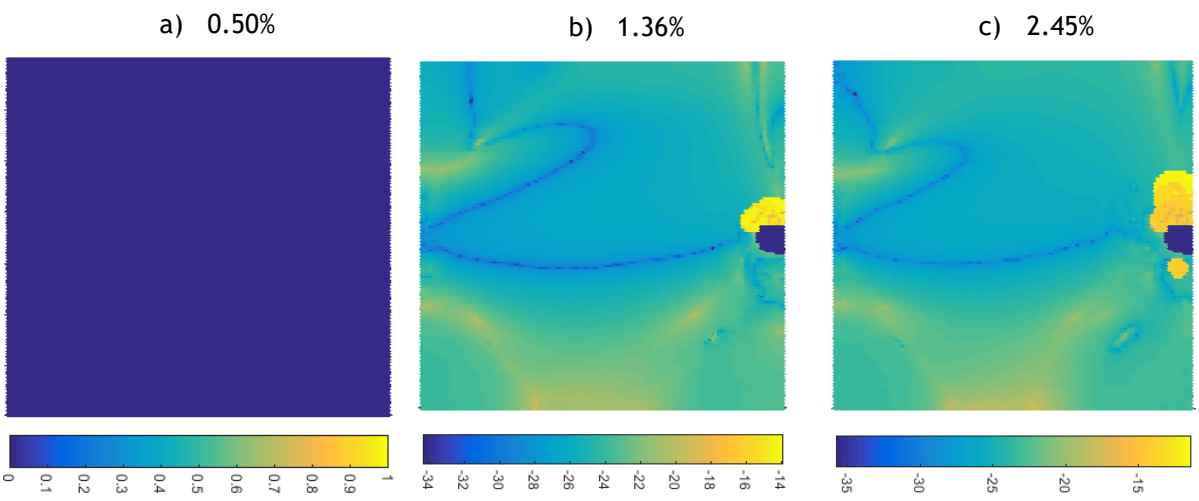

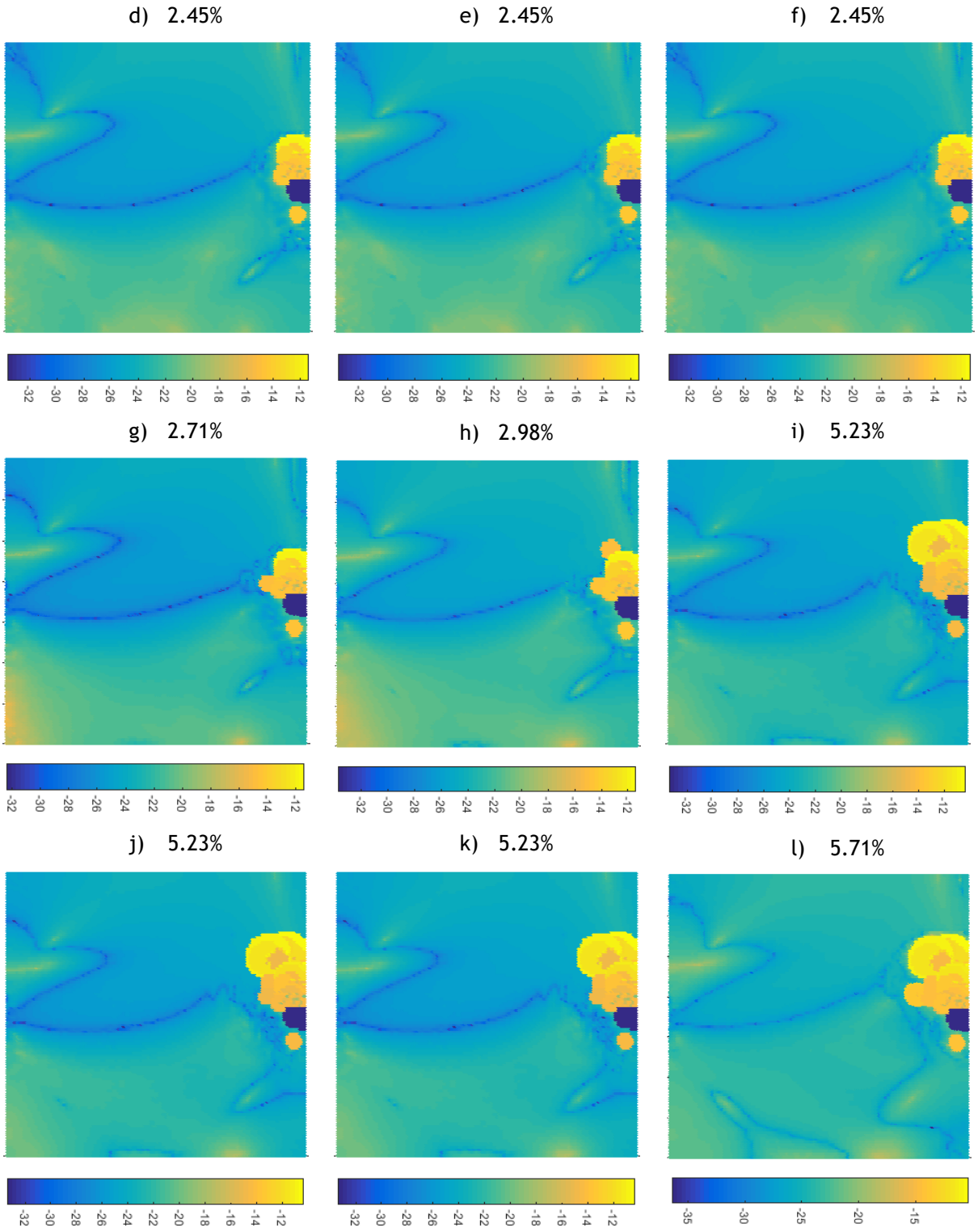

Figure 9.25 - Colour maps of the variation of viscosity – boundary conditions case 1.

The variation of the viscosity is in agreement to what was expected to be obtained with the proposed algorithm, presenting a similar profile to the previous results.

9.2.2 - Boundary Conditions Case 2

The entry was defined as in the previous case. However, the exit, while maintaining the same length was modified in order to be kept in the lower portion of the same wall on which it was initially placed, as seen in **Figure 9.26**.

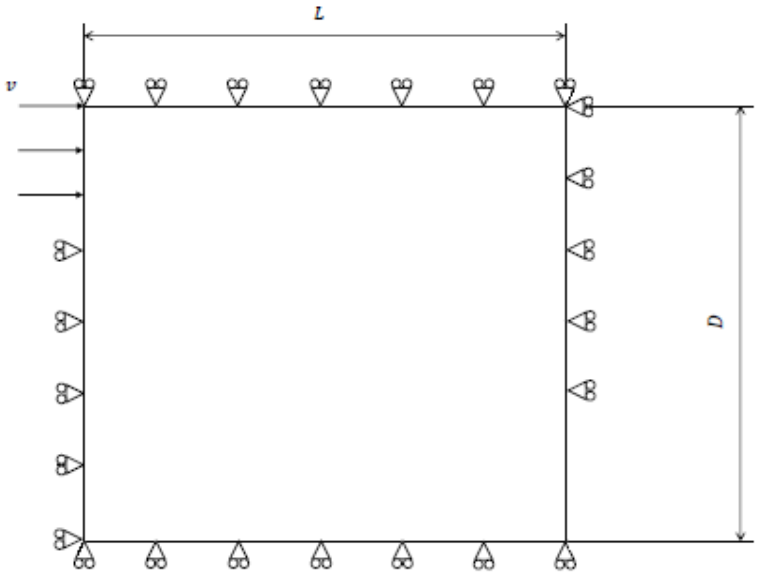

Figure 9.26 - Representation of the boundary conditions of case 2.

a) Clot Growth

The following figure represents the clot growth until the blockage of the flow exit (**Figure 9.27**).

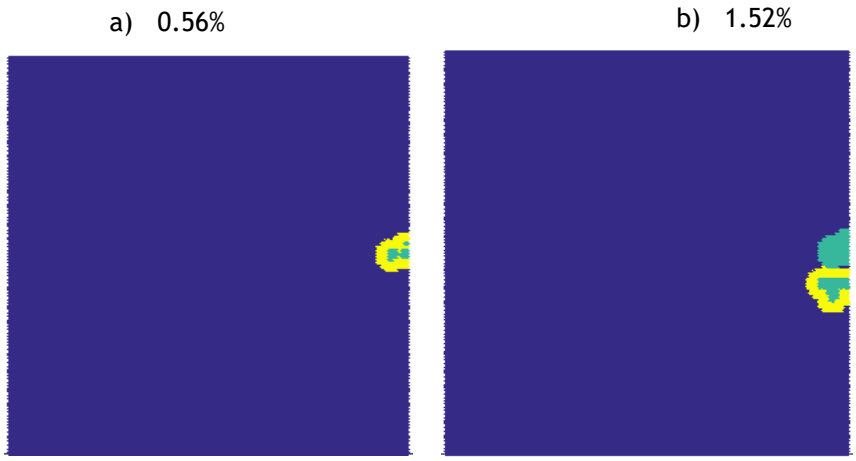

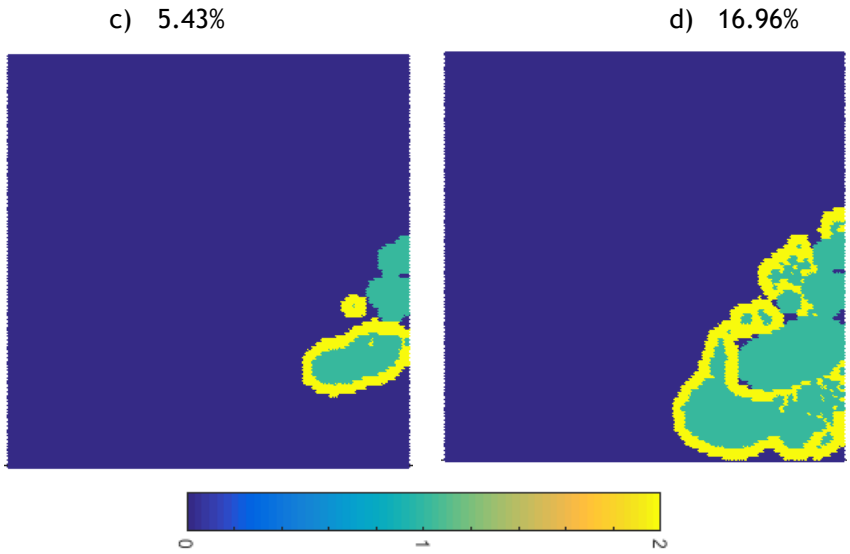

Figure 9.27 - Colour maps of the growth of the clot – boundary conditions case 2. Blue: blood; Green: old clot; Yellow: new clot.

With the alteration of the boundary condition, in this case, the flow exit, it is possible to note that the clot growth begins in the same area as in the previous results, however, the growth is directed to the lower right corner, which is the exit area of the flow, causing its blockage in an initial stage.

b) Concentration of Thrombin

The next colour maps represent the variation of the concentration of the thrombin, in logarithmic scale (**Figure 9.28**).

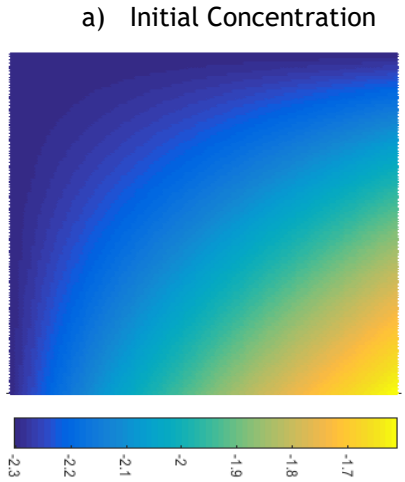

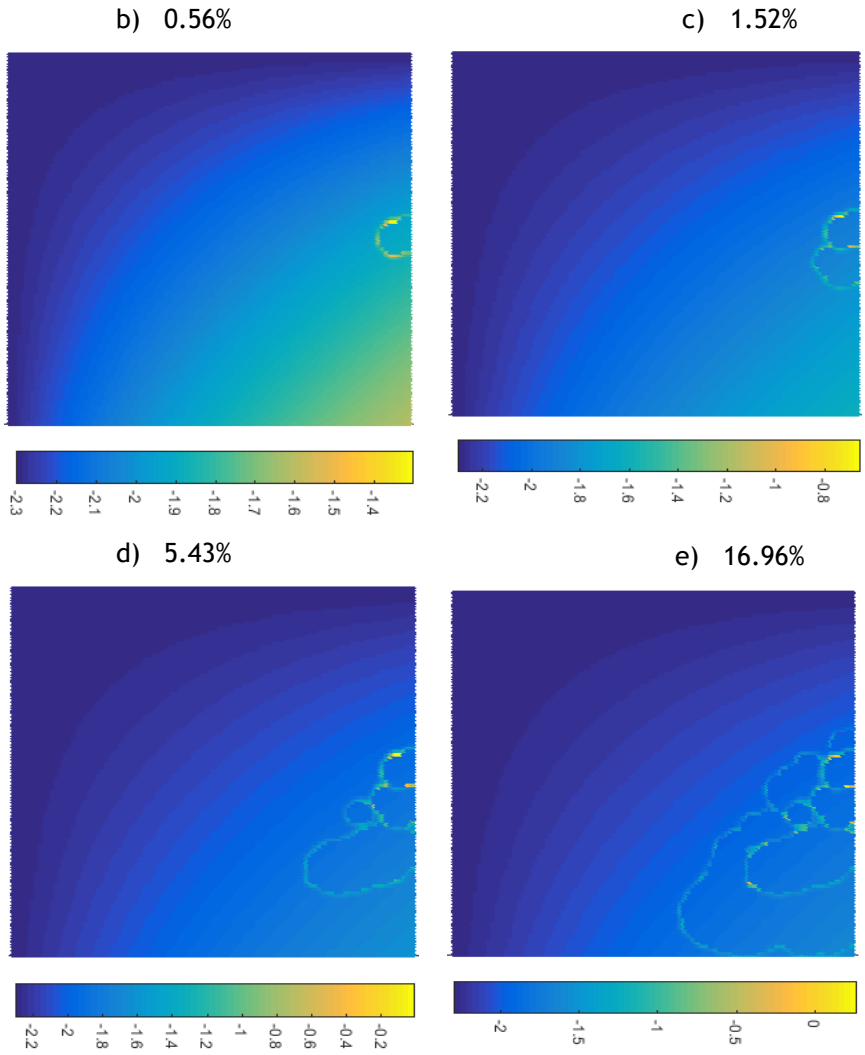

Figure 9.28 - Colour maps of the distribution of the thrombin concentration – boundary conditions case 2.

Analysing the results above, it is possible to see that they are similar to previous ones, maintaining the same features. Moreover, it is noticeable that the clot tends to form in the direction of the focus of the concentration of thrombin.

c) Velocity

The variation of the velocity, along the increments, is presented in the next colour maps (**Figure 9.29**).

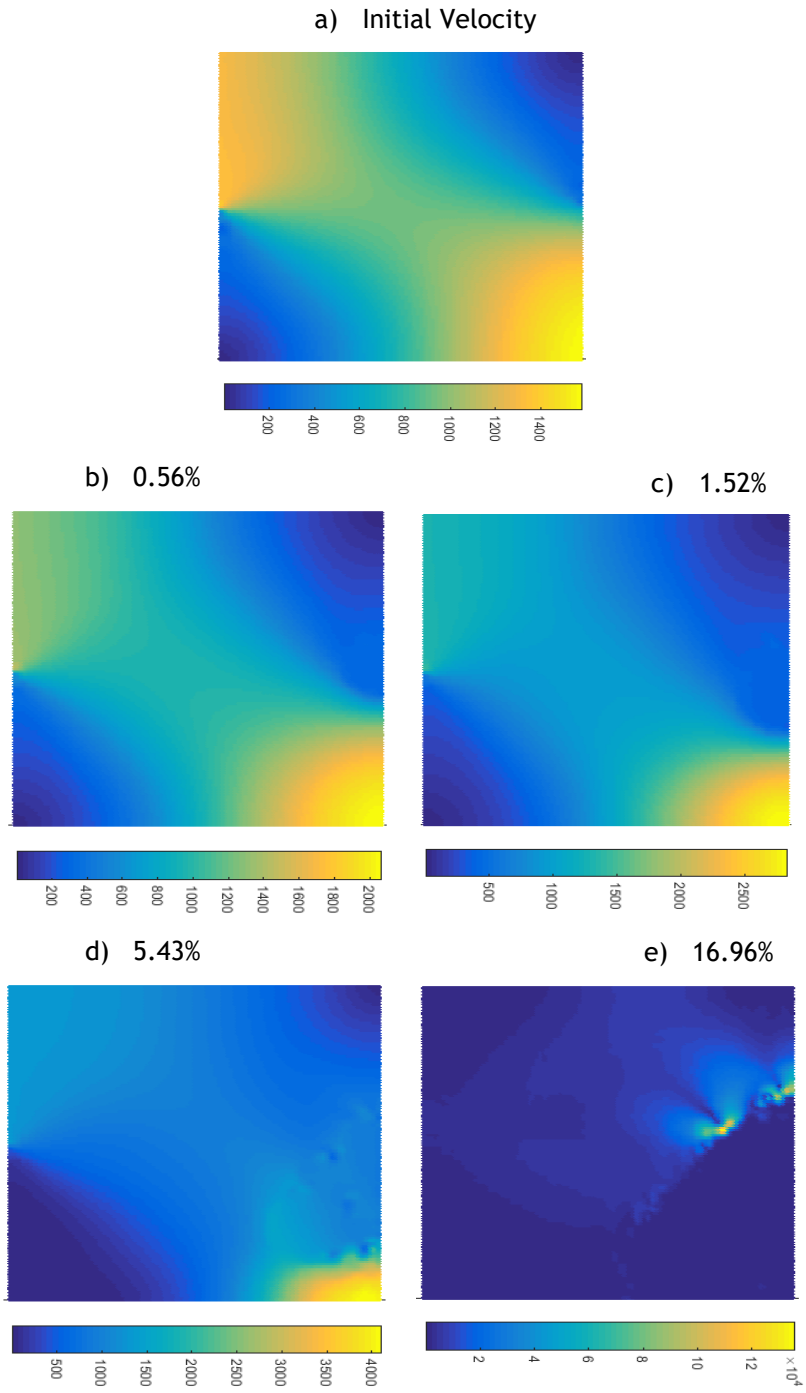

Figure 9.29 - Colour maps of the velocity profiles – boundary conditions case 2.

Analysing the initial velocity profile, that is, without clot, it is noticeable that the higher velocities are in the zones of entry and exit of flow, being this last one presented, in this case, in the right lower corner. In the remaining figures, the velocity profile is quite similar to the velocity profiles which were previously shown, which shows a velocity increase in the area of flow exit,

since the clot tends to block it. In the last increment, due to the complete blockage of that area, the velocity in the domain tends to 0, which is in accordance with the expected.

d) Shear Rate

The following figures represent the variation of the shear rate until the blockage of the flow exit (**Figure 9.30**).

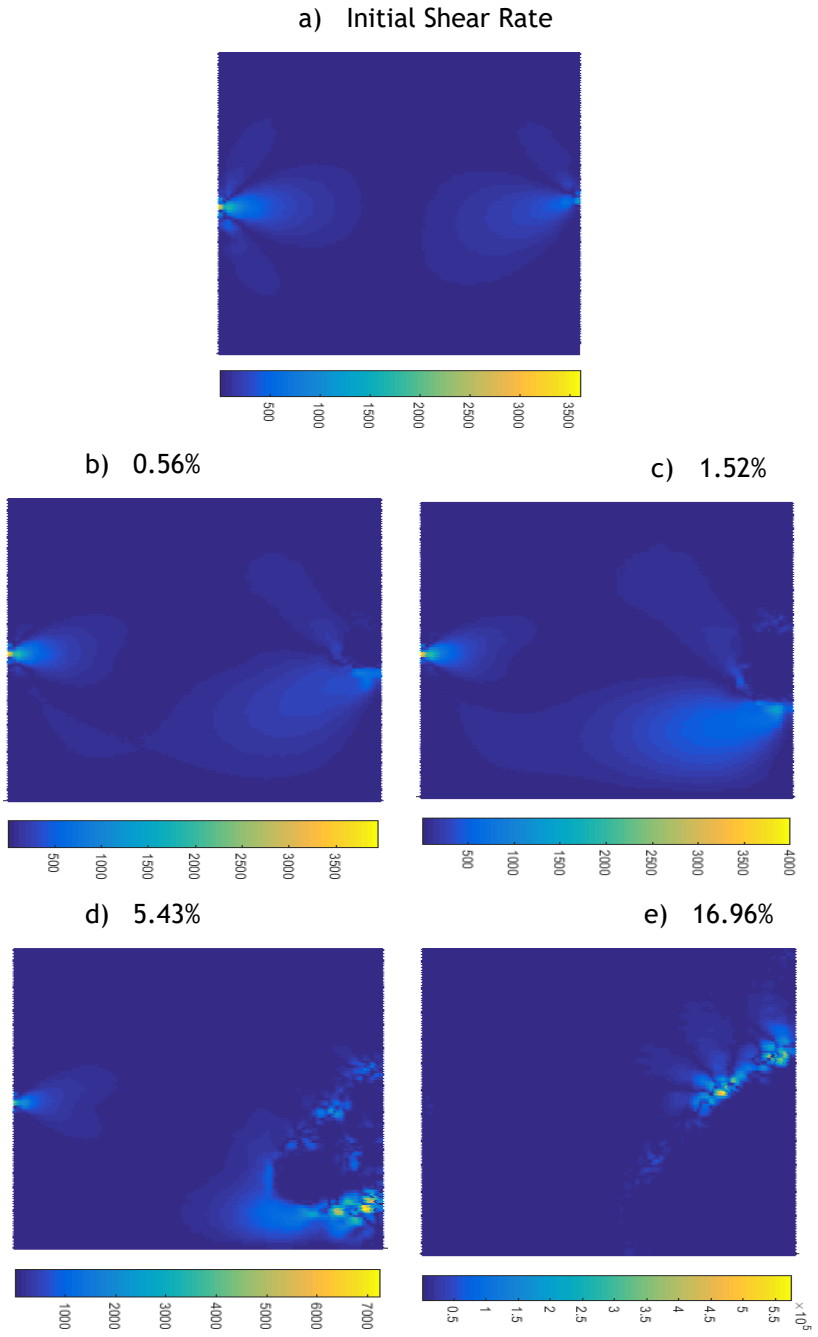

Figure 9.30 - Colour maps of the shear rate profiles – boundary conditions case 2.

When it comes to the initial shear rate profile it is similar to the previous one, presenting higher values near the entry and exit areas. Regarding the remaining figures, these are coherent with the other results and the velocity profiles presented in this case.

e) Viscosity

The following figures represent the variation of the viscosity until the blockage of the flow exit along the increments, being in the same scale as the corresponding ones in the previous sections (**Figure 9.31**).

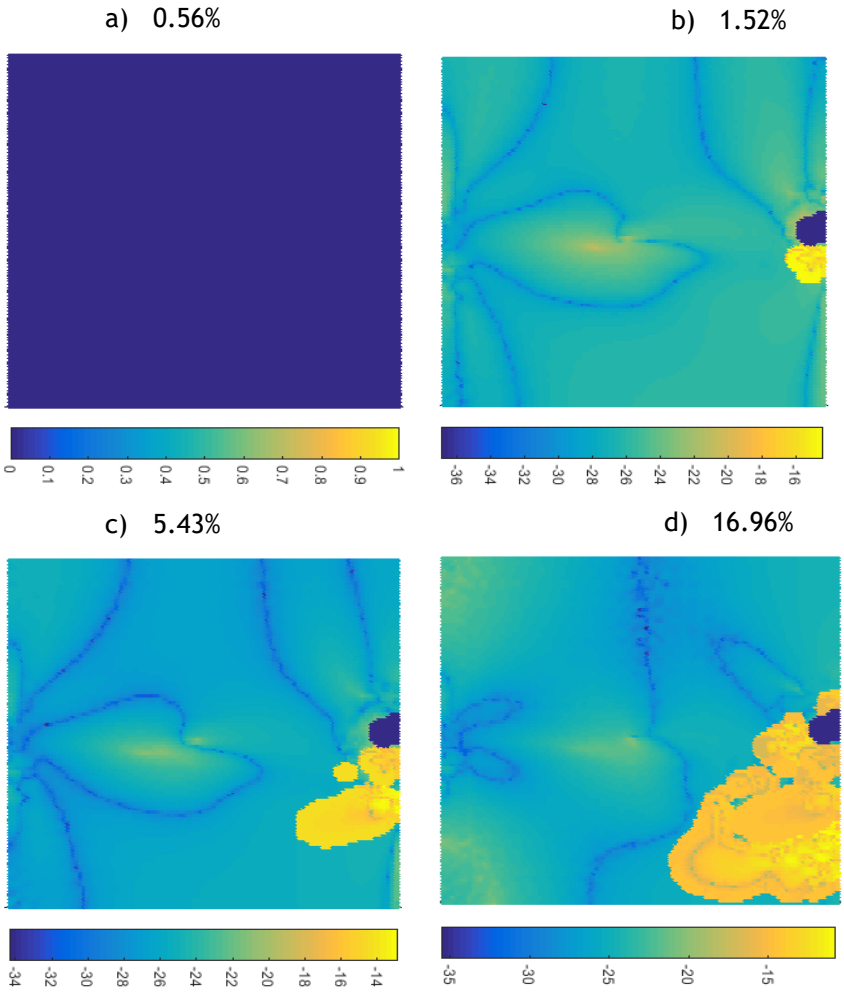

Figure 9.31 - Colour maps of the variation of viscosity – boundary conditions case 2.

The results are adequate to the clot evolution, presenting an increase in the viscosity at each increment, as well as, being in agreement with the previous ones, which makes them satisfactory.

9.2.3 - Boundary Conditions Case 3

Similarly to the previous case, the entry area of the flow was defined in the same way, when it comes to the exit area of the flow, it was placed in the lower right corner of the lower wall, as shown in **Figure 9.32**, maintaining the initially defined length.

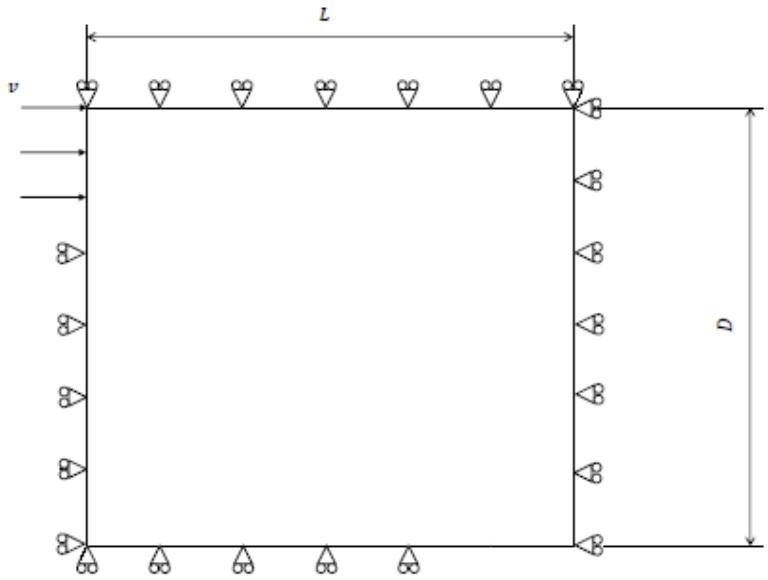

Figure 9.32 - Representation of the boundary conditions of case 3.

a) Clot Growth

The following figure represents the clot growth until the blockage of the flow exit (**Figure 9.33**).

a) 0.58%

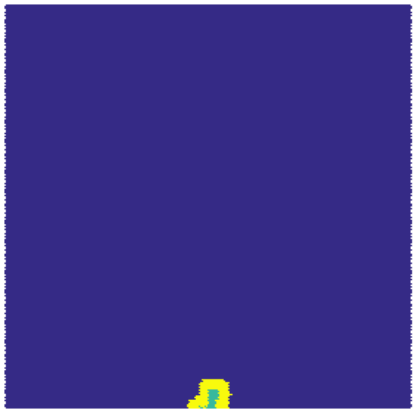

b) 2.09%

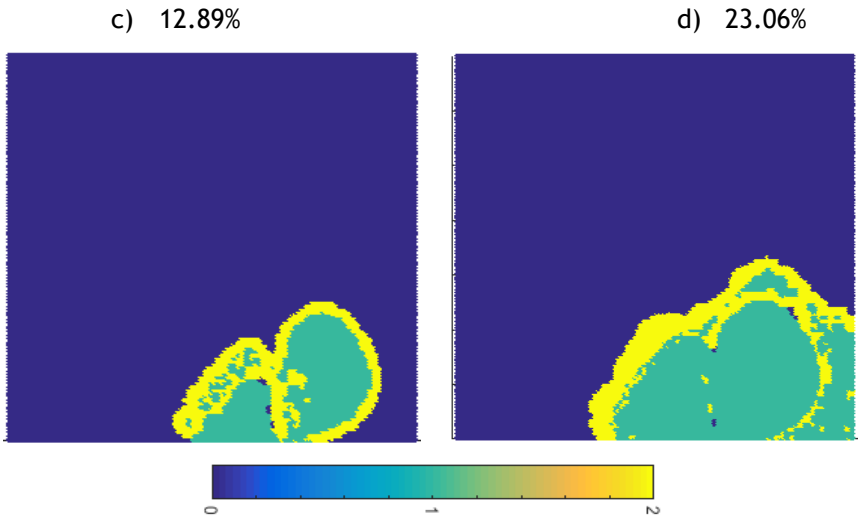

Figure 9.33 - Colour maps of the growth of the clot – boundary conditions case 3. Blue: blood; Green: old clot; Yellow: new clot.

Analysing the previous images, the position where the clot began to grow was altered with the alteration of the boundary condition of the flow exit. In this case, the clot initiates its growth on the lower wall of the domain. However, similar to what happened in the previous case, the clot growth is directed to the flow exit which causes its blockage.

b) Concentration of Thrombin

The following figure represents the variation of thrombin due to the clot growth (**Figure 9.34**).

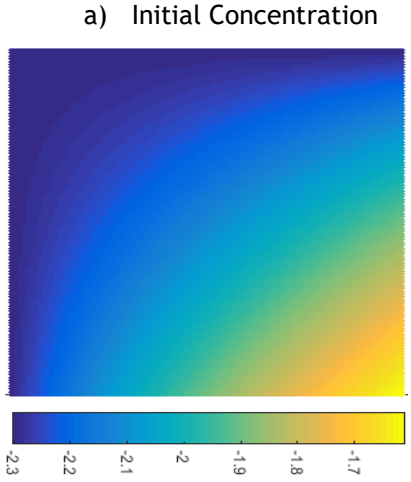

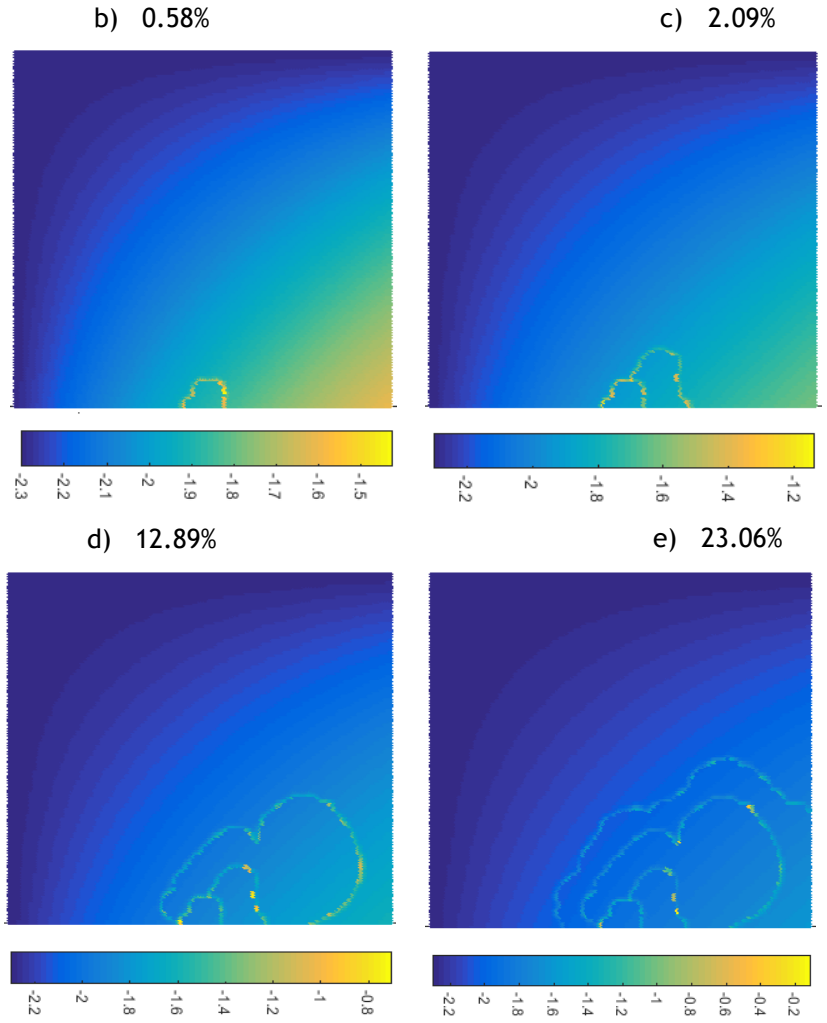

Figure 9.34 - Colour maps of the distribution of the thrombin concentration – boundary conditions case 3.

The presented profiles are similar to the previous ones, presenting the same pattern of concentration growth, since the clot grows in the area of higher thrombin concentration, its growth is faster and larger.

c) Velocity

The following figure represents the variation of the velocity until the blockage of the flow exit (**Figure 9.35**).

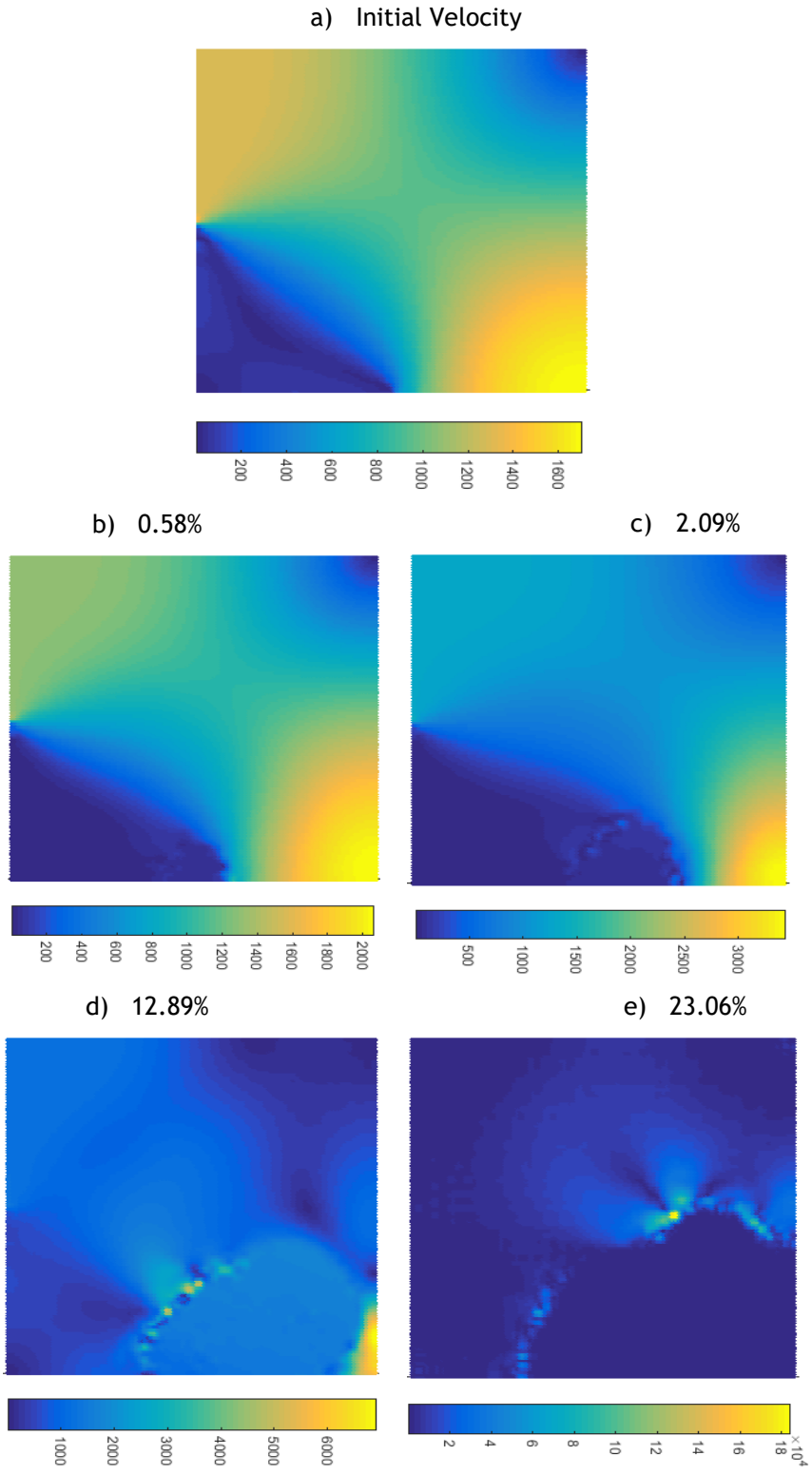

Figure 9.35 - Colour maps of the velocity profiles – boundary conditions case 3.

The initial profile is similar to the one presented in case 2, presenting the higher values of velocity in the same areas. Such can be explain by the fact that they present the outlet in similar zones.

With the growth of the clot, the variation of velocity is similar to the ones that were presented in the previous examples. Like them, the velocity increases in the zone of blockage. However, the representation of this zone is now defined in another position since the boundary condition is presented in a different wall of the domain, as well as, due to the growth of the clot in a new place.

d) Shear Rate

The variation of the shear is represented in the next colour maps (**Figure 9.36**).

a) Initial Shear Rate

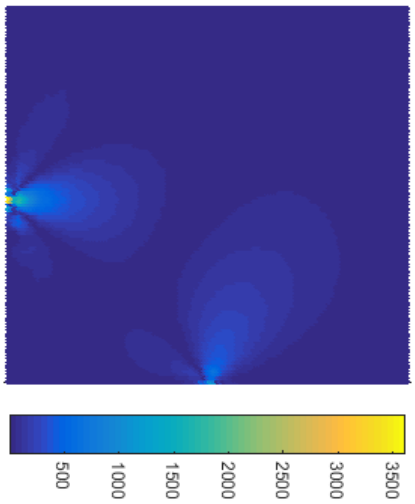

b) 0.58%

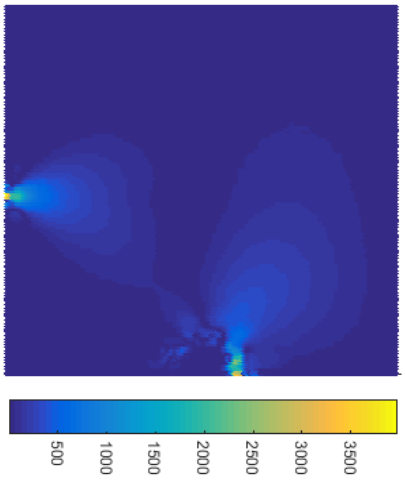

c) 2.09%

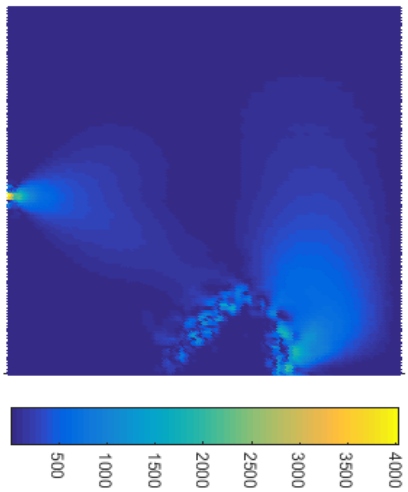

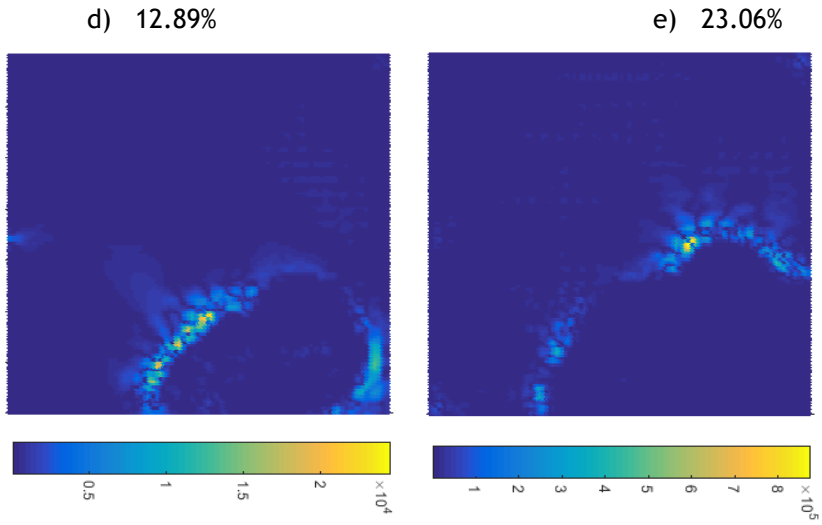

Figure 9.36 - Colour maps of the shear rate profiles – boundary conditions case 3.

The initial shear rate profile slightly differs from the previous ones since, now, the higher values of shear are not in symmetric zones. Although the profile in the inlet maintained, it is possible to see that higher values of shear exit in the middle of the lower section of the domain.
Regarding the variation of shear due to the clot growth, this follows the same configuration of the previous cases.

e) Viscosity

Finally, the colour maps of the variation of the viscosity are presented below (**Figure 9.37**). Note that the same representation that was assumed previously is used to represent them.

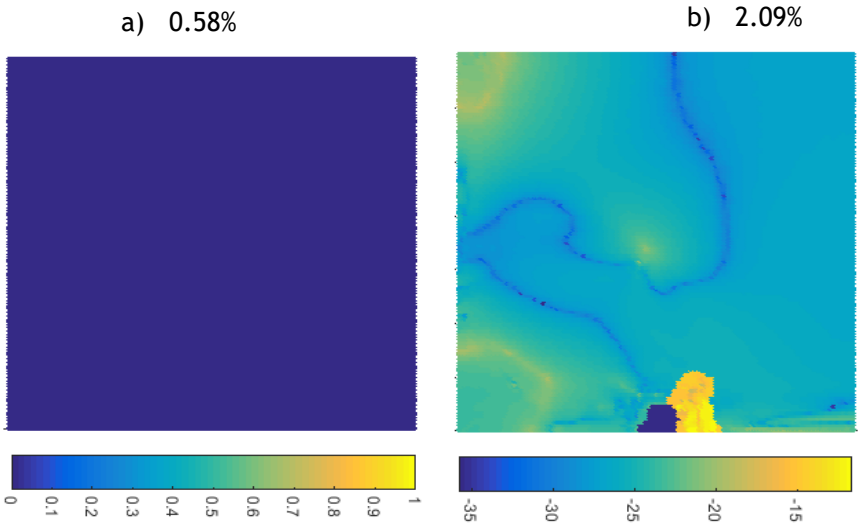

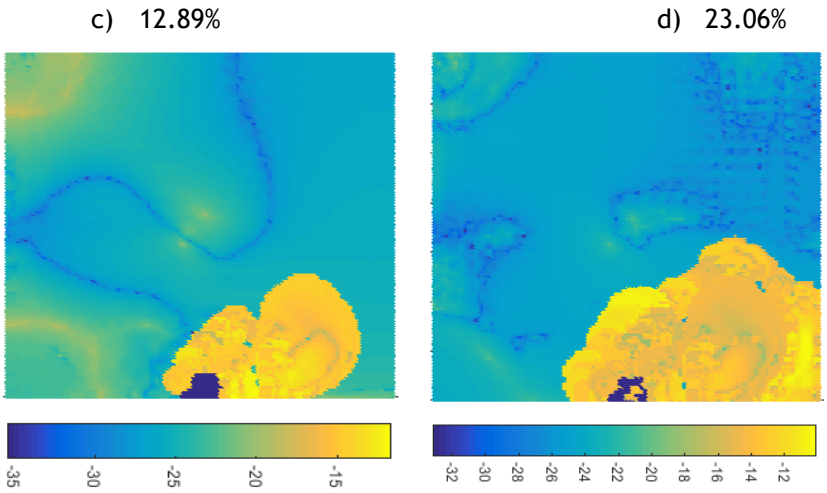

Figure 9.37 - Colour maps of the variation of the viscosity – boundary conditions case 3.

Once again, the variation of the viscosity over the increments is coherent and in agreement with what was expected since, in each one, an increase on this parameter occurs, which promotes satisfactory results.

Summing up, the modification of the boundary conditions affects the clot growth, not only in the time taken in this process, but also in the position where the clot is initially formed. Due to that, the variation of the parameters, such as the velocity or the shear rate, are also affected, being characteristic of the type of boundary conditions used.

That way, the definition of these constrains are important when referring to the appearance and growth of the clot so, it is something that should be carefully chosen.

To finish, a comparison between all cases, including the one presented in section **8.2.4.1** ("standard case"), is shown, taking into account the time taken by each one to reach a specific percentage of Clot Fraction. This comparison is performed in the graphic below (**Figure 9.38**)

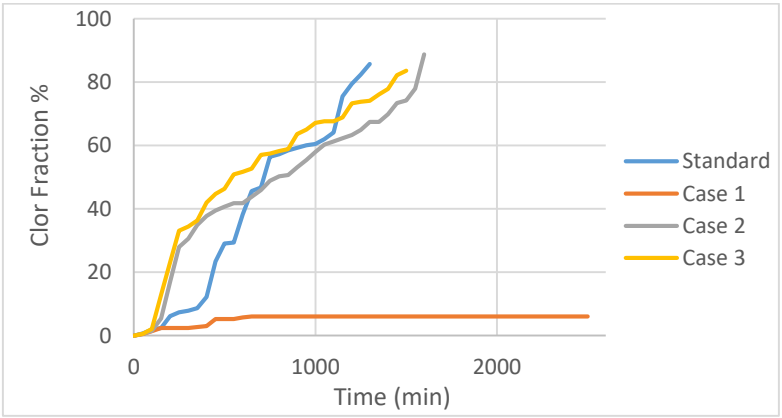

Figure 9.38 - Variation of the Clot Fraction due to the alteration of the boundary conditions.

When comparing all cases, it is possible to conclude that the standard case (results presented in section **8.2.4.1**) and the last two cases present similar curves, being the case 1 the one which differs the most, since this does not present growth from the 600 min.

Regarding cases 2 and 3, it is visible that they present a faster growth in an initial phase, when compared with the standard case. Despite this, for higher Clot Fractions, they all tend to reach it in similar times. However, note that it is important to know how the clot grows in each step time, since the blockage of the outlet is dependent on various variables and parameters (as seen in the colour maps) and, for this reason, this comparison in not sufficient to understand the behaviour of the growth process.

Chapter 10

Conclusion

Cardiovascular diseases, where coagulation disorders are included, are a critical problem of the modern society, being one of the leading causes of mortality around the world. Consequently, the interest in developing new techniques to understand this type of diseases, as well as assisting in the diagnosis, treatment or even in disease prevention, have increased in the last years. Thus, computational methods emerged as an innovation that allows for the study of haemodynamics.

The aim of this work was to create a new algorithm to simulate the formation of clots. Since the process of the coagulation is complex and not completely understood, the existent algorithms to simulate this process are limited and most are focused in specific phases of the process or in a specific component.

The designed algorithm, even in a preliminary phase, is a numerical tool capable of to simulate the appearance and growth of a clot, allowing to study the evolution of the clot over a time and its implication in the whole domain. Summing up, the algorithm generates an initial concentration of thrombin, and evaluate which points present a concentration of thrombin higher than the basal value, and that are in a specific range of shear rate. The points that satisfy these conditions have their viscosity modify according the created model of growth and, for each one, a radius is created, being also based in that model. After that, this radius is used to promote the clot growth. After that, the process occur iteratively and the concentration of thrombin is modify in the points that are not clot, which promote the growth of the clot. Thus, the growth is depend on numerical parameters (such as $Magnitude$, $Action\ Radius$ and thrombin concentration) that can be initially defined by the user.

The designed algorithm was tested with simple benchmark examples, being an initial satisfactory approach to understand the influence of this process in the blood flow. The obtained results are suitable since they mimic the expected behaviour of the appearance of a clot, namely in terms of viscosity or velocity of the domain.

Analysing the results, it was possible to conclude that the algorithm is strongly dependent on the values of two parameters $Magnitude$ and $Action\ Radius$ being necessary to use a suitable combination of these to promote moderate growth, avoiding a high computational time. However, sudden growths should be avoided because they can spin the process out of control.

After defining the combination of these parameters it becomes possible to analyse different variables associated with the used formulation, namely viscosity, velocity, thrombin concentration and shear rate. Their analysis allowed for the verification of the influence of the clot growth on the flux and its properties but also the viability of the used code, which is one of the main objectives of this work.

Regarding the velocity and shear rate, their values are in agreement since these are directly proportional and their variation over time is adequate to the presence of the clot and its growth. Besides that, knowing that the shear rate is one of the triggers of the coagulation in the created algorithm, the growth occurs between the intervals of values defined in the algorithm. The viscosity of the points that would be defined as clot was seen to have altered, which led to its increase in those points. This difference in viscosities is evident when compared to the initial viscosities. Lastly, when analysing the thrombin concentration it is clear that it increases in the points close to the clot but defined as fluid, as was defined by the algorithm. This way, it is possible to conclude that the algorithm presented satisfactory and adequate results and no running errors.

In order to verify the algorithm's behaviour in different situations from the initially defined, two new tests were created: variation of the thrombin focus and alteration of the boundary conditions. With the first one, it was possible to verify that the clot growth depends on the position of the focus, which may lead to a faster growth altering its position and consequently the thrombin distribution along the domain. Regarding the change of the boundary conditions, the same type of dependency was verified, since it influences the initial shear rate profiles of the flow and may lead to a faster and larger growth or at another position of the domain different from the initially defined. However, note that these two variations are inter-dependable since they influence the shear rate and the concentration parameters, the triggers of coagulation in this algorithm. This way, these parameters should be imposed in a thoughtful and adequate manner to each situation.

On the other hand, it is important to note that the new phenomenological curve developed to modify the viscosity of the integration points and to make the clot growth was created by the author, taking into account the literature. However, this process should be more realistic and consider other clot growth factors rather only the thrombin.

Regarding the methods used to solve similar numerical problems, it is possible to conclude that FEM is the preferable method in this field. However, meshless methods present large potential because they allow to obtain smother fields and more accurate results with less nodes. On the other hand, meshless methods are computationally more expensive. Concerning RPIM, it is important to stress that there are no studies performed with RPIM regarding this topic. And regarding the other advanced discretization techniques, such as particle methods, the number of published works is still much reduced (as shown in Chapter 5). However, the results here presented permit to understand that RPIM allows to obtain suitable and satisfactory results when combined with the new proposed algorithm.

Since it is a preliminary work on the topic, several improvements and developments can be introduced in the new proposed algorithm in future works, namely:

- Introduction of other coagulation factors, such as the platelets, in order to verify the influence in the clot growth and to promote a more realistic results;
- The concentration of the thrombin should be based on diffusion equations that describe the process in a real development. These equations can be found in the literature;
- Test the algorithm with 3D domains;
- Use more complex and realistic structures, such arteries and veins obtained with medical imaging techniques, to verify the viability of the algorithm in clinical scenarios;
- Other numeric schemes can be used, which can be interesting to study, since the created radius to increase the concentration of thrombin and to promote the clot growth are depended on this;
- Instead of RPIM, other methods, such as FEM or other meshless methods, can be used to understand which method is more suitable for this type of analysis.

To conclude, the author emphasizes that this algorithm is preliminary. Nevertheless, it was shown that the proposed new algorithm promotes accurate and satisfactory results, being a potential numerical tool do simulate the process of formation and growth of a clot.

References

1. Castellano, J.M., et al., *Promoción de la salud cardiovascular global: estrategias, retos y oportunidades*. Revista Española de Cardiología, 2014. **67**(9): p. 724-730.
2. Laslett, L.J., et al., *The worldwide environment of cardiovascular disease: prevalence, diagnosis, therapy, and policy issues: a report from the American College of Cardiology*. Journal of the American College of Cardiology, 2012. **60**(25 Supplement): p. S1-S49.
3. Mozaffarian, D., *Scourge of Global Cardiovascular Disease: Time for Health Care Systems Reform and Precision Population Health*. Journal of the American College of Cardiology, 2017.
4. Wurie, H.R. and F.P. Cappuccio, *Cardiovascular disease in low-and middle-income countries: an urgent priority*. 2012, Taylor & Francis.
5. Tomaselli, G., et al., *Government continues to have an important role in promoting cardiovascular health*. American Heart Journal, 2018. **198**: p. 160-165.
6. El-Sayed, M.S., Z.E.-S. Ali, and S. Ahmadizad, *Exercise and training effects on blood haemostasis in health and disease*. Sports medicine, 2004. **34**(3): p. 181-200.
7. Jackson, S.P., *Arterial thrombosis—insidious, unpredictable and deadly*. Nature medicine, 2011. **17**(11): p. 1423.
8. Jessup, M. and S. Brozena, *Heart failure*. N Engl J Med, 2003. **348**(20): p. 2007-18.
9. Machlus, K.R., M.M. Aleman, and A.S. Wolberg, *Update on venous thromboembolism: risk factors, mechanisms, and treatments*. Arteriosclerosis, thrombosis, and vascular biology, 2011. **31**(3): p. 476-478.
10. Aleman, M.M., et al., *Fibrinogen and red blood cells in venous thrombosis*. Thrombosis research, 2014. **133**: p. S38-S40.
11. Formaggia, L., A. Quarteroni, and A. Veneziani, *Cardiovascular Mathematics: Modeling and simulation of the circulatory system*. Vol. 1. 2010: Springer Science & Business Media.
12. Taylor, C.A., T.J. Hughes, and C.K. Zarins, *Finite element modeling of blood flow in arteries*. Computer methods in applied mechanics and engineering, 1998. **158**(1-2): p. 155-196.
13. Bathe, K.J. and H. Zhang, *Finite element developments for general fluid flows with structural interactions*. International Journal for Numerical Methods in Engineering, 2004. **60**(1): p. 213-232.
14. Mackerle, J., *Finite element analyses and simulations in biomedicine: a bibliography (1985-1999)*. Engineering computations, 2000. **17**(7): p. 813-856.
15. Mackerle, J., *Finite element modelling and simulations in cardiovascular mechanics and cardiology: A bibliography 1993–2004*. Computer methods in biomechanics and biomedical engineering, 2005. **8**(2): p. 59-81.
16. Fasano, A. and A. Sequeira, *Hemorheology and Hemodynamics*, in *Hemomath*. 2017, Springer. p. 1-77.

17. Junqueira, L.C., J. Carneiro, and R.O. Kelley, *Basic histology: text & atlas*. Vol. 11. 2003: McGraw-Hill New York.
18. Hoskins, P.R., P.V. Lawford, and B.J. Doyle, *Cardiovascular biomechanics*. 2017: Springer.
19. Widmaier, E.P., et al., *Vander's human physiology: the mechanisms of body function*. 2008: Boston: McGraw-Hill Higher Education.
20. Wootton, D.M. and D.N. Ku, *Fluid mechanics of vascular systems, diseases, and thrombosis.* Annual review of biomedical engineering, 1999. **1**(1): p. 299-329.
21. Berling, C. and L. Hall, *An NMR assessment of the rheological properties of blood and its constituents: A review.* NMR in Biomedicine, 1989. **2**(1): p. 1-6.
22. Sochi, T., *Non-Newtonian rheology in blood circulation.* arXiv preprint arXiv:1306.2067, 2013.
23. Ikeda, Y., et al., *The role of von Willebrand factor and fibrinogen in platelet aggregation under varying shear stress.* The Journal of clinical investigation, 1991. **87**(4): p. 1234-1240.
24. Errill, E., *Rheology of blood.* Physiological reviews, 1969. **49**(4): p. 863-888.
25. Pavlova, J., A. Fasano, and A. Sequeira, *Numerical simulations of a reduced model for blood coagulation.* Zeitschrift für angewandte Mathematik und Physik, 2016. **67**(2): p. 28.
26. Baskurt, O.K. and H.J. Meiselman. *Blood rheology and hemodynamics*. in *Seminars in thrombosis and hemostasis*. 2003. Copyright© 2003 by Thieme Medical Publishers, Inc., 333 Seventh Avenue, New York, NY 10001, USA. Tel.:+ 1 (212) 584-4662.
27. Diamond, S.L., *Systems analysis of thrombus formation.* Circulation research, 2016. **118**(9): p. 1348-1362.
28. Lobanov, A. and T. Starozhilova, *The effect of convective flows on blood coagulation processes.* Pathophysiology of haemostasis and thrombosis, 2005. **34**(2-3): p. 121-134.
29. Dahlbäck, B., *Blood coagulation.* The Lancet, 2000. **355**(9215): p. 1627-1632.
30. Ahn, S.H., et al., *Histologic features of acute thrombi retrieved from stroke patients during mechanical reperfusion therapy.* International Journal of Stroke, 2016. **11**(9): p. 1036-1044.
31. Butenas, S. and K. Mann, *Blood coagulation.* Biochemistry (Moscow), 2002. **67**(1): p. 3-12.
32. Gale, A.J., *Continuing education course# 2: current understanding of hemostasis.* Toxicologic pathology, 2011. **39**(1): p. 273-280.
33. Davie, E.W., K. Fujikawa, and W. Kisiel, *The coagulation cascade: initiation, maintenance, and regulation.* Biochemistry, 1991. **30**(43): p. 10363-10370.
34. Butenas, S., et al., *Tissue factor in thrombosis and hemorrhage.* Surgery, 2007. **142**(4): p. S2-S14.
35. Salzman, E., *The events that lead to thrombosis.* Bulletin of the New York Academy of Medicine, 1972. **48**(2): p. 225.
36. VanPutte, C.L., et al., *Seeley's anatomy & physiology*. 2014, New York, NY: McGraw-Hill.
37. Furie, B., *Pathogenesis of thrombosis.* ASH Education Program Book, 2009. **2009**(1): p. 255-258.
38. Rubio-Jurado, B., et al., *The clinical significance of coagulation and the inflammatory response in autoimmunity.* Clinical reviews in allergy & immunology, 2012. **42**(2): p. 172-180.
39. Elizondo, P. and A.L. Fogelson, *A mathematical model of venous thrombosis initiation.* Biophysical journal, 2016. **111**(12): p. 2722-2734.
40. Sagripanti, A. and A. Carpi, *Natural anticoagulants, aging, and thromboembolism.* Experimental gerontology, 1998. **33**(7-8): p. 891-896.
41. Klement, P., P. Liao, and L. Bajzar, *A novel approach to arterial thrombolysis.* Blood, 1999. **94**(8): p. 2735-2743.
42. Minnema, M., et al., *Activation of clotting factors XI and IX in patients with acute myocardial infarction.* Arteriosclerosis, thrombosis, and vascular biology, 2000. **20**(11): p. 2489-2493.
43. Kaibara, M., *Rheology of blood coagulation.* Biorheology, 1996. **33**(2): p. 101-117.
44. Mann, K.G., et al., *Models of blood coagulation.* Blood Cells, Molecules, and Diseases, 2006. **36**(2): p. 108-117.

45. Wang, N.-T. and A.L. Fogelson, *Computational methods for continuum models of platelet aggregation.* Journal of Computational Physics, 1999. **151**(2): p. 649-675.
46. Hoffman, M. and D.M. Monroe III, *A cell-based model of hemostasis.* Thrombosis and haemostasis, 2001. **85**(06): p. 958-965.
47. Fogelson, A.L., Y.H. Hussain, and K. Leiderman, *Blood clot formation under flow: the importance of factor XI depends strongly on platelet count.* Biophysical journal, 2012. **102**(1): p. 10-18.
48. Susree, M., M.A. Panteleev, and M. Anand, *Coated platelets introduce significant delay in onset of peak thrombin production: theoretical predictions.* Journal of theoretical biology, 2018. **453**: p. 108-116.
49. Bodnár, T. and A. Sequeira, *Numerical simulation of the coagulation dynamics of blood.* Computational and Mathematical Methods in Medicine, 2008. **9**(2): p. 83-104.
50. Anand, M., K. Rajagopal, and K. Rajagopal, *A model incorporating some of the mechanical and biochemical factors underlying clot formation and dissolution in flowing blood.* Computational and mathematical methods in medicine, 2003. **5**(3-4): p. 183-218.
51. Leonard, E., *The role of flow in thrombogenesis.* Bulletin of the new York Academy of Medicine, 1972. **48**(2): p. 273.
52. Dobrovolsky, A. and E. Titaeva, *The fibrinolysis system: regulation of activity and physiologic functions of its main components.* Biochemistry (Moscow), 2002. **67**(1): p. 99-108.
53. Hellums, J.D., *1993 Whitaker Lecture: biorheology in thrombosis research.* Annals of biomedical engineering, 1994. **22**(5): p. 445-455.
54. Mody, N.A. and M.R. King, *Three-dimensional simulations of a platelet-shaped spheroid near a wall in shear flow.* Physics of Fluids, 2005. **17**(11): p. 113302.
55. Tosenberger, A., N. Bessonov, and V. Volpert, *Influence of fibrinogen deficiency on clot formation in flow by hybrid model.* Mathematical Modelling of Natural Phenomena, 2015. **10**(1): p. 36-47.
56. Cito, S., M.D. Mazzeo, and L. Badimon, *A review of macroscopic thrombus modeling methods.* Thrombosis research, 2013. **131**(2): p. 116-124.
57. Ataullakhanov, F.I. and M.A. Panteleev, *Mathematical modeling and computer simulation in blood coagulation.* Pathophysiology of haemostasis and thrombosis, 2005. **34**(2-3): p. 60-70.
58. Xu, Z., et al., *Multiscale model of fibrin accumulation on the blood clot surface and platelet dynamics*, in *Methods in cell biology*. 2012, Elsevier. p. 367-388.
59. Xu, Z., et al., *A multiscale model of thrombus development.* Journal of the Royal Society Interface, 2008. **5**(24): p. 705-722.
60. Casa, L.D., D.H. Deaton, and D.N. Ku, *Role of high shear rate in thrombosis.* Journal of vascular surgery, 2015. **61**(4): p. 1068-1080.
61. Wang, J. and G. Liu, *A point interpolation meshless method based on radial basis functions.* International Journal for Numerical Methods in Engineering, 2002. **54**(11): p. 1623-1648.
62. Peyroteo, M., et al., *Mechanical bone remodelling: Comparative study of distinct numerical approaches.* Engineering Analysis with Boundary Elements, 2018.
63. Belinha, J., et al., *The analysis of laminated plates using distinct advanced discretization meshless techniques.* Composite Structures, 2016. **143**: p. 165-179.
64. Belinha, J., et al., *The natural neighbor radial point interpolation method extended to the crack growth simulation.* International Journal of Applied Mechanics, 2016. **8**(01): p. 1650006.
65. Fish, J. and T. Belytschko, *A first course in finite elements*. Vol. 1. 2007: John Wiley & Sons New York.
66. Geng, J.-P., K.B. Tan, and G.-R. Liu, *Application of finite element analysis in implant dentistry: a review of the literature.* The Journal of prosthetic dentistry, 2001. **85**(6): p. 585-598.

67. Pironneau, O. and O. Pironneau, *Finite element methods for fluids*. 1989: Wiley Chichester.
68. Belinha, J., *Meshless Methods: The Future of Computational Biomechanical Simulation.* J Biom Biostat 2016. **7**: p. 325.
69. Liu, G.-R. and S.S. Quek, *The finite element method: a practical course*. 2013: Butterworth-Heinemann.
70. Chandran, K.B., S.E. Rittgers, and A.P. Yoganathan, *Biofluid mechanics: the human circulation*. 2006: CRC press.
71. Trivedi, S., *Finite element analysis: A boon to dentistry.* Journal of oral biology and craniofacial research, 2014. **4**(3): p. 200-203.
72. Parashar, S.K. and J.K. Sharma, *A review on application of finite element modelling in bone biomechanics*. Perspectives in Science, 2016. **8**: p. 696-698.
73. Kamada, H., et al., *A three-dimensional particle simulation of the formation and collapse of a primary thrombus.* International Journal for Numerical Methods in Biomedical Engineering, 2010. **26**(3-4): p. 488-500.
74. Piqueiro, L.G., et al., *A 2D stress analysis of zirconia dental implants: A comparison study*, in *Biodental Engineering IV*. 2017, CRC Press. p. 37-40.
75. Belytschko, T., et al., *Meshless methods: an overview and recent developments.* Computer methods in applied mechanics and engineering, 1996. **139**(1-4): p. 3-47.
76. El Zahab, Z., E. Divo, and A. Kassab, *A localized collocation meshless method (LCMM) for incompressible flows CFD modeling with applications to transient hemodynamics.* Engineering analysis with boundary elements, 2009. **33**(8-9): p. 1045-1061.
77. Belinha, J., *Meshless Methods in Biomechanics*. 1 ed. Lecture Notes in Computational Vision and Biomechanics. 2014: Springer. 320.
78. Tavares, C., et al., *The elasto-plastic response of the bone tissue due to the insertion of dental implants.* Procedia Engineering, 2015. **110**: p. 37-44.
79. Braun, J. and M. Sambridge, *A numerical method for solving partial differential equations on highly irregular evolving grids.* Nature, 1995. **376**(6542): p. 655.
80. Sukumar, N., B. Moran, and T. Belytschko, *The natural element method in solid mechanics.* International journal for numerical methods in engineering, 1998. **43**(5): p. 839-887.
81. Cueto, E., M. Doblaré, and L. Gracia, *Imposing essential boundary conditions in the natural element method by means of density-scaled α-shapes.* International journal for numerical methods in engineering, 2000. **49**(4): p. 519-546.
82. Liu, G.-R. and Y. Gu, *A point interpolation method for two-dimensional solids.* International Journal for Numerical Methods in Engineering, 2001. **50**(4): p. 937-951.
83. Wang, J. and G. Liu, *On the optimal shape parameters of radial basis functions used for 2-D meshless methods.* Computer methods in applied mechanics and engineering, 2002. **191**(23-24): p. 2611-2630.
84. Belinha, J., et al., *The natural neighbor radial point interpolation method in computational fracture mechanics: a 2D preliminary study.* International Journal of Computational Methods, 2017. **14**(04): p. 1750045.
85. Zienkiewicz, O., Y. Liu, and G. Huang, *Error estimation and adaptivity in flow formulation for forming problems.* International Journal for Numerical Methods in Engineering, 1988. **25**(1): p. 23-42.
86. Zienkiewicz, O., *Flow formulation for numerical solution of forming processes*. 1984.
87. Zienkiewicz, O., E. Oñae, and J. Heinrich, *A general formulation for coupled thermal flow of metals using finite elements.* International Journal for Numerical Methods in Engineering, 1981. **17**(10): p. 1497-1514.
88. Mori, D., et al., *Simulation of platelet adhesion and aggregation regulated by fibrinogen and von Willebrand factor.* Thrombosis and haemostasis, 2008. **99**(01): p. 108-115.
89. Sorensen, E.N., et al., *Computational simulation of platelet deposition and activation: I. Model development and properties.* Annals of biomedical engineering, 1999. **27**(4): p. 436-448.

90. Sorensen, E.N., et al., *Computational Simulation of Platelet Deposition and Activation: II. Results for Poiseuille Flow over Collagen.* Annals of Biomedical Engineering, 1999. **27**(4): p. 449–458.
91. Chung, T., *Computational fluid dynamics*. 2010: Cambridge university press.
92. Turner, M., *Stiffness and deflection analysis of complex structures.* journal of the Aeronautical Sciences, 1956. **23**(9): p. 805-823.
93. Horlock, J., *European Report: Finite Element Methods in Flow Problems.* Journal of Fluids Engineering, 1974. **96**(3): p. 197-197.
94. Zienkiewicz, O.C., P. Mayer, and Y.K. Cheung, *Solution of anisotropic seepage by finite elements.* Journal of the Engineering Mechanics Division, 1966. **92**(1): p. 111-120.
95. Martin, H.C., *Finite element analysis of fluid flows*. 1968, WASHINGTON UNIV SEATTLE DEPT OF AERONAUTICS AND ASTRONAUTICS.
96. Oden, J.T. and L.C. Wellford, *Analysis of flow of viscous fluids by the finite-element method.* AIAA Journal, 1972. **10**(12): p. 1590-1599.
97. Reddi, M.M., *Finite-Element Solution of the Incompressible Lubrication Problem.* Journal of Lubrication Technology, 1969. **91**(3): p. 524-533.
98. Argyris, J., G. Mareczek, and D. Scharpf, *Two-and three-dimensional flow analysis using finite elements.* Nuclear Engineering and Design, 1970. **11**(2): p. 230-236.
99. Oden, J.T., *A general theory of finite elements. II. Applications.* International Journal for Numerical Methods in Engineering, 1969. **1**(3): p. 247-259.
100. Oden, J. and D. Somogyi. *Finite element applications in fluid dynamics*. in *Proc. ASCE*. 1969.
101. Oden, J.T., *Finite element formulation of problems of finite deformation and irreversible thermodynamics of nonlinear continua-A survey and extension of recent developments.* 1971.
102. Eidelberg, B. and J. Booker, *Application of finite element methods to lubrication: squeeze films between porous surfaces.* Journal of Lubrication Technology, 1976. **98**(1): p. 175-179.
103. Baskharone, E., *Fluid Mechanics Finite Element Applications. In The Finite Element Method with Heat Transfer and Fluid Mechanics Applications.* Cambridge: Cambridge University, 2013: p. 106-113.
104. Porenta, G., D. Young, and T. Rogge, *A finite-element model of blood flow in arteries including taper, branches, and obstructions.* Journal of biomechanical engineering, 1986. **108**(2): p. 161-167.
105. Parker, D., C. Taylor, and K. Wang. *Imaged based 3D solid model construction of human arteries for blood flow simulations*. in *Engineering in Medicine and Biology Society, 1998. Proceedings of the 20th Annual International Conference of the IEEE*. 1998. IEEE.
106. Ray, G. and N. Davids, *Shear stress analysis of blood-endothelial surface in inlet section of artery with plugging.* J Biomech, 1970. **3**(1): p. 99-110.
107. Baaijens, J. and J. Janssen, *Numerical analysis of steady generalized Newtonian blood flow in a 2D model of the carotid artery bifurcation.* Biorheology, 1993. **30**(1): p. 63-74.
108. Chakravarty, S., P. Mandal, and A. Mandal, *Mathematical model of pulsatile blood flow in a distensible aortic bifurcation subject to body acceleration.* International Journal of Engineering Science, 2000. **38**(2): p. 215-238.
109. Perktold, K. and G. Rappitsch, *Computer simulation of local blood flow and vessel mechanics in a compliant carotid artery bifurcation model.* Journal of biomechanics, 1995. **28**(7): p. 845-856.
110. Lee, S.H., H.G. Choi, and J.Y. Yool, *Finite element simulation of blood flow in a flexible carotid artery bifurcation.* Journal of Mechanical Science and Technology, 2012. **26**(5): p. 1355-1361.
111. Hoogstraten, H., et al., *Numerical simulation of blood flow in an artery with two successive bends.* Journal of biomechanics, 1996. **29**(8): p. 1075-1083.

112. Milner, J.S., et al., *Hemodynamics of human carotid artery bifurcations: computational studies with models reconstructed from magnetic resonance imaging of normal subjects*. Journal of vascular surgery, 1998. **28**(1): p. 143-156.
113. Oshima, M., et al., *Finite element simulation of blood flow in the cerebral artery*. Computer methods in applied mechanics and engineering, 2001. **191**(6-7): p. 661-671.
114. Nithiarasu, P., *Robust Finite Element Approaches to Systemic Circulation Using the Locally Conservative Galerkin (LCG) Method*. Proceedings of the Indian National Science Academy, 2016. **82**(2).
115. Formaggia, L., D. Lamponi, and A. Quarteroni, *One-dimensional models for blood flow in arteries*. Journal of engineering mathematics, 2003. **47**(3-4): p. 251-276.
116. Urquiza, S., et al., *Multidimensional modelling for the carotid artery blood flow*. Computer Methods in Applied Mechanics and Engineering, 2006. **195**(33-36): p. 4002-4017.
117. Tang, D., et al., *Wall stress and strain analysis using a three-dimensional thick-wall model with fluid–structure interactions for blood flow in carotid arteries with stenoses*. Computers & Structures, 1999. **72**(1-3): p. 341-356.
118. Inzoli, F., F. Migliavacca, and G. Pennati, *Numerical analysis of steady flow in aorto-coronary bypass 3-D model*. Journal of Biomechanical Engineering, 1996. **118**(2): p. 172-179.
119. Bertolotti, C. and V. Deplano, *Three-dimensional numerical simulations of flow through a stenosed coronary bypass*. Journal of Biomechanics, 2000. **33**(8): p. 1011-1022.
120. Affeld, K., et al., *Fluid mechanics of the stagnation point flow chamber and its platelet deposition*. Artificial Organs, 1995. **19**(7): p. 597-602.
121. Bluestein, D., et al., *Steady flow in an aneurysm model: correlation between fluid dynamics and blood platelet deposition*. Journal of biomechanical engineering, 1996. **118**(3): p. 280-286.
122. Mower, W.R., W.J. Quiñones, and S.S. Gambhir, *Effect of intraluminal thrombus on abdominal aortic aneurysm wall stress*. Journal of vascular surgery, 1997. **26**(4): p. 602-608.
123. Wang, D.H., et al., *Mechanical properties and microstructure of intraluminal thrombus from abdominal aortic aneurysm*. Journal of biomechanical engineering, 2001. **123**(6): p. 536-539.
124. Li, Z.-Y., et al., *Impact of calcification and intraluminal thrombus on the computed wall stresses of abdominal aortic aneurysm*. Journal of vascular surgery, 2008. **47**(5): p. 928-935.
125. Bluestein, D., et al., *Fluid mechanics of arterial stenosis: relationship to the development of mural thrombus*. Annals of biomedical engineering, 1997. **25**(2): p. 344.
126. Karner, G. and K. Perktold, *The influence of flow on the concentration of platelet active substances in the vicinity of mural microthrombi*. COMPUTER METHODS IN BIOMECHANICS AND BIO MEDICAL ENGINEERING, 1998. **1**(4): p. 285-301.
127. Wootton, D.M., A.S. Popel, and B. Rita Alevriadou, *An experimental and theoretical study on the dissolution of mural fibrin clots by tissue-type plasminogen activator*. Biotechnology and bioengineering, 2002. **77**(4): p. 405-419.
128. Weller, F.F., *Platelet deposition in non-parallel flow*. Journal of mathematical biology, 2008. **57**(3): p. 333-359.
129. Weller, F.F., *A free boundary problem modeling thrombus growth*. Journal of mathematical biology, 2010. **61**(6): p. 805-818.
130. Tokarev, A., et al., *Continuous mathematical model of platelet thrombus formation in blood flow*. Russian Journal of Numerical Analysis and Mathematical Modelling, 2012. **27**(2): p. 191-212.
131. Voronov, R.S., et al., *Simulation of intrathrombus fluid and solute transport using in vivo clot structures with single platelet resolution*. Annals of biomedical engineering, 2013. **41**(6): p. 1297-1307.
132. Abolfazli, E., N. Fatouraee, and B. Vahidi, *Dynamics of motion of a clot through an arterial bifurcation: a finite element analysis*. Fluid Dynamics Research, 2014. **46**(5): p. 055505.

133. Lu, Y., et al., *Multiscale simulation of thrombus growth and vessel occlusion triggered by collagen/tissue factor using a data-driven model of combinatorial platelet signalling*. Mathematical medicine and biology: a journal of the IMA, 2016. **34**(4): p. 523-546.
134. Vanegas-Acosta, J. and D. Garzón-Alvarado, *Mathematical model of the coagulation in the bone–dental implant interface*. Computers in biology and medicine, 2010. **40**(10): p. 791-801.
135. Kovářík, K., J. Mužík, and M. Mahmood, *A meshless solution of two-dimensional unsteady flow*. Engineering Analysis with Boundary Elements, 2012. **36**(5): p. 738-743.
136. Katz, A.J., *Meshless methods for computational fluid dynamics*. 2009: Stanford University.
137. Garg, R., H.C. Thakur, and B. Tripathi, *A Review of Applications of Meshfree Methods in the area of Heat Transfer and Fluid Flow: MLPG method in particular*. Int. Res. J. Eng. Tech, 2015. **2**(4): p. 329-338.
138. Grilli, S.T., J. Skourup, and I.A. Svendsen, *An efficient boundary element method for nonlinear water waves*. Engineering Analysis with Boundary Elements, 1989. **6**(2): p. 97-107.
139. Kikani, J., *Application of boundary element method to streamline generation and pressure transient testing*. 1989, Stanford University.
140. Holmes, D.W., J.R. Williams, and P. Tilke, *Smooth particle hydrodynamics simulations of low Reynolds number flows through porous media*. 2000.
141. Löhner, R., et al., *A finite point method for compressible flow*. International Journal for Numerical Methods in Engineering, 2002. **53**(8): p. 1765-1779.
142. Noutcheuwa, R.K. and R.G. Owens, *A new incompressible smoothed particle hydrodynamics-immersed boundary method*. Int. J. Numer. Anal. Model. Series B, 2012. **3**(2): p. 126-167.
143. Lin, H. and S. Atluri, *Meshless local Petrov-Galerkin(MLPG) method for convection diffusion problems*. CMES(Computer Modelling in Engineering & Sciences), 2000. **1**(2): p. 45-60.
144. Singh, I., *Application of meshless EFG method in fluid flow problems*. Sadhana, 2004. **29**(3): p. 285-296.
145. Bhargava, R. and S. Singh, *Numerical simulation of unsteady MHD flow and heat transfer of a second grade fluid with viscous dissipation and joule heating using meshfree approach*. World Academy of Science, Engineering and Technology, 2012. **66**: p. 1215.
146. Mužík, J. *Simulating Couette Flow Using the Meshless Local Petrov-Galerkin Method*. in *Applied Mechanics and Materials*. 2014. Trans Tech Publ.
147. Tsubota, K.-i., S. Wada, and T. Yamaguchi, *Particle method for computer simulation of red blood cell motion in blood flow*. Computer Methods and programs in biomedicine, 2006. **83**(2): p. 139-146.
148. Qin, Y., et al., *Computational evaluation of smoothed particle hydrodynamics for implementing blood flow modelling through CT reconstructed arteries*. Journal of X-ray Science and Technology, 2017. **25**(2): p. 213-232.
149. Caballero, A., et al., *Modeling left ventricular blood flow using smoothed particle hydrodynamics*. Cardiovascular engineering and technology, 2017. **8**(4): p. 465-479.
150. Karimi, A. and R. Razaghi, *Interaction of the blood components and plaque in a stenotic coronary artery*. Artery Research, 2018. **24**: p. 47-61.
151. Mori, D., et al., *Computational study on effect of red blood cells on primary thrombus formation*. Thrombosis research, 2008. **123**(1): p. 114-121.
152. Kamada, H., et al., *Computational study on effect of stenosis on primary thrombus formation*. Biorheology, 2011. **48**(2): p. 99-114.
153. Sughimoto, K., et al., *Total cavopulmonary connection is superior to atriopulmonary connection Fontan in preventing thrombus formation: computer simulation of flow-related blood coagulation*. Pediatric cardiology, 2015. **36**(7): p. 1436-1441.
154. Chui, Y.-P. and P.-A. Heng, *A meshless rheological model for blood-vessel interaction in endovascular simulation*. Progress in biophysics and molecular biology, 2010. **103**(2-3): p. 252-261.

155. Rubenstein, D., W. Yin, and M.D. Frame, *Biofluid mechanics: an introduction to fluid mechanics, macrocirculation, and microcirculation*. 2015: Academic Press.
156. Siebert, M.W. and P.S. Fodor. *Newtonian and non-newtonian blood flow over a backward-facing step–a case study*. in *Proceedings of the COMSOL Conference, Boston*. 2009.
157. Brant, W.E.T.c.c., ultrasound. Philadelphia: Lippincott Williams & Wilkins., 2001.
158. He, L. and J. Pan. *Hemodynamics simulation of the intracranial bifurcation vessel with different shape*. in *2010 3rd International Conference on Biomedical Engineering and Informatics*. 2010. IEEE.